universität wien

DIPLOMARBEIT

Feldfortsetzung nach unten – Vergleich ausgewählter Methoden

und

Reduktion zum Pol auf unebenen Flächen

Verfasser: Niko Kompein

angestrebter akademischer Grad

Magister der Naturwissenschaften (Mag. rer. nat.)

Wien, 2011

Matrikelnummer:	0505524
Studienkennzahl lt. Studienblatt:	A416
Studienrichtung lt. Studienblatt:	Geophysik
Betreuer:	Ao. Univ.-Prof. Dr. Bruno Meurers

Downward field continuation – Comparing selected methods

and

RTP on arbitrary surface

diploma thesis
to achieve the degree of
master of natural sciences
"Magister der Naturwissenschaften"

prepared at
institute of meteorology and geophysics
university Vienna

submitted by

Mr. Niko KOMPEIN

with mentoring of
Prof. Dr. Bruno MEURERS

Vienna July 2011

I was trying to get consent for all the pictures shown in this thesis. Nevertheless, if there are Copyright infringements please contact me.

Content:

1. Problem-Setting / Motivation 7

2. Model-fields 12

2.1. ...for downward field continuation 12
2.1.1. Synthetic data set 12
2.1.2. "Real data" dataset Vulcano 13
2.1.3. "Real data" dataset Vulcano, local and regional part 16
2.2. ...for reduction to pole on arbitrary surface 18
2.2.1. model-field parameters for reduction to pole 18
2.2.2. Simple datasets 19
2.2.3. More realistic dataset of Vulcano (coarse) 21
2.2.4. Vulcano with 100m · 100m spacing (fine) 22
2.2.5. Real dataset of Socorro 22

3. Compared methods for downward field continuation 23

3.1. Field augmentation 25
3.2. Cooper 29
3.2.1. Different Cooper approaches 29
3.2.1.1. Finite difference approaches for a two-dimensional field 29
3.2.1.1.1. Cooper approach FD mixed horizontal derivative (fa) 30
3.2.1.1.2. Cooper approach FD mixed horizontal derivative (af) 31
3.2.1.1.3. Cooper approach FD GK-X derivative (fa) 31
3.2.1.1.4. Cooper approach FD GK-X derivative (af) 31
3.2.1.1.5. Cooper approach FD GK-Y derivative (fa) 31
3.2.1.1.6. Cooper approach FD GK-Y derivative (af) 31
3.2.1.1.7. Cooper approach FD 2nd vertical derivative (fa) 31
3.2.1.1.8. Cooper approach FD 2nd vertical derivative (af) 31
3.2.1.1.9. Cooper approach FD 1st vertical derivative (fa) 31
3.2.1.1.10. Cooper approach FD 1st vertical derivative (af) 32
3.2.1.2. Bi-cubic splines approaches for two-dimensional fields 32
3.2.1.2.1. Cooper approach BS mixed horizontal derivative (fa) 33
3.2.1.2.2. Cooper approach BS mixed horizontal derivative (af) 33
3.2.1.2.3. Cooper approach BS GK-X derivative (fa) 33
3.2.1.2.4. Cooper approach BS GK-X derivative (af) 33
3.2.1.2.5. Cooper approach BS GK-Y derivative (fa) 33
3.2.1.2.6. Cooper approach BS GK-Y derivative (af) 33
3.2.1.2.7. Cooper approach BS 2nd vertical derivative (fa) 33
3.2.1.2.8. Cooper approach BS 2nd vertical derivative (af) 34
3.2.1.2.9. Cooper approach BS 1st vertical derivative (fa) 34
3.2.1.2.10. Cooper approach BS 1st vertical derivative (af) 34
3.3. Fedi and Florio / ISVD 34
3.4. FFT Fast Fourier Transform 37
3.5. Pasteka's approach based on the Tikhonov algorithm 38

4. Reduction to pole on arbitrary surfaces 39

4.1. Considerations on the measured data in magnetic surveys 39
4.2. Reduction to pole on plane surfaces 41
4.3. Adjustment of magnetic fields with Xia on arbitrary surfaces 43

5. Results: 46

5.1. Results, downward field continuation 48

5.1.1. Simple dataset....48
5.1.1.1. Model-field and field of different approaches in -50m....48
5.1.1.2. Errors of different approaches in -50m....51
5.1.1.3. Improved errors of Cooper approaches in -50m....54
5.1.1.4. cross-sections of the error-fields in -50m....55
5.1.1.5. Relative errors of different approaches in -50m....58
5.1.1.6. 2D cross-sections of the relative field errors in -50m depth....62
5.1.1.7. Fields of different approaches in -300m....64
5.1.1.8. Errors of different approaches in -300m....66
5.1.1.9. Improved errors of Cooper approaches in -300m....69
5.1.1.10. cross-sections of the error-fields in -300m....70
5.1.1.11. Relative errors of different approaches in -300m....73
5.1.1.12. 2D cross-sections of the relative field errors in -300m depth....75
5.1.2. Vulcano dataset local part....77
5.1.2.1. Local fields with 10m x 10m grid including regional part in -50m . .77
5.1.2.2. Errors, local area. 10m · 10m sampling interval in -50m.....83
5.1.2.3. 2D cross-sections of error fields in -50m....86
5.1.2.4. Relative errors of local field in -50m.....89
5.1.2.5. 2D cross-sections of relative errors local field in -50m....91
5.1.3. Discussion: Disastrous results of Cooper's approaches when regional field is used for augmentation....93
5.1.3.1. BS3af, BS3fa....93
5.1.3.2. BS4af, BS4fa....94
5.1.4. Whole Vulcano area....96
5.1.4.1. Fields continued to -50m. 100m · 100m sampling interval.....96
5.1.4.2. Errors of the different approaches in -50m. Sampling interval 100m · 100m.....98
5.1.4.3. Relative error in -50m. Sampling interval 100m · 100m....100
5.1.4.4. Fields of the different approaches in -130m. Sampling interval 100m · 100m....102
5.1.4.5. Errors of the different approaches in -130m. Sampling interval 100m · 100m.....104
5.1.4.6. relative error in -130m. Sampling interval 100m · 100m....107
5.2. Results, reduction to pole (RTP) on arbitrary surface....110
5.2.1. Simple datasets....110
5.2.1.1. Inclination 10°....110
5.2.1.2. Inclination 30°....111
5.2.1.3. Inclination 50°....113
5.2.1.4. Inclination 70°....114
5.2.2. More realistic dataset of Vulcano 500m · 500m....116
5.2.3. More realistic dataset Vulcano 100m · 100m....117
5.2.4. Real dataset of Socorro....118
6. Conclusion / Zusammenfassung....119
6.1. ...for downward field continuation / für die Feldfortsetzung nach unten....119
6.1.1. FFT....119
6.1.2. Cooper....119
6.1.3. ISVD....121
6.1.4. Tikhonov....122
6.2. ...for reduction to pole on arbitrary surfaces / für die Reduktion zum Pol auf beliebigen Flächen....124
6.2.1. ...for the simple dataset / für den simplen Datensatz....124
6.2.2. ...for the more realistic dataset of Vulcano / für den realistischeren

Datensatz von Vulcano....125
6.2.3. ...for the real dataset of Socorro / für den echten Datensatz von Soccoro 126
7. Acknowledgements....128
8. References....129
9. Appendix....131
9.1. Equations....131
9.1.1. Truncation parameter for ISVD approach....131
9.2. Index....131
9.3. List of figures:....132
10. Lebenslauf....145

1. Problem-Setting / Motivation

There are two major topics in this thesis. The first is concerning the errors made by some selected methods for downward field-continuation. The second one is aimed at the error influence of topography on the reduction to pole process.
/ In dieser Arbeit werden zwei Hauptthemen behandelt. Der erste Themenblock beschäftigt sich mit dem Vergleich ausgewählter Methoden zur Feldfortsetzung nach unten. Im zweiten Teil wird der Einfluss der Topographie auf den Fehler der Reduktion zum Pol untersucht.

All dataset used in field continuation processes are in form of discrete data. Therefore aliasing and leaking is a inherent problem. Upward field-continuation is a smoothing operation and is therefore a stable process in terms of slightly varying the input dataset while the resulting dataset of this filtering process is also changing faintly. On the other hand downward continuation is an unstable filter process, cause a small variation in the input dataset, turns out into a huge alteration in the resulting dataset causing it to oscillate with comparable big magnitudes with respect to the change in the input. This oscillating character gets bigger the closer to a causing source the downward field-continuation is done. Nevertheless, downward field-continuation may only be done if it is certain that there are actually no sources in the region of continuation. For this reason many scientist round the world have tried to develop methods for a more stable downward field-continuation. There are several more or less well known field continuation methods like classical *FFT (BRACEWELL 1978)*, *(XIA 1993), (IVAN 1994), (COOPER 2004)*, *Integrated second vertical derivative (FEDI and FLORIO 2002)* or *(TIKHONOV 1968)*. Through different methods the influence of aliasing, leaking and maybe oscillations in downward continuation processes may be minimized. The first part of this thesis is aimed on finding the most stable method for downward continuation of some selected methods for potential field data.
/ Alle Daten für Feldfortsetzungsprozesse liegen in diskreter Form vor. Daher sind Aliasing und Leaking zwei unausweichliche Probleme. Die Feldfortsetzung nach oben ist eine Glättungsoperation und daher ein stabiler Operator, oder anders gesprochen, ändert sich das Eingangssignal nur leicht, so ändert sich auch das Ausgangssignal nur gering. Auf der anderen Seite ist die Feldfortsetzung nach unten aber ein instabiler Operator, da eine kleine Änderung des Eingangssignals in einer riesengroßen Änderung des Ausgangssignals mündet, vielleicht noch verstärkt durch zahlreiche und starke Oszillationen. Diese Oszillationen werden stärker je näher die Feldfortsetzung zur Quelle durchgeführt wird. Nichtsdestotrotz, Feldfortsetzung nach unten ist nur erlaubt solange Quellenfreiheit gegeben ist. Aus diesem Grunde haben sich viele Wissenschaftler rund um den Globus damit beschäftigt stabilere Verfahren für die Feldfortsetzung nach unten zu entwickeln. Es exestieren einige mehr oder weniger bekannte Verfahren für die Feldfortsetzung wie z.B. FFT (BRACEWELL 1978), (XIA 1993), (IVAN 1994), COOPER 2004), Integrated second vertical derivative (FEDI and FLORIO 2002) oder (TIKHONOV 1968). Durch die unterschiedlichen Methoden soll der Einfluss von Aliasing und Leaking, sowie möglicherweise existente Oszillationen verursacht durch den Feldfortsetzungsprozess nach unten, minimiert werden. Daher ist das Ziel des ersten Teils dieser Diplomarbeit die Bestimmung der bestmöglichen Methode zur Feldfortsetzung von Potentialfeldern nach unten.

The methods to be investigated are classical *FFT*, *Cooper*, *ISVD* and *Tikhonov / Pasteka*. All the methods tested here do need equidistant spaced datasets on a plane surface as input data on the contrary to (IVAN 1994) which can also use data on different spaced

locations and heights. For synthetic datasets equidistant spaced field information on a plane surface represents no further problem but the frequency content in such datasets is often poor. Therefore real world datasets would be a better idea to test such methods. Real world data is most of the times only available at one topographic height/depth and therefore comparison of downward continued fields wouldn't be possible. Further on observations from real world data are never ever perfectly equidistant-spaced.
/ Die zu untersuchenden Methoden in dieser Arbeit sind FFT, Cooper, ISVD und Tikhonov / Pasteka. Im Gegensatz zu (IVAN 1994) benötigen alle hier untersuchten Methoden equidistant auf einer Ebene angeordnete Daten. Im Fall synthetischer Daten führt dies zu keinem Problem, aber der Frequenzinhalt solcher synthetischer Datensätze ist eher gering und daher kaum vergleichbar mit echten Felddaten. Deshalb wäre es eine kluge Idee diese Methoden an echten Felddaten zu testen. Da aber echte Felddaten meist nur in einer topographischen Höhe/Tiefe bekannt sind, wäre der Vergleich der Ergebnisse der einzelnen Methoden in anderen Tiefen als dem Beobachtungsniveau nicht möglich. Des weiteren sind echte Felddaten nie auf einem perfekt equidistanten Raster vorhanden.

Therefore a source distribution had to be found, which re-produced the potential field observed, vanishes at infinity (definition of a potential field) and is harmonic in the area of interest. These are the basics for *equivalent-source* (*EQS*) principles, which were used to gain sources for different model-field datasets. Those sources were utilized to reproduce the measured field at equidistant spaced sampling-points with acceptable accuracy in measurement datum as well as in different plane heights/depths below this datum. Those so gained model-fields were then assumed as “true” fields for comparison with the results of the different approaches as well as input fields (model-fields in assumed 0m height/depth) for them.
/ Aus diesem Grund musste eine Quelleverteilung gefunden werden, die ein beobachtetes Potentialfeld im Beochtungsniveau exakt wiedergibt, gleichzeitig im Unendlichen verschwindet (siehe Definition eines Potentialfeldes) und die an der Stelle der Feldfortzsetzung der Laplace-Gleichung genügt. Das sind allerdings genau die Grundlagen der equivalent-source (EQS) Prinzipien, die verwendet werden um ein Ensemble an Quellen zu erhalten, das die entsprechenden Potentialfelder wiedergibt. Mit Hilfe dieser Quellenverteilungen konnten die beobachteten Felder auf einem equidistantem Raster in ebenen (Mess-)Niveaus, sowie in den entsprechden zu testenden Tiefen mit ausreichender Genauigkeit wiedergegeben werden. Diese so erhaltenen Modellfelder wurden fortan als wahre Felder in den besagten Tiefen angesehen.

As measured field data is often only available in a small area, regional field data from other surveys is frequently used to minimize edge effects and to consider big anomalies influencing the local field part of interest. Regional field informations are most likely only available on a different sampling-point spacing and or height than the local part or just shifted compared to the local part. The tested methods here on the contrary all do need equidistant spaced information on a plane surface. So interpolation needs to be done to get field informations on a equidistant-spaced, plane surface. Further on this leads to interpolation errors especially at the regional part of a field of interest but as well as smaller errors in the local part. In the following chapters there will be a short discussion on this interpolation errors and their influence on the downward field continuation process.
/ Da beobachtete Felddaten oft nur in kleinen Messgebieten vorliegen, werden regionale Felddaten von anderen Messungen in angrenzenden Messgebieten häufig verwendet um Randeffekte zu minimieren und Einflüsse größerer, regionaler Anomalien in Form von langwelligen Trends in den Daten zu berücksichten. Regionalfelddaten

sind meist nur auf unterschiedlichen Rastern und Höhen vorhanden sind als der lokale Bereich (der von Interesse ist). Da aber die hier untersuchten Methoden Daten auf einem equidistantem ebenen Raster benötigen ist eine Interpolation der regionalen und der lokalen Felddaten in ein gemeinsames Raster notwendig. Dies wiederum führt aber zu Interpolationsfehlern, speziell im Regionalfeldbereich, da dort meist der Rasterabstand größer gewählt ist als im lokalen Bereich. Aber auch im lokalen Bereich treten kleinere Fehler auf. In den folgenden Kapiteln folgt daher eine kleine Erörterung zum Thema Interpolationsfehler und deren Einfluss auf die Feldfortsetzung nach unten.

Additional tests concerning field-augmentation techniques are included during those tests for the Cooper and Tikhonov algorithm. As Cooper proposed in his paper *(COOPER 2004)* there are a lot of possible ways to combine filtering in space-domain and wave-number-domain. The tests here include the exchange of a linearly extrapolating field-augmentation technique with a regional field. This regional field could be assumed as a high-sophisticated field-augmentation method. Also there will be tests on the exchange of order for filtering in space-domain and field-augmentation before applying the downward continuation operator or adjusting the size of the cosinus-taper for field-augmentation of Tikhonov's algorithm.
/ Zusätzlich folgen Tests zum Thema Felderweiterung im Zusammenhang mit den Ansätzen von Cooper und Tikhonov. (COOPER 2004) schlug in seinem Artikel einige Möglichkeiten vor Filter im Wellenzahl- und Raum-Bereich zu kombinieren. Diese Tests hier untersuchen den Einfluss des Vertauschens der Reihenfolge von Felderweiterung und Filterung im Raumbereich sowie das gänzliche ersetzen der linear interpolierenden Felderweiterung mit Regionalfelddaten – Die Daten des Regionalfeldes sollten im folgenden angenommen werden als das Ergebniss einer äußert guten Felderweiterungstechnik. Beim verwendeten Tikhonov Algorithmus wird zusätzlich getestet inwieweit der Einfluss einer veränderten Felderweiterungsgröße des implementierten Cosinus-Taper (für die Felderweiterung) ist.

Neglecting the influence of arbitrary surfaces of a survey on the *reduction to pole (RTP)* process is the aim of the second part and the errors gained through this.
/ Die Vernachlässigung einer beliebigen Messgebietsoberfläche auf die Reduktion zum Pol (RTP) und die dabei entstehenden Fehler ist das Ziel des zweiten Teils dieser Arbeit.

In geophysical magnetic surveys ferromagnetic attributes of minerals are used to get first overview informations about a survey area. Since inclination and declination for a given survey area is changing with latitude, longitude and time the reduction to pole process is used to shift anomalies to their correct location with respect to a given inclination and declination. This process neglects temporal changes of the direction of the total field intensity, but as long as they aren't influenced by solar magnetic storms or other short-term magnetic events this assumption can be made. Furthermore reduction to pole operator is applied to the total field anomaly field which is gained by subtracting a suitable regional field (usually from an actual *IGRF* model) from the measured total field intensity. This implies some further restrictions.
/ Bei geophysikalischen Messungen werden häufig ferromagnetische Eigenschaften von Mineralien genutzt um einen ersten Überblick über ein zu untersuchendes Messgebiet zu erhalten. Inklination sowie Deklination hängen in der Regel von geographischer Länge und Breite und der Messzeit ab. Der RTP Operator wird in Folge dessen dazu verwendet magnetischen Anomalien entsprechend Inklination und Deklination an ihre

wahre, horizontale Position zu "verschieben". Die Reduktion zum Pol vernachlässigt dabei aber die zeitliche Änderung der Inklination und Deklination insoweit, dass angenommen wird die Richtung des Hauptfeldes sei für den Zeitraum der Messung konstant. Dies gilt natürlich nicht für Messungen die über Monate hinweg durchgeführt werden. Da die zeitlichen Änderung der Richtung des Hauptfeldes nur langsam vonstatten geht ist diese Vereinfachung aber erlaubt solange keine kurzzeitlichen Änderungen auftreten wie z.B. Sonnenstürme, etc. Auch sollte berücksichtigt werden, dass der RTP Operator auf einen Datensatz angewandt, wird der durch die Subtraktion eines Regionalfeld-Anteils (aus der Berechnung eines IGRF Modells zum Beispiel) vom eigentlichen Messdatensatz entstanden ist. Das impliziert allerdings weitere Annahmen und Bedingungen.

Since the direction of the regional field and the total field intensity is usually different it is important to establish under what conditions the total field anomaly is harmonic and satisfies Laplace's equation. *(BLAKELY 1995)* shows that the total field anomaly satisfies Laplace's equation and is harmonic as long the anomaly field is small compared to the total field and the direction of regional field is approximately constant over the dimensions of the survey area.
/ Da die Richtung des Regionalfeldes und der Totalfeldintensität im Allgemeinen unterschiedlich sind, ist es wichtig klar zu stellen unter welchen Bedingungen die Totalfeld-Anomalie die Laplace Gleichung erfüllt, deren erste Ableitung eindeutig ist und deren zweite Ableitung exestiert und somit eine harmonische Funktion darstellt. (BLAKELY 1995) zeigt das die Totalfeld-Anomalie der Laplace Gleichung genügt und eine harmonische Funktion ist, wenn die Anomalie klein im Vergleich zum Totalintensitätsfeld ist und die Richtung des Regionalfeldes im Messgebiet in etwa als konstant angesehen werden kann.

As magnetic field intensity surveys are always gained on more or less arbitrary surfaces and different spaced sampling-points a field continuation and interpolation upward to a plane surface at a equidistant spaced grid above the highest topography would be done before applying the reduction to pole operator. This would be needed cause the reduction to pole process takes place in wave-number-domain and therefore again uses FFT which is defined only for plane surfaces with equidistant-spaced grid locations. Since our aim is to compare results of reduction to pole on arbitrary surfaces with the true reduction to pole field a method for model-field generation is needed. It was decided to use *(XIA 1993)*'s approach to adjust the fields of interest with given inclination and declination and recalculate the adjusted fields with inclination and declination 0° to get appropriate model-fields. The operator used for reduction to pole in Xia's algorithm on arbitrary surfaces was based on *Poisson's theorem* (DOBRIN 1976).
/ Da magnetischen Messungen eigentlich fast immer auf mehr oder weniger beliebig gestalteten Oberfläche und mit unterschiedlichsten Rasterabständen durchgeführt werden müssen, führt dies wiederum zur Notwendigkeit der Interpolation auf ein equidistantes ebenes Raster, oberhalb der höchsten Topographie, bevor die Reduktion zum Pol korrekt durchgeführt werden kann. Diese Notwendigkeit rührt wieder daher dass die Reduktion zum Pol eine mathematische Operation im Wellenzahl-Bereich ist und deshalb die FFT benötigt. Diese benötigt aber wiederum Daten auf einem equidistanten ebenen Raster, worin das Problem begründet wäre. Das Ziel dieser Arbeit ist es nun genau diese Feldfortsetzung nach oben, auf das Niveau der höchsten Topographie zu vernachlässigen und zu untersuchen wie groß der Fehler bei dieser Vernachlässigung werden kann. Zur Wiedergabe der "wahren" polreduzierter Felddaten auf der Topography wurde daher der Ansatz von (XIA 1993) gewählt. Dieser lässt Inklination und Deklination eines gesuchten Messgebiets in einem iterativen

Anpassungsprozess miteinfließen und gibt anschließend das polreduzierte Feld, verursacht durch die erhaltene Feldverteilung auf der Topographie aus. Diese Feldinformationen werden anschließend als "wahre" RTP-Felder auf der Topographie angesehen. Der verwendete Operator im Xia Algorithmus basiert auf dem Poisson Theorem (DOBRIN 1976) der im Wellenzahl-Bereich wie folgt aussieht.

$$\frac{(\vec{k}\,\vec{s}_0)(\vec{k}\,\vec{m}_0)}{|K|^2} \qquad (1.1)$$

$$\vec{k} = (ik_x, ik_y, \sqrt{k_x^2 + k_y^2}),\ K = (k_x, k_y), \qquad (1.2)$$
$$\vec{s}_0, \vec{m}_0 \ldots \textit{unit vectors of mainfield and magnetization}$$

Further discussions regarding this operator will follow in chapter 4.3. "Adjustment of magnetic fields with Xia on arbitrary surfaces". This additional operator made it at least possible to adjust magnetic fields as long as the frequency content in the model-fields weren't too big. In fact this still caused some problems but through trial and error of extraction of every n-th grid-location and adjustment of the resulting fields, model-fields were gained with more or less acceptable deviations from the original fields.
/ Eine weitere Erörterung bezüglich des verwendeten Operators folgt in Kapitel 4.3. "Adjustment of magnetic fields with Xia on arbitrary surfaces". Dieser zusätzliche Operator machte es erst möglich magnetische Felddaten anzupassen und anschließend die Reduktion zum Pol durchzuführen, zumindest solange der Frequenzinhalt in den untersuchten Datensätzen nicht zu groß ist. Durch Probieren unterschiedlichster Rasterabständen konnten schluss endlich aber doch Datensätze gewonnen werden, die noch ein akzeptabeles Mass an Frequenzinhalt innehatten und gleichzeitig eine Konvergenz des Xia Algorithmus zuließen.

Since such iteration processes like Xia and the preparations before applying reduction to pole takes time and as field-surveys themselves sometimes are time-critical process it would be interesting where and how big the errors are made during reduction to pole by neglecting the influence of topography [PERS. COMM. *Dr. Andreas Ahl*, *Geologische Bundesanstalt, Vienna*].
/ Da iterative Prozesse wie Xia und die Vorarbeiten zur Reduktion zum Pol viel Zeit beanspruchen und magnetische Feldmessungen des Öfteren zeitkritische Prozesse sind, die als günstige Messungen vor den kostenintensiveren Verfahren wichtige vorab Informationen liefern, wäre es von großem Interesse wie groß die Fehler wären, würde man die besagten Feldfortsetzungen nach oben unterlassen. [PERS. COMM. Dr. Andreas Ahl, Geologische Bundesanstalt, Vienna].

2. Model-fields

2.1. ...for downward field continuation

2.1.1. Synthetic data set

For the synthetic data set a triple of synthetic point sources were used.
This model-sources were set along a diagonal line through the model-field.
The point sources were read in and used to calculate a grid file at given locations.

Data of the point sources.:			
Northing [km]	Easting [km]	Depth [km]	Mass [kg]
10	10	0.5	1,00E+012
5	5	5	1,00E+013
15	15	1	1,00E+012

Data of the simple model-fields.:	
sampling interval:	0.1km · 0.1km
Model-field size:	20km · 25km
Amount of nodes:	201 · 251

The field in a depths of 0m, 50m and 300m is therefore.:

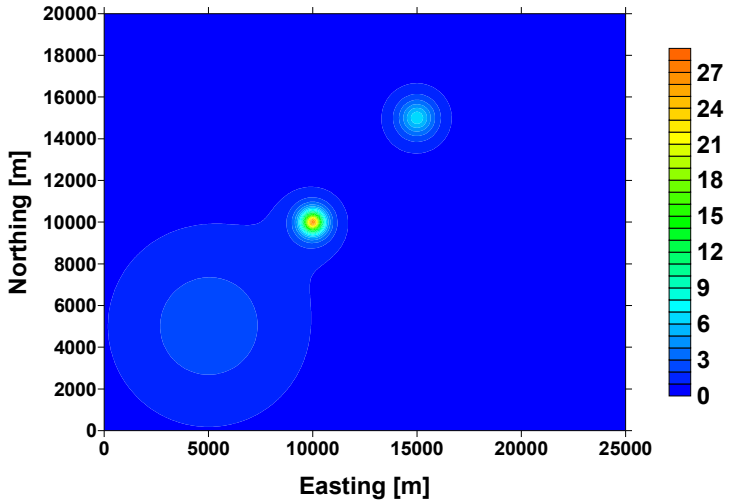


figure 2.1.1.1: model-field in 0m depth. Scale bar in mGal

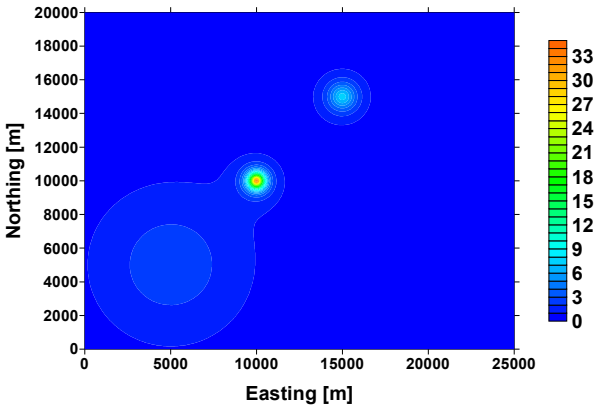


figure 2.1.1.2: model-field in 50m depth. Scale bar in mGal

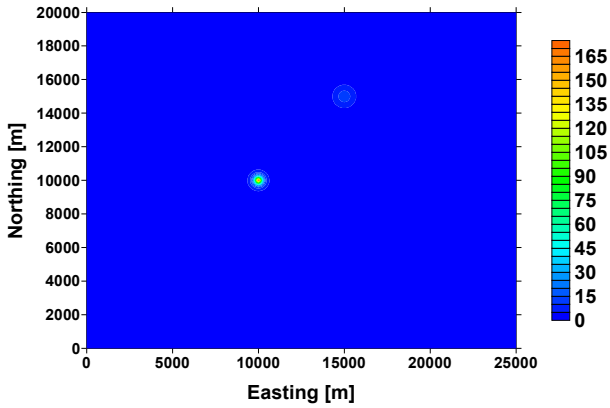


figure 2.1.1.3: model-field in 300m depth. Scale bar in mGal

2.1.2. "Real data" dataset Vulcano

The "real" dataset was sponsored by *GBA* (*Geologische Bundesanstalt, Vienna*). The data was gained at the island *Vulcano* in Italy south of *Lipari* over years of field work and from some recent air borne magnetic surveys to observe the volcanic-complex beneath this island. *(OKUMA, S. et. al. 2006A), (OKUMA, S. et. al. 2006B)*

As the original data were not available at equidistant spaced locations the dataset had to be re-sampled and augmented to a rectangular field by the means of Kriging interpolation. This interpolation to a rectangular dataset with equidistant spaced sampling points was needed for the different approaches that were investigated here. A 100m · 100m grid was chosen. The interpolated dataset was assumed to be on a plain surface in 0m height.

Through a method proposed by *(CORDELL 1992)* based on *equivalent source principles* three different source layers have been obtained. The 100m · 100m potential field A_100 was sampled to a 1000m · 1000m potential field. *Cordell*'s algorithm was used to get deep sources describing the a low frequency content of field A_100.

The deep sources were used to calculate a long wavelength character field B_deep100 at the locations of the original field A_100. This field B_deep100 was subtracted from the original 100m · 100m potential field A_100 to get a residual potential field R1_deep100.

The residual potential field R1_deep100 again was sampled at a 500m · 500m grid. Once again the *Cordell algorithm* was used to get sources for this intermediate deep sources. From these so gained intermediate sources again a field C_inter100 with 100m times 100m spacing was calculated and then subtracted from field R1_deep100 to get the residual field R2_inter100.

The remaining high frequent field R2_inter100 was again used to get the shallowest sources with Cordell's algorithm. The sources gained from field A_100 at 1000m spacing, R1_deep100 at 500m spacing and R2_inter100 at 100m spacing combined in one common file were used to get a list with different source layers for long, intermediate and short wavelength character, which was hereafter used to generate a much more realistic model-field. (See Figure 2.1.2.1)

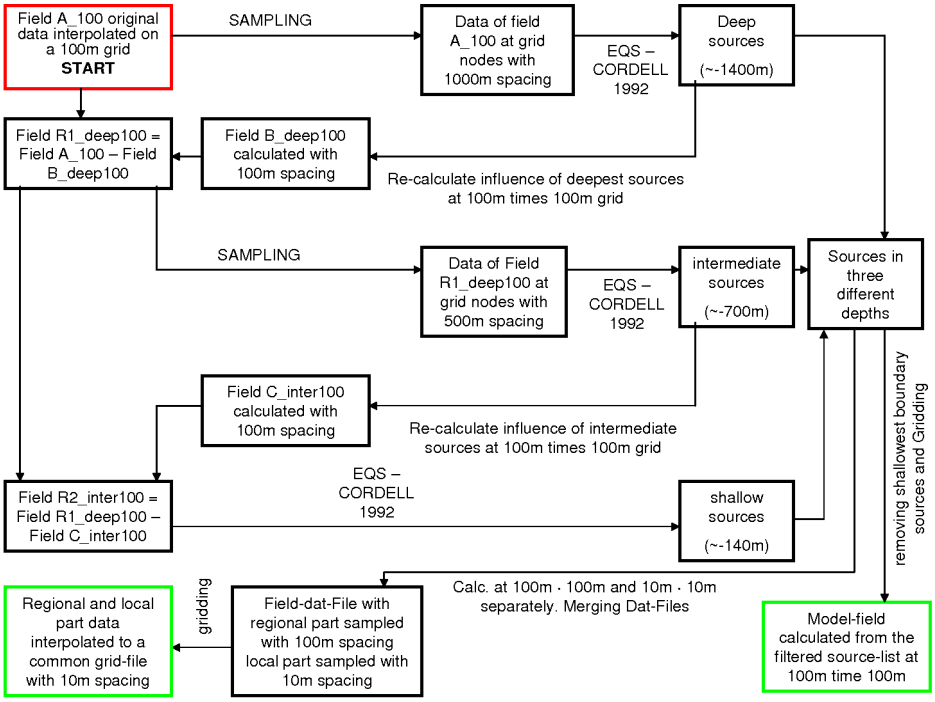


Figure 2.1.2.1: flowchart for model-field generation, RED = START, GREEN = model-fields used for the downward continuation tests

After the whole process *three layers* could be distinguished in around 140m, 700m and 1400m depth. The remaining error to the original field in the assumed zero-level was around ± 8 nT. As it turned out the previously mentioned *Cordell algorithm* produced shallow sources even at the boundaries of the field, which would not cause any problems in simple upward continuation but as the goal to achieve was a stable downward continuation there came up some problems when using these sources.

These shallow boundary sources led to strong gradients at the boundaries of our field of interest, especially the shallowest combined with the used linearly interpolating field-augmentation. As nearly all of our tested methods (except for Tikhonov's approach) for downward continuation used this field-augmentation technique that just extrapolated linearly between the boundary values, the extrapolation of those strong gradients at the boundaries led to high-frequency content which of course was amplified by the downward continuation process. So the shallowest sources near the boundaries had to be filtered out of the list of sources to get comparable results for downward field continuation with the used methods. After that the *adjustment-error* had magnitudes from *-102,50* to *28,96 nT* with a standard deviation of *4,12 nT* compared to the measured field data. This and a further one were the model-fields that the different approaches of *FFT*, *Cooper, Fedi and Florio* and *Tikhonov* were tested on. For the first model-field two depth were tested. One within the range of sampling interval (100m · 100m) and a second one outside this range close to the first source level in around 130m. Depth 1: 50m, Depth 2: 130m

The additional model-field was a small aperture of the whole Vulcano dataset. It was sampled with 10m times 10m and had an inner sampling point spacing of 10m times

10m for the “local” part and a 100m times 100m sampling point spacing for a “regional” part. Further explanations why this additional dataset was tested too will be in the following chapter.

The boundaries of the model-fields for the whole Vulcano dataset are:
(Units in meter.)

Easting min.:	485560,	Easting max.:	505860
Northing min.:	4241560	Northing max.:	4264960

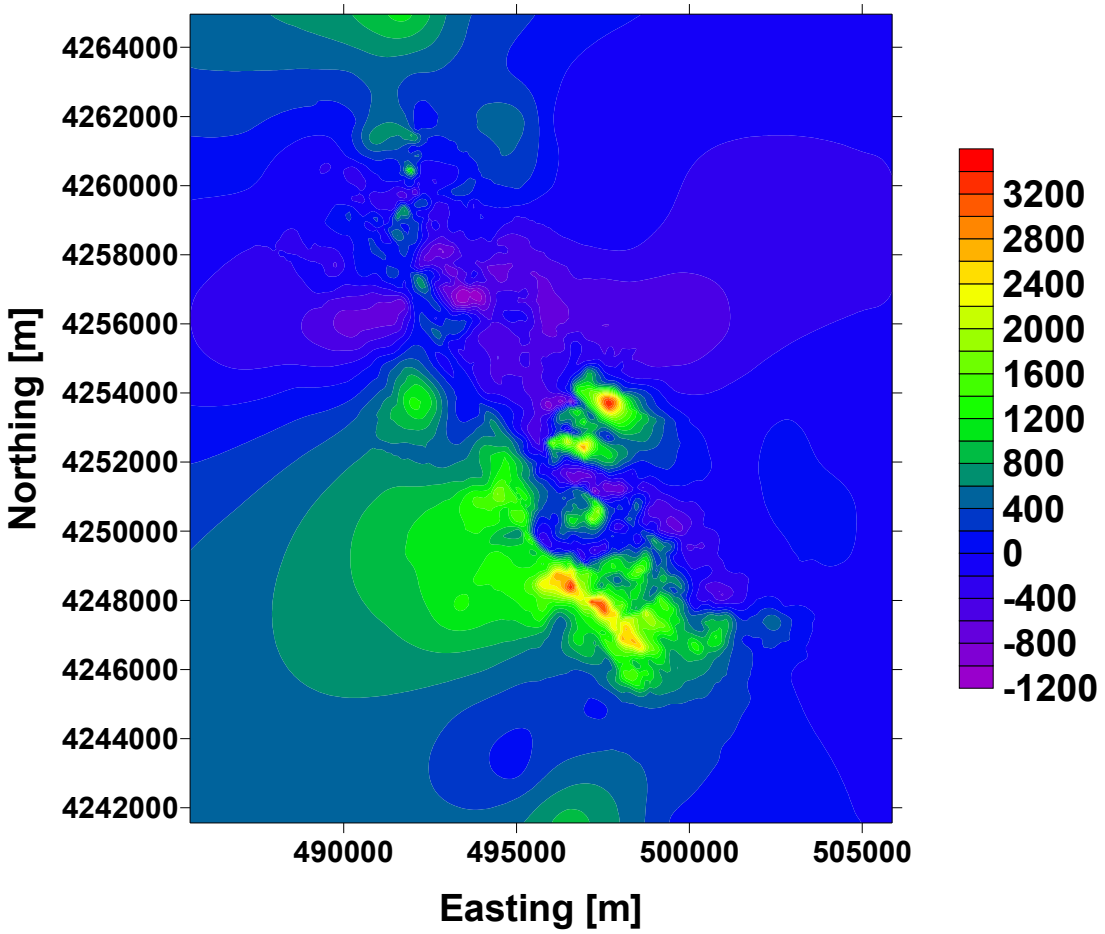


figure 2.1.2.2: model-field in 0m depth 100m · 100m sampling interval. Scale bar in nT

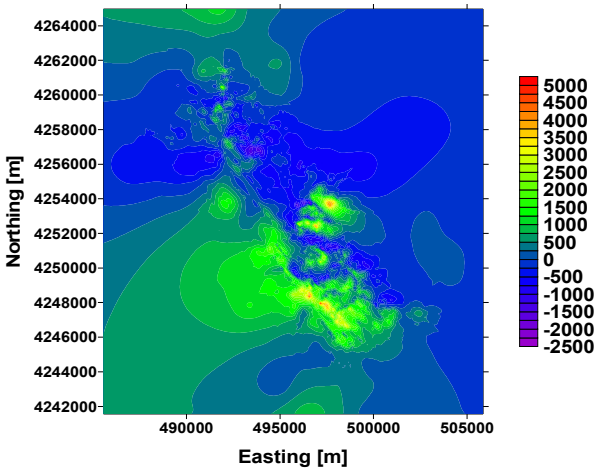


figure 2.1.2.3: model-field in 50m depth 100m · 100m sampling interval. Scale bar in nT

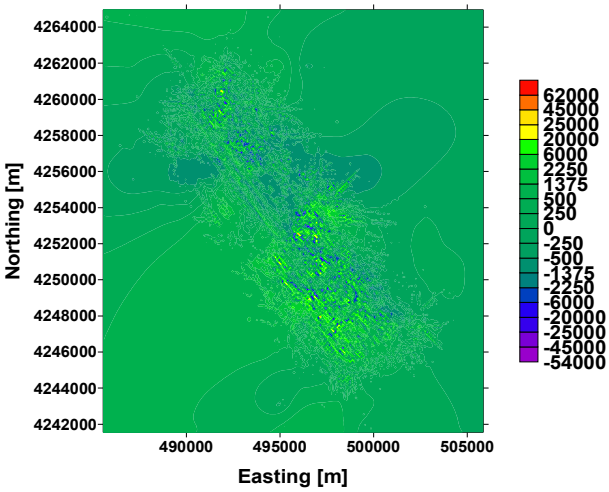


figure 2.1.2.4: model-field in 130m depth 100m · 100m sampling interval. Scale bar in nT

2.1.3. "Real data" dataset Vulcano, local and regional part

Just to make sure how the different approaches behave when they are used to downward continue to depths much greater than the used sampling interval, a third model-field was generated. This third model-field was a small aperture of the above mentioned original one, with 100m · 100m grid spacing, which had its shallowest sources at around -140m. So downward field continuation to depth a multiplicity bigger than the grid-spacing distance is theoretically not possible without downward continuing into regions where sources are located. Therefore a smaller aperture of the previously used 100m x100m grid at a depth of 50m (5 times the new sampling interval of 10m · 10m sampling interval) was used to test the different approaches on downward field continuation to depth bigger than a multiplicity of the grid spacing distance. Surrounding data from the original 100m · 100m grid was used to simulate a regional data set. This dataset was generated from the original source file list gained by the above process but without removing the shallowest sources at boundaries of the whole Vulcano dataset. This was acceptable cause the influence of these shallow boundary sources were nearly constant in this small aperture and was therefore negligible.

regional and local field 10m · 10m spacing:
Easting-min: 495870m
Easting-max: 498650m
Northing-min: 4252270m
Northing-max: 4254450m
219 Rows · 279 Lines
sampling interval: 10m · 10m

local field 10m · 10m spacing:
Easting-min: 496360m
Easting-max: 498160m
Northing-min: 4252760m
Northing-max: 4253960m
121 Rows · 181 Lines
sampling interval: 10m · 10m

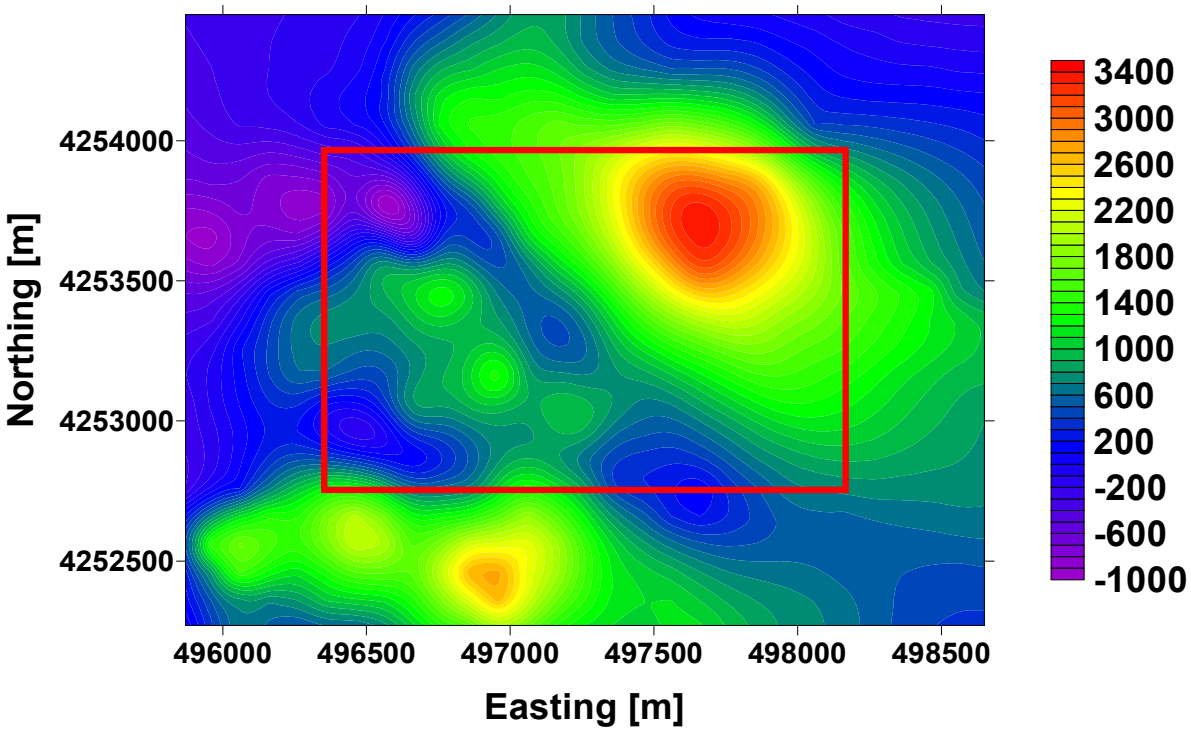


figure 2.1.3.1 model-field in 0m depth, regional (100m · 100m samping point spacing) and local part (10m · 10m samping point spacing) interpolated to 10m · 10m sampling interval. The red rectangle marks the local part of the field which will be discussed in the results. Scale bar in nT

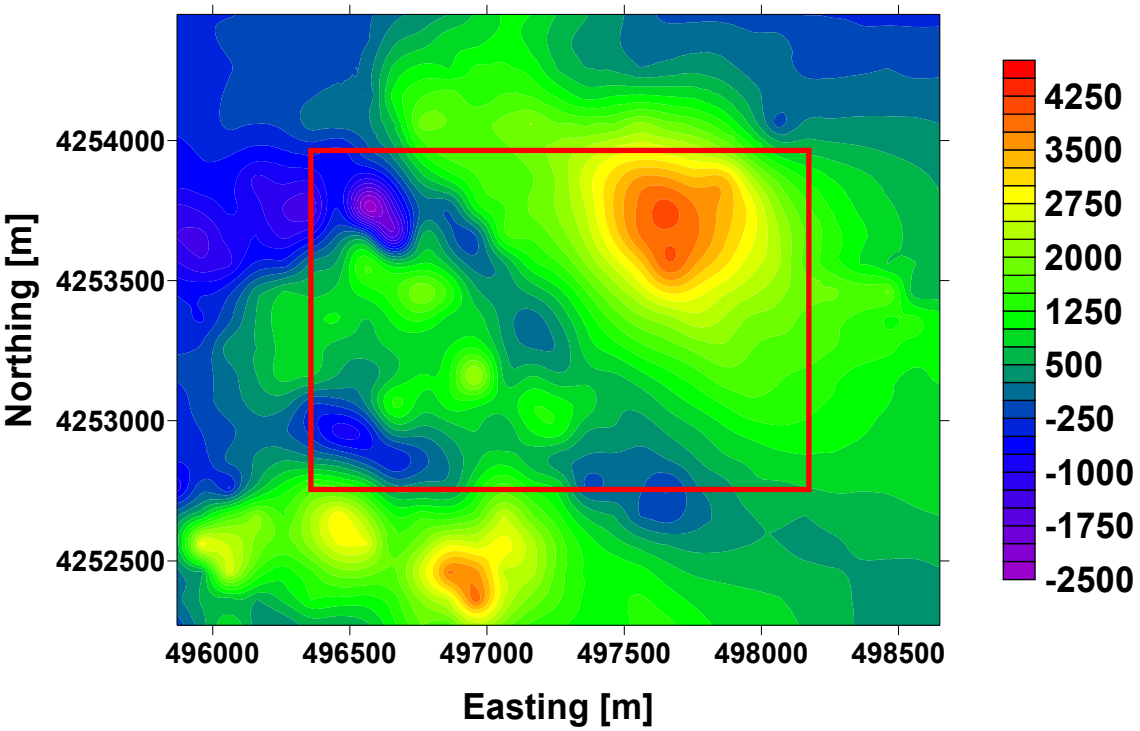


figure 2.1.3.2 model-field in 50m depth 10m · 10m sampling interval. The red rectangle marks the local part of the field which will be discussed in the results. Scale bar in nT.

2.2. ...for reduction to pole on arbitrary surface

2.2.1. model-field parameters for reduction to pole

Simple datasets were used to test the reduction to pole operator on arbitrary surface. The model-fields, were generated by a small program which used homogeneous magnetized spheres representing dipole sources with given inclination and declination in different horizontal and vertical positions. The same program was also used to generate a field with 90° inclination and 0° declination of the same spheres-set as RTP model-field. An *helicopter flight height profile* included in the dataset of *Vulcano* was used to simulate real world topography and locations for the potential fields being adjusted.

The simple dataset consisted of two magnetic dipoles. For these two dipoles the inclination varied from 10 to 70 degree in steps of 20 degree so that 4 different inclinations where tested (10, 30, 50 and 70 degree).

The errors for reduction to pole on arbitrary surfaces where also tested with an algorithm based on a paper by *(XIA 1993)*. Since usually Xia's algorithm is an iteratively used adjustment method for potential-fields through calculation of a equivalent source distributions, there wouldn't be any further problems during this process as long as the conditions mentioned in (XIA 1993) and in 4.3. “Adjustment of magnetic fields with Xia on arbitrary surfaces“ are met (The series contained in the iterative process of Xia converges if Z_0 is bigger than $H = max|h(\vec{r})|$ and therefore the equivalent source layer E is below the observation surface S (*(WHITTAKER AND WATSON 1962)*). Where $H = max|h(\vec{r})|$ is the maximum magnitude of deviation of the surface S from the median topography distance Z_0 with respect to the chosen equivalent source layer E.).

Nevertheless through RTP there is another problem inbound in the adjustment process caused by an operator *A,* containing inclination and declination information, based on *Poisson's theorem*.

$$A = \frac{\left(i\,k_x e_x + i\,k_y e_y + e_z\sqrt{k_x^2 + k_y^2}\right)^2}{k_x^2 + k_y^2} \qquad (2.2.1.1)$$
$$\vec{f} = \vec{m} = (e_x, e_y, e_z)$$

e_x, e_y and e_z are the vector components of the unit vector of the main field and the magnetization respectively. Where $k_x = \frac{2\pi n}{N\Delta x}, k_y = \frac{2\pi m}{M\Delta y}$ with the spacial Nyquist-frequency $k_{Nx} = \frac{\pi}{\Delta x}$ and $k_{Ny} = \frac{\pi}{\Delta y}$ reached as n=N/2 / m=M/2, N·M the amount of nodes and Δx / Δy the grid spacing in x and y spacing respectively

This operator made the adjustment with given inclination and declination as well as the reduction to pole process on topography primarily possible with Xia's algorithm. A further discussion on the behaviour of this operator will be in 4.3. “Adjustment of magnetic fields with Xia on arbitrary surfaces“.

As it it turned out to be very time consuming to develop an algorithm, which would

have made it possible to gather a list of sources, including their inclinations and declinations, to reproduce a more realistic dataset, it was decided to assume *Xia*'s adjusted fields, with RTP already applied and topography considered to be the model-fields for the more realistic datasets. Nevertheless, it maybe possible to gather such informations, if there is enough time for an appropriate algorithm development. Furthermore it should be kept in mind that the results of Xia didn't lead to really accurate results for the more realistic datasets, caused by bad convergence, as was observed in preliminary tests. Therefore the more realistic model-field plots do have informations about the last iteration step's convergence inbound in the plots – Standard-deviation and maximum absolute error respectively.

The inclination and declination of the model-fields were assumed to be I=57.8°and D=0° for the more realistic datasets of Vulcano. The *parameter C* mentioned in *(XIA 1993)* were chosen to be 0.07 for the more realistic and approximately $\frac{1}{2\pi}$ for the real dataset. The chosen value for *parameter C* was just gained through simple trial and error. So maybe a bigger value faster delivers results but also maybe diverges extremely fast. For the more realistic datasets and the real one a maximum of ten thousand iteration steps were chosen.
The real dataset from the island *Socorro* (18° 47' 35" N, 110° 58' 45" W) in the pacific ocean near the Mexican western coastline from a *GBA* survey in this region was used for test purposes on real field data. On this field again the RTP operator was applied, using Xia's algorithm to gain “model-field”-data on topography height and classical RTP neglecting topography on the other hand. The inclination and declination for this field was.: I: 43,73° and D: 8,87° (referring to http://www.ngdc.noaa.gov/geomag/magfield.shtml, National Geophysical Data Center, NOAA for the above mentioned GPS location) for early July, 2009. This dataset contained real topography information. Since the original data was again given on different spaced sampling-points Kriging interpolation was once more used to get a dataset with 50m · 50m grid spacing and corresponding heights, also interpolated with Kriging. Since real, high-frequency content in the Soccoro's dataset prevented an acceptable convergence with Xia at first with the chosen grid-spacing the interpolated data was filtered ten times by a “9 – node Averaging (3x3)” filter contained in “Surfer 8, Golden Software Inc.” before adjustment with Xia.

2.2.2. Simple datasets

The locations of the two spheres used to generate this dipole-fields were.:

	Northing [km]	Easting [km]	Radius [km]	Depth [km]
1.	11,7	10,15	3	2
2.	9,03	11,5	3	2

Permeability κ=0,025
All scale bars are in nT.

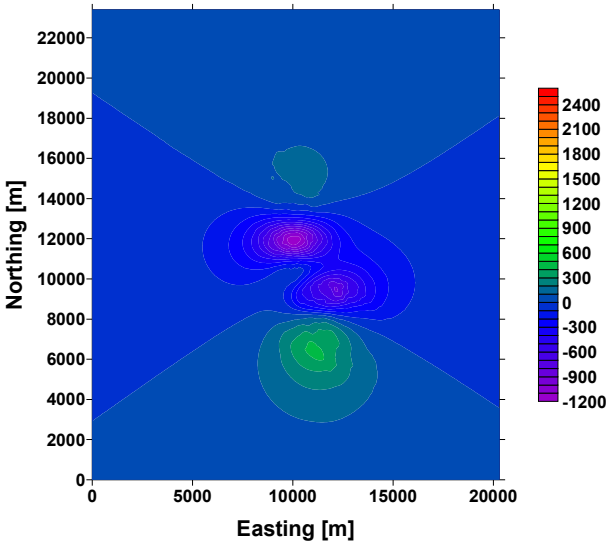


Figure 2.2.2.1: simple model-field 2 sources, inclination 10°

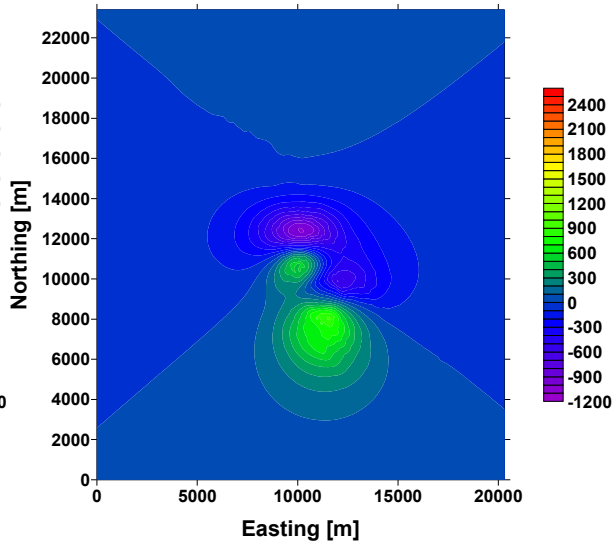


figure 2.2.2.2: simple model-field 2 sources, inclination 30°

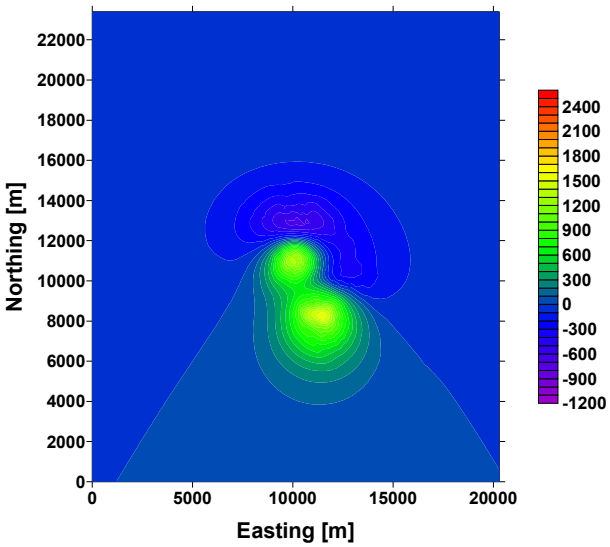


figure 2.2.2.3: simple model-field 2 sources, inclination 50°

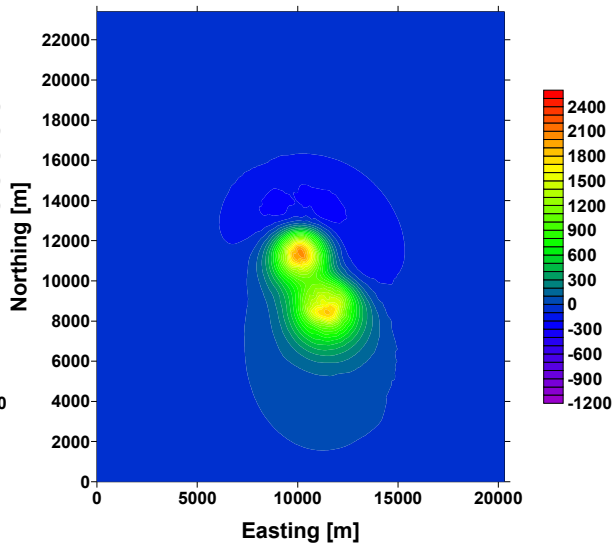


figure 2.2.2.4: simple model-field 2 sources, inclination 70°

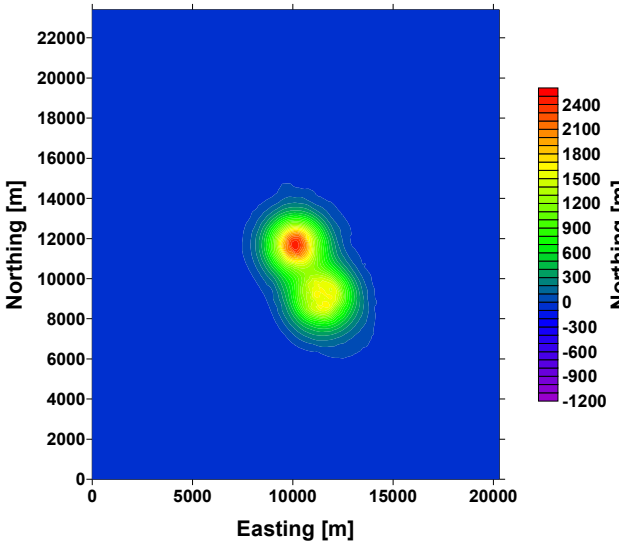


figure 2.2.2.5 simple model-field 2 sources, inclination 90° (true pole-reduced field)

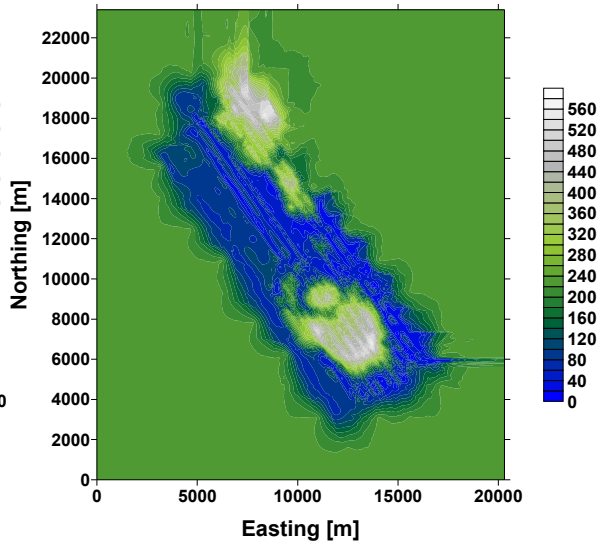


Figure 2.2.2.6: Topography for simple datasets. Scale bar in meter

2.2.3. More realistic dataset of Vulcano (coarse)

The Vulcano dataset was re-sampled to a quite big sampling interval of 500m · 500m to assure a better convergence of the *Xia* algorithm than the with the original grid spacing of 100m times 100m used for "true" RTP field generation. The adjustment for the more complicated fields of course wasn't as good as those of the simple datasets. So for all the "true" RTP fields gained by Xia's algorithm the standard-deviation and the absolute maximum error of the adjusted field – not the pole-reduced field – will be shown in the pole-reduced field-plots.

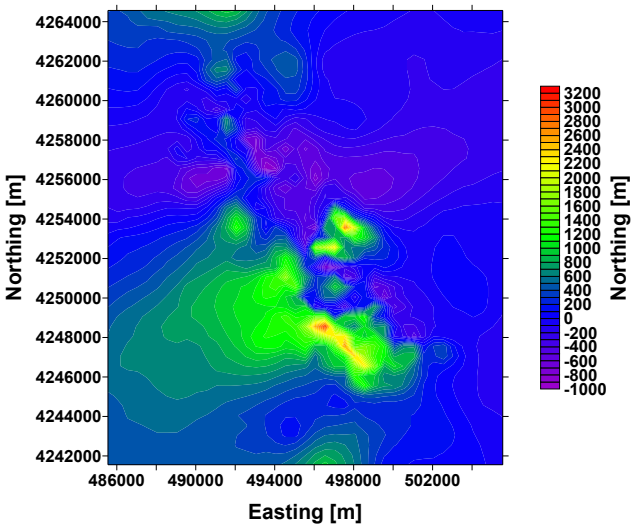


Figure 2.2.3.1: model-field of Vulcano dataset, re-sampled to 500m · 500m. Scale bar in nT.

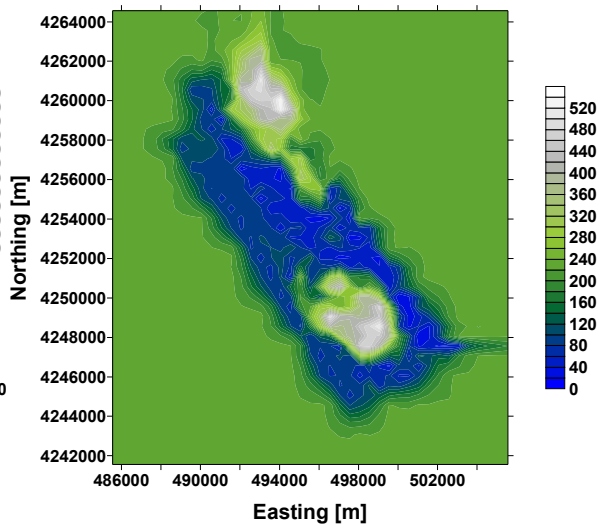


Figure 2.2.3.2: topography field for Vulcano dataset re-sampled to 500m · 500m. Heights in meter.

2.2.4. Vulcano with 100m · 100m spacing (fine)

In this case the Vulcano dataset was taken with its originally sampled spacing of 100m times 100m. It is exactly the same dataset as has been used for the field continuation investigations but with the according topography for it.

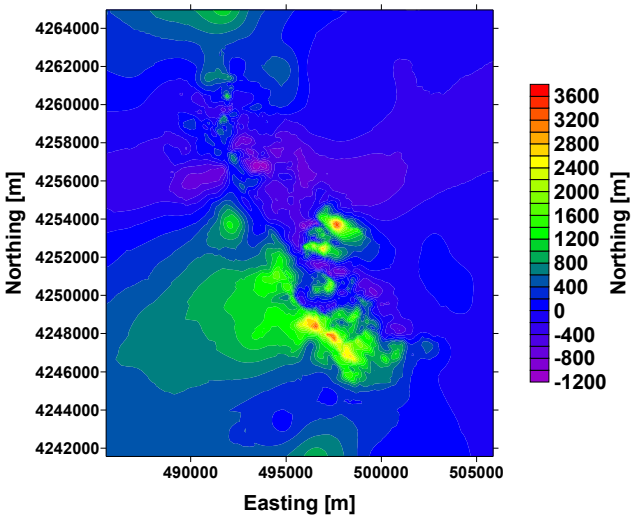


figure 2.2.4.1 model-field Vulcano 100m · 100m grid spacing. Scale bar in nT.

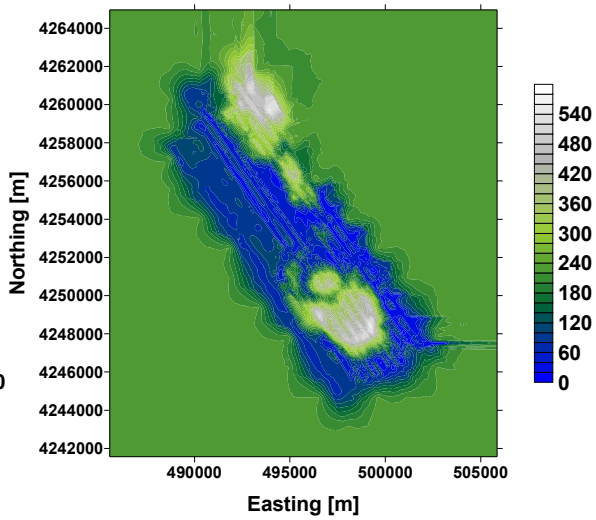


figure 2.2.4.2 topography for Vulcano dataset 100m · 100m grid spacing. Heights in meter.

2.2.5. Real dataset of Socorro

The whole dataset from Socorro included topography-height information. The measured magnetic data were captured around every 20m along a lot of east-west flight-profiles. The datasets were re-sampled at 50m · 50m with 241 rows times 191 columns starting at.:

2068000 North, 498000 East

and ending at:

2080000 North, 507500 East

After grid file generation the topography and the potential-field data both were filtered using a sliding mean value taper 3 times 3 samples big with 10 passes included in Golden Software Inc., Surfer 8, as the measured dataset had so much high-frequency content that Xia's didn't deliver an acceptable adjustment.

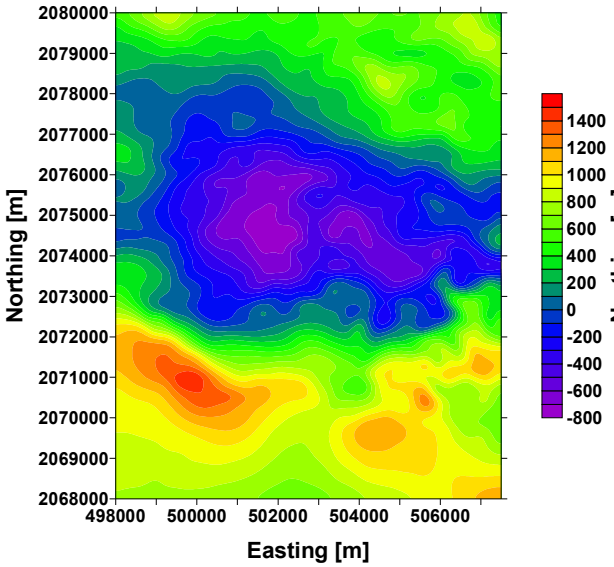


Figure 2.2.5.1: model-field of Socorro, no pole-reduction. Scale bar in nT

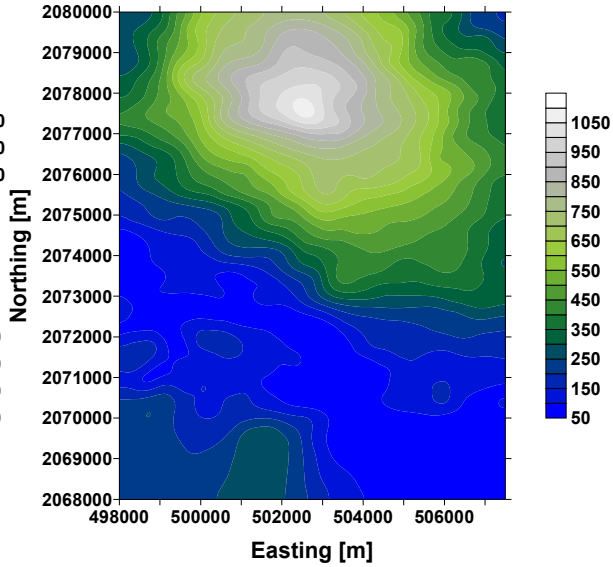


Figure 2.2.5.2: topography of Socorro, heights in meter

3. Compared methods for downward field continuation

The problem of the field continuation downward is an ill posed one. Therefore one aim of this work is to compare some selected methods for downward field continuation. The selected methods are *(COOPER 2004), (FEDI and FLORIO 2002)*, *Roman Pasteka*'s semi automated method based on the *(TIKHONOV 1968)* algorithm as well as *FFT* by *(BRACEWELL 1978)*. These five methods are applied first to a simple dataset of synthetic data (point masses in different depth below the point of observation) and then the results are compared to each other in different depth of continuation. Since real data always contains higher frequency content than simple point masses, the methods needed to be applied to and compared on more realistic data. Therefore a more realistic dataset was used. As this dataset from an area around the island *Vulcano* measured in aero-magnetic surveys where available only at different spaced sampling-points an EQS modelling and field interpolation to a rectangular grid needed to be done to gain model-fields in different plane heights at equidistant spaced locations for comparison with the tested approaches.

Nevertheless the fact that not all approaches appear in the following discussions in chapter 5, they have been investigated too but turned out to be less accurate than those discussed here. The judgement which approaches are better or worse was done through a small program. This program calculated standard deviation and the magnitude-ranges of the errors and printed them in a text file for faster and easier comparability. As there were sometimes strong variations in the resulting fields, a program to split the resulting error fields into smaller parts, was written. So the errors belonging to the edge, intermediate or inner parts were more easy to distinguishable. Regarding to this statistic data the error-files were sorted first for the smallest standard deviation and then separately for the smallest magnitude-range. From both lists the best six were reviewed more precisely and will be discussed here further.

The EQS method used was based on a paper by *(CORDELL 1992)*. He proposed the

following iterative process to get a list of sources at different horizontal and vertical locations. The norm of a given discrete potential field value $f_i(x_i,y_i,z_i)$ minus a potential field caused by a sum of sources at appropriate locations is smaller than an expected error ε.

$$\left| f_i(x_i, y_i, z_i) - \sum_{n=1}^{N} \frac{c_n}{\sqrt{(x_i-\xi_n)^2+(y_i-\eta_n)^2+(z_i-\zeta_n)^2}} \right| < \epsilon \qquad (3.1)$$

The task for Cordell's algorithm is to find a particular ensemble of sources (at the locations (ξ_n,η_n,ζ_n)) whose calculated field fits the data being adjusted and interpolated smoothly between the data points in three dimensions (CORDELL 1992). (1) This is done by removing the mean value of the given potential field of interest. (2) Then by finding the absolute maximum of the residual field $f_i = f_i - \bar{f}_i, \bar{f}_i \ldots mean\,of\ f_i$, the horizontal position for the n-*th* source can be found.

$$|f_{im}| = max|f_i|, f_{im}(x_{im}, y_{im}, z_{im}) = \frac{c_1}{\sqrt{(x_i-\xi_1)^2+(y_i-\eta_1)^2+(z_i-\zeta_1)^2}} \qquad (3.2)$$

The vertical position and the source strength are still unknown at this point of view but can be found by assuming that the source is exactly beneath the maximum.

$$f_{im} = \frac{c_1}{|z_{im}-\zeta_1|} \qquad (3.3)$$

and the depth of the source zeta is proportional to a experimental factor a times the minimum distance to the nearest adjacent sampling location d_{im}.

$$\zeta_1 = a \cdot d_{im}, with\ d_{im} = min\left(\sqrt{(x_{im}-x_n)^2+(y_{im}-y_n)^2+(z_{im}-z_n)^2}\right), n \neq im \qquad (3.4)$$

The proportional factor a in our tests was chosen to be

$$a = 2 \cdot \sqrt{0.5} \qquad (3.5)$$

.

This allows the next closest source location at a point horizontally twice the distance to the next sampling point location. This corresponds to the inflection point of the inverse-distance function (calculation of the inflection point of equation (3.2)). Then the residual is calculated by subtracting the influence source strength c_n from f_i. The residual

$$f_{i+1} = \left| f_i - \sum_{n=1}^{N} \frac{c_n}{\sqrt{(x_i-\xi_n)^2+(y_i-\eta_n)^2+(z_i-\zeta_n)^2}} \right| \qquad (3.6)$$

is again used at the start (1) of the iterative process. The iterative process stops as soon as the norm of the error is smaller than the predefined ε or the the predefined last iteration step is reached.

3.1. Field augmentation

As field transformation is always some kind of filtering the resulting field *t(x)* can be expressed as the convolution of the field *u(x)* with a filter function *f(x)* for continuous data with infinite boundaries.

$$t(x)=u(x)*f(x)=\int_{-\infty}^{\infty} u(x_0)\cdot f(x-x_0)dx_0 \\ =\frac{1}{2\pi}\int_{-\infty}^{\infty} u(\omega)\cdot f(\omega)e^{ikx}dk \qquad (3.1.1)$$

Discrete data on the contrary is only known in a defined area. Therefore the convolution for discrete data becomes finite.

$$t(x_i)=u(x_i)*f(x_i)=\sum_{i=1}^{N} u(x_{0,i})\cdot f(x_i-x_{0,i}) \qquad (3.1.2)$$

This includes that function *u* and filter *f* should be periodic in the interval *i=(1...N)* but for real case survey areas it is not mandatory that the fields observed are periodic. The filter *f* can be chosen in different ways and therefore may be periodic in the interval *i=(1...N)*. So the continues function *u(x)* is sampled to a discrete function $u(x_i)$ but their boundaries are still infinite. As the sum is a finite one, the infinite field $u(x_i)$ gets taped by a rectangular taper in space domain with the boundaries *i=1* and *i=N*. Here the leakage effect has its origin cause the rectangular taper in space domain corresponds to a convolution with sinc – function in the wave-number domain. Additionally there is a leakage effect influence from taping the spectrum of the field in wave-number-domain.

The intention therefore is to reduce the leakage (Gibb's Phenomenon) effect, by field augmentation. The augmentation for FFT, Cooper and ISVD worked as follows.

$$N=A\cdot B \qquad (3.1.3)$$

A...columns, B...rows, N...nodes

A dataset with *N* samples gets augmented by adding additional data points at the boundaries of the original field to a chosen amount N_E defined through *c* and *d.*

$$N_E=(A+c)\cdot(B+d) \qquad (3.1.4)$$

c...augmenting columns, d...augmenting rows, N_E...nodes after field augmentation

The data values between the last value outside of column A and the first of column A are interpolated in a linear way. This is done one column/row after another. For sure this is not the most advanced technique and maybe causes high frequency content in the downward continued fields. Since the Cooper approaches use filters in space domain and frequency domain it was also tested if filtering in space domain before or after field augmentation results in a better approach.

One significant example for the purpose of these tests is the following. A simple test field, continued to depth Z, by one of Cooper's approaches, using 2nd order vertical derivatives includes the Laplace equation, which itself uses 2nd order horizontal derivatives in two directions.

$$\frac{\partial^2 U(x_i)}{\partial x_3^2} = -\frac{\partial^2 U(x_i)}{\partial x_1^2} - \frac{\partial^2 U(x_i)}{\partial x_2^2}, \; U(x_i) \ldots \textit{potential field} \qquad (3.1.5)$$

If the field augmentation is applied before filtering with Laplace equation and field continuation, then the field augmentation produces a area at the north-eastern end of the original field, which is influenced by both field augmentation directions before filtering with Laplace equation takes place (see figure 3.1.1 area marked in pink and original field size marked in red).

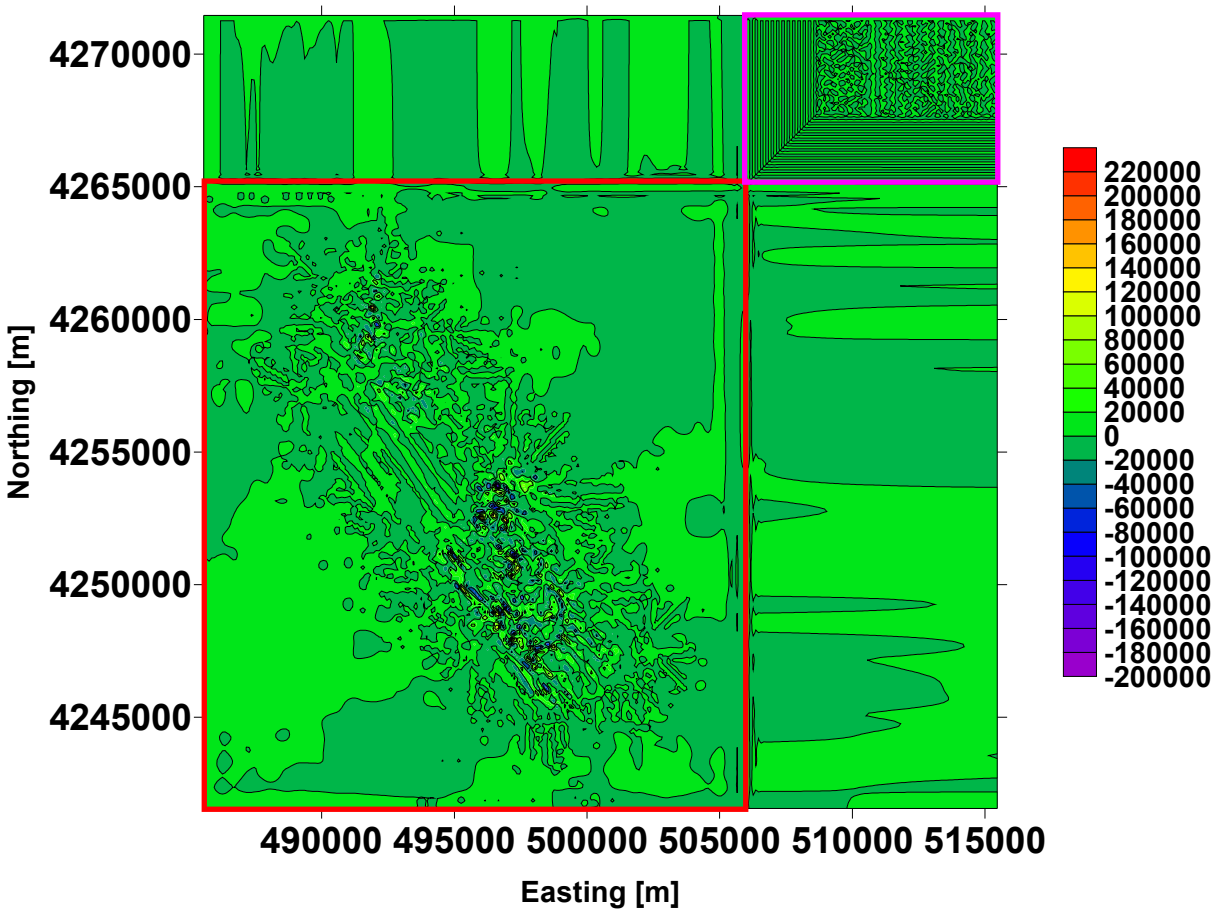


figure 3.1.1 potential field with problematic area (PINK) of two dimensional linearly interpolating field-augmentation for 1st and 2nd order vertical derivative calculation by Laplace's equation. Original field size marked by RED rectangular. Scale bar in nT per square-kilometer.

So the area where the field augmentation produced a maybe strong oscillating augmented part is filtered by the Laplace equation in space domain, as well as the downward field continuation operator in wave-number domain.

$$e^{-|K|\Delta z}$$
$$\Delta z \ldots depth\, to\, continue\, field\, to\, (\, positive\, downward\,) \qquad (3.1.6)$$
$$|K| \ldots magnitude\, of\, wave-number\, vector$$

If the field augmentation takes place after the application of the Laplace equation filter, maybe the influence caused by field augmentation is smaller than in the above mentioned order. This is the aim of this test.

The augmentation used by Tikhonov's / Pasteka's algorithm makes use of a cosine-taper to smooth the boundary values of the original field to zero-level with a defined percental augmentation distance with respect to the original field size. The standard percental rate is defined in the source code of Tikhonov's / Pasteka's algorithm with 15%. In 5.1.2 “Vulcano dataset local part“ there are some tests where the percental rate for field augmentation is changed to 0% as well as 50%. In the same chapter a “regional” field part is assumed as some high-sophisticated field-augmentation technique (See 2.1 “...for downward field continuation“). Additionally another test comparing the linearly interpolating field-augmentation with the regional field, as some the result of some high-sophisticated augmentation technique, is also shown in chapter 5.1.2. “Vulcano dataset local part“, for the best approaches of each separate ranking.

3.2. Cooper

According to *(COOPER 2004)* there are several ways to combine horizontal derivatives in space-domain and integration in wave number-domain so that downward field continuation is not any more completely unstable. *Cooper* had some interesting ideas belonging those combinations and some of them are made to a topic in this thesis.
He recommended to use horizontal derivatives in space-domain in combination with inverse operators in wave-number domain, according to those used in space domain. The horizontal derivatives in space-domain can be assumed as some kind of high-pass filters. After that he proposed to apply the field continuation operator which has a high-pass filter characteristic too when used to downward continue a field to the depth $\mathbf{Z_D}$ below the observation surface. The appropriate (with respect to the derivative operator used in space domain) inverse derivative operator in wave number-domain should be applied at last. *Cooper* also proposed to get rid of the disturbing long wavelength character of the downward continued fields by adding the error of the selected approach in observation level to the downward continued field in depth $\mathbf{Z_D}$.

The combination of these filter pairs and improvements for these approaches should lead to a better downward continued field than FFT. The order of horizontal derivative in space-domain and "vertical integration" in wave number-domain may be exchanged if needed.

This thesis investigated the influences of this change in augmentation-filter-order too. Especially the influence of filtering after and before field augmentation while using Cooper's approaches. Therefore a lot more approaches were tested. In the next chapter the naming convention for these approaches can be found.

3.2.1. Different Cooper approaches

3.2.1.1. Finite difference approaches for a two-dimensional field

The finite difference method used, is based on gathering the value-difference between two adjacent data points and dividing it through the distance between those data points. The result is plotted exactly at the location between the chosen data points. In fact this reduces the amount of data points per direction by one per finite difference and direction calculated. So in a two-dimensional field this reduces the nodes by

$$-a \cdot m - b \cdot n + n \cdot m \qquad (3.2.1.1.1)$$

where

n,m...amount of derivatives in direction x/a and/or y/b

a...amount of columns, b...amount of rows (before derivation)

cause

$$(a-n) \cdot (b-m) = a \cdot b - b \cdot n - a \cdot m + n \cdot m \qquad (3.2.1.1.2)$$

The differential exchanged by the finite difference is given for the first derivative in x direction for a two-dimensional field by

$$f(x+\Delta\frac{x}{2,}y)=\frac{(f(x+\Delta x,y)-f(x,y))}{\Delta x} \qquad (3.2.1.1.3)$$

Δx...distance in direction x between two adjacent points

f(x,y)...two-dimensional field with a (columns) times b (rows) nodes

This means that the origin point is shifted by $\frac{\Delta x}{2}$ inside the original field and the last point is shifted too by this amount inside the original field. So the new derivative field in x-direction is reduced by one column or row, depending on which coordinate system is used.

The second derivative in direction x is therefore

$$f(x+\Delta x,y)=\frac{f(x+2\Delta x,y)-2f(x+\Delta x,y)+f(x,y)}{\Delta x^2} \qquad (3.2.1.1.4)$$

Again it should be mentioned that the origin is again shifted by $\frac{\Delta x}{2}$ according to the first derivative field. So the new origin is now located exactly one data point nearer to the centre of the original field in x-direction. The resulting field is reduced by two columns or rows in relation to the original field.
The vertical and 2nd vertical derivatives used too in this thesis are gained by *Laplace equation*.

$$\Delta U=0=\frac{\partial^2 U}{\partial x^2}+\frac{\partial^2 U}{\partial y^2}+\frac{\partial^2 U}{\partial z^2} \qquad (3.2.1.1.5)$$

So

$$-\frac{\partial^2 U}{\partial x^2}-\frac{\partial^2 U}{\partial y^2}=\frac{\partial^2 U}{\partial z^2} \qquad (3.2.1.1.6)$$

For 2nd vertical derivatives the 2nd horizontal derivatives of the original fields are used by the means of equation 3.2.1.1.6.

The 1st vertical derivatives are gained by assuming that the original field is a gravimetric or total field intensity magnetic field and calculating the according potentials by the means of FFT. Then applying inverse vertical derivative operator in wave-number-domain. After that inverse FFT should be applied and the resulting field is assumed to be the potential of the field of interest in space-domain. equation 3.2.1.1.6 applied to this so gained potential solves the problem for 1st vertical derivative of the original field.

3.2.1.1.1. Cooper approach FD mixed horizontal derivative (fa)

Using finite differences, 1st: mixed horizontal derivative in space domain, 2nd:

field augmentation in space-domain, 3rd: FFT, 4th: continuation to datum of interest 5th: inverse mixed horizontal derivative in wave number-domain and inverse FFT. Further called *FD0fa*.

3.2.1.1.2. Cooper approach FD mixed horizontal derivative (af)

Using finite differences, 1st: field augmentation in space-domain, 2nd: mixed horizontal derivative in space domain, 3rd: FFT, 4th: continuation to datum of interest 5th: inverse mixed horizontal derivative in wave number-domain and inverse FFT. Further called *FD0af*.

3.2.1.1.3. Cooper approach FD GK-X derivative (fa)

Using finite differences, 1st: horizontal derivative Gauss Krüger x-direction in space domain, 2nd: field augmentation in space-domain, 3rd: FFT, 4th: continuation to datum of interest, 5th: inverse horizontal derivative in wave number-domain and inverse FFT. Further called *FD1fa*.

3.2.1.1.4. Cooper approach FD GK-X derivative (af)

Using finite differences, 1st: field augmentation in space-domain, 2nd: horizontal derivative Gauss Krüger x-direction in space domain, 3rd: FFT, 4th: continuation to datum of interest, 5th: inverse horizontal derivative in wave number-domain and inverse FFT. Further called *FD1af*.

3.2.1.1.5. Cooper approach FD GK-Y derivative (fa)

Using finite differences, 1st: horizontal derivative Gauss Krüger y-direction in space domain, 2nd: field augmentation in space-domain, 3rd: FFT, 4th: continuation to datum of interest, 5th: inverse horizontal derivative in wave number-domain and inverse FFT. Further called *FD2fa*.

3.2.1.1.6. Cooper approach FD GK-Y derivative (af)

Using finite differences, 1st: field augmentation in space-domain, 2nd: horizontal derivative Gauss Krüger y-direction in space domain, 3rd: FFT, 4th: continuation to datum of interest, 5th: inverse horizontal derivative in wave number-domain and inverse FFT. Further called *FD2af*.

3.2.1.1.7. Cooper approach FD 2nd vertical derivative (fa)

Using finite differences, 1st: separate 2nd order horizontal derivative in space domain for x and y direction, 2nd: through Laplace equation calculation of 2nd vertical derivative, 3rd: field augmentation in space-domain, 4th: continuation to datum of interest, 5th: inverse 2nd order vertical integration in wave number-domain and inverse FFT. Further called *FD3fa*.

3.2.1.1.8. Cooper approach FD 2nd vertical derivative (af)

Using finite differences, 1st: field augmentation in space-domain, 2nd: separate 2nd order horizontal derivative in space domain for x and y direction, 3rd: through *Laplace equation* calculation of 2nd vertical derivative, 4th: continuation to datum of interest, 5th: inverse 2nd order vertical integration in wave number-domain and inverse FFT. Further called *FD3af*.

3.2.1.1.9. Cooper approach FD 1st vertical derivative (fa)

Using finite differences, 1st: FFT, 2nd: inverse 1st order vertical derivative in

wave number-domain, 3rd: inverse FFT, 4th: separate 2nd order horizontal derivative in space domain for x and y direction, 5th: 2nd order vertical derivative through *Laplace equation*, 6th: field augmentation in space-domain, 7th: FFT, 8th: continuation to datum of interest, 9th: inverse 1st order vertical derivative in wave-number-domain and inverse FFT. Further called *FD4fa*.

3.2.1.1.10. Cooper approach FD 1st vertical derivative (af)

Using finite differences, 1st: field augmentation in space-domain, 2nd: FFT, 3rd: inverse 1st order vertical derivative in wave number-domain, 4th: inverse FFT, 5th: separate 2nd order horizontal derivative in space domain for x and y direction, 6th: 2nd order vertical derivative through Laplace equation, 7th: FFT, 8th: continuation to datum of interest, 9th: inverse 1st order vertical derivative in wave-number-domain and inverse FFT. Further called *FD4af*.

3.2.1.2. Bi-cubic splines approaches for two-dimensional fields

Bi-cubic splines approach is an alternative to finite differences when horizontal derivatives are of interest. For an A · B potential field the horizontal derivatives can be calculated by the means of bi-cubic splines. Originally the continues bi-cubic splines interpolation functions where intended to be used as method for calculation of unevenly spaced data values on an equispaced array but the bi-cubic splines method includes horizontal derivatives calculation too. The major difference to *finite differences* is that bi-cubic splines is based on *boundary and continuity conditions*.

The function

$$U(x,y)=U_{ij}(x,y)=\sum_{k=0}^{3}\sum_{l=0}^{3} c_{ijkl}(x-x_i)^k(y-y_j)^l \qquad (3.2.1.2.1)$$

c_{ijkl}*...represents 16 coefficients needed to form the potential field*

using two cubic polynomials represents the potential field which is of interest. The coefficients c_{ijkl} are the 16 unknowns to be calculated. The boundary conditions are defined as follows.

$$\frac{\partial U}{\partial x}\Big|_{x=x_i,\,y=y_j}=r_{ij} \qquad (3.2.1.2.2) \text{ for } i=1,A \text{ and } j=1,\ldots,B$$

$$\frac{\partial U}{\partial y}\Big|_{x=x_i,\,y=y_j}=s_{ij} \qquad (3.2.1.2.3) \text{for } i=1,\ldots,A \text{ and } j=1,B$$

$$\frac{\partial^2 U}{\partial x\,\partial y}\Big|_{x=x_i,\,y=y_j}=t_{ij} \qquad (3.2.1.2.4) \text{for } i=1,A \text{ and } j=1,B$$

This means that the values for the horizontal derivatives in x-direction and y direction have to be known at the boundaries of the field. (see 3.2.1.2.2 and 3.2.1.2.3)

The mixed horizontal derivative in equation 3.2.1.2.4 means just that these derivatives too have to be known at the boundaries of the field.

The continuity conditions defines that the following horizontal derivatives need to be steady at every point within the field.

$$\frac{\partial U}{\partial x}, \frac{\partial U}{\partial y}, \frac{\partial^2 U}{\partial x \partial y} \qquad \textit{(3.2.1.2.5) have to be steady}$$

Through the boundary and continuity conditions the coefficients c_{ijkl} can be calculated.

3.2.1.2.1. Cooper approach BS mixed horizontal derivative (fa)

Using bi-cubic splines, 1st: mixed horizontal derivative in space domain, 2nd: field augmentation in space-domain, 3rd: FFT, 4th: continuation to datum of interest 5th: inverse mixed horizontal derivative in wave number-domain and inverse FFT. Further called *BS0fa.*

3.2.1.2.2. Cooper approach BS mixed horizontal derivative (af)

Using bi-cubic splines, 1st: field augmentation in space-domain, 2nd: mixed horizontal derivative in space domain, 3rd: FFT, 4th: continuation to datum of interest 5th: inverse mixed horizontal derivative in wave number-domain and inverse FFT. Further called *BS0af.*

3.2.1.2.3. Cooper approach BS GK-X derivative (fa)

Using bi-cubic splines, 1st: horizontal derivative Gauss Krüger x-direction in space domain, 2nd: field augmentation in space-domain, 3rd: FFT, 4th: continuation to datum of interest, 5th: inverse horizontal derivative in wave number-domain and inverse FFT. Further called *BS1fa*.

3.2.1.2.4. Cooper approach BS GK-X derivative (af)

Using bi-cubic splines, 1st: field augmentation in space-domain, 2nd: horizontal derivative Gauss Krüger x-direction in space domain, 3rd: FFT, 4th: continuation to datum of interest, 5th: inverse horizontal derivative in wave number-domain and inverse FFT. Further called *BS1af.*

3.2.1.2.5. Cooper approach BS GK-Y derivative (fa)

Using bi-cubic splines, 1st: horizontal derivative Gauss Krüger y-direction in space domain, 2nd: field augmentation in space-domain, 3rd: FFT, 4th: continuation to datum of interest, 5th: inverse horizontal derivative in wave number-domain and inverse FFT. Further called *BS2fa*.

3.2.1.2.6. Cooper approach BS GK-Y derivative (af)

Using bi-cubic splines, 1st: field augmentation in space-domain, 2nd: horizontal derivative Gauss Krüger y-direction in space domain, 3rd: FFT, 4th: continuation to datum of interest, 5th: inverse horizontal derivative in wave number-domain and inverse FFT. Further called *BS2af.*

3.2.1.2.7. Cooper approach BS 2nd vertical derivative (fa)

Using bi-cubic splines, 1st: separate 2nd order horizontal derivative in space domain for x and y direction, 2nd: through Laplace equation calculation of 2nd vertical derivative, 3rd: field augmentation in space-domain, 4th: continuation to

datum of interest, 5th: inverse 2nd order vertical integration in wave number-domain and inverse FFT. Further called *BS3fa*.

3.2.1.2.8. Cooper approach BS 2nd vertical derivative (af)

Using bi-cubic splines, 1st: field augmentation in space-domain, 2nd: separate 2nd order horizontal derivative in space domain for x and y direction, 3rd: through *Laplace equation* calculation of 2nd vertical derivative, 4th: continuation to datum of interest, 5th: inverse 2nd order vertical integration in wave number-domain and inverse FFT. Further called *BS3af*.

3.2.1.2.9. Cooper approach BS 1st vertical derivative (fa)

Using bi-cubic splines, 1st: FFT, 2nd: inverse 1st order vertical derivative in wave number-domain, 3rd: inverse FFT, 4th: separate 2nd order horizontal derivative in space domain for x and y direction, 5th: 2nd order vertical derivative through *Laplace equation*, 6th: field augmentation in space-domain, 7th: FFT, 8th: continuation to datum of interest, 9th: inverse 1st order vertical derivative in wave-number-domain and inverse FFT. Further called *BS4fa*.

3.2.1.2.10. Cooper approach BS 1st vertical derivative (af)

Using bi-cubic splines, 1st: field augmentation in space-domain, 2nd: FFT, 3rd: inverse 1st order vertical derivative in wave number-domain, 4th: inverse FFT, 5th: separate 2nd order horizontal derivative in space domain for x and y direction, 6th: 2nd order vertical derivative through Laplace equation, 7th: FFT, 8th: continuation to datum of interest, 9th: inverse 1st order vertical derivative in wave-number-domain and inverse FFT. Further called *BS4af*.

All approaches removed the augmented part when all other operations were done.

Coopers additional proposal to improve the particular Cooper approaches mentioned above are starting with an ***imp*** at the beginning of the naming convention. For example improved approach ***FD4af*** would be called

impFD4af

It should be mentioned here that an earlier work from *(BERES 2010)* on a similar topic including this Cooper program in fact had some problems with an older version of this algorithm. As Prof. B. Meurers was able to correct some location settings in the Cooper algorithm now this problem is not any more existent and those tests were repeated with the new corrected version of the algorithm.

3.3. Fedi and Florio / ISVD

Fedi and Florio proposed a stable downward continuation approach based on the combination of vertical integration in wave number-domain as well as calculation of nth order of vertical derivatives through Laplace equation in space-domain and then summing them together in a Taylor series with a predefined amount of terms or until a truncation-parameter is reached.

$$U(i,j;Z_D)=\sum_{k=0}^{N}\frac{Z_D^k}{k!}\frac{\partial^k U(i,j;Z_0)}{\partial z^k} \qquad (3.3.1)$$

Z_D...*depth to continue to,*

$U(i,j;Z_0)$...original field with dimension A·B in observation datum

$U(i,j,Z_D)$...downward continued field to depth Z_D

k...index of Taylor series term,

N...maximum amount of Taylor series terms to be calculated

Since there are derivatives included in the ISVD approaches it should be mentioned that those derivatives were realized like the finite difference approaches for Cooper FD mentioned in 3.2.1.1 “Finite difference approaches for a two-dimensional field“

For 2^{nd}, 4^{th}, 6^{th}, 8^{th},...(even) order vertical derivative only “Laplace equation” and the second order horizontal derivatives in x and y direction were used.

The odd order derivatives just starts at the potential of the measured data, gained through FFT of the measured data, inverse vertical derivative in wave-number-domain and inverse FFT. Again after that Laplace equation is used to get 1^{st}, 3^{rd},5^{th}, 7^{th},...(odd) order vertical derivatives.

The amount of terms, the truncation-parameter as well as depth to field continue to had to be specified. In fact *Fedi and Florio*'s *ISVD* approach is a combination of Cooper approach FD3af and FD4af combined within a Taylor-Series and some additional Taylor series terms, cause ISVD uses the inverse vertical derivation in wave-number-domain like in FD4af to get the potential for the original field of interest. After that is makes use of 2^{nd} order horizontal derivatives in x and y direction separately to get the 1^{st} order vertical derivative through Laplace equation. FD3af just directly calculates the 2^{nd} order vertical derivative, also through Laplace equation and 2^{nd} order horizontal derivatives, but this time the original field is taken for the derivations. In the same manner also 3^{rd}, 4^{th} , etc. are calculated (See schematic down below).

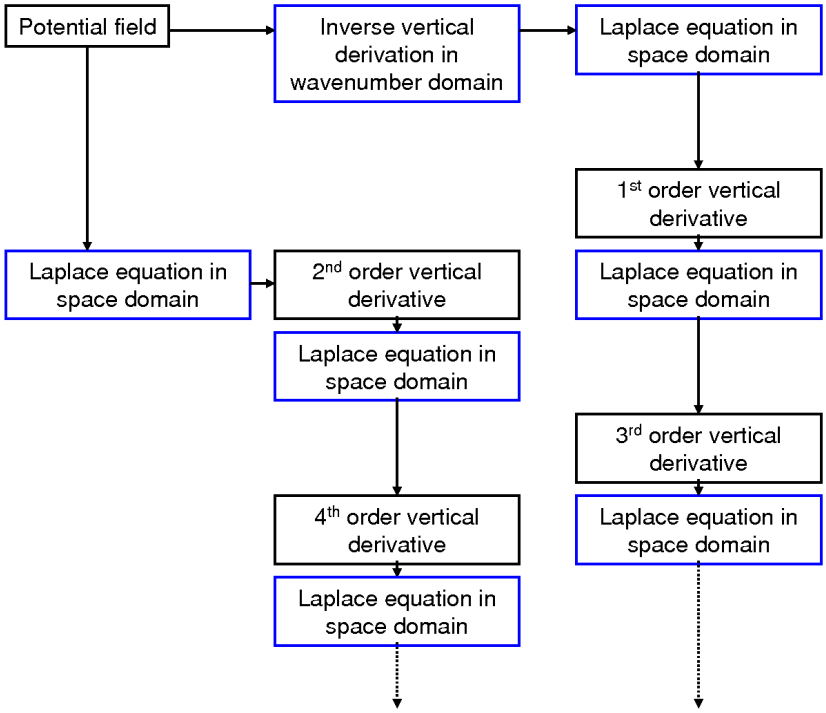


figure 3.3.1 ISVD flowchart for Taylor-series development

Of course linearly interpolating field augmentation was done to reduce "Gibb's phenomenon". All our approach-fields for Cooper, ISVD and FFT were augmented to 300 · 300 data points. Except for the those approach-fields with the regional part. Further naming convention for ***I**ntegrated **S**econd **V**ertical **D**erivative* will be.:

ISVD N X

N...amount of Taylor series terms

X...exponent of truncation-parameter, so

$$truncation-parameter=10^{-X} \qquad (3.3.2)$$

As the amount of terms used is an obvious parameter, only the truncation-parameter is a bit puzzling and may needs some attention. This parameter could be chosen in various ways regarding to *Fedi and Florio*'s Paper concerning this topic.

Our approaches were controlled in the following way. As soon as the truncation parameter was bigger than the the ratio of the variance of the k^{th} Taylor series term, with respect to the variance of the whole Taylor series, the process stopped and put the result in a grid file.

3.4. FFT Fast Fourier Transform

Our algorithm was based on a multivariate complex Fourier transform *(Bracewell 1978)*, using a ***F**ast **F**ourier **T**ransform* algorithm by *R. Singleton 1968*, *Stanford Research Institute*.

In principle the transformation pair for 2D discrete Fourier transformation is:

$$F(u\cdot\Delta k_{1,}v\cdot\Delta k_2)=\sum_{m=0}^{M-1}\sum_{n=0}^{N-1} f(m\cdot\Delta x_{1,}n\cdot\Delta x_2)\cdot e^{-i\left(\frac{2\cdot\pi\cdot u}{M\cdot\Delta x_1}m\cdot\Delta x_1+\frac{2\cdot\pi\cdot v}{N\cdot\Delta x_2}n\cdot\Delta x_2\right)} \qquad (3.4.1)$$

$$f(m\cdot\Delta x_{1,}n\cdot\Delta x_2)= \frac{1}{M\cdot N}\sum_{u=0}^{M-1}\sum_{v=0}^{N-1} f(u\cdot\Delta k_{1,}v\cdot\Delta k_2)\cdot\exp^{i\left(\frac{2\cdot\pi\cdot u}{M\cdot\Delta x_1}m\cdot\Delta x_1+\frac{2\cdot\pi\cdot v}{N\cdot\Delta x_2}n\cdot\Delta x_2\right)} \qquad (3.4.2)$$

$$\begin{aligned} &F(u\cdot\Delta k_{1,}v\cdot\Delta k_2)\ldots spectrum\ of\ input\ function\\ &f(m\cdot\Delta x_{1,}n\cdot\Delta x_2)\ldots input\ \ function\\ &M\ldots rows/columns\\ &N\ldots columns/rows\\ &\Delta x_{1,}\Delta x_2\ldots spacing\ x_1-,\ x_2-direction \end{aligned} \qquad (3.4.3)$$

The field continuation operator

$$\begin{aligned} &e^{-|k_r|\cdot\Delta z}\\ &k_r\ldots radial\ wavenumber\\ &\Delta z\ldots vertical\ \ field\ continuation\ distance(\ positive\ upward\ ) \end{aligned} \qquad (3.4.4)$$

applied to the spectrum of the input function delivers the spectrum of the input function in the depth of interest $Z=Z_o+\Delta z$, *positive downward* and $Z_o\ldots observation\ datum$. Of course also aliasing and leakage effects are field continued and therefore filtered by field continuation operator. Downward continuation amplifies high-frequency content in the data as well as upward continuation amplifies low-frequency content. Therefore downward continuation can be assumed as a high-pass frequency filter as well as upward continuation may be assumed as a low-pass filter process.

The inverse Fourier transformation of this filtered spectrum leads to the field continued field in depth Z.

Since FFT / DFT is applied to discrete data, aliasing and Leakage is always an inherent problem but this topic was already discussed in 3.1. “Field augmentation“.

3.5. Pasteka's approach based on the Tikhonov algorithm

Tikhonov proposed to use a low-pass filter operator depending on a regularization parameter α to smooth a downward continued field *F(k,z,α)* in terms of minimization of the error and simultaneous smooth the approximation.

$$F(k,z,\alpha)=e^{-|k_r|z}\frac{1}{1+\alpha k^2 e^{-|k_r|z}} \qquad (3.5.1)$$

The algorithm works as follows:

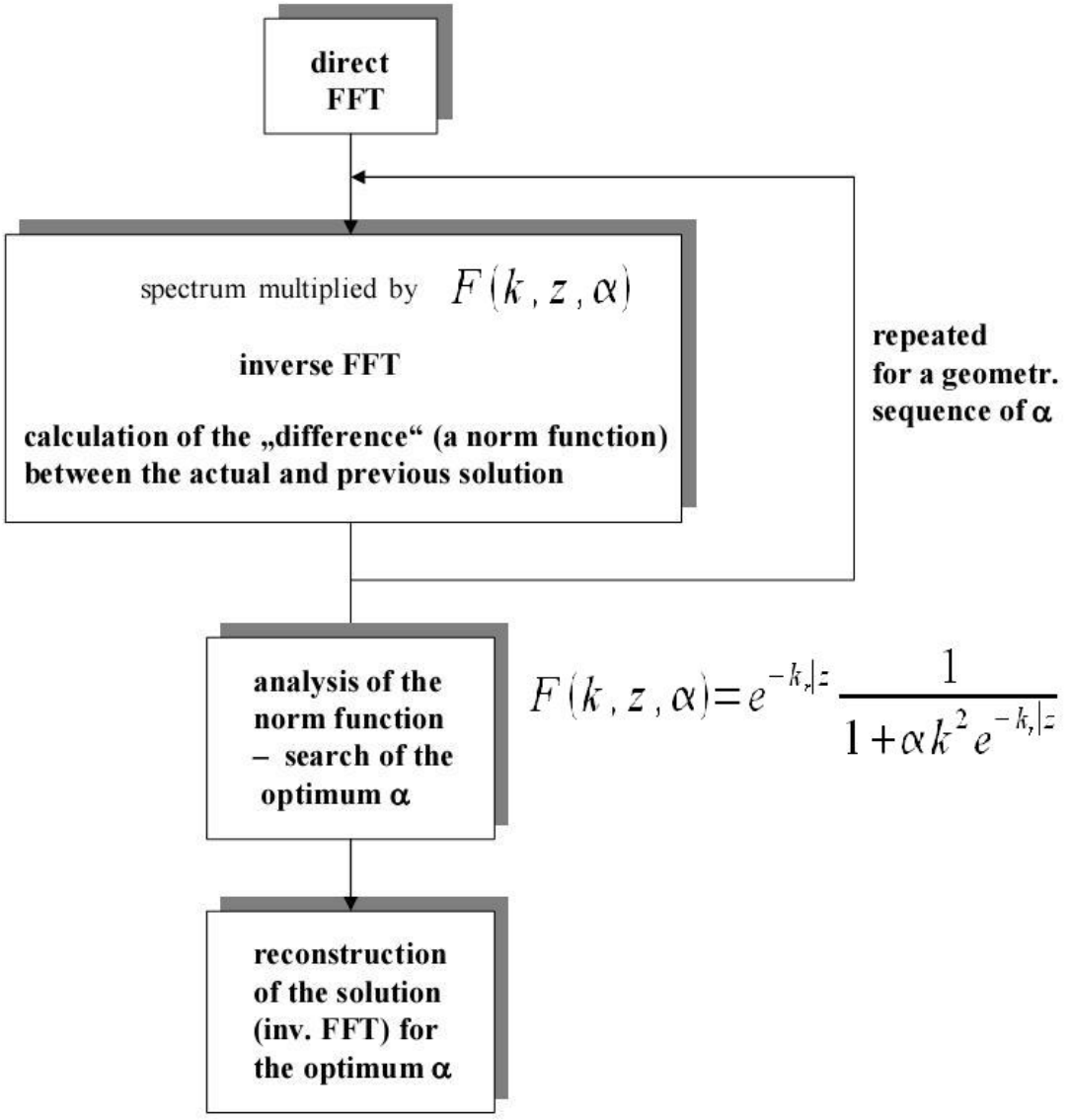


figure 3.5.1 Tikhonov algorithm (with special thanks to Dr. Roman Pasteka, Comenius University of Bratislava)

The different elements of the geometrical sequence for α leads to different absolute errors. Each of the absolute error functions somewhere has its maximum. The resulting function of these maxima is called the C-Norm-function.

$$CNorm(\alpha) = max\left|V(\alpha_k) - V(\alpha_{k+1})\right| \qquad (3.5.2)$$

$V(\alpha_i)$...sequence of solutions depending on the regularization parameter α

The C-Norm-function then is plotted against the regularization parameter α. For the different C-Norm-function values different approximations will result. Each of them is oscillating more or less. Through choice of the global minimum of the C-Norm-function the result with the least squares error and the smoothest one is taken, that still approximates the field in the depth of interest in the best possible way with this algorithm.

Precautions should be made when the automatic determination of the global minimum leads to a minimum which corresponds to the strongly oscillating rightmost edge of the C-Norm function (can be viewed when Tikhonov's / Pasteka's algorithm is applied), which happens often when the range for the L-Norm function was chosen too big (standard values of 10^{-15} to 10^{15} usually works fine, regarding to personal communication with Dr. Roman Pasteka). This leads to over-regularization, so smoothing the output field to strong and should therefore be avoided by manual re-check of the automatically determined global minimum.

4. Reduction to pole on arbitrary surfaces

4.1. Considerations on the measured data in magnetic surveys

Separately reduction to magnetic pole on a arbitrary surface (Dr. Andreas *Ahl* - personal comm. from *GBA - Geologische Bundesanstalt, Vienna)* was tested. As reduction to pole works theoretically on plane surfaces only, the aim for this part was to gather informations about the errors made by neglecting the influence of different observation datums. As Austria is a very mountainous country this would maybe reduce the time consuming field continuation processes needed to get a dataset for classical reduction to pole on a plane surface. Even if the results are bad this would at least deliver informations about the errors made in such cases.

It should be kept in mind that measured data from first overview field surveys often are just magnitude values without direction information measured by a total-field magnetometer *(BLAKELY 1995).*

$$\Delta T = |\vec{T}| - |\vec{F}| \qquad (4.1.1)$$

ΔT...magnitude of total field anomaly, $|T|$...measured total field, $|F|$...regional field (for example from IGRF model)

ΔT forms the basis for the further discussion. Theoretically, exactly calculated *ΔT* is never a harmonic function since the magnitude of a vector never fulfils Laplace equation but with appropriate conditions and approximations *ΔT* can be assumed a harmonic. It is of high importance to know what are those conditions, as reduction to pole theoretically work only in source-free-space. For all our examples regarding this

topic always a source-free-space was assumed.

In fact ΔT is approximately equal to one component of the field produced by the anomalous magnetic source and therefore harmonic if $|F| \gg |\vec{\Delta} F|$ and the direction of the regional field is approximately constant over the dimensions of the of the survey.

Based on *(BLAKELY 1995)*

$$\vec{T} = \vec{F} + \vec{\Delta} F \qquad (4.1.2)$$

The total field $\vec{T}$ consist of a regional field $\vec{F}$ plus a anomaly $\vec{\Delta} F$.

Therefore ΔT is

$$\Delta T = |\vec{F} + \vec{\Delta} F| - |\vec{F}| \neq |\vec{\Delta} F| \qquad (4.1.3)$$

as ΔF is the vector describing the different amount and direction of the anomaly to the regional field and ΔT is just the difference between the arbitrary values of $\vec{T}$ and $\vec{F}$. With the assumption made that the anomaly is small compared to the regional field the following approximation has to be made.

$$\Delta T = |\vec{F} + \vec{\Delta} F| - |\vec{F}| \approx \sqrt{\vec{F} \cdot \vec{F} + 2\vec{F} \cdot \vec{\Delta} F} - |\vec{F}| \qquad (4.1.4)$$

With $\vec{\Delta} F$ << $\vec{F}$ (anomaly small compared to regional field)

and

$$\sqrt{\vec{F} \cdot \vec{F} + 2\vec{F} \cdot \vec{\Delta} F} - |\vec{F}| \approx \sqrt{\vec{F} \cdot \vec{F}} + \frac{2}{2\sqrt{\vec{F} \cdot \vec{F}}} (\vec{F} \cdot \vec{\Delta} F) - |\vec{F}| \qquad (4.1.5)$$

with the assumption that the projection of the total field anomaly $\vec{\Delta} F$ onto the regional field direction $\hat{F}$ (unit vector) is small compared to $\vec{F} \cdot \vec{F}$ and can therefore be developed in a Taylor series for the last square-root term with respect to $\vec{\Delta} F$, stopping after the linear term.

Then the magnitude of the total field anomaly may be assumed as the projection of the total field anomaly $\vec{\Delta} F$ onto the regional field direction $\hat{F}$ (unit vector).

$$\Delta T \approx \hat{F} \cdot \vec{\Delta} F \qquad (4.1.6)$$

As for a given relatively small (compared to earths scales) survey area the direction of the regional field may be assumed as constant, regarding to time and space, Laplace equation is valid for a single component of the anomaly $\vec{\Delta} F$ times a constant factor

$\hat{F}$. Thus the arbitrary value ΔT can be assumed as one component of the magnetic anomaly projected onto regional field direction. For one component of $\vec{\Delta F}$ Laplace equation is valid and thus Laplace equation is valid for ΔT.

$$\nabla^2(\Delta T)=\nabla^2(\hat{F}\cdot\vec{\Delta F})=\hat{F}\cdot\nabla^2(\vec{\Delta F}) \qquad (4.1.7)$$

So when a total field anomaly is named here, one may remember that the arbitrary value ΔT was assumed to be measured but only the projection of $\vec{\Delta F}$, the vector of the anomaly, onto the regional field's $\hat{F}$ unit vector was really calculated with reduction to pole process.

4.2. Reduction to pole on plane surfaces

The reduction to pole process takes place in the wave-number-domain. For a given potential field in space-domain $U(x,y)$ an equivalent function in wave-number-domain $U(k_x,k_y;x_3=Z_0)$ can be calculated through FFT. Z_0 may be the observation datum, assumed to be constant over the whole survey area for our needs. In normal cases Z_0 of course can vary with topography or flight height, etc. So normally a field continuation process needs to be done before the reduction to pole process to a datum above the shallowest source. Only when all data values are continued to a constant height Z_D at a equidistant spaced grid the reduction to pole process may be applied onto real case data. As said before, for our case this is exactly the point to be neglected and the question to be investigated is, how big the errors are made by this negligence.

As theoretically

$$U(x,y;x_3=Z_D)=\frac{1}{4\pi^2}\cdot \iint U(k_x,k_y;x_3=Z_0)\cdot\exp^{-k_r\Delta Z}\cdot\exp^{i(k_x x+k_y y)}dk_x\,dk_y \qquad (4.2.1)$$

$\Delta Z = Z_D - Z_0$ is

with δT the given total field anomaly (formerly called ΔT).

$$\delta T=-s_i\cdot\frac{\partial V}{\partial x_i},\ V(x,y)=n_i\cdot\frac{\partial}{\partial x_i}\overbrace{\left(-\iiint\frac{|m_i|}{4\pi r}dv\right)}^{U},\ m_i=const \qquad (4.2.2)$$

As well as

$$\begin{matrix}\frac{\partial U}{\partial x_1}\\ \frac{\partial U}{\partial x_2}\\ \frac{\partial U}{\partial x_3}\end{matrix} = \frac{1}{4\pi^2}\iint \begin{matrix}ik_1\\ ik_2\\ -k_r\end{matrix} U(k_x, k_y; x_3 = Z_0)\cdot\exp^{-k_r \Delta Z}\cdot\exp^{i(k_x x + k_y y)} dk_x dk_y \qquad (4.2.3)$$

is and therefore *V(x,y)*

$$V(x, y) = \frac{1}{4\pi^2}\cdot \iint (ik_1 n_1 + ik_2 n_2 - k_r n_3) \cdot U(k_x, k_y; x_3 = Z_0)\cdot\exp^{-k_r \Delta Z}\cdot\exp^{i(k_x x + k_y y)} dk_x dk_y \qquad (4.2.4)$$

Referring to the first part of equation 4.2.2 solves the problem for the total field anomaly δT.

$$\delta T(x, y) = \frac{1}{4\pi^2}\cdot \iint -(ik_1 s_1 + ik_2 s_2 - k_r s_3)(ik_1 n_1 + ik_2 n_2 - k_r n_3) \cdot U(k_x, k_y; x_3 = Z_0)\cdot\exp^{-k_r \Delta Z}\cdot\exp^{i(k_x x + k_y y)} dk_x dk_y \qquad (4.2.5)$$

The reduction to pole operator

$$R_p = \frac{{k_r}^2}{(ik_1 s_1 + ik_2 s_2 - k_r s_3)(ik_1 n_1 + ik_2 n_2 - k_r n_3)} \qquad (4.2.6)$$

$n_i \ldots unit\ vector\ of\ |m_i|$

$s_i \ldots unit\ vector\ of\ regional\ field$

is applied to $\delta T(k_1, k_2; Z_D)$

$$\delta T(k_{1,} k_2; Z_D) = -(ik_1 s_1 + ik_2 s_2 - k_r s_3)(ik_1 n_1 + ik_2 n_2 - k_r n_3) \cdot U(k_x, k_y; x_3 = Z_0)\cdot\exp^{-k_r \Delta Z} \qquad (4.2.7)$$

in wave-number-domain

$$\delta T_p(k_{1,} k_2; Z_D) = R_p \cdot \delta T(k_{1,} k_2; Z_D) \qquad (4.2.8)$$

to get the transformed field with

$$s_i = n_i = (0,0,1) \qquad (4.2.9)$$

.

This shifts the anomalies literally exactly over their "true" horizontal location.

4.3. Adjustment of magnetic fields with Xia on arbitrary surfaces

According to *(XIA 1993)* the gravitational effect of a horizontal density distribution below a observation surface can be represented in wave-number-domain by equation (4.3.1).

$$g(K) = \bar{g}(K)\, e^{-|K| \cdot Z(\vec{r})}$$
$$g(K) \ldots \textit{gravity anomaly on observation surface } S \qquad (4.3.1)$$
$$\bar{g}(K) \ldots \textit{gravity anomaly on equivalent source layer } E$$

$\bar{g}(K) = 2\pi G \sigma(K)$ contains the gravitational constant G and the density distribution $\sigma(K)$ on the plane equivalent source layer E. The exponential term is the wave-field extrapolation operator containing the wavenumber $K=(k_x,k_y)$ and $Z(r)$ the vertical distance between the observation surface S and the equivalent source layer E (see figure 4.3.1). $\vec{r}$ =(x,y) with x and y describing the x-y-plane.

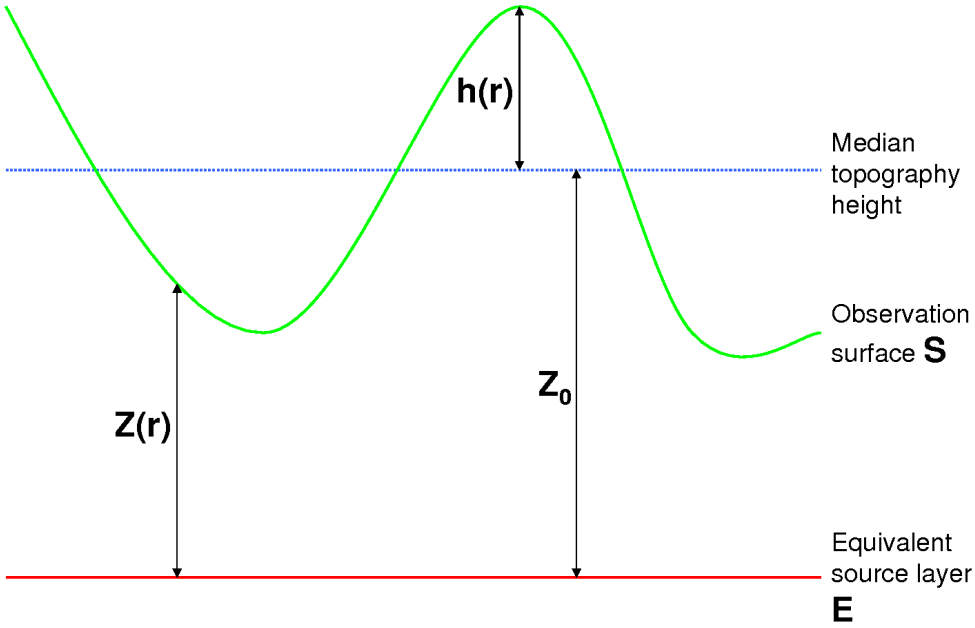


figure 4.3.1 Geometry of the plane of the equivalent source E (red) and the observation surface S (green) as well as the median topography height (blue)

Z_0 is the median distance between the equivalent source layer E and the observation surface S and $h(\vec{r})$ is the topographic change relative to Z_0. Therefore

$$Z(\vec{r}) = Z_0 + h(\vec{r}) \qquad (4.3.2)$$

and equation (4.3.1) can be written as

$$g(K) = \bar{g}(K) e^{-|K| \cdot Z_0} \cdot e^{-|K| \cdot h(\vec{r})} \qquad (4.3.3)$$

Through Taylor series development of the exponential term containing the topographic change $h(\vec{r})$

$$e^{-|K| \cdot h(\vec{r})} = \sum_{n=0}^{\infty} \frac{[-|K| \cdot h(\vec{r})]^n}{n!} \qquad (4.3.4)$$

and applying inverse Fourier transform to both sides of equation (4.3.3), we obtain

$$g(\vec{r}) = 2\pi G \sum_{n=0}^{\infty} \frac{h^n(\vec{r})}{n!} \cdot F^{-1}[\sigma(K) \cdot e^{-|K| Z_0} \cdot |-K|^n] \qquad (4.3.5)$$

F^{-1} is the inverse Fourier transformation operator. Equation (4.3.5) is later used in an gravitational iterative process and was originally derived by *(PARKER 1973)* and others separately. This series converges if Z_0 is bigger than $H = max|h(\vec{r})|$ and therefore the equivalent source layer E is below the observation surface S (*(WHITTAKER AND WATSON 1962)*). Based on Poisson's relation (e.g., *(DOBRIN 1976))* an equation for the magnetic anomaly can be written *(PARKER 1973)*.

$$T(K) = 2\pi \frac{(\tilde{k} \cdot \vec{f}) \cdot (\tilde{k} \cdot \vec{m})}{|K|^2} \cdot J(K) \cdot e^{-|K| \cdot Z_0} \sum_{n=0}^{\infty} \frac{[-|K| \cdot h(\vec{r})]^n}{n!} \qquad (4.3.6)$$

By applying the inverse Fourier transformation operator to both sides of the equation again the formula for the iterative process as proposed by *(XIA 1993)* can be found.

$$T(\vec{r}) = 2\pi \sum_{n=0}^{\infty} \frac{h^n(\vec{r})}{n!} F^{-1}\left[\frac{(\tilde{k} \cdot \vec{f}) \cdot (\tilde{k} \cdot \vec{m})}{|K|^2} \cdot J(K) \cdot e^{-|K| \cdot Z_0} \cdot |-K|^n \right] \qquad (4.3.7)$$

Where $\tilde{k} = (ik_x, ik_y, \sqrt{k_x^2 + k_y^2})$ and $\vec{f}, \vec{m}$ are the unit vectors of earth's main field and the magnetization respectively.

For reduction to pole process by Xia and for simplification the direction of the main field and magnetization have been assumed as equal and therefore the unit vector of them are the same too. The Poisson's theorem (DOBRIN 1976) applied to equation (4.3.5) alters the adjustment. Therefore the operator *A* is discussed here a bit more in particular.

$$A=\frac{(\tilde{k}\cdot\vec{f})\cdot(\tilde{k}\cdot\vec{m})}{|K|^2} \qquad (4.3.8)$$

$$A=\frac{\left(i\,k_x e_x+i\,k_y e_y+e_z\sqrt{k_x^2+k_y^2}\right)^2}{k_x^2+k_y^2} \qquad (4.3.9)$$
$$\vec{f}=\vec{m}=(e_x,e_y,e_z)$$

e_x, e_y and e_z are the vector components of the unit vector of the main field and the magnetization respectively. Where $k_x=\frac{2\pi n}{N\Delta x}, k_y=\frac{2\pi m}{M\Delta y}$ with the spacial Nyquist-frequency $k_{Ny}=\frac{\pi}{\Delta x}$ reached when n=N/2 and m=M/2 with N·M the amount of nodes and delta x and delta y the grid spacing in x and y spacing respectively. By investigating the limits of equation (4.3.9) as $|K|$ approaches zero, the operator turns out to be only defined for $|K|>0$. Nevertheless the operator split into magnitude and phase information shows a saddle point as $|K|$ approaches zero for the magnitude $|A|$ and a more complex structure for the phase *arg(A)*.

$$|A|=e_z^2-\frac{(e_x k_x+e_y k_y)^2}{k_x^2+k_y^2}\quad,$$
$$arg(A)=\arctan\left(\frac{2\,e_z(e_x k_x+e_y k_y)\cdot\sqrt{k_x^2+k_y^2}}{e_z^2(k_x^2+k_y^2)-(e_x k_x+e_y k_y)^2}\right) \qquad (4.3.10)$$

Since there is no real limit for the operator A derivable as $|K|$ approaches zero at the magnitude, phase as well as real and imaginary part of A may be shown here to define the problem more clearly.

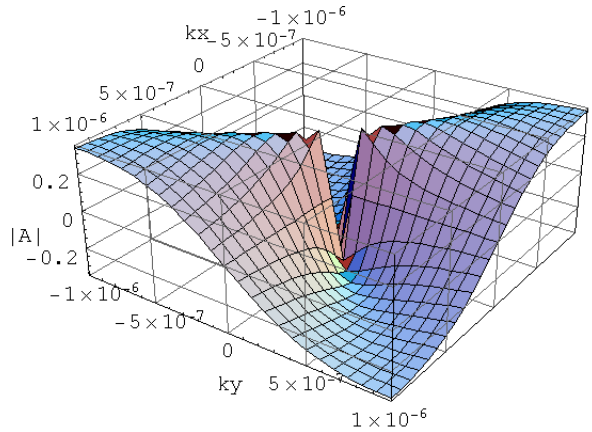


figure 4.3.2 Magnitude of Poisson's theorem operator

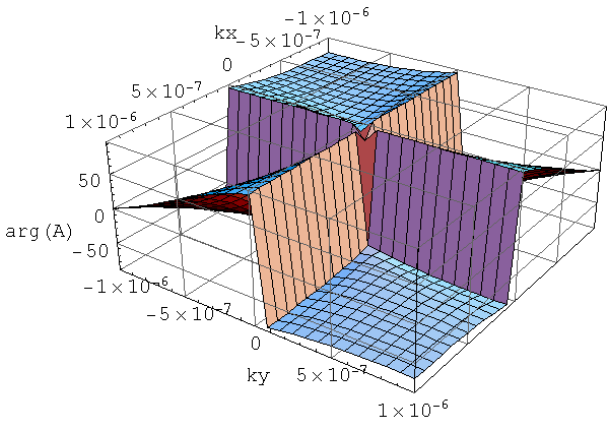


figure 4.3.3 Phase of Poisson's theorem operator

The magnitude of Poisson's theorem operator seems to quite stable but the phase information turns out have a phase reversal when cross from $k_x < 0$, $k_y > 0$ to $k_x > 0$, $k_y < 0$ diagonally over the origin point. Additionally the real and imaginary parts contain

clear jump discontinuities.

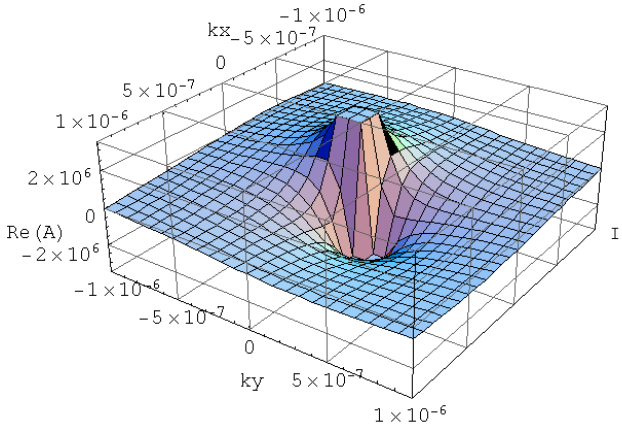


figure 4.3.4 real part of A, a strong jump discontinuity as |K| approaches zero

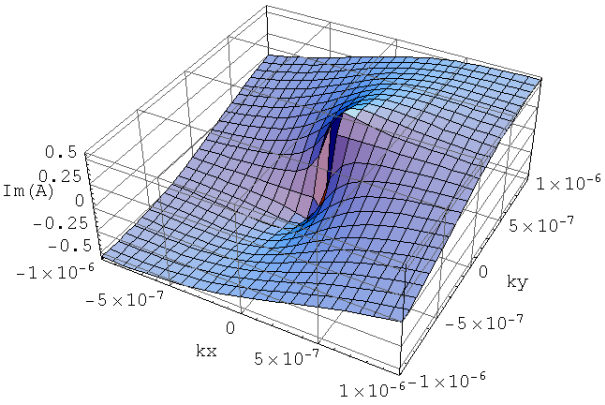


figure 4.3.5 imaginary part of A, another weaker jump discontinuity as |K| approaches zero

So unfortunately there is no real limit for the operator A but as $|K|$ approaches zero only corresponds to the average of a potential-field being adjusted and those potential-fields are only anomalies in our case, this is just an offset in the data adjusted by Xia and therefore for the adjustment of anomaly data quite uninteresting. For computational purposes in our case the value of $T(\vec{r})$ as $|K|$ approaches zero was chosen to be zero.

5. Results:

Our different approaches led to a multiplicity of results which needed to be tested in an objective manner and so these approaches were tested on different statistical information. To get the most objective results first of all the error-fields were separated in an outer, intermediate and inner area in order reduce edge effect influences in the statistical informations. Then the standard deviation of the errors of the different parts (outer, intermediate, inner) of the approaches and the error ranges (magnitudes) were compared separately. The best six results for every separate region were weighted corresponding to the importance of the error analysis of the investigated region and were then taken and combined in one best of ranking for one complete dataset. So outer area most important, means if an approach is not in the ranking of the best six for this region then this is weighted with a big factor. Is an approach not listed in the best six ranking of the innermost part the the factor for this is small. A medium factor corresponds in the same way for the intermediate area.

As the different approaches did not deal with the problem of different mean values in the data a small program was written to remove the mean values of the model-field data as well as those of the fields of the different approaches and plot logarithmic relative error-fields for them.

$$lre = \log_{10}\left(\frac{error(i,j)+\varepsilon}{max|V(i,j)|}\right) \qquad (5.1)$$

lre...logarithmic relative offset free error to absolute maximum of offset free model-field

i...column index, j...row index, V(i,j)... offset free model-field,

error(i,j)...zero-mean error of approach XY

ε...small nominal positive value to prevent the numerical process from instability as error(i,j) approaches 0, chosen in this thesis to be 10^{-15}

Needles to say that there is no information about the exact amount of error at a given station in this data but the relative maximum can be seen and whether data result is a stable solution or already remarkably oscillating (caused by the logarithmic scaling).

Hereafter only the best thirteen for each depth were chosen. Since the ISVD approaches reduced the field size with every two Taylor series terms by 2 nodes in easting as well as northing direction, first the best 6 of ISVD for each depth were distinguished. These 6 best ISVD approaches were then compared to the best Cooper and FFT as well as Tikhonov / Pasteka approaches. So there are always 13 approaches to be compared but sometimes there there are the results of the FFT within the list and sometimes not, depending on the ranking of FFT results.

For the Vulcano local + regional part – dataset, there are some additional approaches. They concern with the alteration of standard settings for the field-augmentation distance of Tikhonov / Pasteka as well as exchange of the regional part of the field with the linearly interpolating field-augmentation for the best approaches in the ranking. So for those tests there are more results displayed.

5.1. Results, downward field continuation

5.1.1. Simple dataset

5.1.1.1. Model-field and field of different approaches in -50m

All Scale bars are in mGal.

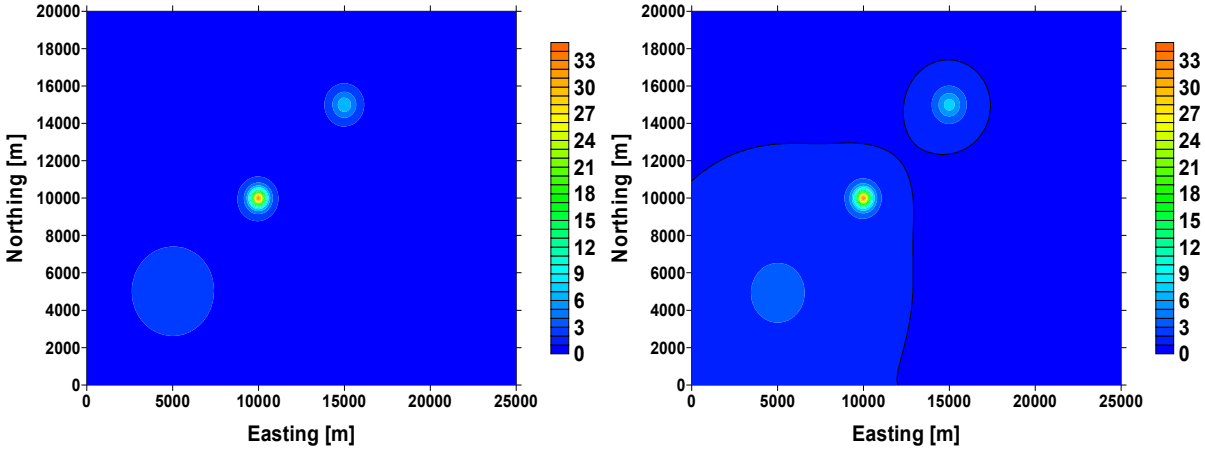


figure 5.1.1.1.1: FFT

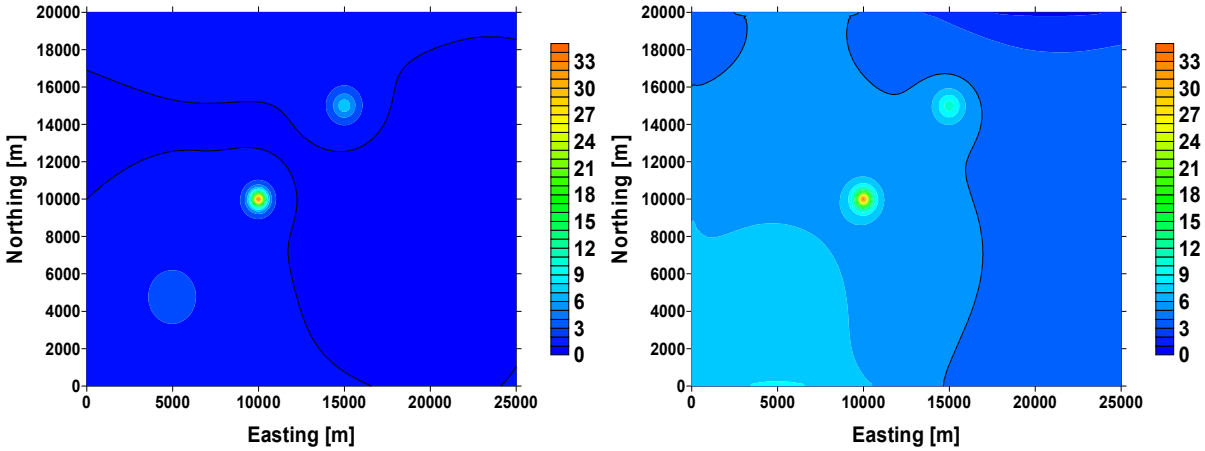


figure 5.1.1.1.2: Cooper approach BS4af

figure 5.1.1.1.3: Cooper approach BS3fa

figure 5.1.1.1.4: Cooper approach BS4fa

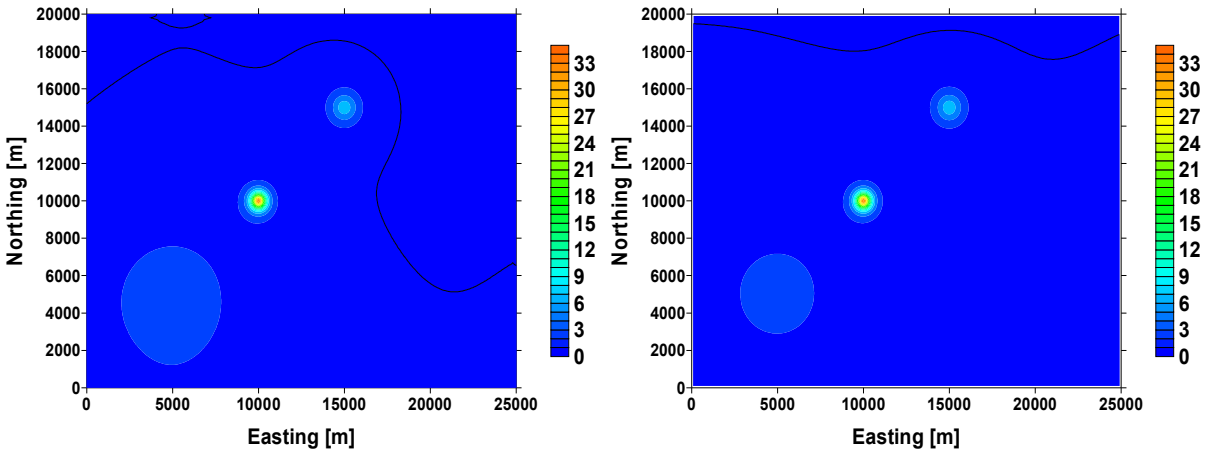


figure 5.1.1.1.5: Cooper approach BS3af

figure 5.1.1.1.6: Cooper approach FD3fa

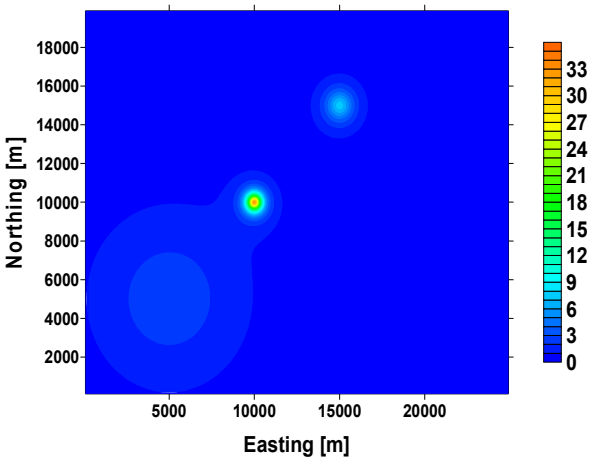


figure 5.1.1.1.7: ISVD 6 30

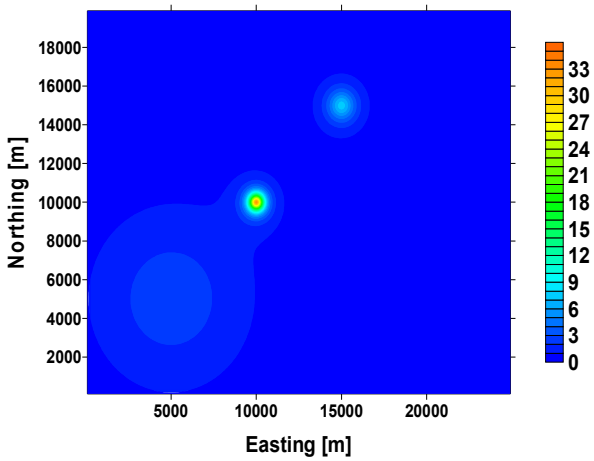


figure 5.1.1.1.8: ISVD 20 6

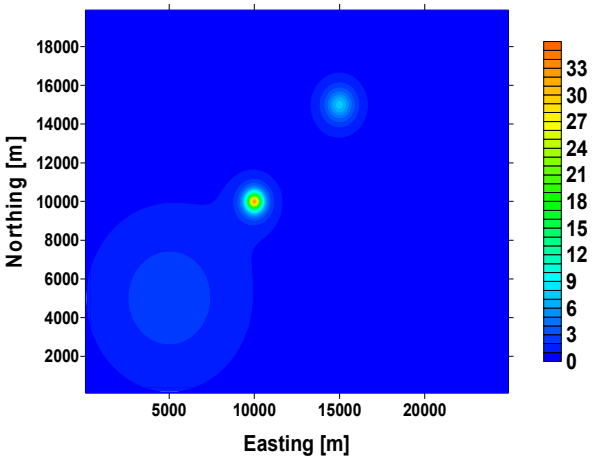


figure 5.1.1.1.9: ISVD 8 30

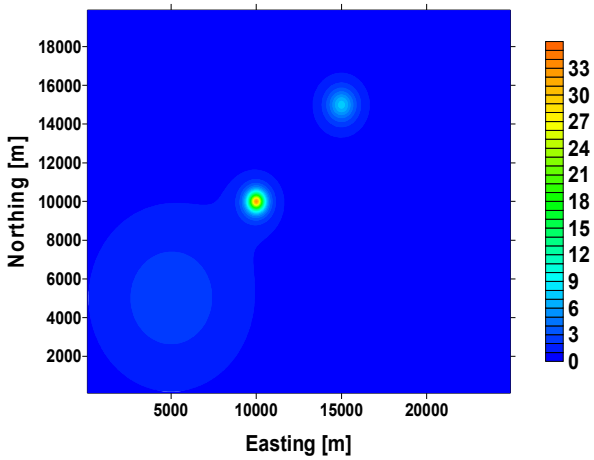


figure 5.1.1.1.10: ISVD 4 30

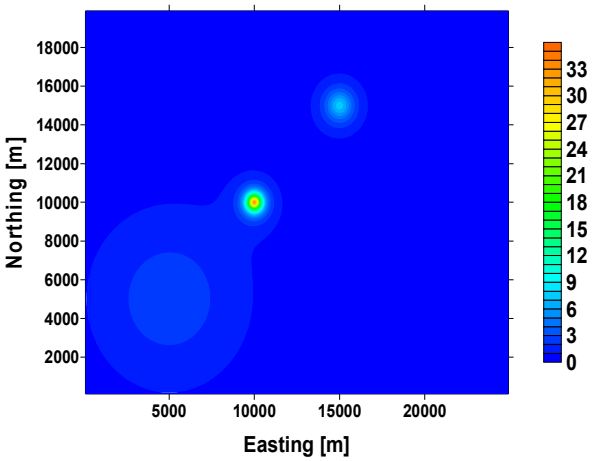


figure 5.1.1.1.11: ISVD 7 30

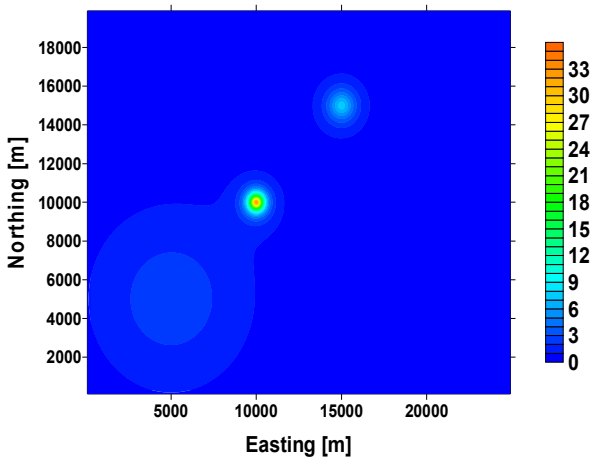


figure 5.1.1.1.12: ISVD 5 30

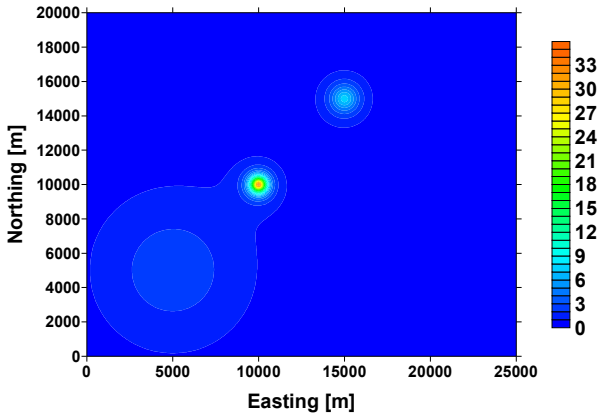


figure 5.1.1.1.13 Tikhonov / Pasteka

It can be seen in figure 5.1.1.1.1 that the field is stable for FFT within the sampling interval interval and the magnitude is equal to that of the model-field in figure 2.1.1.2. Nevertheless there is a slight difference in the long wavelength character of the field. This will be more obvious when looking at the relative failure-energy-field subsequently.

The fields gained by ISVD approach seem to be nearly all the same and in fact they are, sometimes caused by the use of Taylor series terms as well as the truncation-parameter. Furthermore the ISVD approaches will be just called by their amount of Taylor series terms or their break off parameter depending to on which parameter is more important. There seems to be some major similarities to FFT results at least in 50m depth. As the paper of *Fedi and Florio* noticed the best results are for around seven Taylor series terms or comparable truncation-parameter, at least for 50m. For 300m depth it isn't.

Tikhonov's approach in figure 5.1.1.1.13 looks quite similar to the ISVD approaches and the model-field. From this point of view there are no oscillations visible.

5.1.1.2. Errors of different approaches in -50m

All scale bars in mGal.

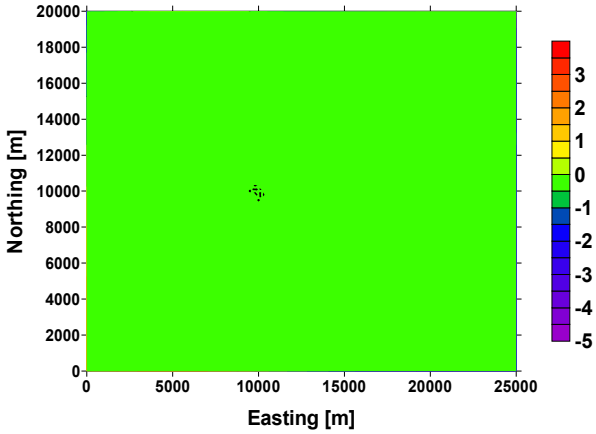


figure 5.1.1.2.1: error FFT

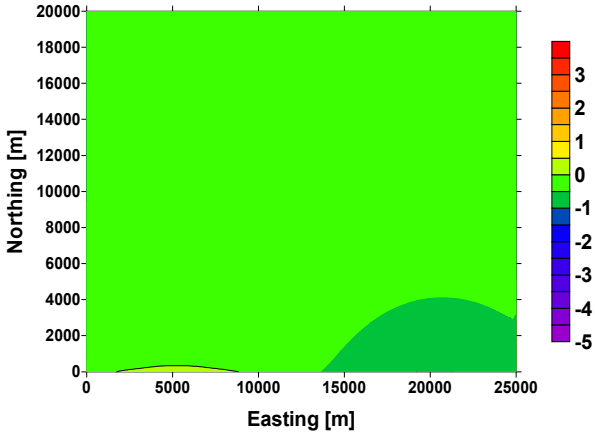


figure 5.1.1.2.2: error Cooper approach BS4af

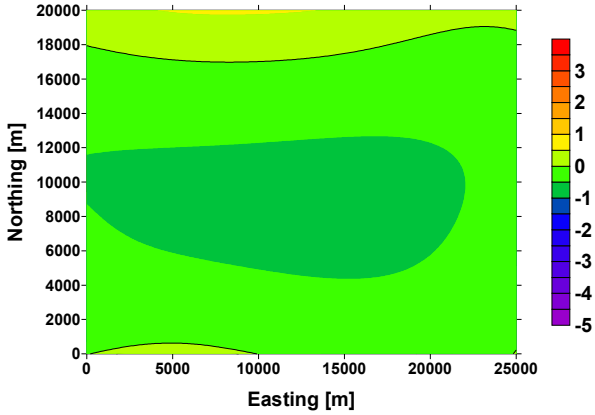


figure 5.1.1.2.3 error Cooper approach BS3fa

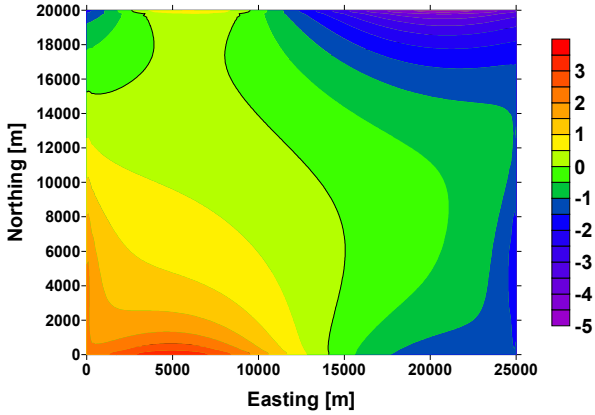


figure 5.1.1.2.4: error Cooper approach BS4fa

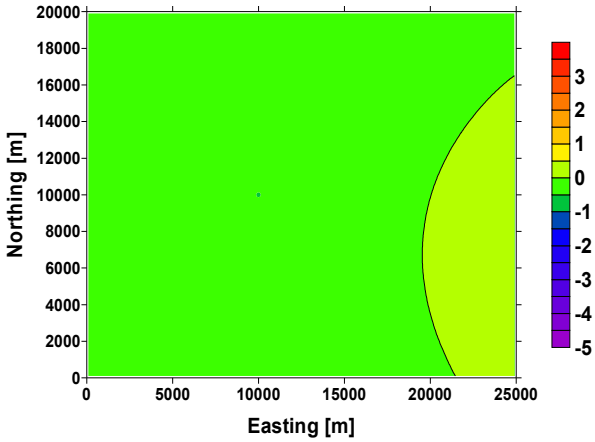


figure 5.1.1.2.5: error Cooper approach FD3fa

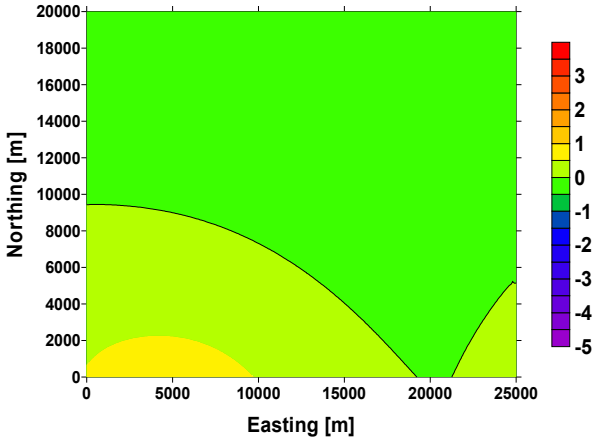


figure 5.1.1.2.6 error Cooper approach BS3af

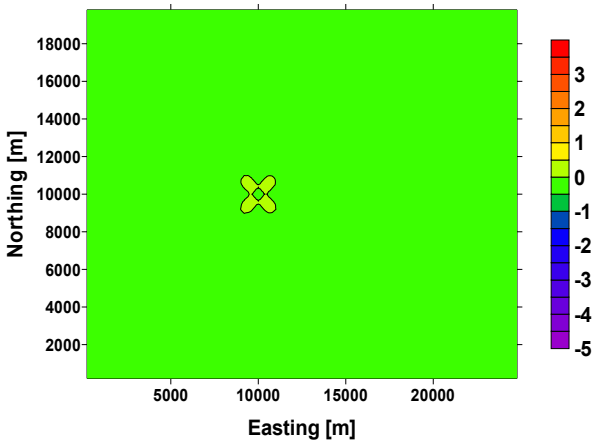


figure 5.1.1.2.7: error ISVD 8 30

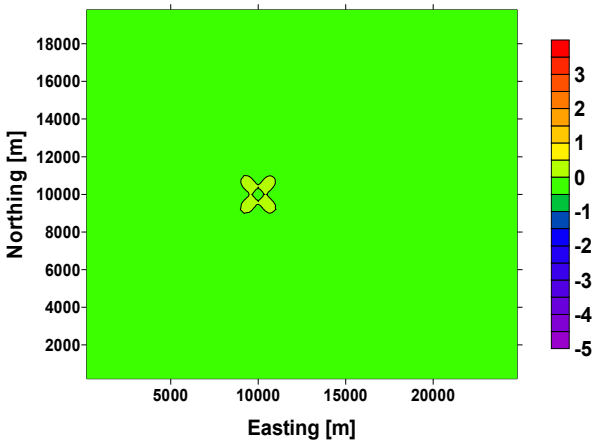


figure 5.1.1.2.8: error ISVD 6 30

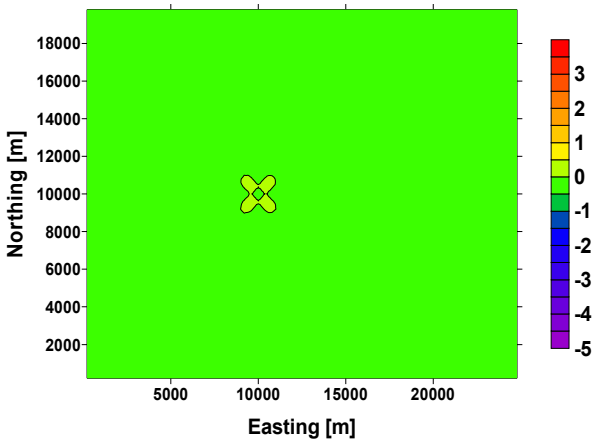


figure 5.1.1.2.9: error ISVD 7 30

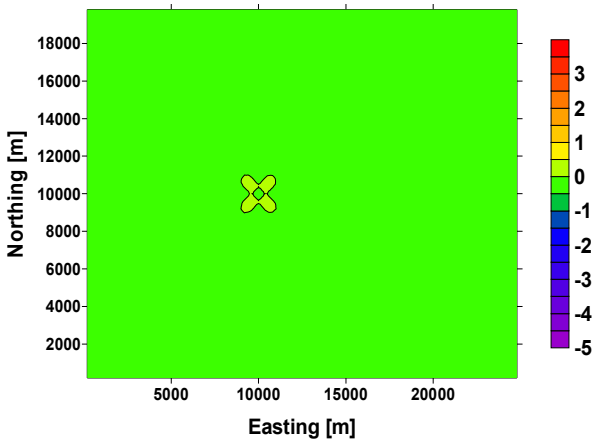


figure 5.1.1.2.10: error ISVD 20 6

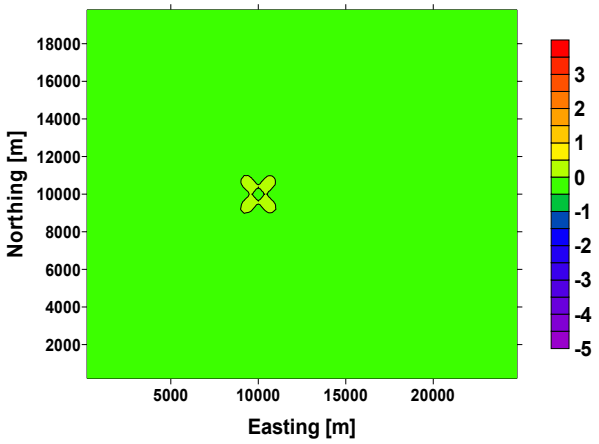


figure 5.1.1.2.11: error ISVD 4 30

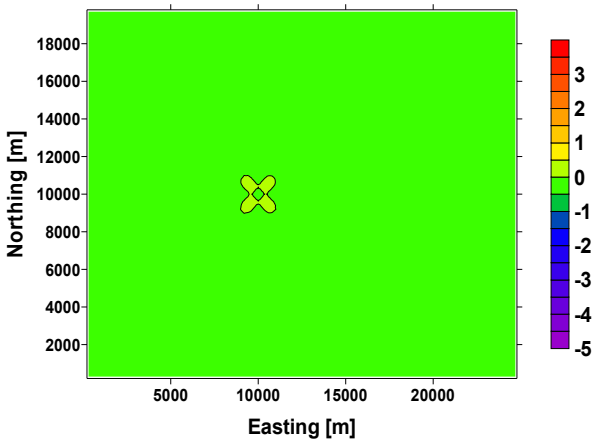


figure 5.1.1.2.12: error ISVD 5 30

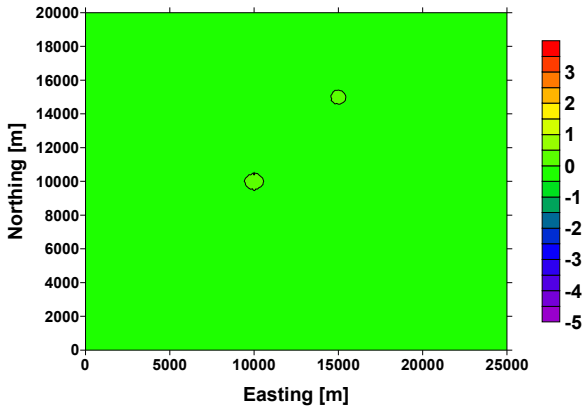


figure 5.1.1.2.13 error Tikhonov / Pasteka

As for the fields of Cooper approaches one can say there are a lot of different long wavelength characters inbound in the data which obviously disturbs these approaches to work appropriately. Cooper proposes here to reduce these effects by subtracting the error of the according approach in measurement datum, which means in our case, the error in 0m. These so gained errors will be mentioned hereafter as improved errors and will be addressed later on in 5.1.1.3 and 5.1.1.9. In the further chapters the improved fields, errors and relative logarithmic relative error fields can be distinguished by the naming convention. All cooper-fields that use the cooper proposal for improvement will include an “IMP” within the name. Though all ISVD approaches look the same for this simple dataset the best 6 results will be shown regardless if they all look the same or not. So the reader of this thesis may recognize for himself how small the difference between them is. If in the following chapters nearly equal results exist only the best (of ISVD, Cooper/FFT or Tikhonov) with respect to the ranking will be shown.

Tikhonov on the other hand seems to be very good. There is no obvious long wavelength character visible in the error and there are only small errors at the two shallower anomalies. So the best choice here may be the Tikhonov /Pasteka approach.

5.1.1.3. Improved errors of Cooper approaches in -50m

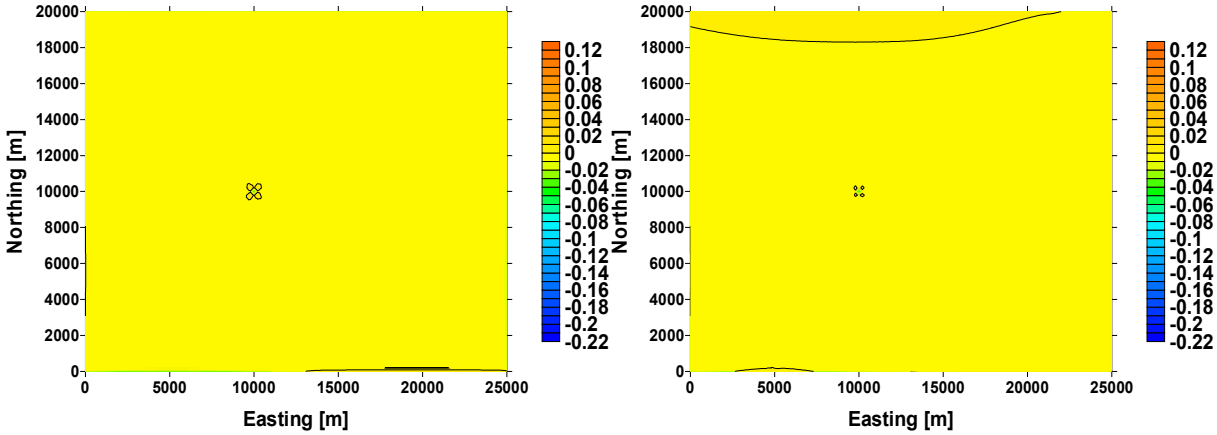


figure 5.1.1.3.1: error Cooper approach impBS4af

figure 5.1.1.3.2: error Cooper approach impBS3fa

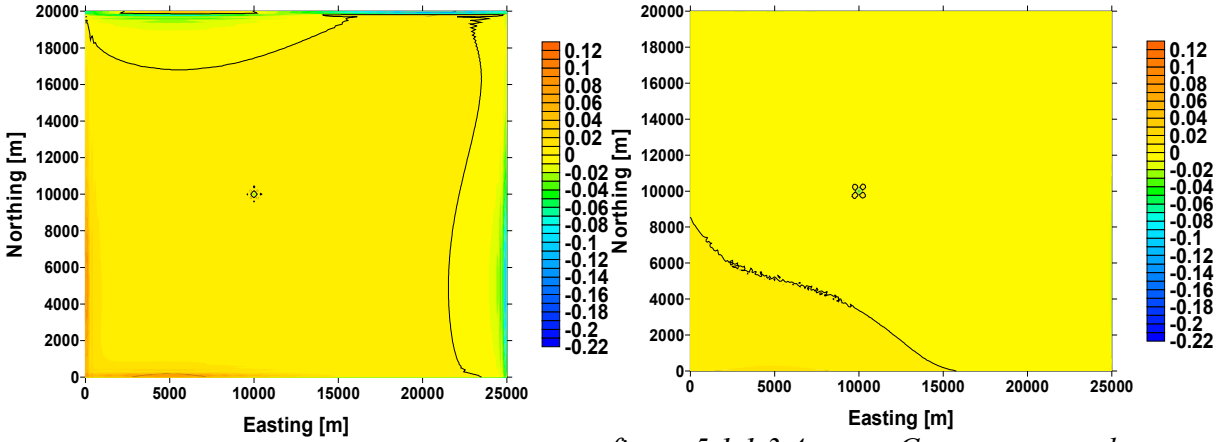


figure 5.1.1.3.3: error Cooper approach impBS4fa

figure 5.1.1.3.4: error Cooper approach impBS3af

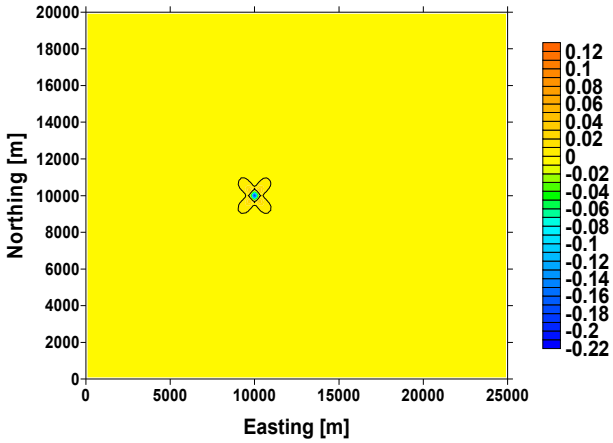


figure 5.1.1.3.5: error Cooper approach impFD3fa

It is obvious that there is still some long wavelength character remaining in the data after Coopers special error improvement. Only in figure 5.1.1.3.1 and figure 5.1.1.3.5 the improvement removed the long wavelength character nearly completely,

nevertheless a small error remains at the close area around the shallowest anomaly. This error also is evident in all other Cooper approaches. At the centre of the shallowest anomaly there is always a negative error. There is positive error along the axes of derivation. This error is also evident in the derivatives. This will be discussed later. As one may have seen the bi-cubic splines approaches dominate the list of the best 6 Cooper approaches in 50m depth. For the more realistic data set of *Vulcano* this is different.

5.1.1.4. cross-sections of the error-fields in -50m

To better see a may existent pattern in the error-fields 2D cross-sections were plotted against the horizontal distance to first point [m]. This first point for the synthetic data set with the three point sources at given locations was located at.:

285,74 East, 316,63 North

The 2D cross-section points were located along a diagonal line. See figure 5.1.1.4.1.

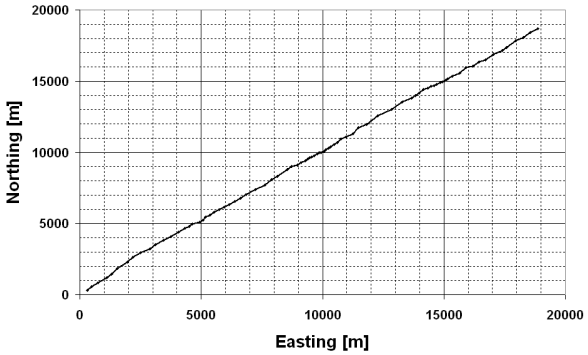


figure 5.1.1.4.1 cross-section path

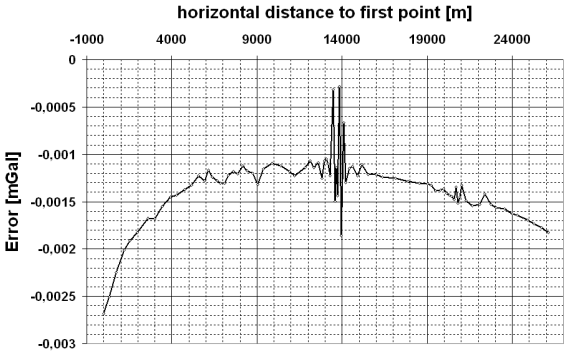


figure 5.1.1.4.2: CS error FFT

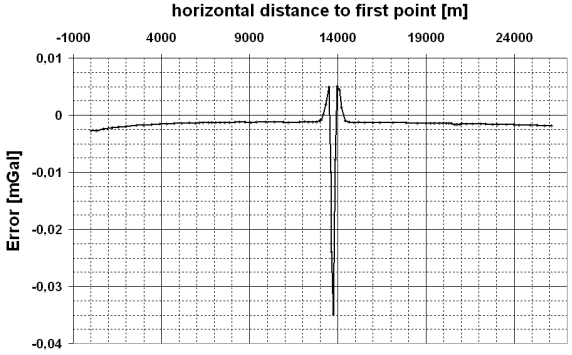


figure 5.1.1.4.3: CS error Cooper approach impBS4af

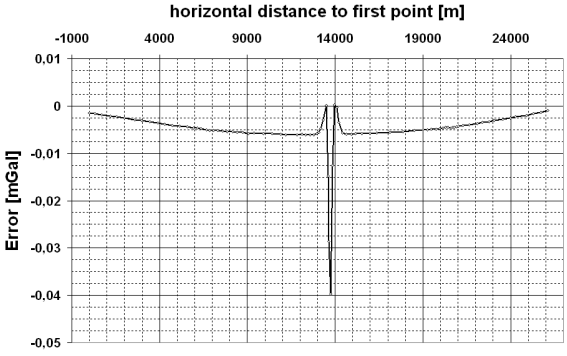


figure 5.1.1.4.4: CS error Cooper approach impBS3fa

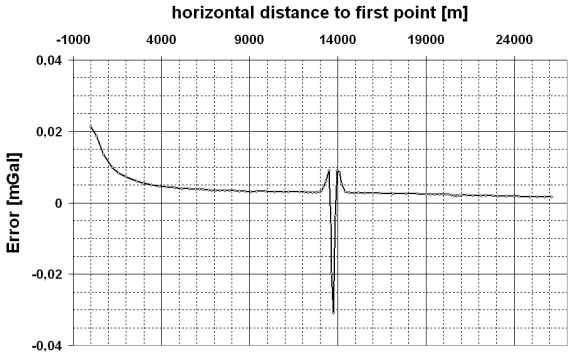


figure 5.1.1.4.5: CS error Cooper approach impBS4fa

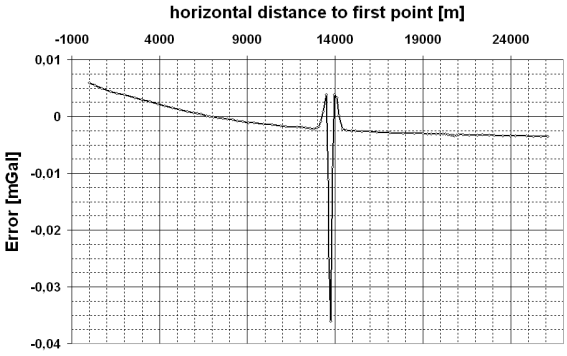


figure 5.1.1.4.6: CS error Cooper approach impBS3af

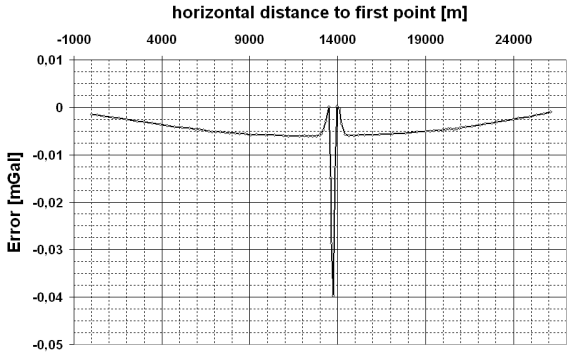


figure 5.1.1.4.7: CS error Cooper approach impFD3fa

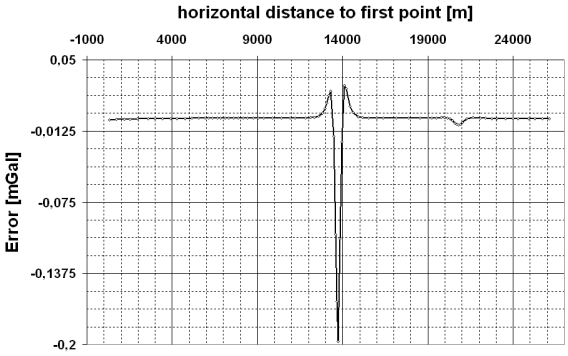


figure 5.1.1.4.8: CS error ISVD 6 30

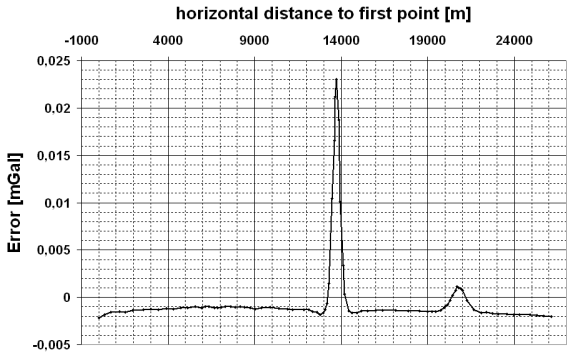


figure 5.1.1.4.9 CS error Tikhonov / Pasteka

The FFT error in figure 5.1.1.4.2 has a clearly visible oscillating character at the location of the shallowest anomaly and even at the location of the anomaly at 1km depth there is some slightly visible oscillation. May some experienced eye also see some oscillation at the deepest source location but if it is so, its faint. There is some kind of a long wavelength structure evident in the error which may be best described by the word "cap-structure" cause the error is more negative at the edges and has its maximum at the centre. Here it is completely negative but this may be influenced by a different mean value of the model-field and the field of FFT approach. This and the following mean difference influences will be discussed later on in the *lre*-plots..

In figure 5.1.1.4.3 Cooper's approach with bi-cubic splines, first field augmenting and after that using 1st vertical derivative filter, including the improvement method proposed by Cooper and explained earlier in this text, shows a quite stable solution. Only the location of the shallowest anomaly again is obviously oscillating in a close area around. The magnitude seems to be a bit bigger than the FFT error but at least is more stable in the areas more farer from the anomalies. There is just a faint "cap-strucure" visible and the error is nearly completely negative. Only at the close edges of the shallowest anomaly there are some peaks that turned out to be a typical phenomenon for this Cooper approach.

Coopers next approach in figure 5.1.1.4.4 uses nearly the same work-flow but the "cap-structure" has changed into some kind of "bowl-structure". This could be caused by an exchange of filter and field augmentation order or by the additional filter process of "vertical integration" in wave number-domain. The comparison of the rest according

approaches - which are not shown here, cause their standard deviation and magnitude were far away of the first six ranks - seemed to pinpoint out the exchange of order for filtering and field augmentation as the cause for this change in the structure of the error. Nevertheless it may be interesting to look into this more closely in a separate work.

figure 5.1.1.4.5 and figure 5.1.1.4.6 look like there is some trend obvious in the error, but when one compares the previously mentioned error fields it is clear that both have this trend, but only figure 5.1.1.4.6 is having a true trend structure. figure 5.1.1.4.5's trend is more a influence of some edge effects of the error-field itself. Both again oscillate a bit in a close area around the shallowest anomaly. This turns out to be a characteristic error structure for Cooper as well as ISVD approaches.

The only finite difference approach from Cooper existent in the list of the best 12 approaches in figure 5.1.1.4.7 shows nearly no difference in the 2D cross-section to figure 5.1.1.4.4 but as can be seen in the according error-fields (figure 5.1.1.3.2 and figure 5.1.1.3.5) that this may be just some coincident caused by some incongruous 2D cross-section path and so may be neglected.

The 2D cross-sections of the best ISVD approaches, ISVD 6 30, ISVD 20 6, ISVD 8 30, ISVD 7 30, ISVD 4 30 and ISVD 5 30 all look the same and even the maximum and minimum values seem to be equal although the amount of Taylor series terms used and truncation-parameters are different. The best of them regarding the numerical ranking can be seen in figure 5.1.1.4.8. There is no real trend distinguishable and the local maxima and minima of the errors are at the locations of the anomalies. These maxima and minima appear to be of the same shape as that of the Cooper approaches also shown in this ranking, but with bigger minima and maxima values.

Tikhonov shows a major difference to all other approaches. The peak of the error at the shallowest anomaly is positive at this depth. All the following errors will show a similar behaviour like the ISVD and Cooper approaches with negative peaks at the locations of the shallowest anomalies. This fact has been checked twice as it looked like an systematic error, caused by the interpreter but twice it turned out to be true. This fact could may be a starting point for further investigations on Tikhonov's / Pasteka's approach.

5.1.1.5. Relative errors of different approaches in -50m

The relative errors shown in the following figures are the logarithmic mean free relative errors with respect to the absolute maxima of the according model-field. All values displayed are gained through equation 5.1. The black isolines just pinpoints out the original model-field. All scale bars are dimensionless.

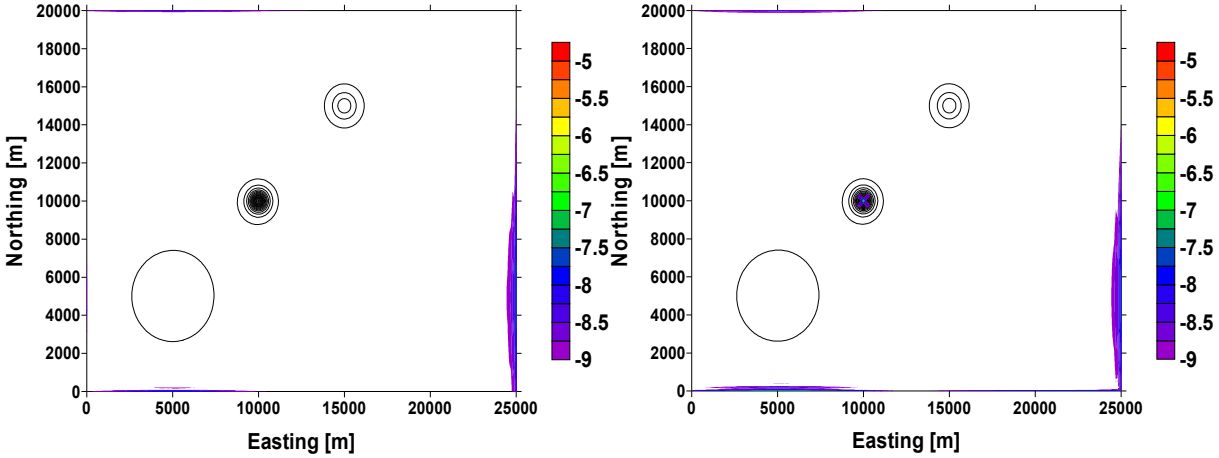


figure 5.1.1.5.1: lre FFT

figure 5.1.1.5.2: lre Cooper approach impBS4af

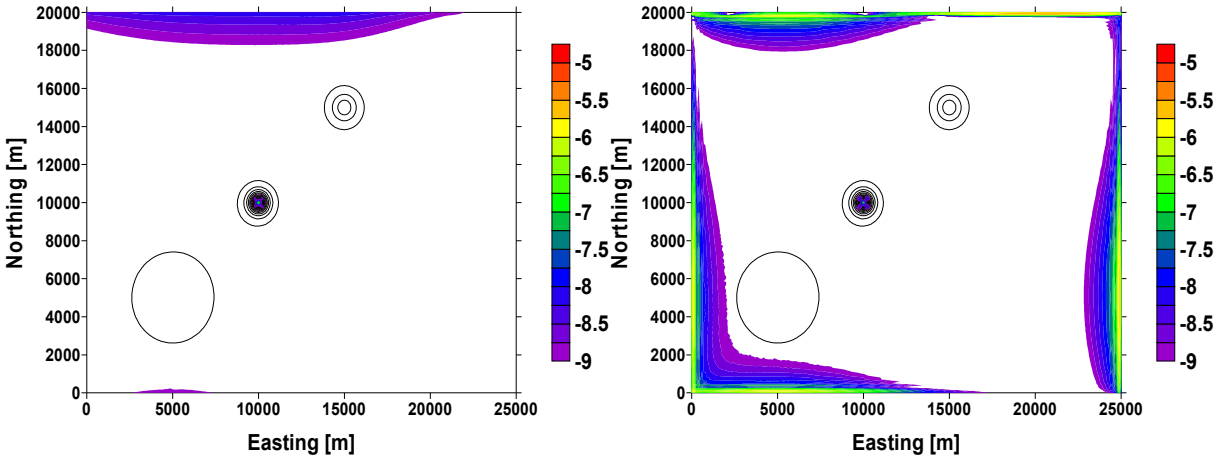


figure 5.1.1.5.3: lre Cooper approach impBS3fa

figure 5.1.1.5.4: lre Cooper approach impBS4fa

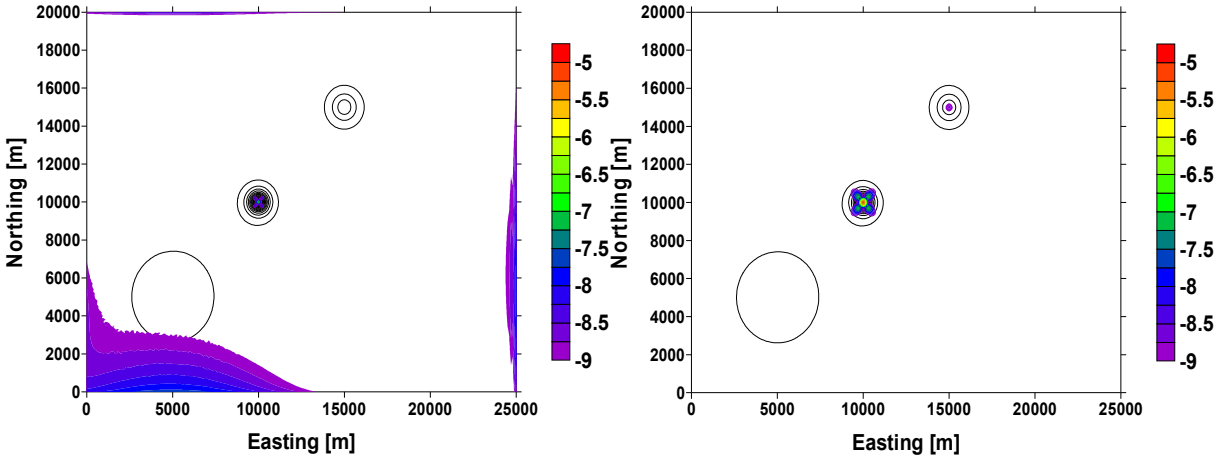


Figure 5.1.1.5.5: lre Cooper approach impBS3af

figure 5.1.1.5.6: lre Cooper approach impFD3fa

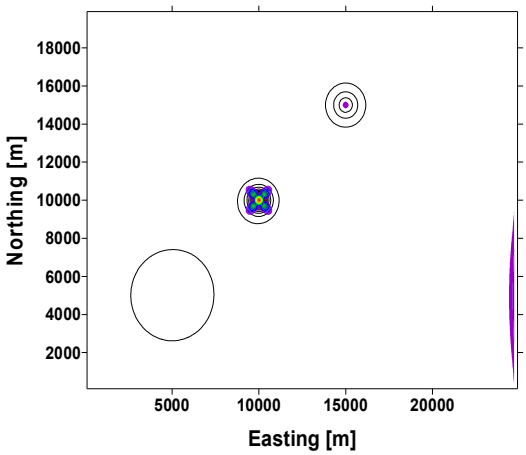


figure 5.1.1.5.7: lre ISVD 6 30

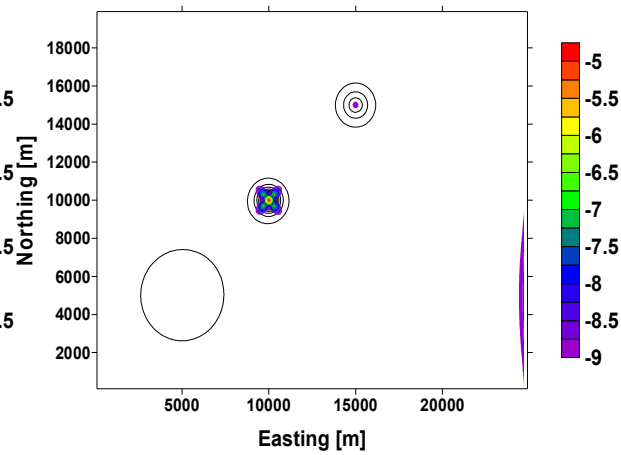


figure 5.1.1.5.8: lre ISVD 20 6

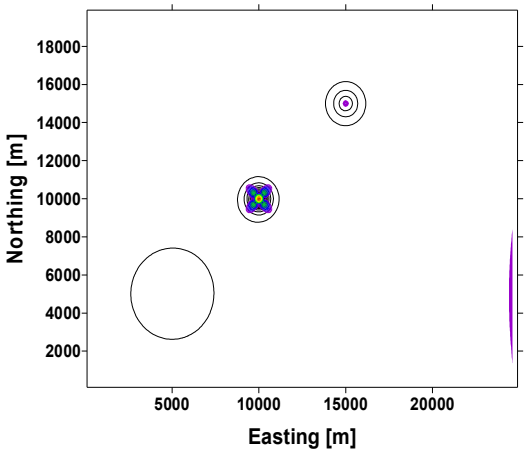


figure 5.1.1.5.9: lre ISVD 8 30

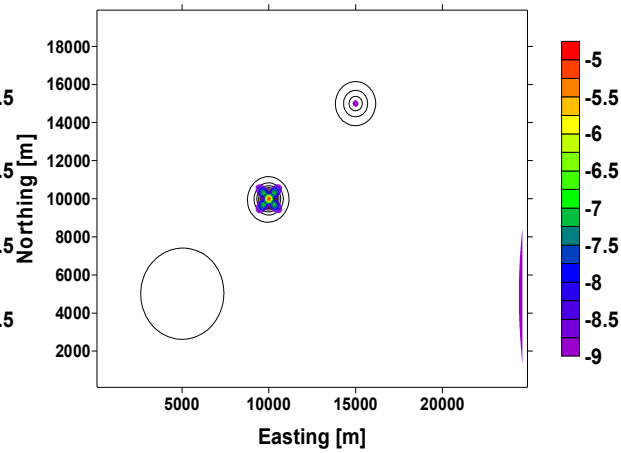


figure 5.1.1.5.10: lre ISVD 7 30

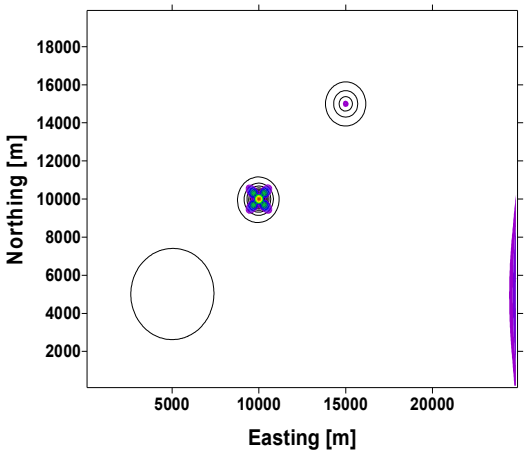


figure 5.1.1.5.11: lre ISVD 4 30

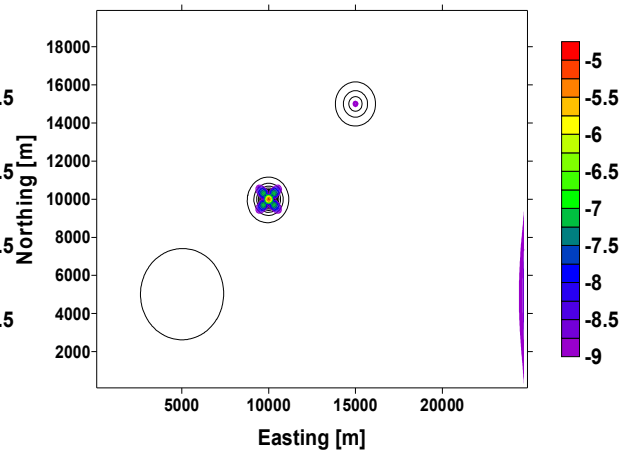


Figure 5.1.1.5.12: lre ISVD 5 30

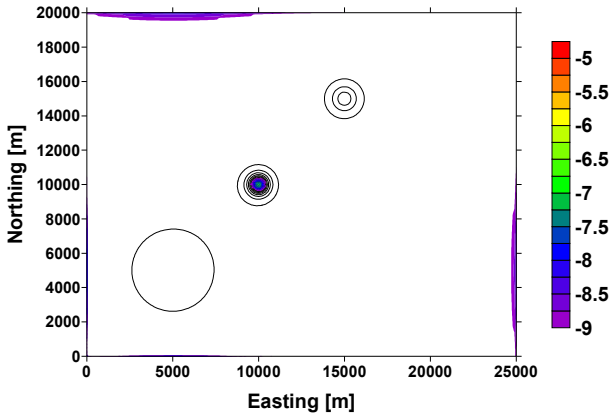


figure 5.1.1.5.13 lre Tikhonov / Pasteka

In figure 5.1.1.5.1 the relative error of the FFT approach shows a quite stable behaviour. Just at the edges of the field there are some faint errors, although they are not of a oscillating character. One may recognize that the oscillations at the location of the anomalies nearly disappeared. It will be shown in the following chapter that the error is still evident but compared to the absolute maximum of the model-field it seems negligible.

figure 5.1.1.5.2 shows the best result of Cooper approaches. Compared to the quite stable structure of the relative error of FFT approach there is a slight decrease in stability at the edges as one can see at the lower and rightmost edge of the field which looks like typical edge effects also seen in FFT results but not so strong.

In figure 5.1.1.5.3 Cooper's proposal to reduce the influence of long wavelength error by subtracting the error in measurement level from the field in depth Z shows to be not as good as intended to be. Still there is the long wavelength character visible. Only here it is more easier to see that the relative maximum of the error is in the northern end of the field and again the error has quite distinguishable local maximum at the location of the shallowest anomaly.

Cooper's approach with bi-cubic splines first building 1st vertical derivative and then field augmenting is quite stable in the middle but starts to become unstable at the edges. The local extrema at the location of the shallowest anomaly nearly disappeared in relation to the model-field value. See figure 5.1.1.5.4. Strong edge effect are visible.

Figure 5.1.1.5.5: Again Cooper's approach to reduce the error turns out to be not as reliable as expected. Still there is a strong long wavelength character visible. Compared to the FFT result there are additional errors at the locations of the anomalies which do not oscillate still but are definitely not to be preferred to the FFT approach.

First time using finite differences for building the 2nd vertical derivative shown in figure 5.1.1.5.6 reveals a strong peak at the location of the shallowest anomaly. Nevertheless it looks quite stable compared to the bi-cubic splines solutions and as can be seen later turns out to be similar to the ISVD results..

figure 5.1.1.5.7 to Figure 5.1.1.5.12 all seem to have nearly the same relative error

structure. The error at the location of the shallowest anomalies are clearly visible which leads to the assumption that the errors for ISVD method at the shallowest anomalies are quite big, at least compared to the rest of the error-field data of the ISVD approach. This would be consistent with the 2D cross-sections of the ISVD errors where the biggest error is located at the centre of the shallowest anomaly. The different amount of Taylor series terms or truncation parameter used just makes some minor difference in the relative error fields as may be seen in the south-eastern corners of the fields. As Fedi and Florio recommended 7 Taylor series terms is quite as good as 8 terms. 6 terms increases the error at the borders, even if it is a faint increase.

Tikhonov's approach seems to have a small nearly not existent long-wavelength character too. The relative error at the location of the shallowest anomaly looks smaller than the relative errors of ISVD and Cooper maybe equal to FFT.

5.1.1.6. 2D cross-sections of the relative field errors in -50m depth

Again the cross-section profile mentioned earlier was used to get the cross-sections of the relative errors.

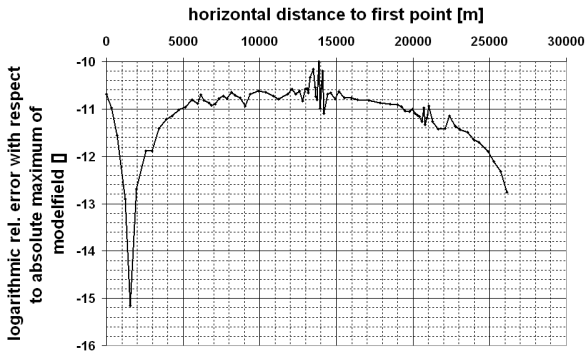


figure 5.1.1.6.1: CS lre FFT

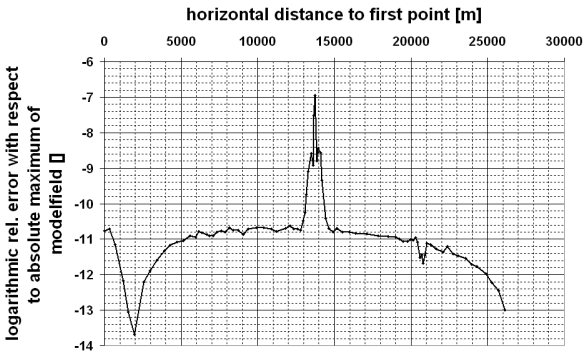


figure 5.1.1.6.2: CS lre Cooper approach impBS4af

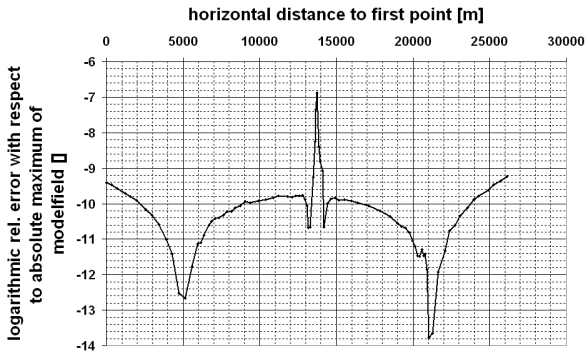


figure 5.1.1.6.3: CS lre Cooper approach impBS3fa

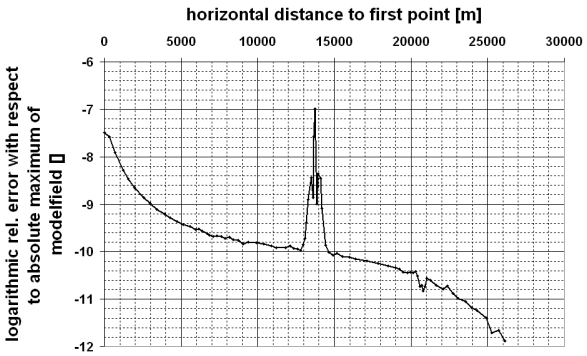


figure 5.1.1.6.4: CS lre Cooper approach impBS4fa

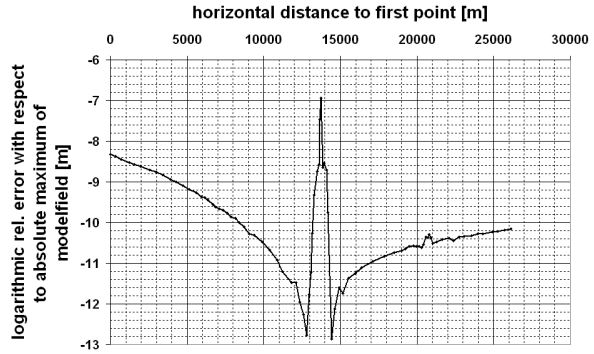


figure 5.1.1.6.5: CS lre Cooper approach impBS3af

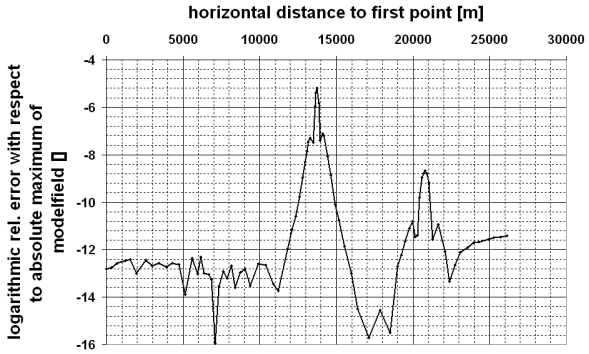


figure 5.1.1.6.6: CS lre Cooper approach impFD3fa

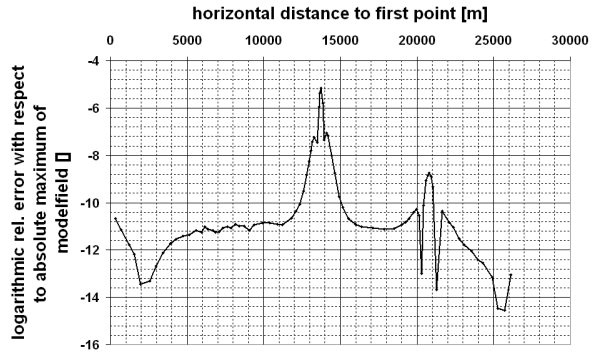


figure 5.1.1.6.7: CS lre ISVD 6 30

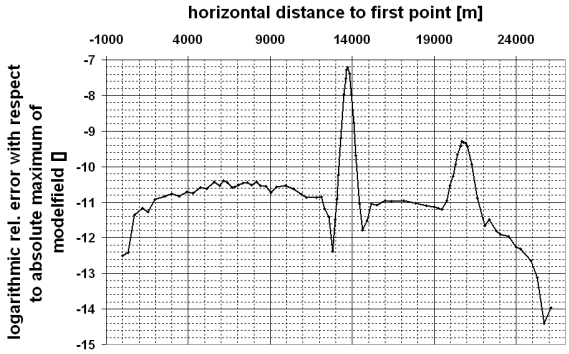


figure 5.1.1.6.8 CS lre Tikhonov / Pasteka

For all the 2D cross-section plots a logarithmic scaling of the z-axis was chosen, to better see the small and big errors within one plot. One may keep in mind that all these Cooper 2D cross-section plots are improved by the Cooper's proposal to reduce the error by subtracting the error in observation level.

figure 5.1.1.6.1 showing the relative FFT 2D cross-section turns out to be most unstable at the location of the anomalies albeit the amplitudes seem to be very small. The relative error is quite constant, just at the edges of the field there seems to be an improvement of the relative error as it tends to zero-level but then increases again to a value bigger than in the inner area of the field.

The best Cooper approach in figure 5.1.1.6.2 looks similar but has a bigger relative error range than figure 5.1.1.6.1. Even with the cooper proposed improvement it is not capable to outperform the result of the FFT in figure 5.1.1.6.1.

figure 5.1.1.6.3 needs just a short look at the magnitude to see that this result is out of competition like the approach before, cause the mean value of this relative error field is quite big compared to FFT's. Still it should be mentioned there is this small improvement at the locations of the two deeper anomalies. Again the relatively big error at the edges of the field are visible.

The next following Cooper approach in figure 5.1.1.6.4 using again bi-cubic splines to get the 1st vertical derivative and then field augmenting before FFT is applied, reveals a quite different result compared to the other Cooper approaches, as the relative error increases at the south-western edge of the field and a clear trend in the data is visible.

It's error range is bigger than that of FFT and so this result seems to be out of competition.

figure 5.1.1.6.5's relative error range is somewhere in the middle of the ranking. The error seems to be quite small around the shallowest anomaly but then again increases to the edges of the field. The maximum of the error at the location of the shallowest anomaly is again a lot bigger than that of FFT and so this result seems to be out of competition too.

figure 5.1.1.6.6 showing a finite difference cooper approach looks quite unstable in the whole field on the contrary to simple contour plot which looked stable except at the location of the shallowest anomaly.

figure 5.1.1.6.7 showing the best of the ISVD relative errors has a quite bigger relative error than Cooper and FFT. ISVD can not compete to Cooper bi-cubic splines and FFT results. Only The last Cooper approach using finite differences for the derivatives has a similar relative error at the location of the shallowest anomaly.

The approach of Tikhonov / Pasteka maybe oscillates a bit but the amplitudes of those oscillations are a lot smaller than those of ISVD and Cooper. Anyway the FFT approach reveals oscillations too but the amplitudes of those oscillations are smaller than those of all other.

5.1.1.7. Fields of different approaches in -300m

All scale bars are in mGal.

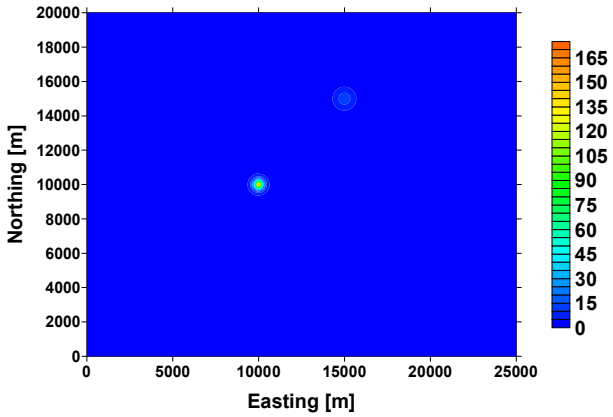


figure 5.1.1.7.1 model-field in -300m

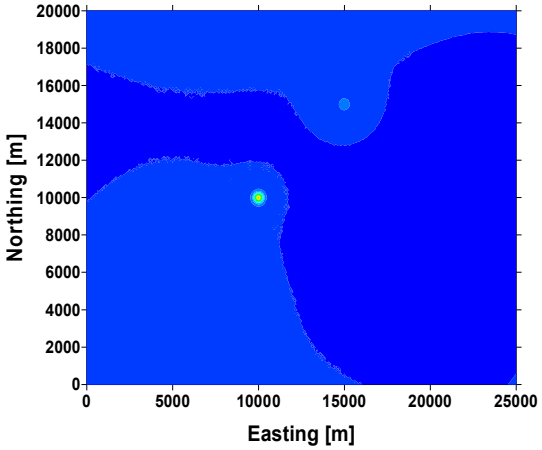


figure 5.1.1.7.2: Cooper approach BS3fa

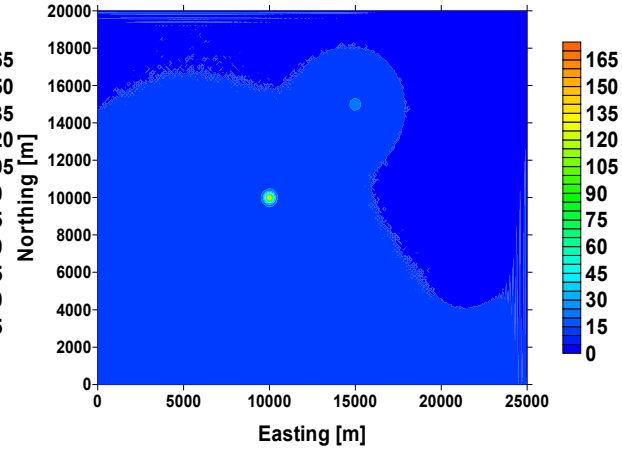


figure 5.1.1.7.3: Cooper approach BS3af

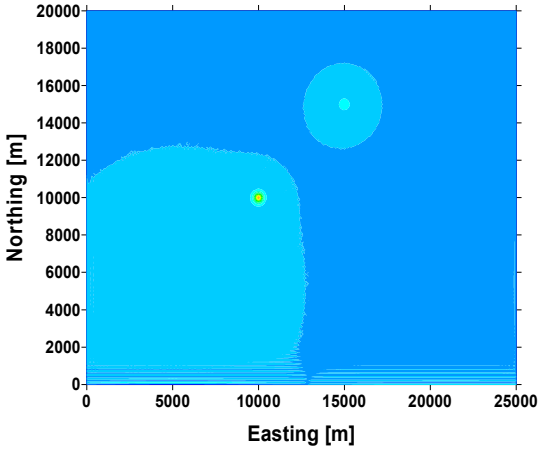


figure 5.1.1.7.4: Cooper approach BS4af

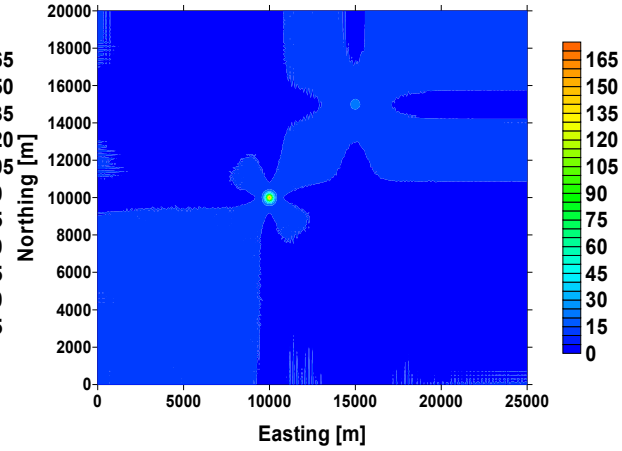


figure 5.1.1.7.5: Cooper approach BS0fa

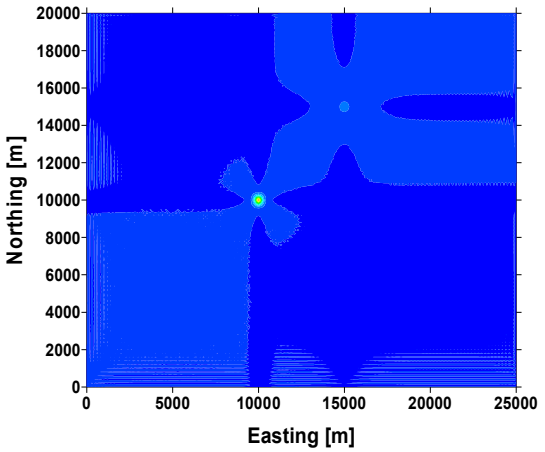


figure 5.1.1.7.6: Cooper approach BS0af

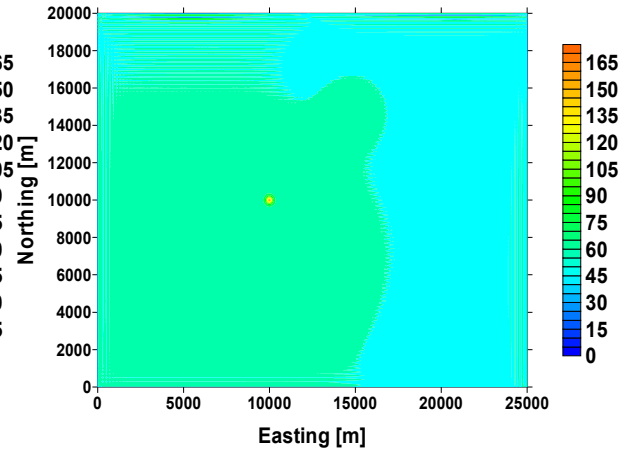


figure 5.1.1.7.7: Cooper approach BS4fa

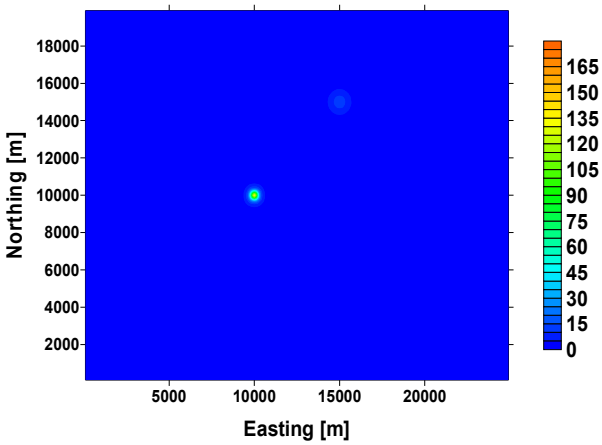


figure 5.1.1.7.8: ISVD 8 30

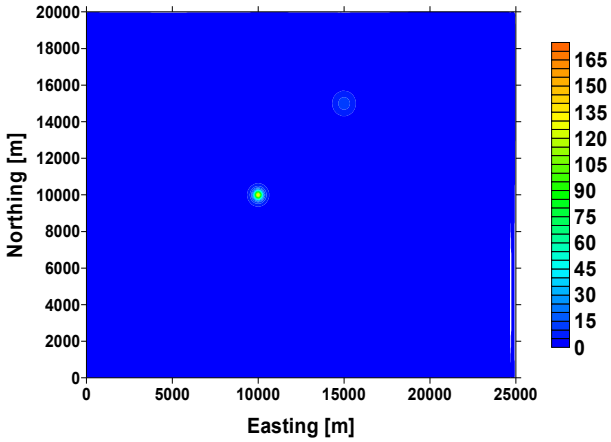


figure 5.1.1.7.9 Tikhonov / Pasteka

The best approach of ISVD, ISVD 8 30 (figure 5.1.1.7.8) looks the same and as stable as ISVD 20 3, ISVD 20 4, ISVD 20 5, ISVD 20 6, ISVD 7 30, which are the other best 5 ISVD approaches.

All Cooper approaches in -300m (figure 5.1.1.7.2 to figure 5.1.1.7.7) contain strong oscillation effect, spread over the whole field. Of course the edge effects are increased, compared to the results in -50m. The fact that no finite difference approach is in the ranking, is maybe caused by the strong oscillations within the data in this depth. One may see that there are a mixed derivative approaches in the ranking now too.

Tikhonov / Pasteka delivers a quite stable result nearly not to differ from the model-field. Maybe errors fields better depicts the difference.

5.1.1.8. Errors of different approaches in -300m

All scale bars are in mGal.

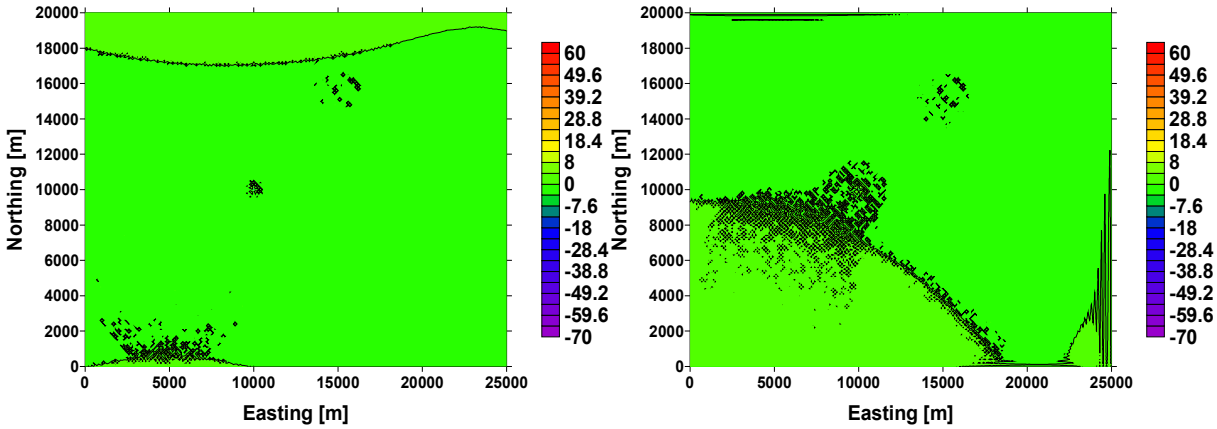


figure 5.1.1.8.1: error Cooper approach BS3fa *Figure 5.1.1.8.2: error Cooper approach BS3af*

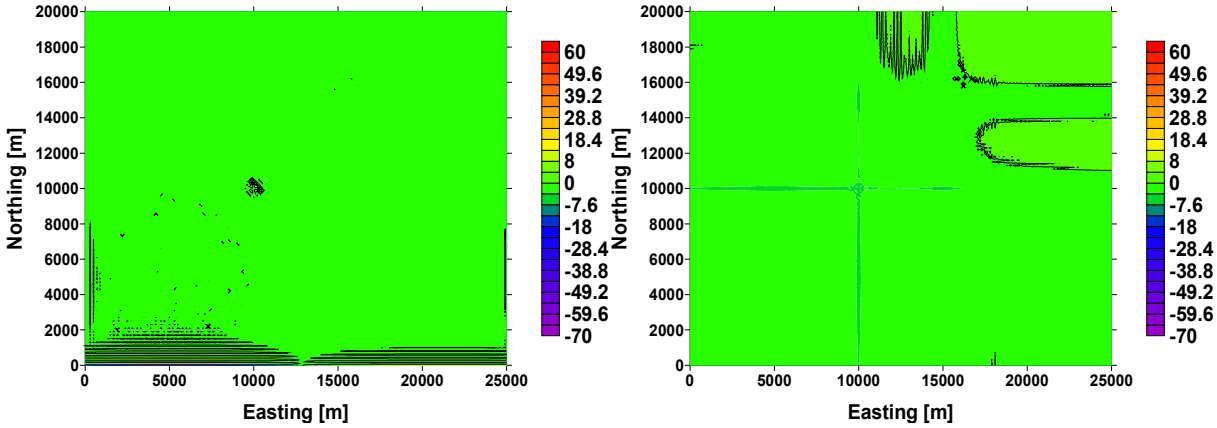


figure 5.1.1.8.3: error Cooper approach BS4af *figure 5.1.1.8.4: error Cooper approach BS0fa*

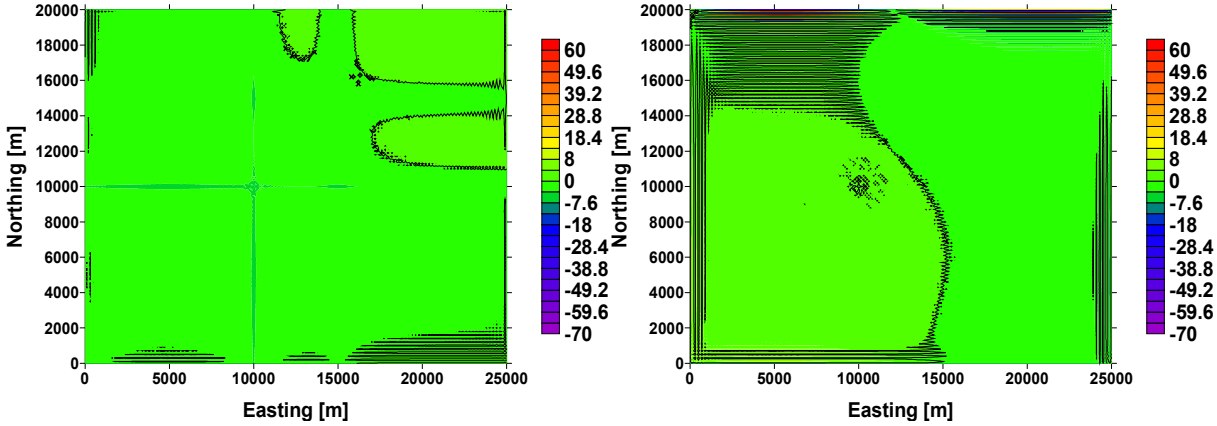


figure 5.1.1.8.5: error Cooper approach BS0af *figure 5.1.1.8.6: error Cooper approach BS4fa*

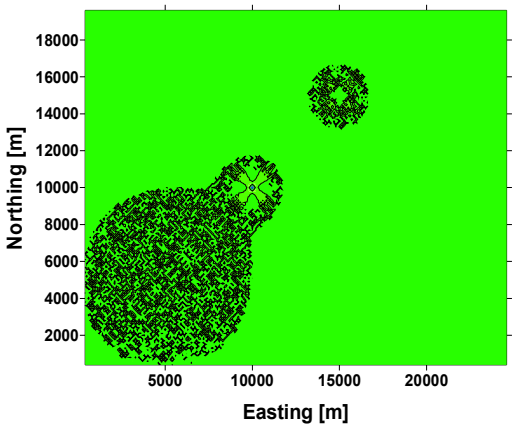


figure 5.1.1.8.7: error ISVD 8 30

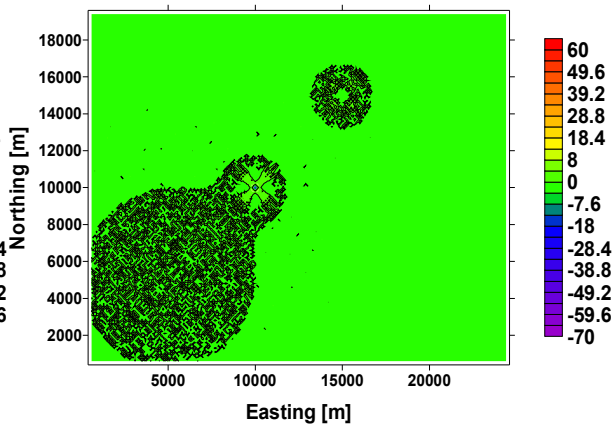


figure 5.1.1.8.8: error ISVD 20 3

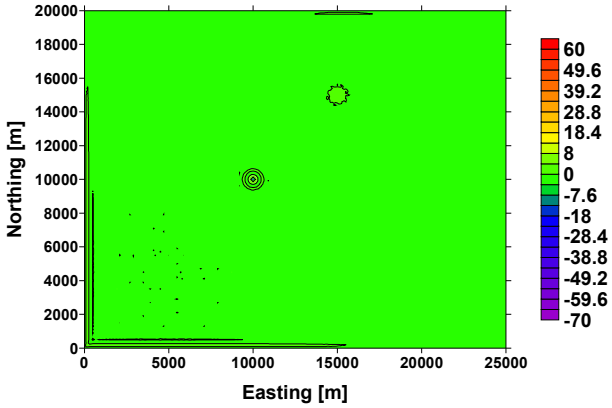


figure 5.1.1.8.9 error Tikhonov / Pasteka

ISVD 20 4, ISVD 20 5, ISVD 20 6 look exactly the same as ISVD 20 3 (figure 5.1.1.8.8). ISVD 7 30 can't be differed from ISVD 8 30 (figure 5.1.1.8.7).

figure 5.1.1.8.1 and Figure 5.1.1.8.2 show a quite distinguishable long wavelength part and is strongly oscillating especially at the locations of the anomalies. There are strong oscillations visible in both error fields.

Cooper's first 1st vertical derivative approach in -300m in the ranking (figure 5.1.1.8.3) could be mistaken for a good result at first sight but when one looks at the still oscillating edges and the slight oscillation at the location of the shallowest anomaly as well as the faint oscillations at the deepest anomaly it is clear that this approach should not been chosen in this depth.

The first mixed approach in the ranking (figure 5.1.1.8.4) has a quite typical error structure for this kind of approach. The faint stripe-formed structures along the derivative axes crossing each other at the locations of the anomalies are a typical error-structure of all mixed derivative Cooper approaches. Again strong oscillations dominate the error field. Edge effect are faint but distinguishable. Remarkable also is the fact that this is the only approach having just negative errors.

The next approach in figure 5.1.1.8.5 uses the same derivative method but the order of field augmentation and filtering is again changed so that the edge effects increased in amplitude and occurrence. As one will see in the following chapter even the

improvements made by Cooper's proposal do not remove this structure.

figure 5.1.1.8.6 shows the second 1st vertical derivative approach. This one is not improved through Cooper's zero-level-error-reduction proposal as was mentioned in the last chapter too. Oscillations are spreading over the whole field even in the more inner area where no anomaly is located.

figure 5.1.1.8.7 to figure 5.1.1.8.8 are again nearly the same. Just some small more or less increasing oscillations are visible. The most and intensest of them at the locations of the anomalies whereupon the deepest anomaly is the one with the biggest area of oscillations around but the faintest and the shallowest one has the smallest area of oscillations but the strongest in amplitude. As all the ISVD and Cooper approaches in -300m do have oscillations inbound its hard to tell which one is the best. The following chapters hopefully will help to decide which one to take at which depths deeper than the spacing of the grid.

Tikhonov's / Pasteka's approach already oscillates faintly. In comparison to the other approaches is seems to be the stablest field continuation for this depth and the used simple dataset. There are also edge effects visible at the lower left corner of the error field.

5.1.1.9. Improved errors of Cooper approaches in -300m

All scale bars are in mGal.

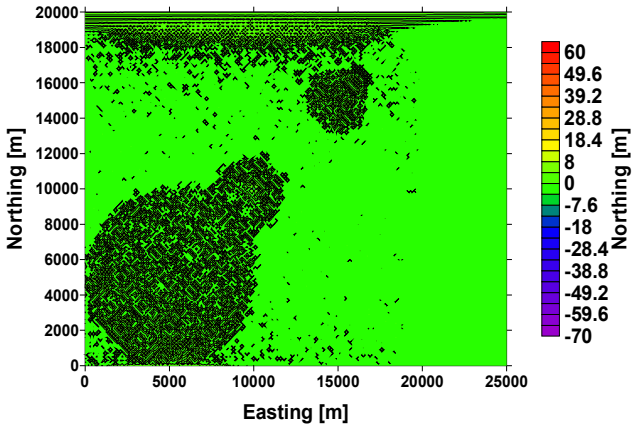


figure 5.1.1.9.1: error Cooper approach impBS3fa

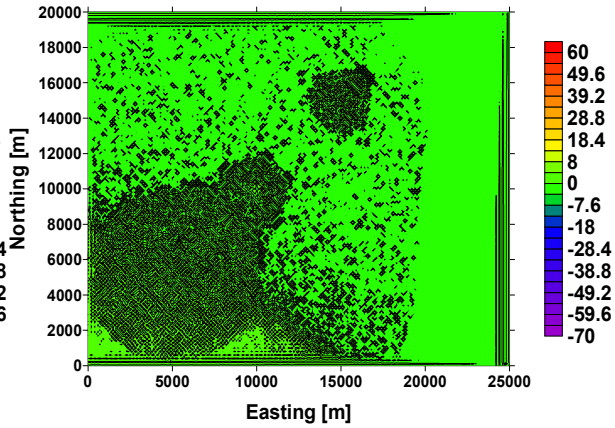


figure 5.1.1.9.2: error Cooper approach impBS3af

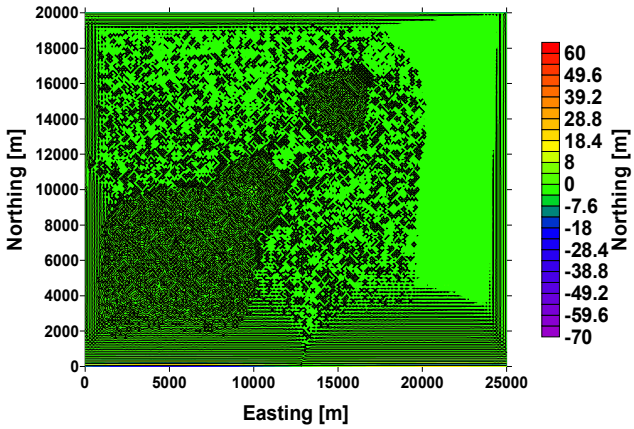


figure 5.1.1.9.3: error Cooper approach impBS4af

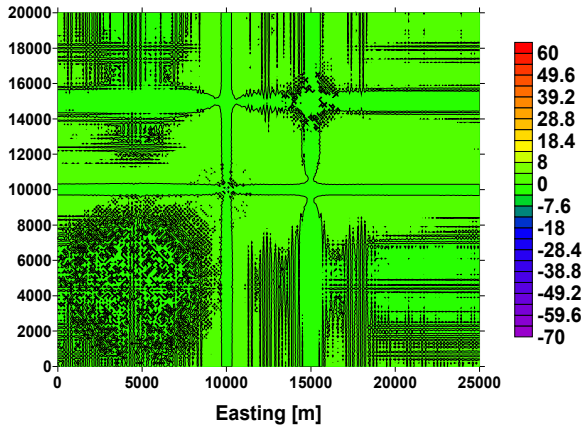


figure 5.1.1.9.4: error Cooper approach impBS0fa

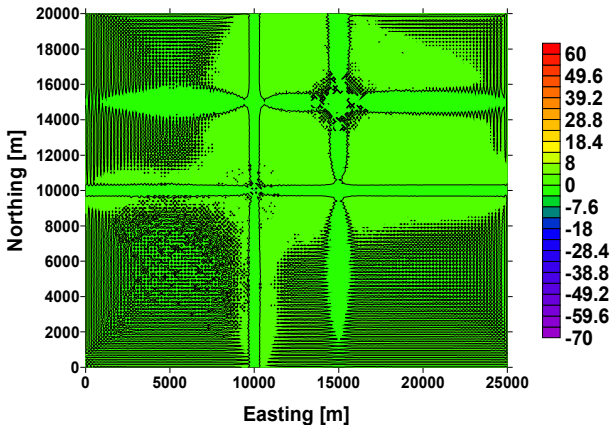


figure 5.1.1.9.5: error Cooper approach impBS0af

As expected the improvement for the Cooper approaches didn't really improved the results, as the error ranges stayed as they where or even increased. The edge effects as well as oscillations did not disappear. Cooper's improvement was only intended to remove long wavelength information from the data but no high frequency noise. (for example: edge effects or oscillations) Nevertheless through these “improvements” the long wavelength information could be removed partly. The oscillations, which where mentioned in the last chapter are now visible to the readers eye more clearly. They are small in amplitude in the more inner part but reach their maxima and minima at the boundaries.

As one may again is able to see the stripe-formed structures within the improved mixed derivatives approaches too (figure 5.1.1.9.4 and figure 5.1.1.9.5). The edge effect is very strong in these two approaches.

5.1.1.10. cross-sections of the error-fields in -300m

Again the cross-section profile is the same as in 50m depth.

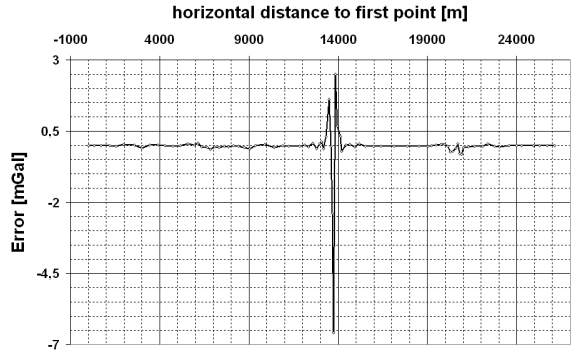


figure 5.1.1.10.1: CS error Cooper approach impBS3fa

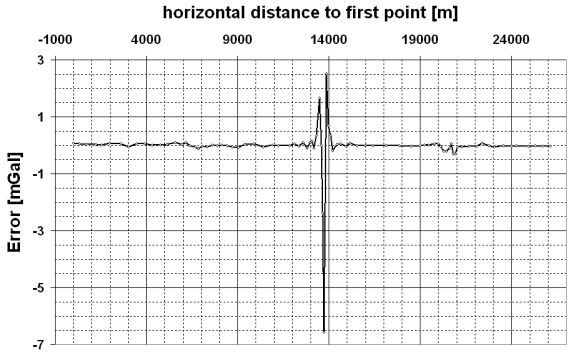


figure 5.1.1.10.2: CS error Cooper approach impBSaf

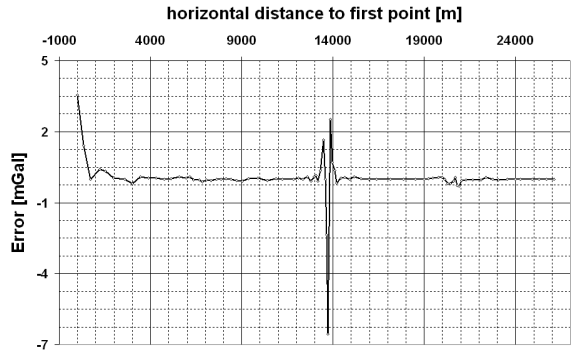


figure 5.1.1.10.3: CS error Cooper approach impBS4af

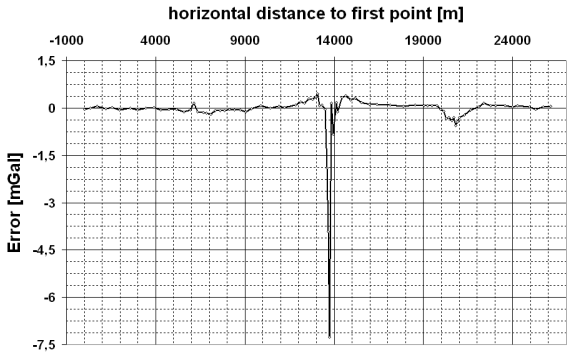


figure 5.1.1.10.4: CS error Cooper approach impBS0fa

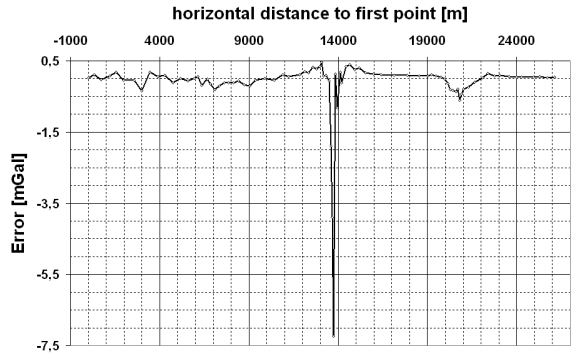


figure 5.1.1.10.5: CS error Cooper approach impBS0af

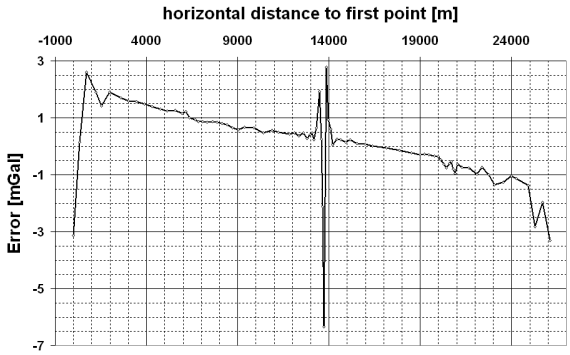


figure 5.1.1.10.6: CS error Cooper approach BS4fa

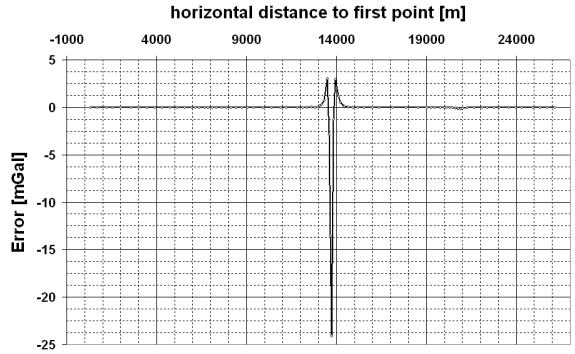


figure 5.1.1.10.7: CS error ISVD 8 30

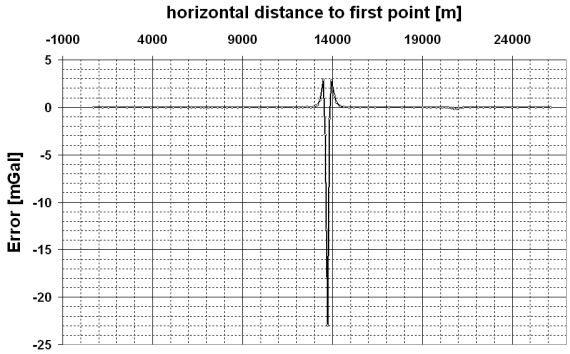


figure 5.1.1.10.8: CS error ISVD 20 3

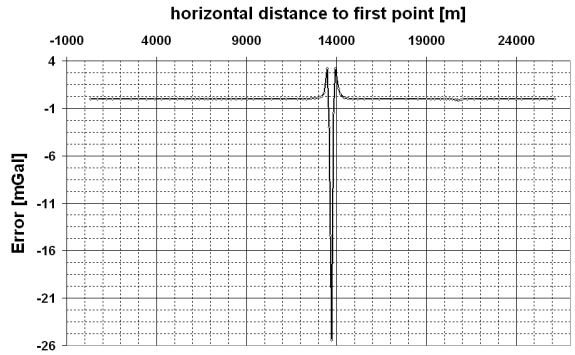


figure 5.1.1.10.9: CS error ISVD 7 30

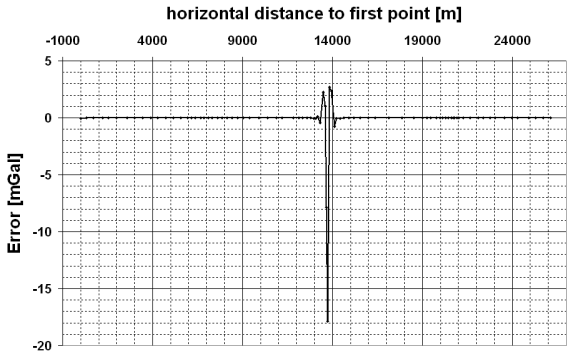


figure 5.1.1.10.10 CS error Tikhonov / Pasteka

As the reader of this thesis may recognize at first sight all Cooper results are slightly oscillating but the last Cooper approach in figure 5.1.1.10.6 shows there is still a trend visible in the error-data. This is may be caused by the negligence of the zero-level-error-reduction proposed by Cooper.
All the results have a negative peak at the location of the shallowest anomaly as well as a very small peak at the location of the north-eastern anomaly.
Normally the 1st and 2nd vertical derivatives approaches show some positive peaks at the approximate locations of the inflection points of the fields. The mixed derivative approaches do oscillate a bit more over the whole data field and their errors are nearly all negative. These so typical positive peaks in the area close to the inflection points of the model-field, are present in mixed derivative approaches too but not so strong in amplitude.
All the ISVD approaches show nearly the same error plot. Compared to the error range of Coopers approaches ISVD is extremely good at the locations where no anomalies exist, nevertheless the errors at the locations of the anomalies, especially the shallowest is around 3 times bigger than the Cooper approach errors. ISVD 20 4, ISVD 20 5 and ISVD 20 6 also in the ranking of the best 6 ISVD approaches (but not shown here) all look the same as ISVD 20 3 (figure 5.1.1.10.8). The best ISVD approach in the ranking is ISVD 8 30 (figure 5.1.1.10.7) but looking more closely at the error range of ISVD 20 3 shows a bit smaller error range than ISVD 8 30. In fact the recommended 7 Taylor series terms approach (figure 5.1.1.10.9) of Fedi and Florio here turns out to be the worst of the 6 ISVD results as one may sees while again looking at the error range. Generally ISVD still looks like its a stable solution in the depth of -300m.

Tikhonov's / Pasteka's approach looks very similar too the ISVD approaches. The amplitude of the error may be a bit smaller at the location of the shallowest anomaly.

5.1.1.11. Relative errors of different approaches in -300m

All scale bars are dimensionless.

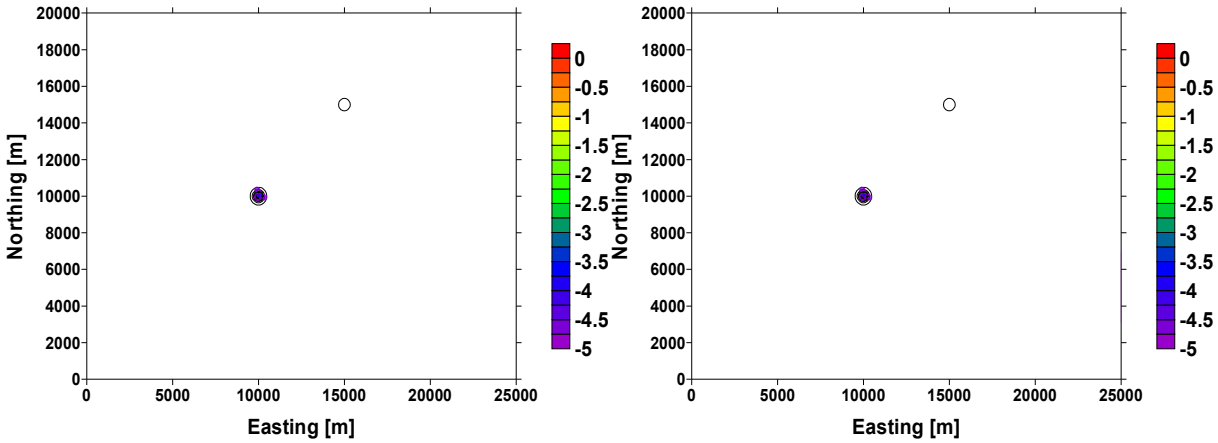


figure 5.1.1.11.1: lre Cooper approach impBS3fa

figure 5.1.1.11.2: lre Cooper approach impBS3af

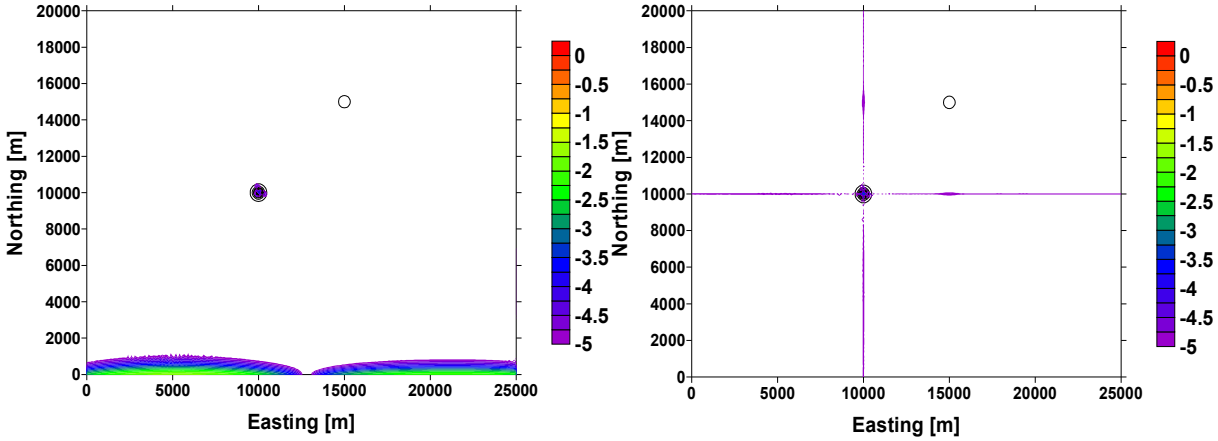


figure 5.1.1.11.3: lre Cooper approach impBS4af

figure 5.1.1.11.4: lre Cooper approach impBS0fa

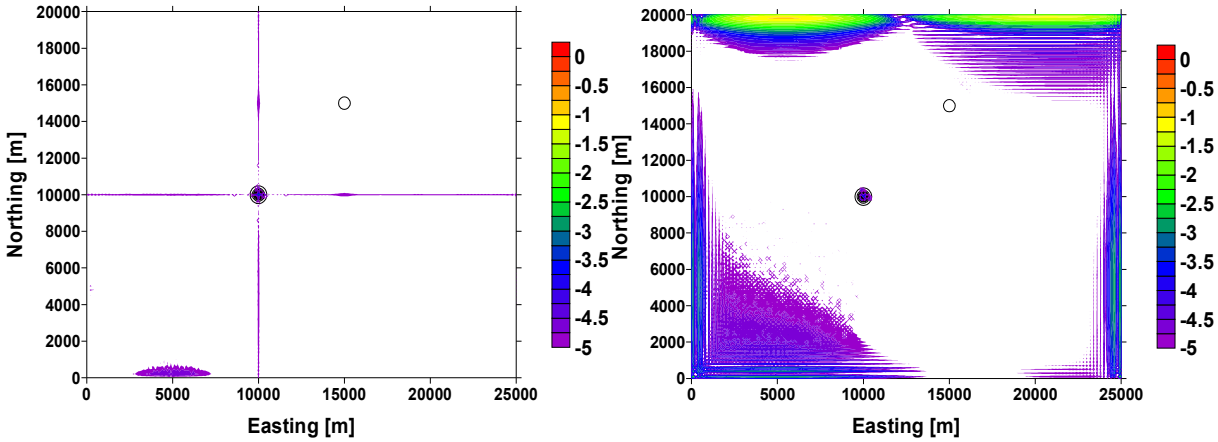


figure 5.1.1.11.5: lre Cooper approach impBS0af

figure 5.1.1.11.6: lre Cooper approach BS4fa

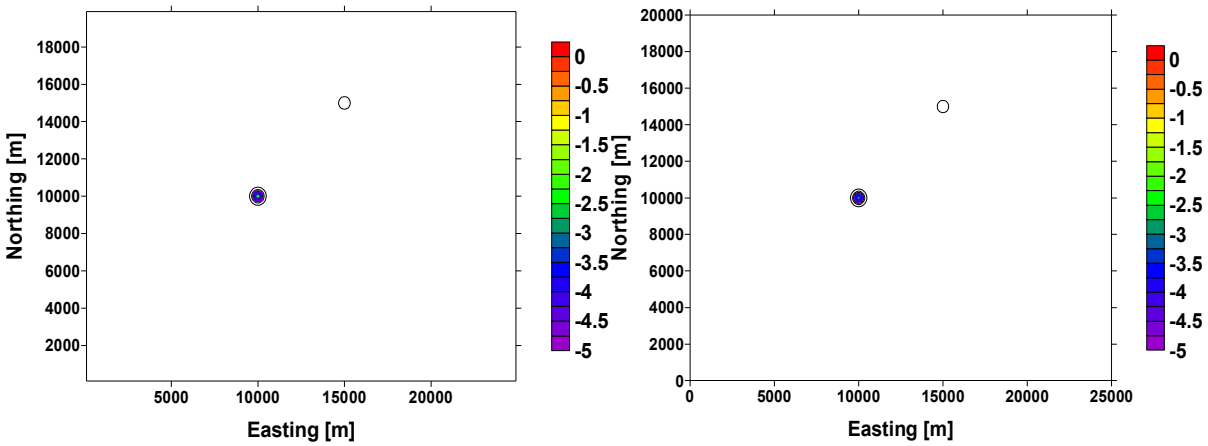


figure 5.1.1.11.7: lre ISVD 8 30

figure 5.1.1.11.8 lre Tikhonov / Pasteka

figure 5.1.1.11.1 and figure 5.1.1.11.2 showing the improved 2nd vertical derivative approaches seem to be quite stable and have their error maximum at the location of the shallowest anomaly. It is very interesting too, that the last Cooper approach in figure 5.1.1.11.6 using no zero-level-error-reduction as proposed by Cooper was at least quite stable in the more inner part of the field. Nevertheless edge effects were quite distinguishable still and maybe are so strong in amplitude that oscillations in the more inner part of the field are just not visible cause there amplitude were to small compared to that of the edge effects.

Regardless of which ISVD approach in the ranking of the best six is viewed, all look the same. Therefore only the best in the ranking is shown here. The rest of the six ISVD approaches are: *ISVD 20 3, ISVD 20 4, ISVD 20 5, ISVD 20 6* and *ISVD 7 30.* From this point of view ISVD may be preferred ot other the other kind of approaches.

figure 5.1.1.11.8 showing the relative error of Tikhonov's / Pasteka's approach looks quite as good as the ISVD approach. To decide between ISVD and Tikhonov in this example is maybe possible from the cross-sections of those relative errors. The lre-plots do not show enough differences to decide which one to take.

5.1.1.12. 2D cross-sections of the relative field errors in -300m depth

As in all the other cross-sections above, the cross-section used is shown in figure 5.1.1.4.1.

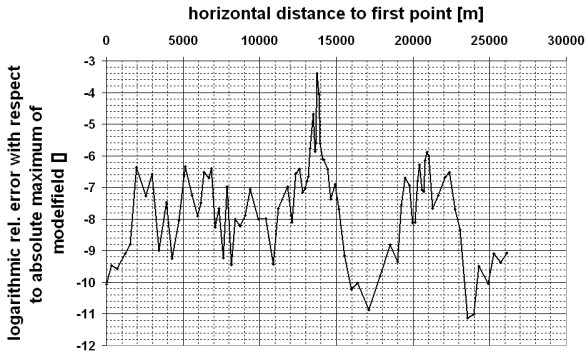


figure 5.1.1.12.1: CS lre Cooper approach impBS3fa

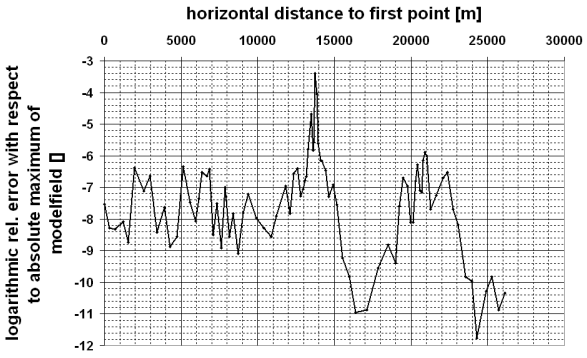


figure 5.1.1.12.2: CS lre Cooper approach impBS3af

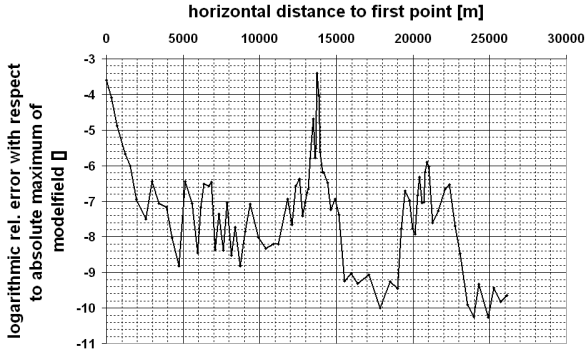


figure 5.1.1.12.3: CS lre Cooper approach impBS4af

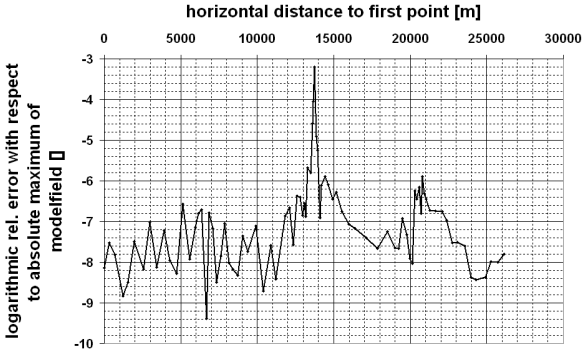


figure 5.1.1.12.4: CS lre Cooper approach impBS0fa

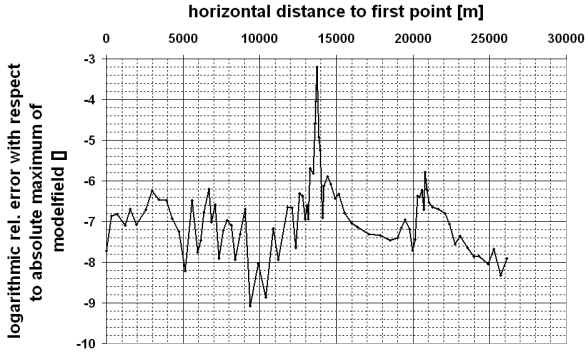


figure 5.1.1.12.5: CS lre Cooper approach impBS0af

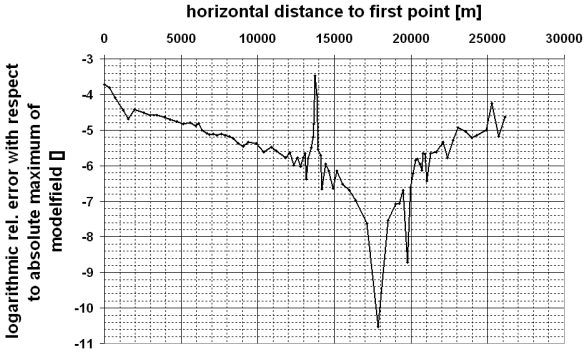


figure 5.1.1.12.6: CS lre Cooper approach BS4fa

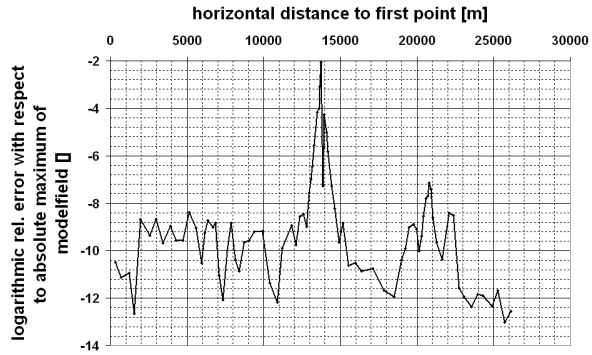


figure 5.1.1.12.7: CS lre ISVD 8 30

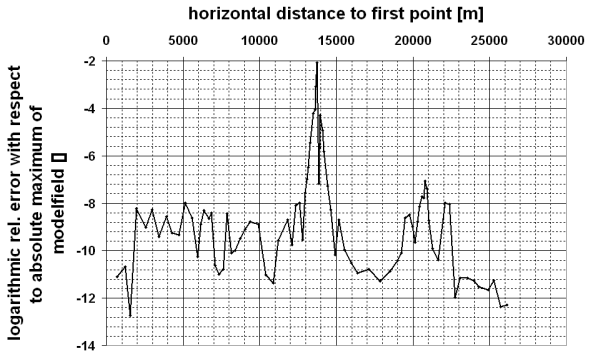


figure 5.1.1.12.8: CS lre ISVD 20 3

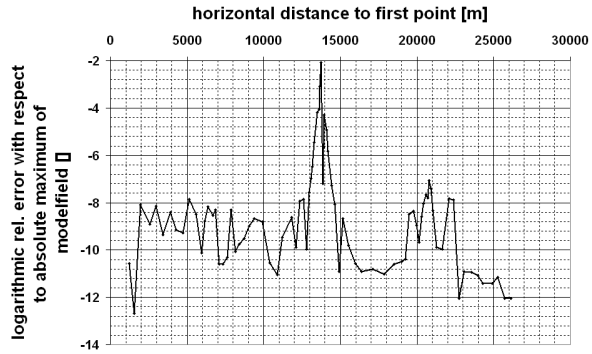


figure 5.1.1.12.9: CS lre ISVD 20 4

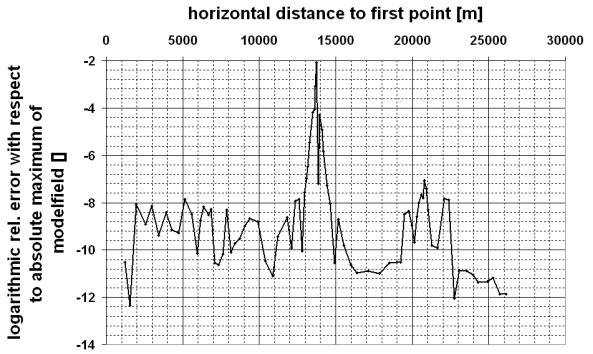


figure 5.1.1.12.10: CS lre ISVD 20 5

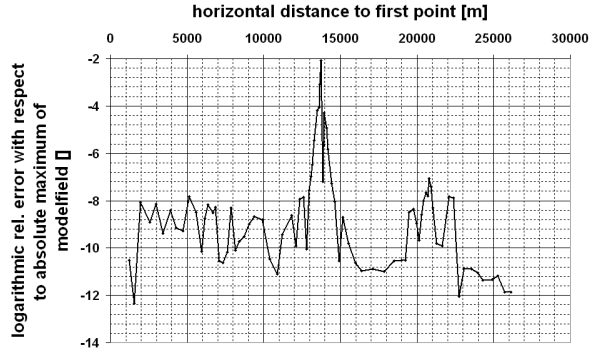


figure 5.1.1.12.11: CS lre ISVD 20 6

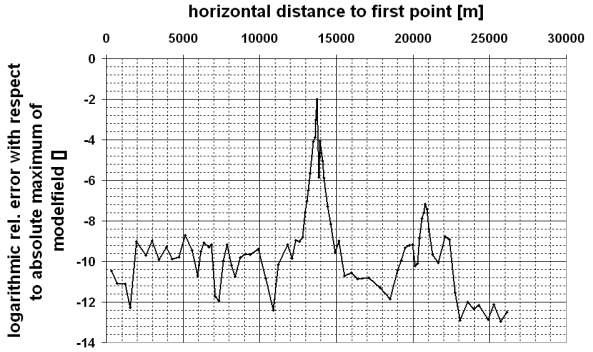


figure 5.1.1.12.12: CS lre ISVD 7 30

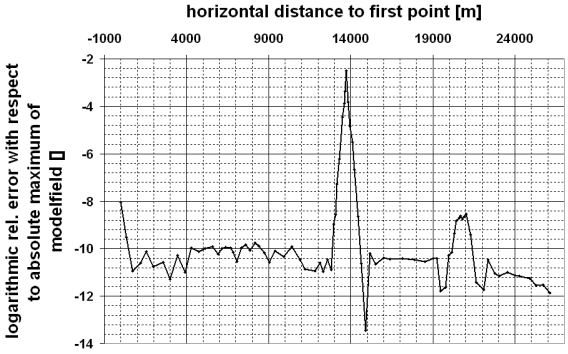


figure 5.1.1.12.13 CS lre Tikhonov / Pasteka

As one can already see at first sight all results, those of Cooper and those of ISVD are oscillating. Even though the amplitudes of the oscillations seen in the ISVD plots are small compared to them of cooper's approaches. All cross-sections also do have in common that there is a peak in the logarithmic relative error at the location of the shallowest anomaly and a smaller peak at the location of the intermediate anomaly.

Both Cooper approaches using 1st vertical derivatives seem to be have a trend inbound in the data (figure 5.1.1.12.3 and figure 5.1.1.12.6).

The mixed-horizontal derivatives in figure 5.1.1.12.4 and figure 5.1.1.12.5 do have a bit better logarithmic relative error but the amplitudes at the location of the shallowest are still increasing to around a thousandth of the model-field maximum. The exchange of filter and field-augmentation seems to make nearly no difference in this two approaches.

The result for the improved 2nd vertical derivative approach in figure 5.1.1.12.1 seem to be the best choice, as the logarithmic relative error seem to be quite small and at the location of the shallowest anomaly is nearly a tenth than that of the ISVD approaches (figure 5.1.1.12.7 to figure 5.1.1.12.12). In these CS it can also be seen how small the difference in the errors is from 7 to 8 Taylor series terms is.

Even though Tikhonov seems to oscillate already close to the source, the amplitudes of these oscillations compared to the ISVD approaches may be a bit smaller at least at the locations where no sources are located. The maximum error amplitudes on the other hand of Cooper's approaches are all at least 10 times smaller but the amplitudes of the oscillations of those approaches are bigger than those of Tikhonov. Therefore Tikhonov may be preferred to ISVD, Cooper and FFT in this case.

5.1.2. Vulcano dataset local part

5.1.2.1. Local fields with 10m x 10m grid including regional part in -50m

The regional part with sampling points at a 100m times 100m grid-spacing and the local part with sampling points at a 10m times 10m grid-spacing together were interpolated at a 10m · 10m grid-spacing using the regional field boundaries.

regional and local field 10m · 10m spacing:
Easting-min: 495870m
Easting-max: 498650m
Northing-min: 4252270m
Northing-max: 4254450m
219 Rows · 279 Lines

The interpolation that took place was based on a Kriging algorithm included in the Software “Golden Software, Surfer Ver. 8”. This small aperture of the whole Vulcano dataset was then downward continued with the different approaches. The local field borders

local field 10m · 10m spacing:
Easting-min: 496360m
Easting-max: 498160m
Northing-min: 4252760m
Northing-max: 4253960m
121 Rows · 181 Lines

were used to extract the local field parts from the downward continued fields. Their was no additional field augmentation done, except for some additional tests for Tikhonov's / Pasteka's algorithm as the standard settings for the Tikhonov algorithm were set by default to 15% field-augmentation with a cosine-taper window. So the results for 0, 15 and 50% field-augmentation with the cosine-taper were plotted here too. Additionally to those tests for the best approach of each ranking the the regional field was exchanged by the linearly interpolating field-augmentation for the ISVD approaches only as the results of Cooper were badly oscillating already with the regional field as field-augmentation assumed. Since Tikhonov's / Pasteka's algorithm used a cosine-taper function for percental field-augmentation distance calculation with respect to the original field size the percental rate was chosen, so that the resulting augmented field had nearly the same amount of nodes, as directional depending field-augmentation was not possible with this algorithm.

For all other approaches tested here the regional part may be assumed as the augmented part, gained from some high sophisticated method for field augmentation. This should be an investigation on the stability of the different approaches when continuing to depth deeper than the used sampling interval of 10m · 10m but with an additional regional field part around. For a better comparison the one chosen depth is the same one as used in the earlier mentioned 100m · 100m grid of Vulcano's dataset (-50m). The whole field including the regional and local field part can be seen in figure 2.1.3.2.

Furthermore it should be remembered here that the used algorithm for Tikhonov's / Pasteka's approach included a field augmentation process with a cosine-taper. This taper was used to get different approaches with field-augmentation of the regional field including local part to get three different fields for downward field continuation. 1.) no additional field-augmentation, 2.) additional 15% field-augmentation (standard setting) and 3.) additional 50% field augmentation with respect to the regional field size.

The used model-field gained from a regional and a local part with different grid spacings, was interpolated at a common 10m grid-spacing interval. The regional field data had sampling-points only at 100m grid-spacing interval and so there are interpolation errors made by the used Kriging interpolation in the regional part as well as smaller errors in the local part, compared to the exactly calculated field.

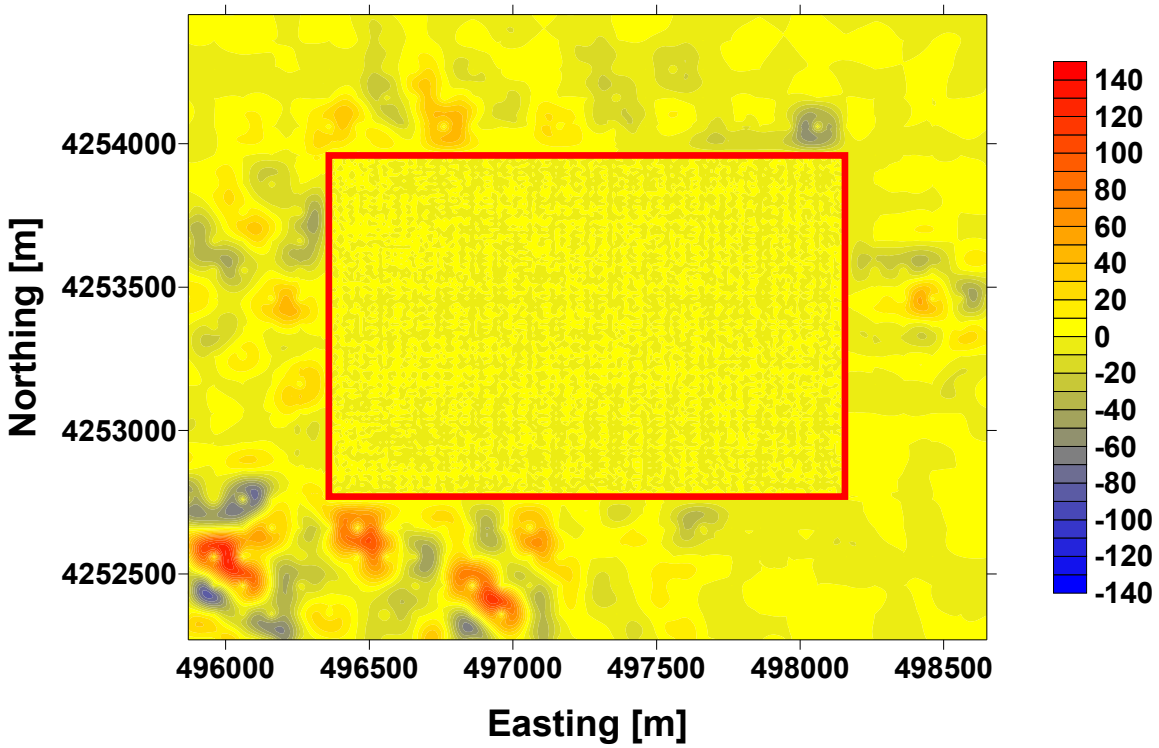


figure 5.1.2.1.1 Error of Kriging interpolation in 0m. The red rectangle marks the local/regional field boundary. Scale bar in nT.

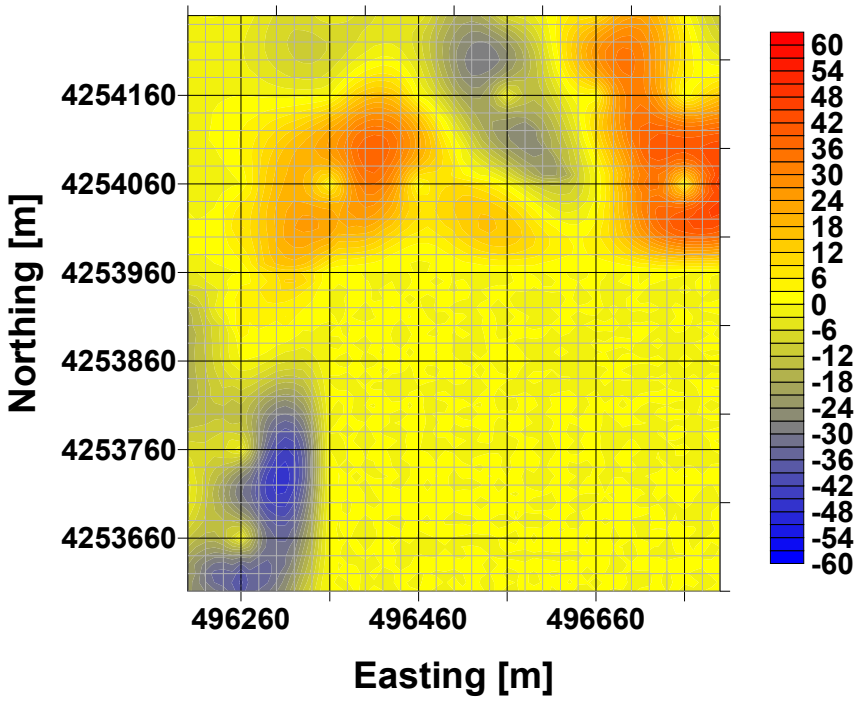


figure 5.1.2.1.2 The black lines mark the 100m grid, the grey lines mark the 10m grid. Upper left corner of the model-field. The biggest errors are in the regional part. Smaller errors are also in the local part of around ± 3nT.

Kriging causes high frequent content in the regional as well as local part as can be seen

by comparing grid-locations of the 10m grid with direction changes of the isolines. There are changes of direction of those isolines between the interpolation points which is caused by this interpolation. This high frequent content is downward continued too in the following tests.

Even further tests (not shown here) have turned out that by replacing the Kriging interpolated data in the local part the true data leads to strong gradients at the boundaries of the local field. This would have been downward continued too. Another reason is that real world data is never measured and therefore available on a perfectly equidistant spaced grid, in a regional area or even the local area of interest and therefore needs to be interpolated to a equidistant spaced grid in some way. Therefore this option was discarded. So interpolation is always a part of process for the here tested methods.

Therefore it was decided to accept the errors made by the Kriging interpolation and use the completely Kriging interpolated field for the following tests.

Further on only the local part of that field will be discussed as this will be the area of interest for real field operations if one of the following approaches emerges to be stable enough. All Scale bars are in nT.

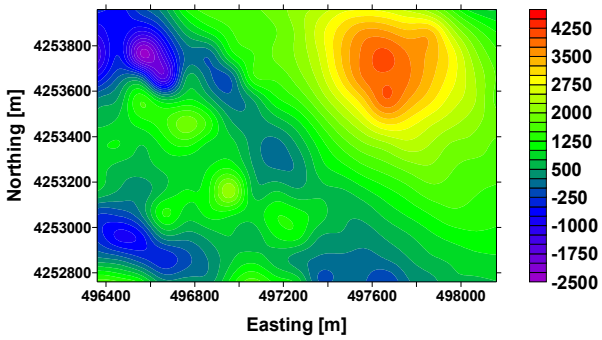


figure 5.1.2.1.3: local part of the model-field with 10m · 10m sampling interval in -50m.

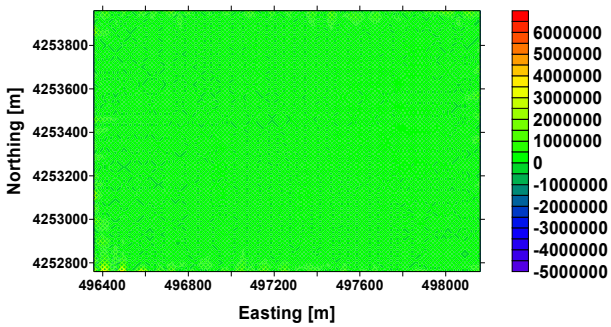


figure 5.1.2.1.4: Cooper approach impBS3af

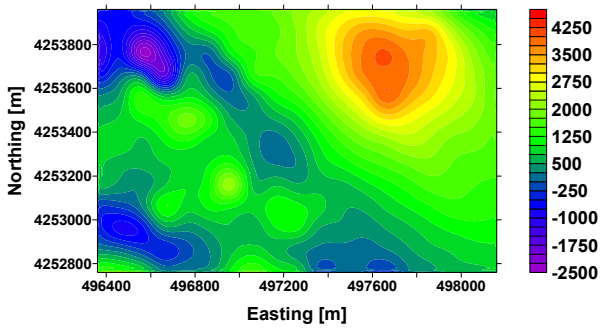


figure 5.1.2.1.5: ISVD 4 30

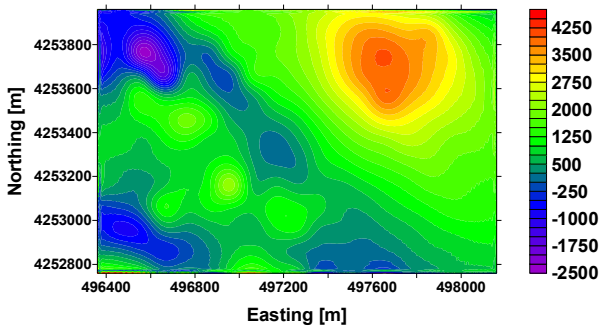


figure 5.1.2.1.6: ISVD 6 30

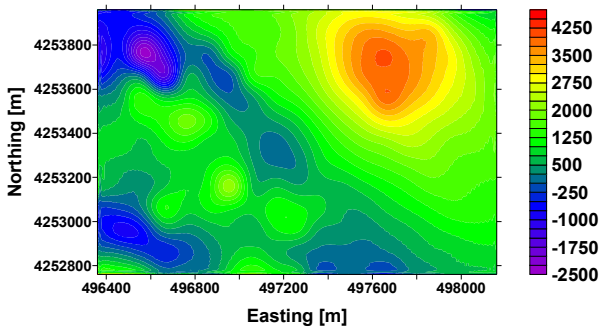


figure 5.1.2.1.7: ISVD 5 30

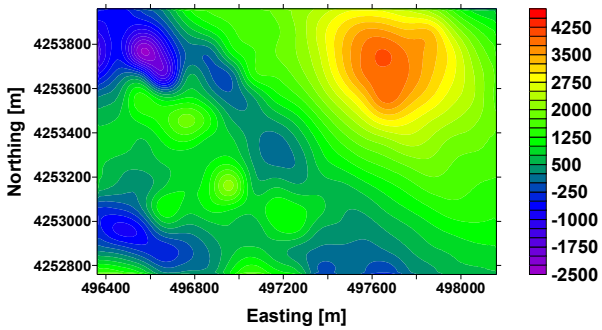


figure 5.1.2.1.8 ISVD 3 30

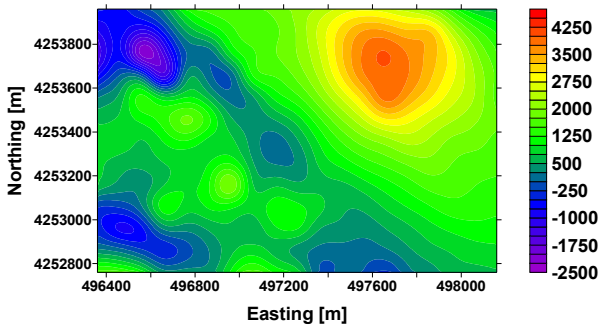


figure 5.1.2.1.9: ISVD 2 30

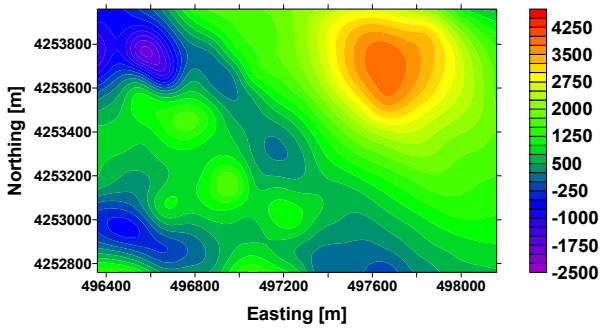


figure 5.1.2.1.10: ISVD 1 30

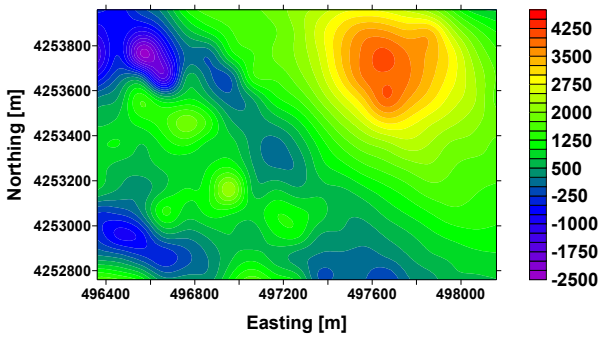


figure 5.1.2.1.11: local part of the model-field with 10m · 10m sampling interval in -50m.

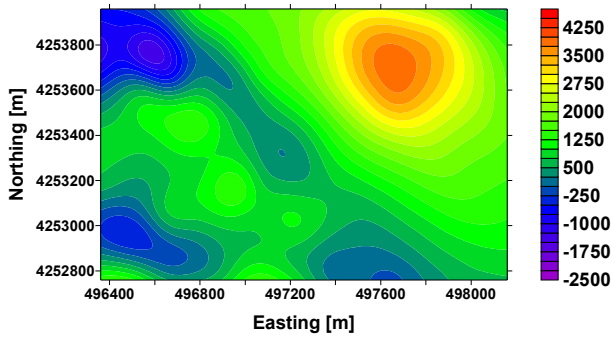


figure 5.1.2.1.12 Tikhonov without field-augmentation

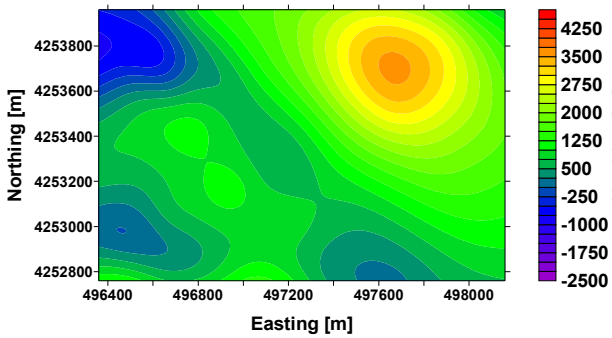


figure 5.1.2.1.13 Tikhonov with 15% field-augmentation (standard setting)

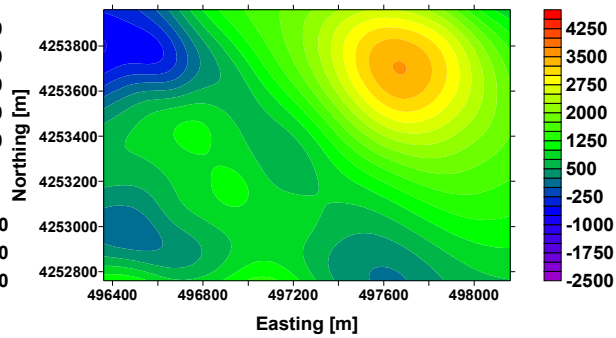


figure 5.1.2.1.14 Tikhonov with 50% field-augmentation

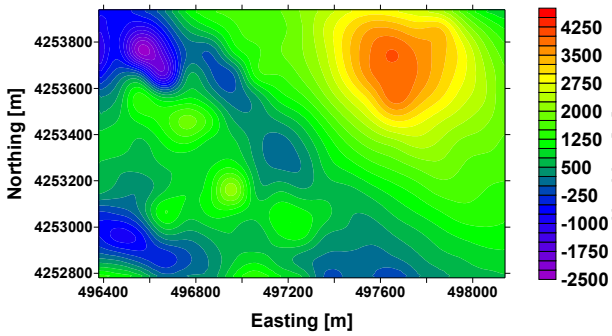


figure 5.1.2.1.15 ISVD 4 30 (regional part exchanged by linear field augmentation to same field size like regional field)

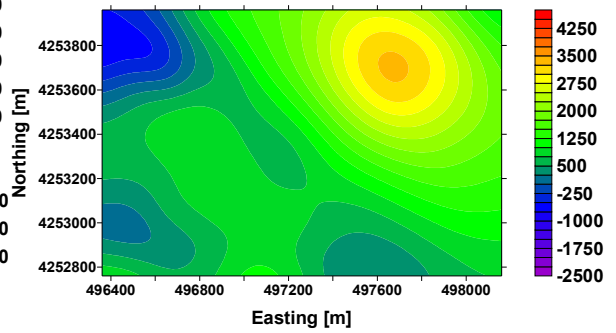


figure 5.1.2.1.16 Tikhonov with 67% field augmentation (corresponds to same amount of nodes like regional field + local field)

Comparing the model-field in figure 5.1.2.1.3 with the approach field of Cooper in figure 5.1.2.1.4 of course reveals at first, there is a remarkable big difference in the scale bar of figure 5.1.2.1.3 compared to that of figure figure 5.1.2.1.4. The other best five Cooper / FFT approaches behave like the on shown above. Therefore this best one in the ranking is discussed here by proxy for all the other Cooper / FFT approaches. In fact all the Cooper approaches include a strong oscillating character. As there is such a big difference between model-field and Cooper's approaches the error of Cooper's best approach for this case will only be displayed in histogram form with a bin width of 100

nT. Further will there be a discussion on the two best filters used and if those big errors may originate from them on page 92ff, “Discussion: Disastrous results of Cooper's approaches when regional field is used for augmentation“. Nevertheless will there be a discussion on the later results of Cooper's approaches where the 100m · 100m grid of Vulcano were used in chapter 5.1.4..

As for the ISVD approaches of Fedi and Florio shown in figure 5.1.2.1.9 to figure 5.1.2.1.7 one can tell that they look far more better than the Cooper approaches. On the other side the first three ISVD approaches look white stable even at the edges but in exchange the details within the local field have vanished partly. Further discussion in the next chapter will show more clearly where the biggest errors occur.

5.1.2.2. Errors, local area. 10m · 10m sampling interval in -50m.

All scale bars are in nT.

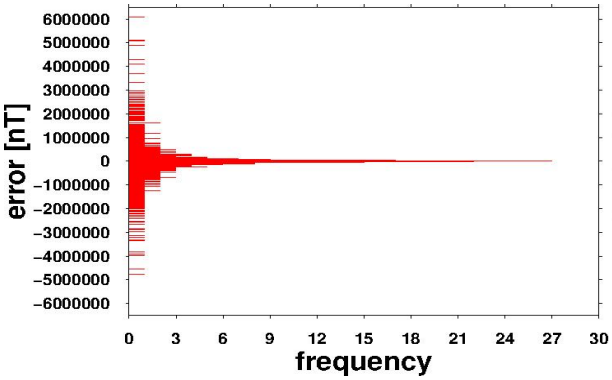


figure 5.1.2.2.1: error distribution Cooper approach impBS3af, bin width 100nT

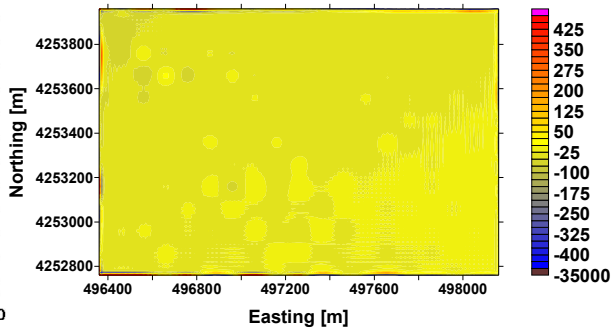


figure 5.1.2.2.2: error ISVD 4 30

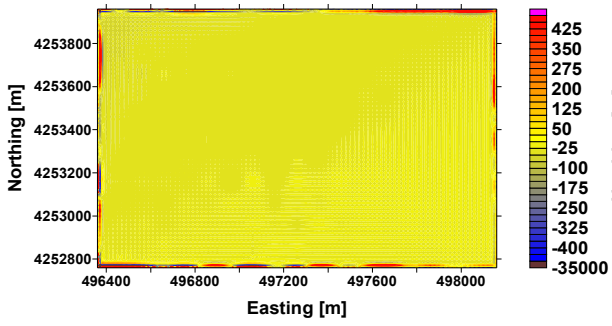


figure 5.1.2.2.3: error ISVD 6 30

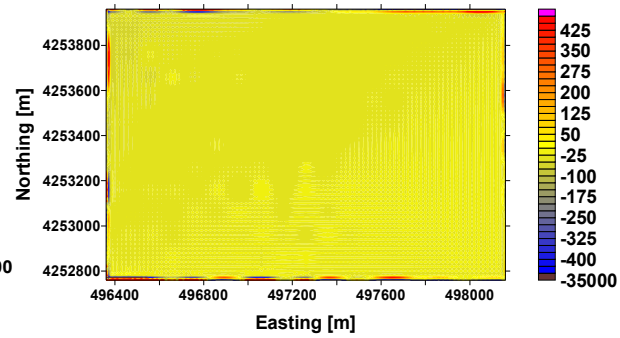


figure 5.1.2.2.4: error ISVD 5 30

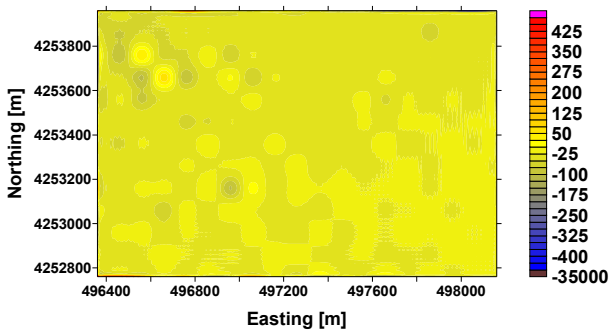


figure 5.1.2.2.5 error ISVD 3 30

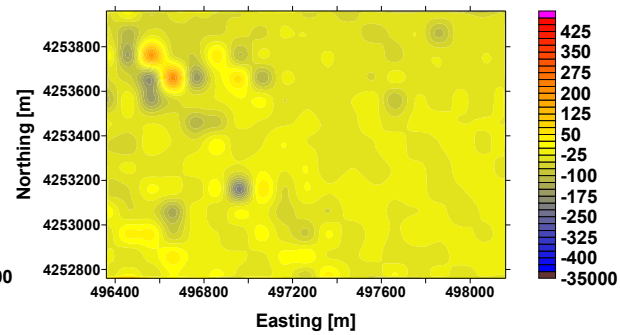


figure 5.1.2.2.6: error ISVD 2 30

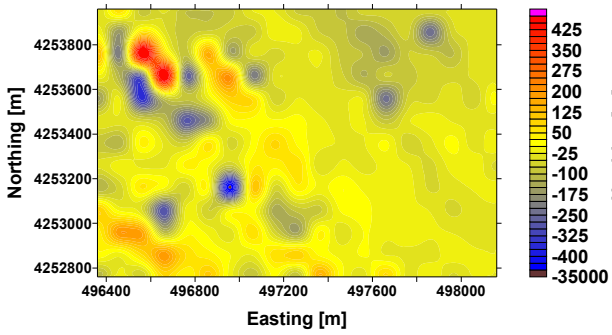


figure 5.1.2.2.7: error ISVD 1 30

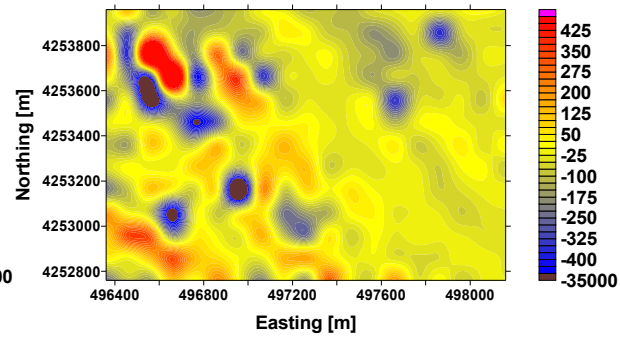


figure 5.1.2.2.8 error Tikhonov without field-augmentation

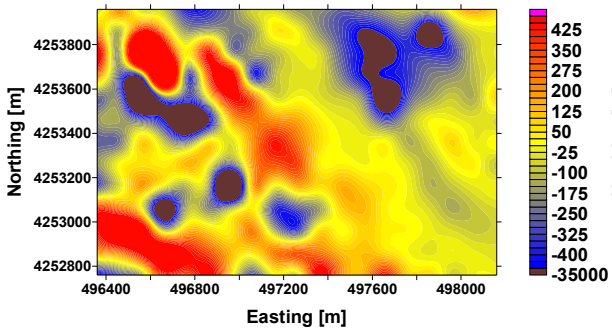


figure 5.1.2.2.9 error Tikhonov with 15% field-augmentation (standard setting)

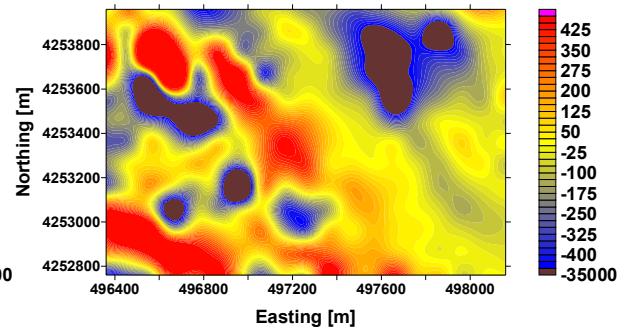


figure 5.1.2.2.10 error Tikhonov with 50% field-augmentation

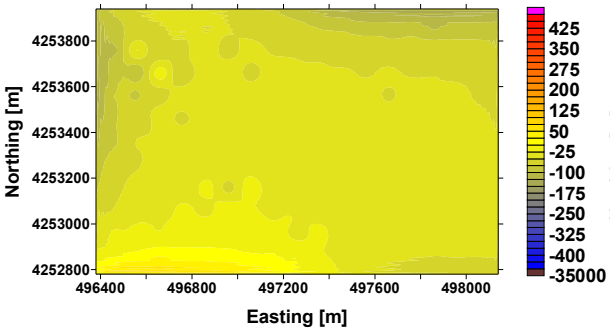


figure 5.1.2.2.11 error ISVD 4 30 (regional part exchanged by linear field augmentation to same field size like regional field)

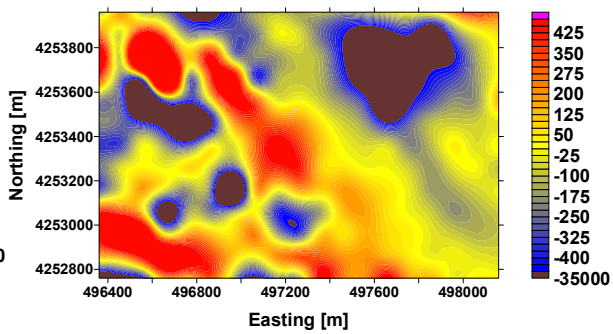


figure 5.1.2.2.12 error Tikhonov with 67% field augmentation (corresponds to same amount of nodes like regional field + local field)

As was mentioned earlier the errors of all Cooper approach are wide out of range (see figure 5.1.2.1.4) even of the used model field in figure 5.1.2.1.3 and of course the oscillations are spread over the whole local field. For these reasons there will be no further discussion on the Cooper approaches except for the according used filters (2nd vertical derivative, 1st vertical derivative, etc.) as these errors may origin from them. It should only be mentioned that the histogram of the cooper approaches seem to be nearly a Gaussian and so very likely to be random distributed which would fit the oscillating character of the cooper results. The displayed histogram is typical for all the other Cooper approaches not shown here too. The most errors occur around 0 nT but even with this chosen small bin width there are already a lot of bigger errors visible in this histogram. The remaining histograms of the cooper approaches not shown, only differ to the one displayed through their lower amount of errors around 0nT.

ISVD 3 30,ISVD 2 30 and ISVD 1 30 are the only one which show major errors in the inner part of the local field.

figure 5.1.2.2.2 showing the ISVD 4 30 has a still acceptable stable behaviour at the edges as their magnitudes are small. Compared to figure 5.1.2.2.11 showing the other approach with 4 Taylor series terms the regional field seams to improve the approach at least at the edges of the local field part. The “high-sophisticated” field-augmentation approach in figure 5.1.2.2.2 showing the error of the more inner part of the field tends to be zero or a negative value in a range of -50 to -100 nT. This may be the best choice. One may see that there is a difference between Fedi's and Florio's suggested amount of Taylor series terms- Fedi and Florio proposed to use around 7 terms to get a appropriate and a result which has a acceptable non oscillation character. -. This is maybe caused by the additional regional field used to downward continue the model-field plus regional part. If one should have to chose between regional field data for field-augmentation and linearly interpolating between the boundary values regional field should definitely be preferred at least when ISVD is used for downward field-continuation.

figure 5.1.2.2.3 shows the error of ISVD 6 30. As expected there are stronger edge effects compared to figure 5.1.2.2.2 but as can be seen in the following chapter with the advancement in the more inner part of the field. One may take this on account when using ISVD approach under similar circumstances.

figure 5.1.2.2.4 looks quite similar to figure 5.1.2.2.3 but there are some differences visible at the edges were strongest oscillations appear. Further investigation through 2D cross-sections in the following chapter will show more clearly on what costs the difference of one Taylor series term will be balanced.

Of course figure figure 5.1.2.2.7 and figure 5.1.2.2.6 are quite stable but the immense cost of accuracy at the more inner part of the field seems to be quite irritating.

Although Tikhonov's / Pasteka's standard settings used an additional field-augmentation the errors made in the local area are severe. The additional tests with the included cosine-taper field-augmentation in Dr. Pasteka's algorithm used 1.) no field-augmentation and 2.) 50% field-augmenation too. Here can be seen the big errors made by the too strong regularization even though it is at least better than the errors made by Cooper. Interesting too is the better result without any field-augmentation. It looks like that additional field-augmentation leads to stronger regularization than no field-augmentation in this case. Maybe a starting point for further investigations. Additionally the Tikhonov approach using 67% field-augmentation distance with respect to the local field size turns out to be even worse than the Tikhonov approach using 50% field-augmentation with regional field.

5.1.2.3. 2D cross-sections of error fields in -50m

Location of starting point for cross-section.: 496684 East, 4252892 North

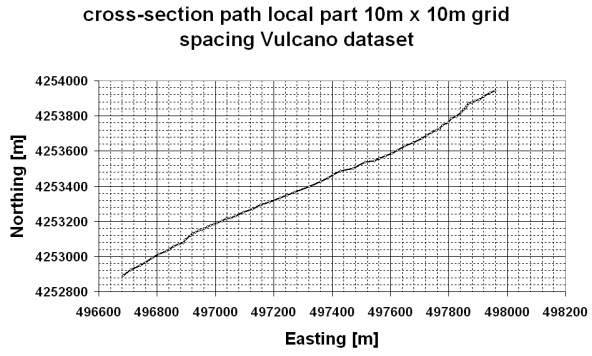


figure 5.1.2.3.1: cross-section path for local field in Vulcano without regional field part.

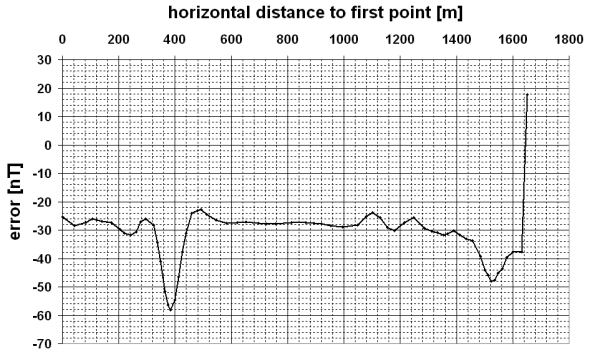


figure 5.1.2.3.2: CS error ISVD 4 30

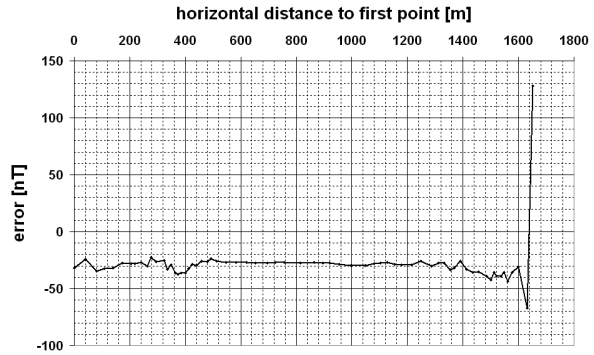


figure 5.1.2.3.3: CS error ISVD 6 30

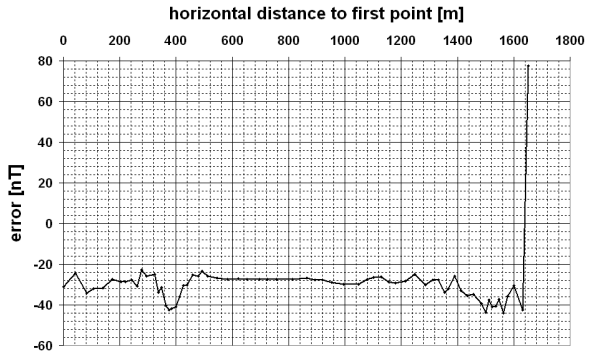


figure 5.1.2.3.4: CS error ISVD 5 30

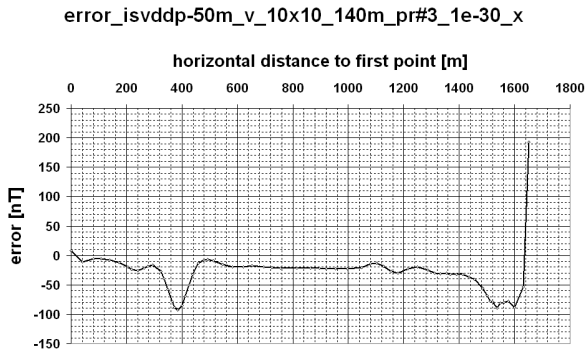


figure 5.1.2.3.5 CS error ISVD 3 30

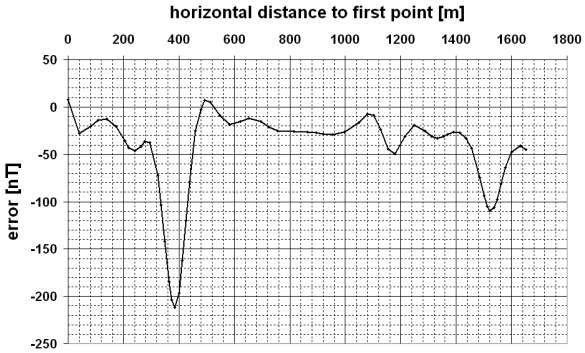


figure 5.1.2.3.6: CS error ISVD 2 30

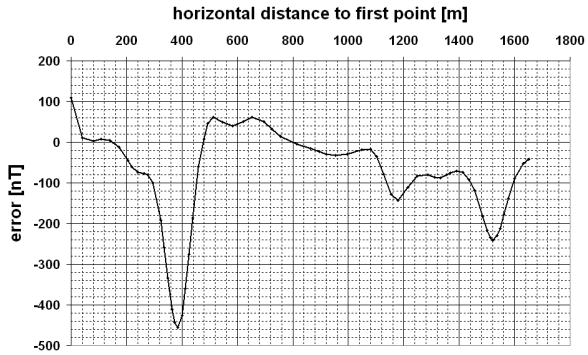


figure 5.1.2.3.7: CS error ISVD 1 30

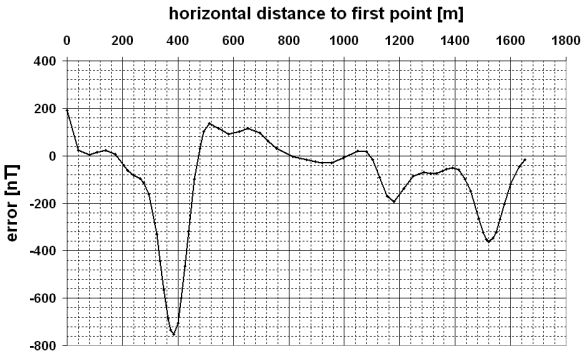


figure 5.1.2.3.8 CS error Tikhonov without field-augmentation

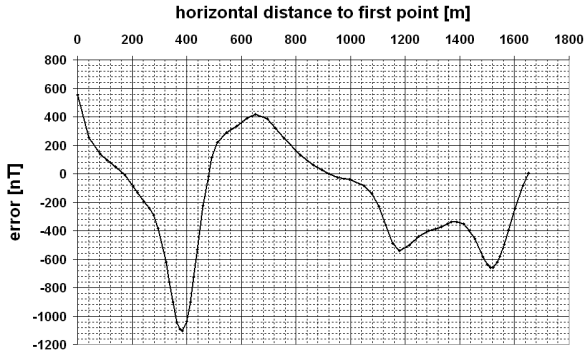


figure 5.1.2.3.9 CS error Tikhonov with 15% field-augmentation

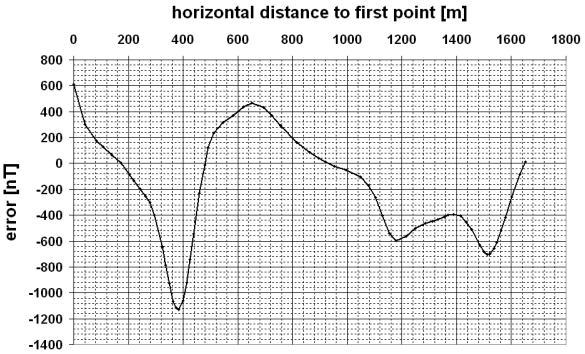


figure 5.1.2.3.10 CS error Tikhonov with 50% field-augmentation

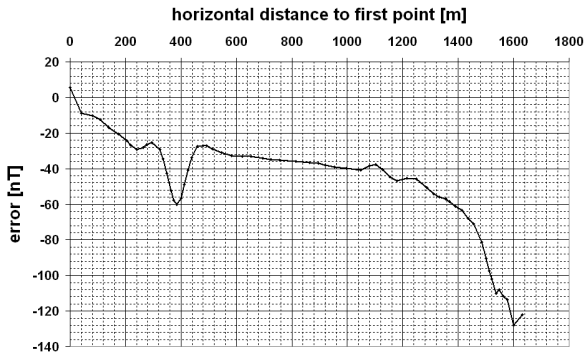


figure 5.1.2.3.11 CS error ISVD 4 30 (regional part exchanged by linear field augmentation to same field size like regional field)

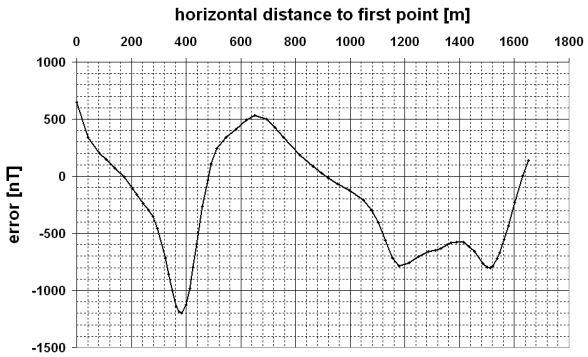


figure 5.1.2.3.12 CS error Tikhonov with 67% field-augmentation (corresponds to same amount of nodes like regional field + local field)

figure 5.1.2.3.7, figure 5.1.2.3.6 (ISVDs) and figure 5.1.2.3.8 (Tikhonov) do have a common typical error structure inbound. A more or less dominant peak at the location of the model-field maximum. One can check this for oneself by checking the according coordinates at 4253160 North and 496960 East. So this turns out to be a typical effect of ISVD and Tikhonov too which is very interesting. If there is a positive peak at the model-field then there is a negative peak at the error-field data at the same location. The shallower the source of this peak is in the model-field the stronger is the negative peak in the error-field.

ISVD 4 30 (figure 5.1.2.3.2)here again turns out to be very stable albeit there is a major peak at the north-eastern end which is most likely caused by edge effects.

figure 5.1.2.3.3 and figure 5.1.2.3.4 look quite stable but do have a strong peak in the error cross-section at the right / north-eastern end of the cross-section. It is obvious that the increasing amount of terms used for ISVD minimizes the errors in the inner part of the field albeit edge effects like oscillations increase with increasing amount of terms used when a dataset with regional field information is used for field continuation.

As all ISVD approaches tend to have oscillations inbound as well as the Cooper approaches – but Cooper's are wide out of range – ISVD with 4 terms used (figure 5.1.2.3.2) seems to be a good compromise between stability and accuracy, as 5 terms seem to increase edge effecting oscillation too much (figure 5.1.2.3.4)and 3 terms decreases accuracy for the fields produced. This all should be mentioned under the premiss that a regional field was downward continued too and only the local part is of interest.

In the CS of the ISVD 4 30 with linear interpolating field-augmentation used instead of the regional field there is a clear trend visible in the local field data. That is consistent with error plot too, where the field at the southern end seems to be a bit bigger than that at the northern one. The magnitude of the error range is definitely around 60% bigger compared to the regional field version.

The three Tikhonov approaches left all do have results that are overregularized compared to the better ISVD approaches. Very interesting is the fact that with increasing amount of field-augmentation distance the magnitude of the error-range seems to increase too, regardless if regional field information is used or cosine-taper is applied to local field boundaries. In fact the earlier mentioned Tikhonov / Pasteka approach using no field-augmentation but with regional field information delivers the best Tikhonov / Pasteka result.

5.1.2.4. Relative errors of local field in -50m.

All scale bars are dimensionless.

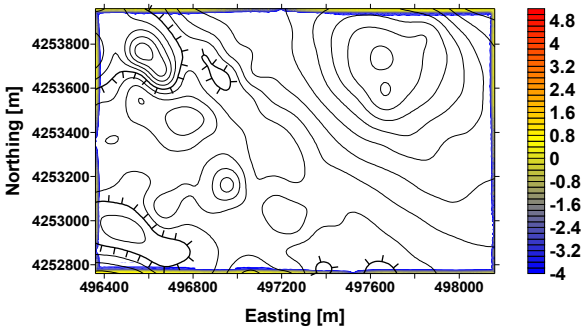


figure 5.1.2.4.1: lre ISVD 4 30

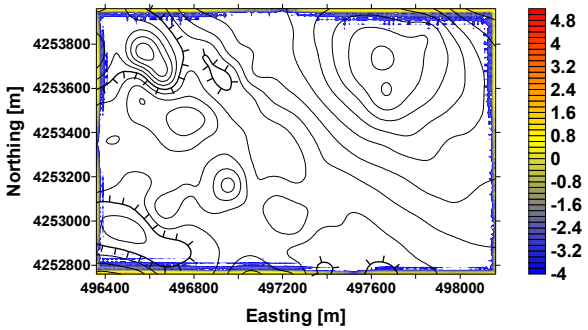


figure 5.1.2.4.2: lre ISVD 5 30

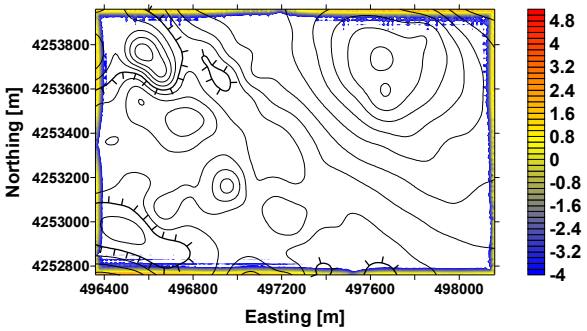


figure 5.1.2.4.3: lre ISVD 6 30

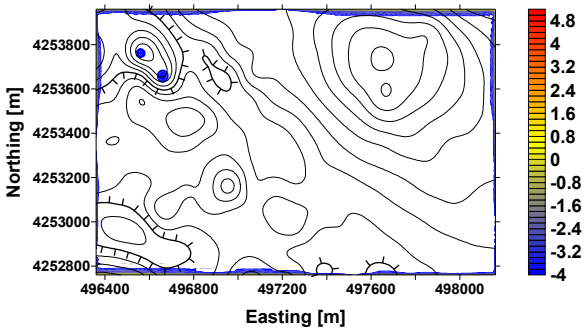


figure 5.1.2.4.4 lre ISVD 3 30

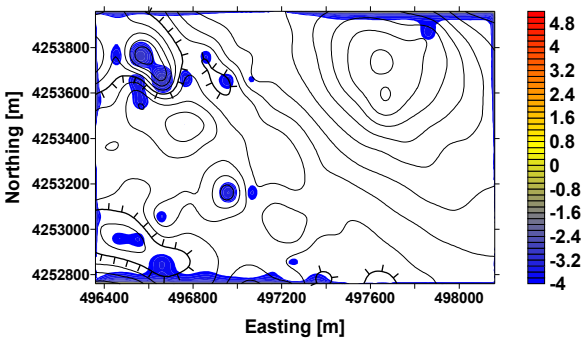


figure 5.1.2.4.5: lre ISVD 2 30

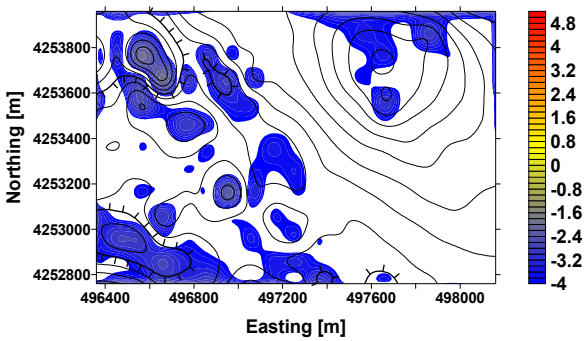


figure 5.1.2.4.6: lre ISVD 1 30

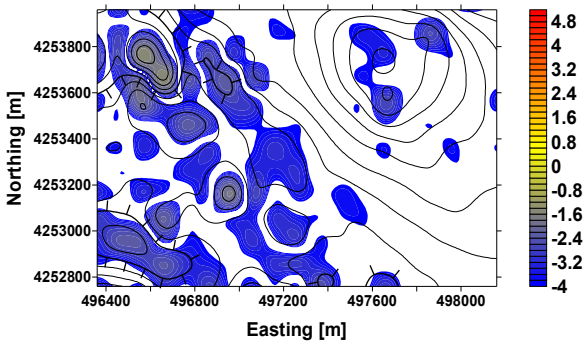


figure 5.1.2.4.7 lre Tikhonov without field-augment

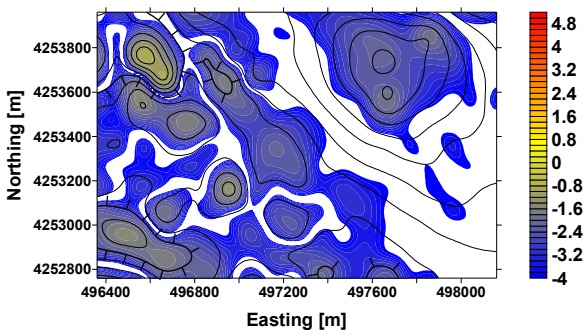


figure 5.1.2.4.8 lre Tikhonov with 15% field-augmentation

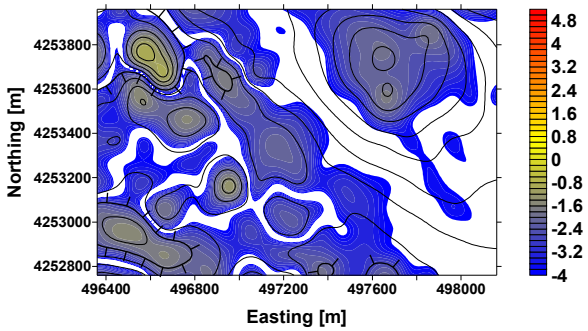


figure 5.1.2.4.9 lre Tikhonov with 50% field-augmentation

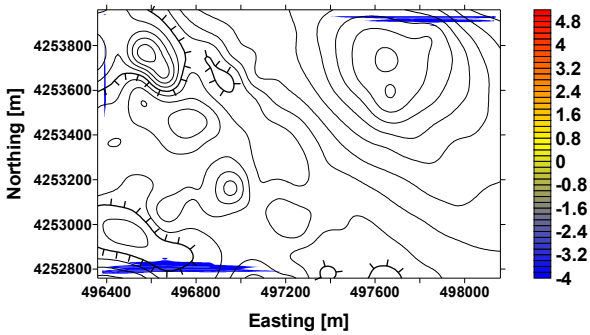


figure 5.1.2.4.10 lre ISVD 4 30 (regional part exchanged by linear field augmentation to same field size like regional field)

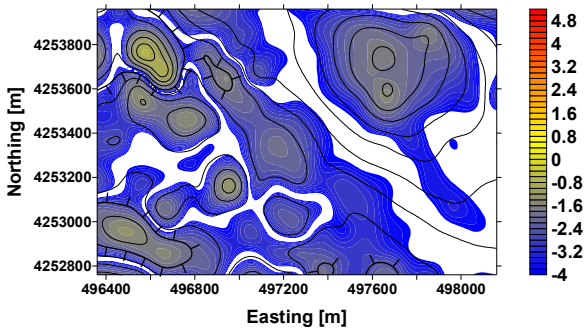


figure 5.1.2.4.11 lre Tikhonov with 67% field-augmentation (corresponds to same amount of nodes like regional field + local field)

Again viewing the relative errors of the different approaches turns out to be a good solution to compare the results for oscillation effects. Here it is obvious why 4 terms (figure 5.1.2.4.1) should be preferred to 5 and 6 terms (figure 5.1.2.4.2 figure 5.1.2.4.3). One is may able to see why ISVD 4 30 in figure 5.1.2.4.1 reveals the best choice with such a continuation depth, field augmentation technique and given data point spacing. All other approaches do have to big errors in the inner area or oscillations dominate at the boundaries.

figure 5.1.2.4.7 again depicts that the biggest errors occur in the areas of interest at the locations where the biggest anomalies existed. Therefore Tikhonov / Pasteka should not be preferred when field parameters are comparable to those used here to the ISVD approaches. Very interesting though is the nearly same result for Tikhonov with standard field-augmentation settings and for Tikhonov with 50% field-augmentation. This can be explained in the following way. The biggest errors occur in both approaches at the same locations and with nearly the same magnitude. On the contrary the smallest errors differ a lot (which can't be seen in this plots here caused by the adapted scale bar to fit the other approaches more accurately). The smallest errors with the standard

settings are around ten thousand times smaller than those made with 50% field-augmentation.

5.1.2.5. 2D cross-sections of relative errors local field in -50m

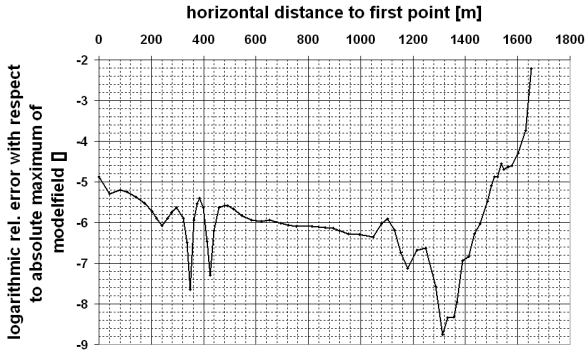


figure 5.1.2.5.1: CS lre ISVD 4 30

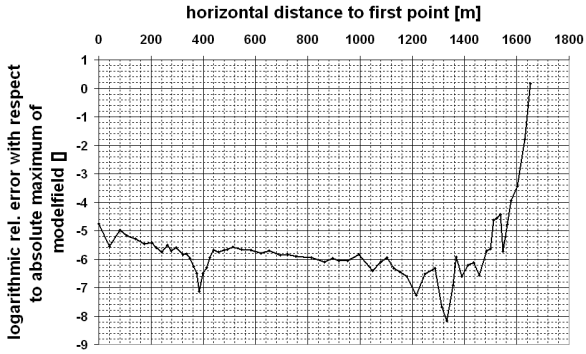


figure 5.1.2.5.2: CS lre ISVD 6 30

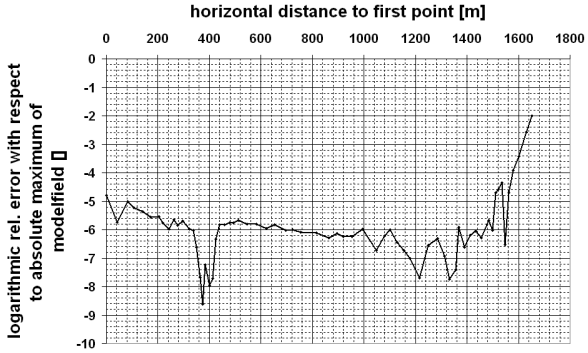


figure 5.1.2.5.3: CS lre ISVD 5 30

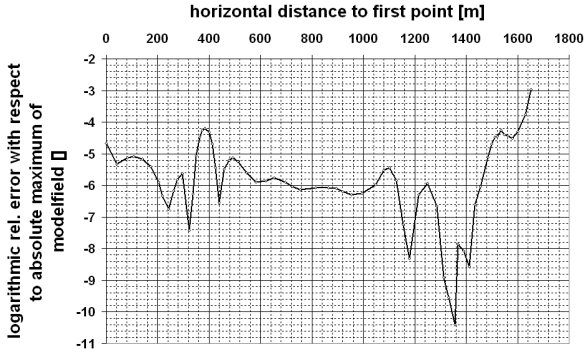


figure 5.1.2.5.4 CS lre ISVD 3 30

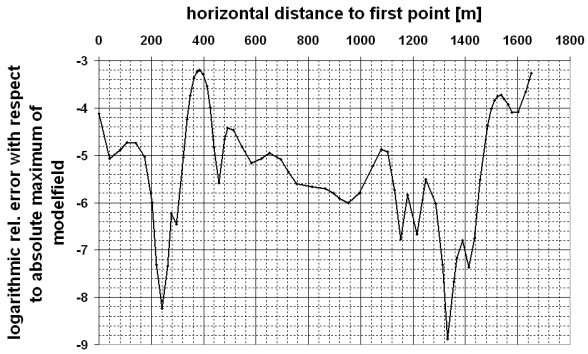


figure 5.1.2.5.5: CS lre ISVD 2 30

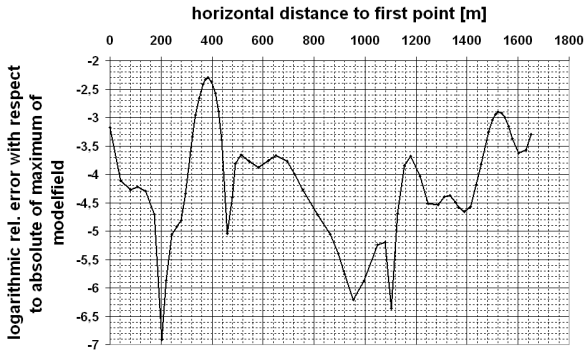


figure 5.1.2.5.6: CS lre ISVD 1 30

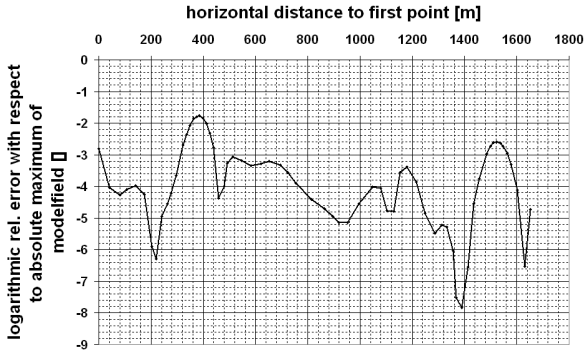


figure 5.1.2.5.7 CS lre Tikhonov without field-augmentation

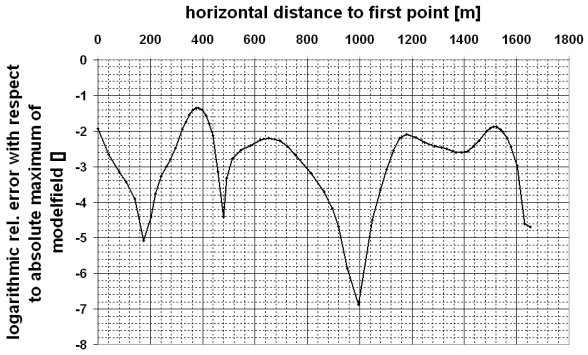


figure 5.1.2.5.8 CS lre Tikhonov with 15% field-augmentation

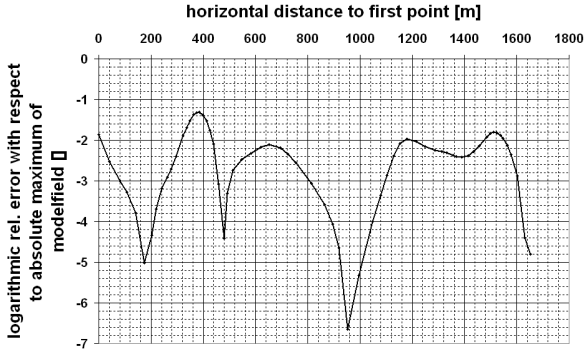


figure 5.1.2.5.9 CS lre Tikhonov with 50% field-augmentation

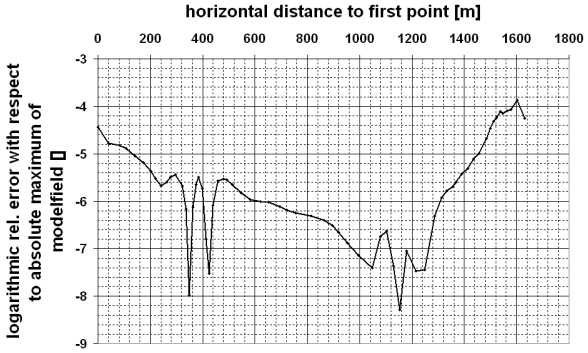


figure 5.1.2.5.10 CS lre ISVD 4 30 (regional part exchanged by linear field augmentation to same field size like regional field)

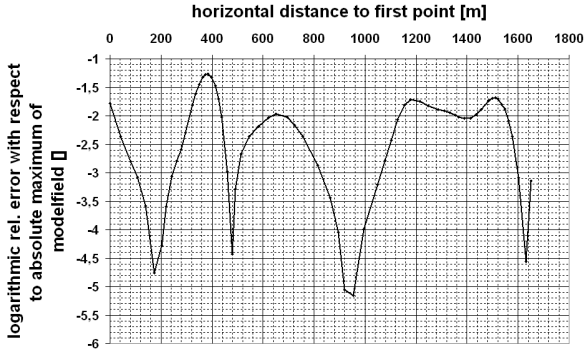


figure 5.1.2.5.11 CS lre Tikhonov with 67% field-augmentation (corresponds to same amount of nodes like regional field + local field)

Of course the logarithmic relative error cross-sections shown in figure 5.1.2.5.6 and figure 5.1.2.5.5 are worse than then most of the other approaches and the 6 Taylor series terms approach is the best in the inner part also in oscillates obviously and has just a big peak at the north-eastern edge most likely be caused by oscillations from edge effects. ISVD 4 30 (figure 5.1.2.5.1) and ISVD 5 30 (figure 5.1.2.5.3) seem to have a slightly less oscillation influenced outer area than the 6 terms approach. ISVD 4 30 using regional field information therefore seems to be the best choice here.

The remaining ISVD approaches all seem to have bigger errors in the inner part (ISVD 3 30) or just a trend in dataset (ISVD 4 30 with regional field exchanged by linearly interpolating field-augmentation.)

All the Tikhonov approaches do not seem to oscillate a lot even though the relative errors are big compared to all other ISVD approaches.

5.1.3. Discussion: Disastrous results of Cooper's approaches when regional field is used for augmentation

As there were no classical field augmentation applied at all the results for first field augmented or first filtered approaches were the same.

5.1.3.1. BS3af, BS3fa

Scale bars for figure 5.1.3.1.1, figure 5.1.3.1.2 and figure 5.1.3.1.3are in nT/km^2. Scale bar for figure 5.1.3.1.4 is dimensionless.

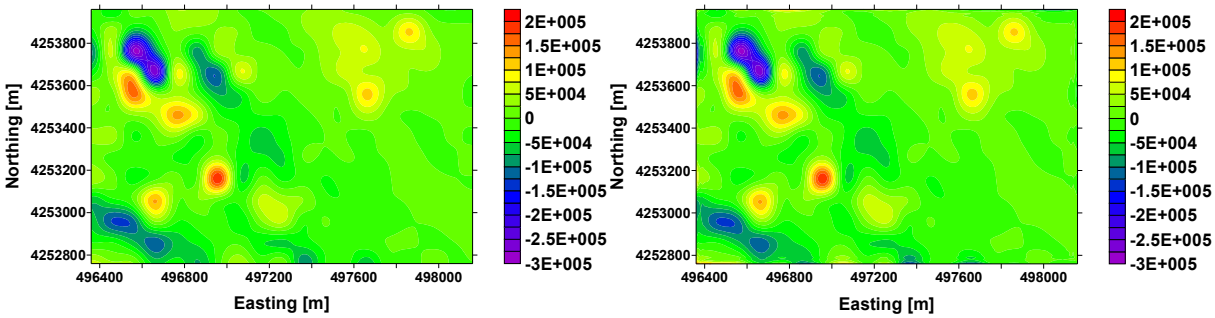


figure 5.1.3.1.1: true derivative

figure 5.1.3.1.2: BS3af / BS3fa derivative

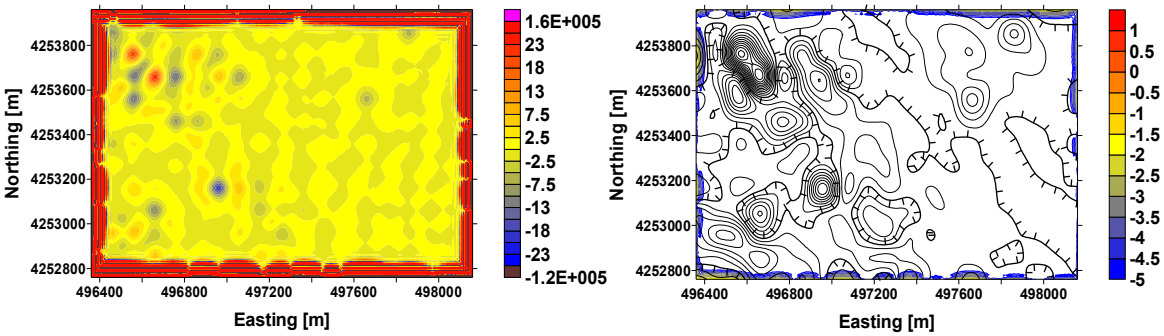


figure 5.1.3.1.3: error BS3af / BS3fa derivative

figure 5.1.3.1.4: lre BS3af / BS3fa derivative

As one can obviously see there are strong oscillation effects at the edges of the local field in figure 5.1.3.1.3 and figure 5.1.3.1.4. These oscillations effects already visible in the filter error will be continued to -50m which explains the results of all Cooper approaches using the 2nd vertical derivative approach.

5.1.3.2. BS4af, BS4fa

Scale bar for Figure 5.1.3.2.1, figure 5.1.3.2.2 and figure 5.1.3.2.3 are in in nT/km.
Scale bar for figure 5.1.3.2.4 is dimensionless.

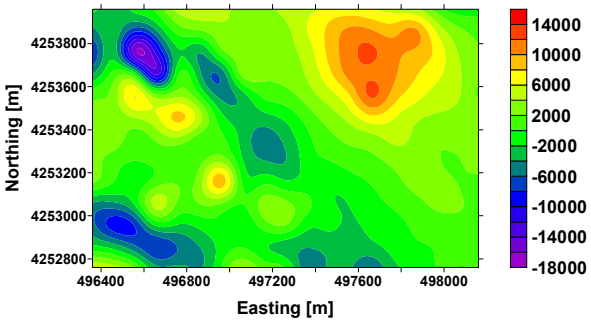


Figure 5.1.3.2.1: true derivative

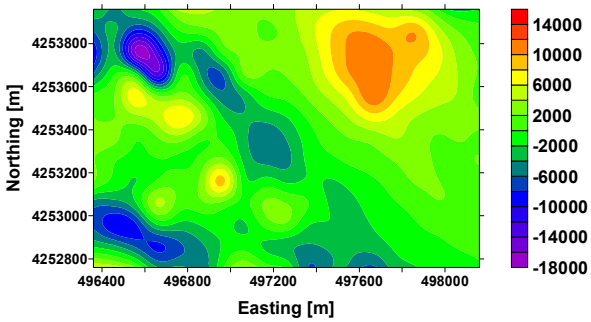


figure 5.1.3.2.2: BS4af / BS4fa derivative

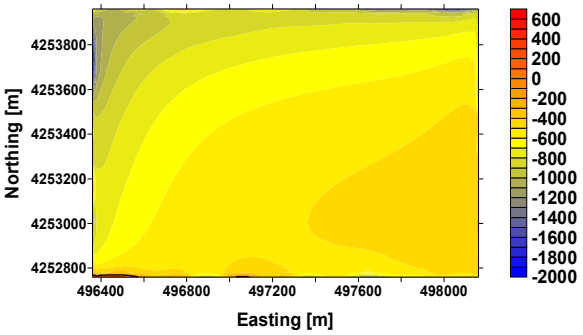


figure 5.1.3.2.3: error BS4af / BS4fa derivative

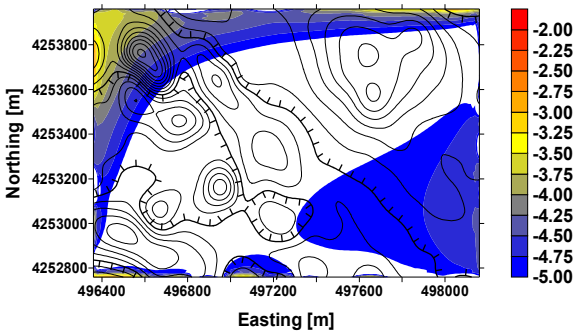


figure 5.1.3.2.4 lre BS4af / BS4fa derivative

Here the oscillation effect at the edge of the local field is nearly not existent but there is still a relatively strong increase in the error at the edges as can be seen in figure 5.1.3.2.4. The errors in the inner part of the local field seem to be small compared to those at the edges of the local field. From this point of view BS4af / BS4fa looks quite stable. Maybe the following investigation on the error of the regional part will help.

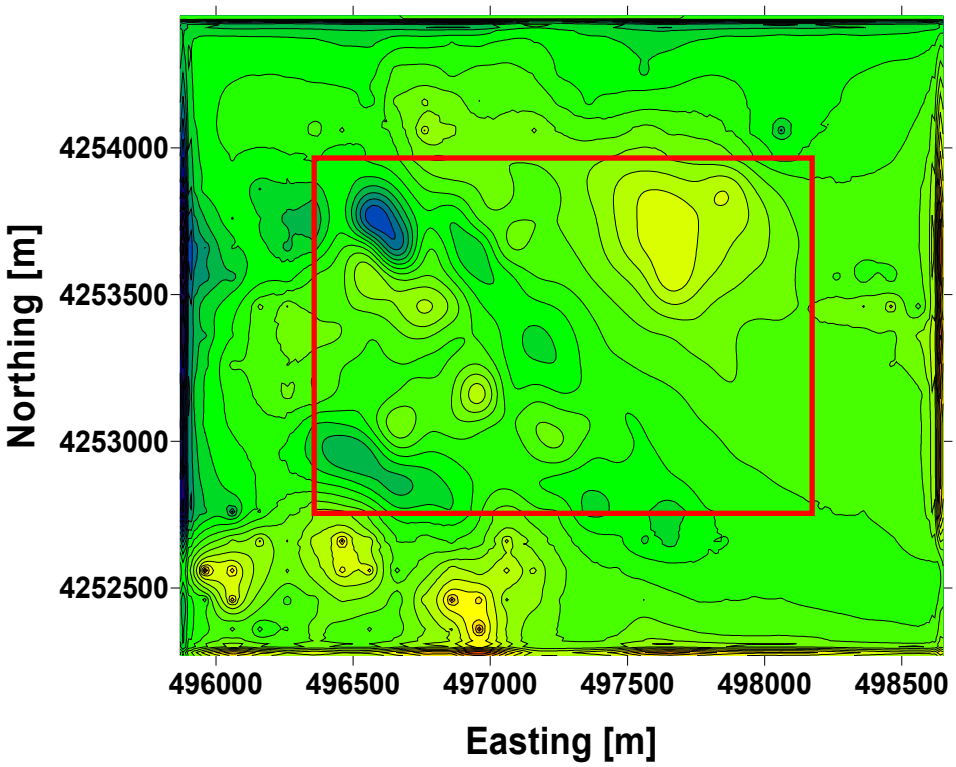


figure 5.1.3.2.5 BS4af / BS4fa derivative including regional part. Scale bar in nT/km

Even if the local field part looks quite stable, the regional part of figure 5.1.3.2.5 is oscillating already and there is a lot of high frequency content inbound in the regional area of the field. Especially the boundaries of the regional field seem to be quite unstable. Furthermore, the field contains some artefacts maybe caused by the used interpolation algorithm in the regional field part. As this is the field which was downward continued all the high frequency content of the regional part was amplified as well. Therefore the error of BS4af / BS4fa was also caused by the vertical derivative used.

5.1.4. Whole Vulcano area

5.1.4.1. Fields continued to -50m. 100m · 100m sampling interval.

All Scale bars in nT.

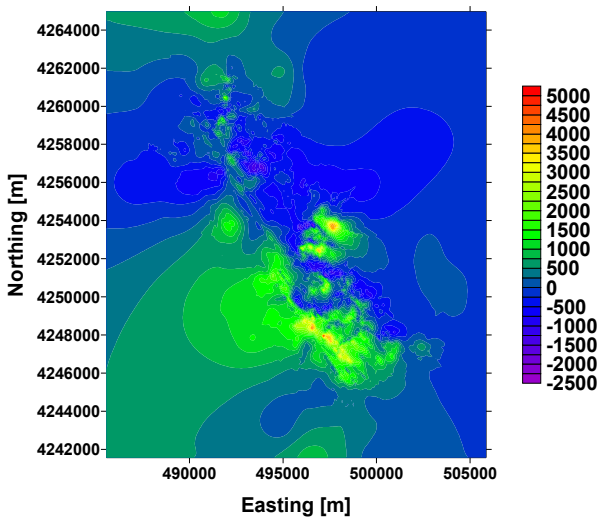


figure 5.1.4.1.1: model-field in 50m depth

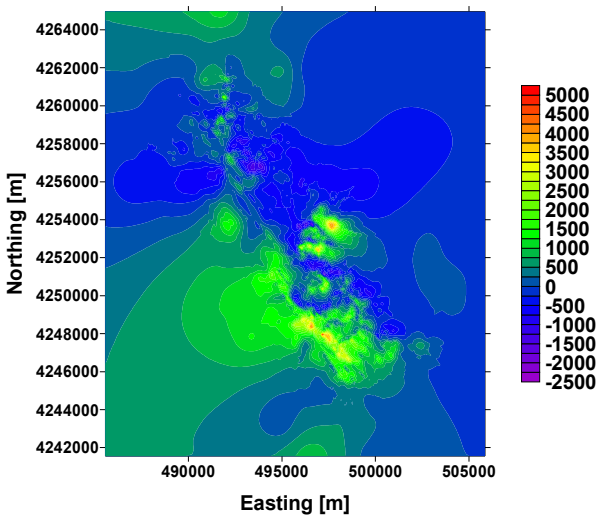


figure 5.1.4.1.2: FFT

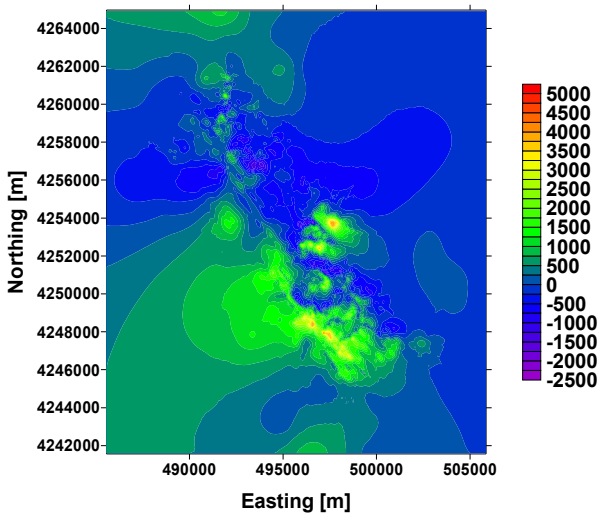


figure 5.1.4.1.3: Cooper approach impFD1af

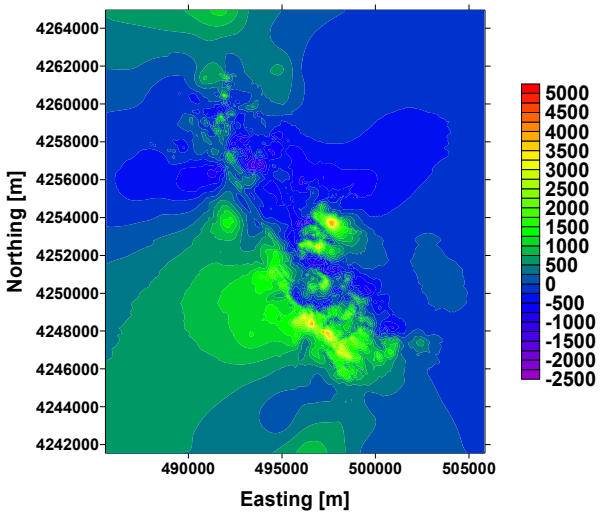


figure 5.1.4.1.4: Cooper approach impFD2af

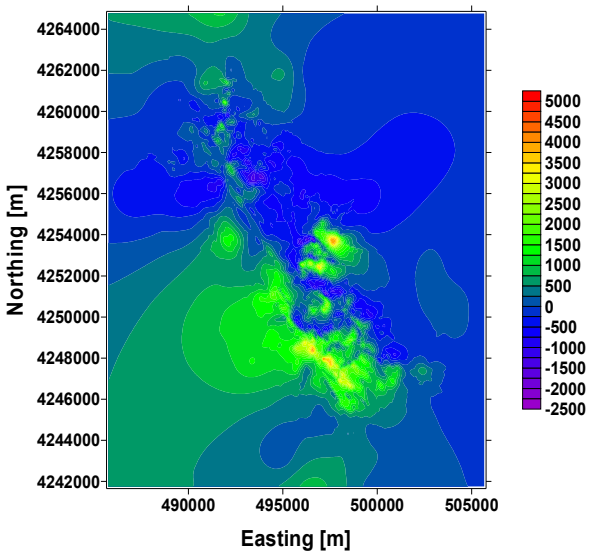


figure 5.1.4.1.5: ISVD 4 30

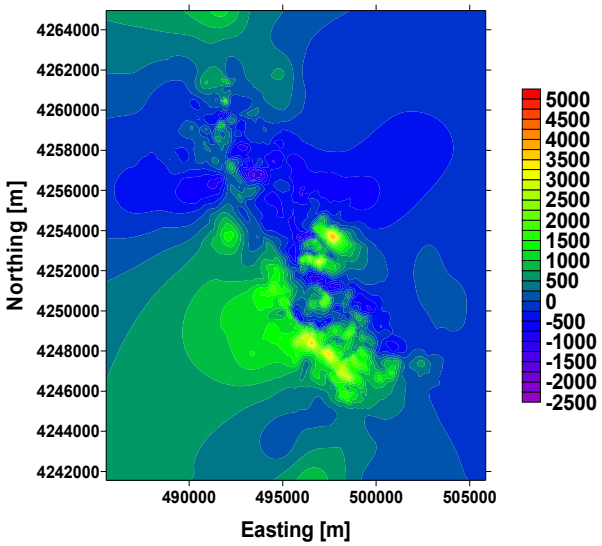


figure 5.1.4.1.6 Tikhonov / Pasteka

Tough these approaches are different the resulting fields are hardly distinguishable from another. Remarkable is also the dominant Cooper finite difference (FD) approach, which is contrary to the results shown in the local field part with 10m · 10m sampling interval, where Coopers bi-cubic splines (BS) dominated - Nevertheless the results of Cooper BS in the local area of the smaller 10m · 10m field where definitely completely useless cause of their oscillating character. Here all results seem to be stable, which is maybe caused by the fact that the downward continuation distance is small compared to the sampling interval in this example. Cooper's approach *impFD1af* and *impFD1fa* look exactly the same as well as Cooper's approach *impFD2af* and *impFD2fa.* Even Cooper's approach *FD2af* is like *impFD2af*. For this reason only the Cooper approaches *impFD1af* and *impFD2af* are shown. All the ISVD approaches look the same, only the field size is different cause of the different amount of terms used for field continuation. For this reason only the first in the ranking is shown here. The rest (*ISVD 6 30*, *ISVD 20 9*, *ISVD 20 4*, *ISVD 20 10* and *ISVD 20 8*) will only be discussed in the following chapters. Remarkable though in the simple model-field the Cooper approaches using Laplace equation to get 2nd and 1st order vertical derivatives dominated the ranking, here not even one such approach is in the ranking of the first six Cooper approaches.

FFT as well as *ISVD 4 30* can't be differed to the used model-field from this point of view.

ImpFD1af is quite similar to the *FFT* result but there are some small differences best seen in south-western direction from the centre of the field between 1000 and 1500 nT in bright green. The curvature of the isoline is a bit more stronger than that of the model-field at location 4250000 north, 492500 east.

ImpFD2af is covered with small artefacts that can be seen at all isolines in the field. Cooper himself mentioned these artefacts in his paper which are perpendicular to the derivation direction used - In this case derivation was in direction west-east. - and in fact the artefacts look like some high-frequency noise which leads to small “steps” in the north-south direction.

There seems to be no remarkable difference between the Tikhonov / Pasteka approach and the model-field. May the error plots reveal some major differences.

5.1.4.2. Errors of the different approaches in -50m. Sampling interval 100m · 100m.

All Scale bars in nT.

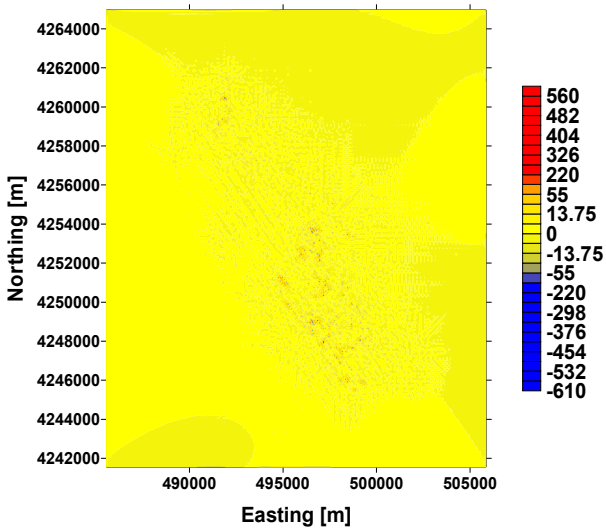


figure 5.1.4.2.1: error FFT

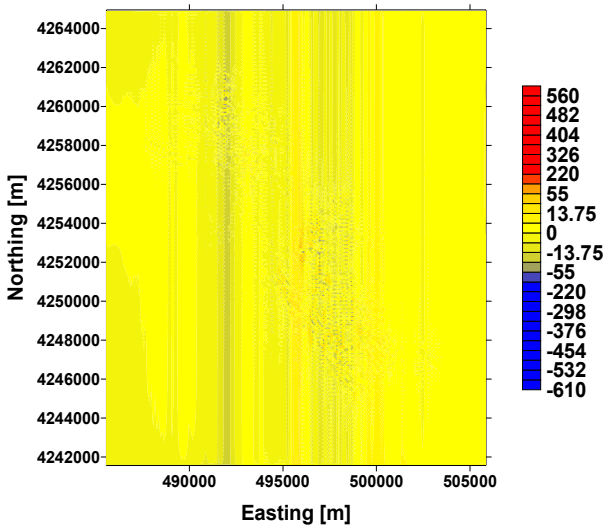


figure 5.1.4.2.2: error Cooper approach impFD1af

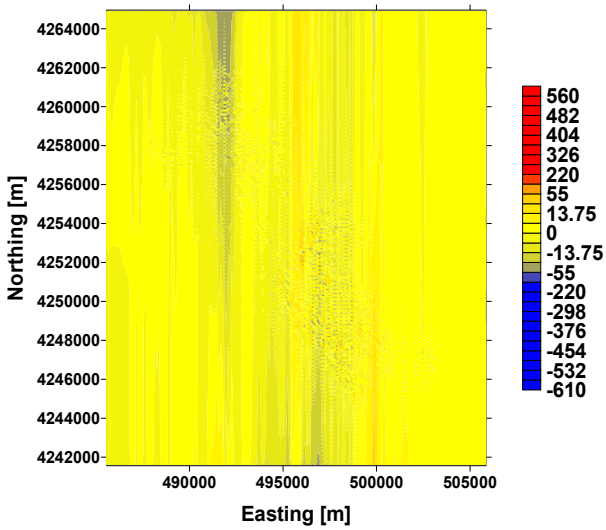


figure 5.1.4.2.3: error Cooper approach impFD1fa

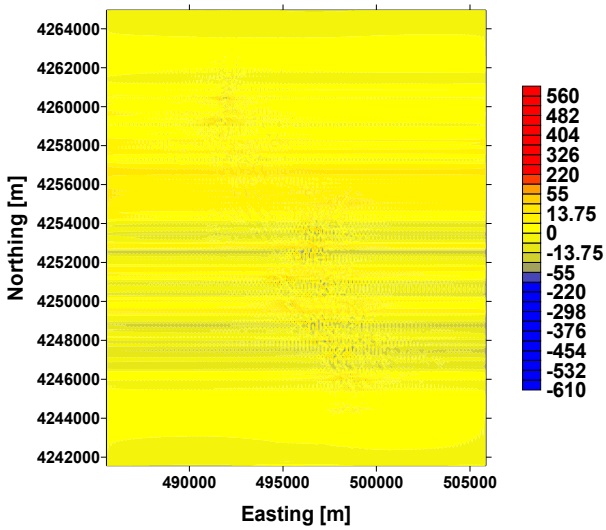


figure 5.1.4.2.4: error Cooper approach impFD2af

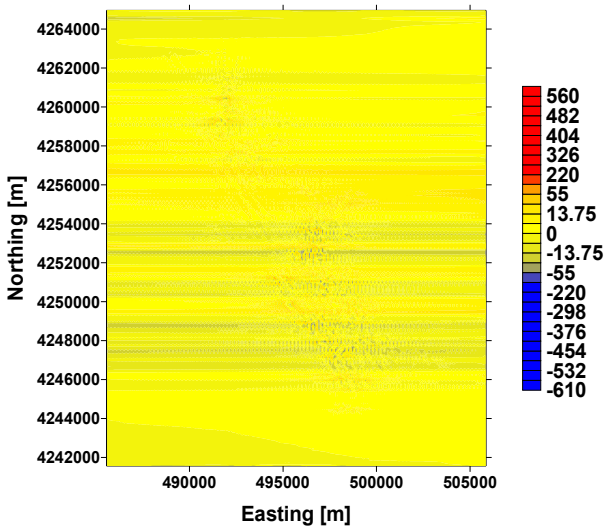


figure 5.1.4.2.5: error Cooper approach impFD2fa

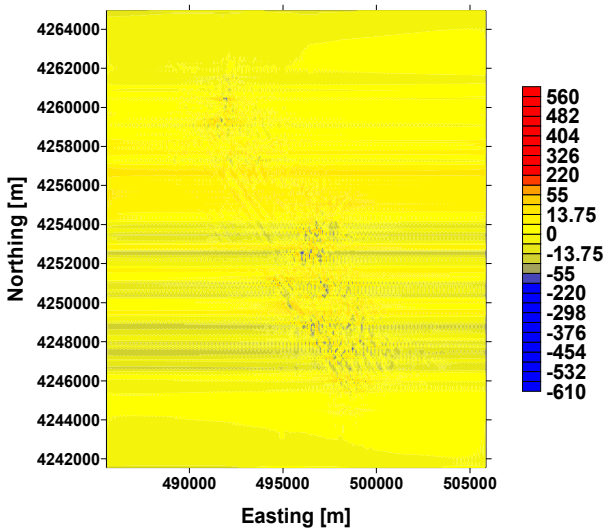


figure 5.1.4.2.6: error Cooper approach FD2af

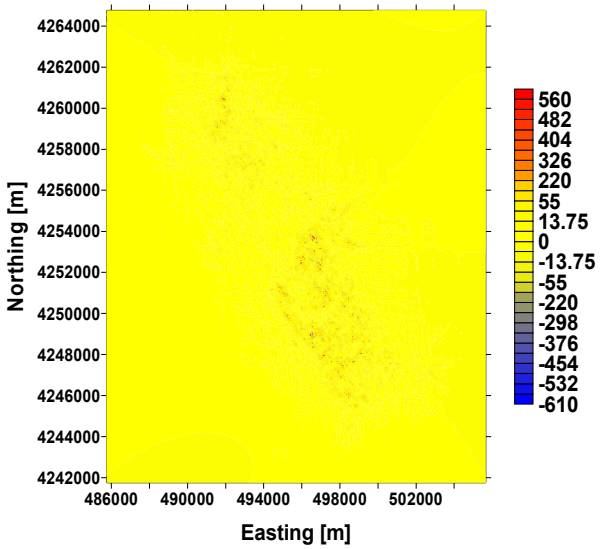


figure 5.1.4.2.7: error ISVD 4 30

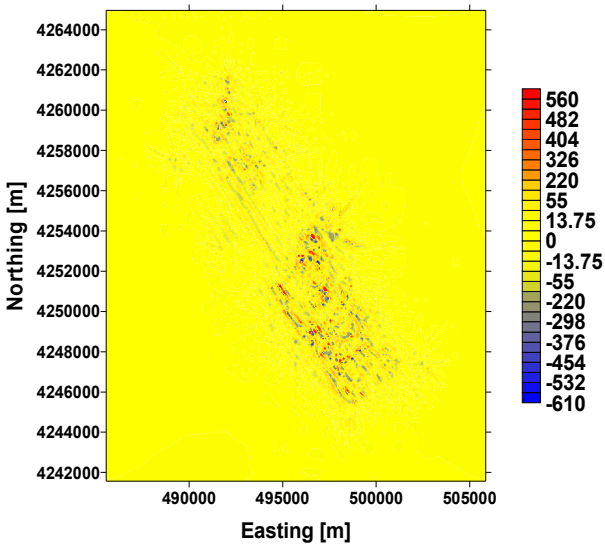


figure 5.1.4.2.8 error Tikhonov / Pasteka

Again all ISVD approaches look the same and so only *ISVD 4 30* is shown here cause it was the best in the ranking. The errors now show some differences in the Cooper approaches that were not visible in the approach fields above. The different derivation directions can be seen here very clearly through the stripe-formed anomalies in the error-fields parallel to the derivation direction.

The FFT approach and the Cooper approaches seem to be more accurate than first assumed – remembering the results in the 10m · 10m sampling interval field - . As can be seen the error structure, ISVD and FFT seem to be the nearly the same. Only the scale seems to be different. Just from the view of the error maxima and minima Cooper's approaches shown in figure 5.1.4.2.4 and figure 5.1.4.2.5 seem to be the better choice than ISVD. Further investigation in the relative logarithmic relative error may reveal different results. From this point of view classical *FFT* seems to be the best approach.

The improvement through Cooper's proposal to remove the long-wavelength character of the the error can be seen by comparing figure 5.1.4.2.4 and figure 5.1.4.2.6. The typical stripe-formed anomalies are not altered a lot but the removal of the long-wavelength character also highlighted the magnitude of the residual errors at the locations of the strongest anomalies compared to the rest of the error field.

The comparison of the ISVD approach and the Tikhonov / Pasteka approach shows some major similarities in this example but the errors made by Tikhonov are bigger in amplitude as well as spreading area than ISVD. This similarities may be an interesting point for further investigations.

5.1.4.3. Relative error in -50m. Sampling interval 100m · 100m

All scale bars are dimensionless.

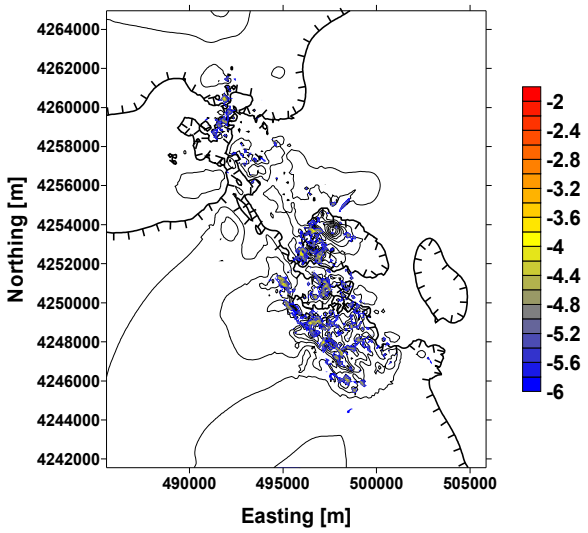


figure 5.1.4.3.1: lre FFT

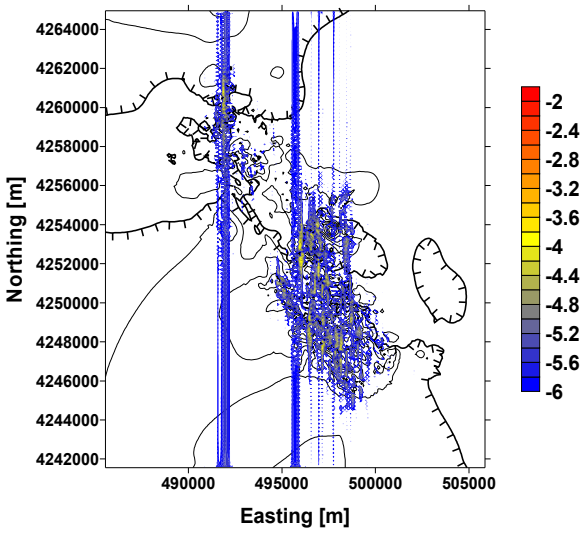


figure 5.1.4.3.2: lre Cooper appraoch impFD1af

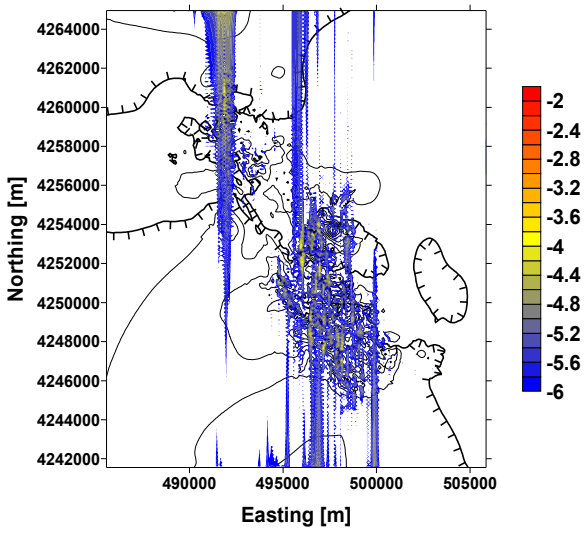


figure 5.1.4.3.3: lre Cooper approach impFD1fa

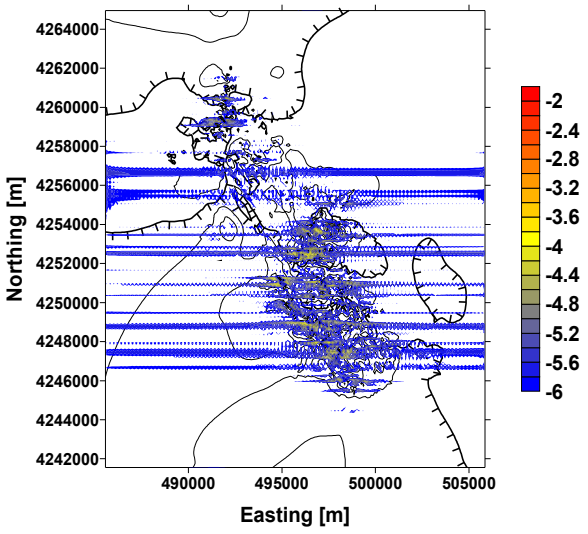


figure 5.1.4.3.4: lre Cooper approach impFD2af

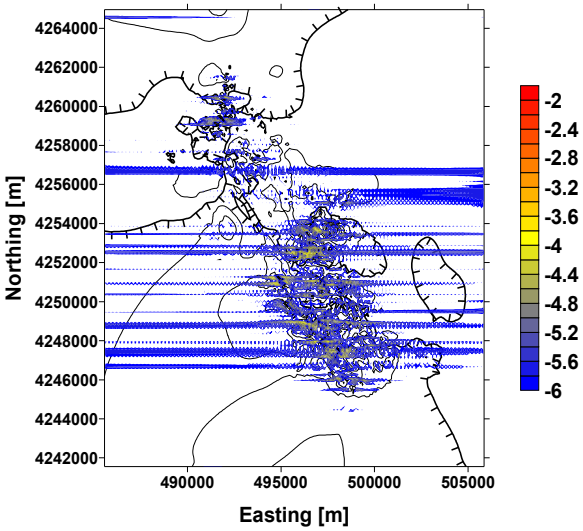


figure 5.1.4.3.5: lre Cooper approach impFD2fa

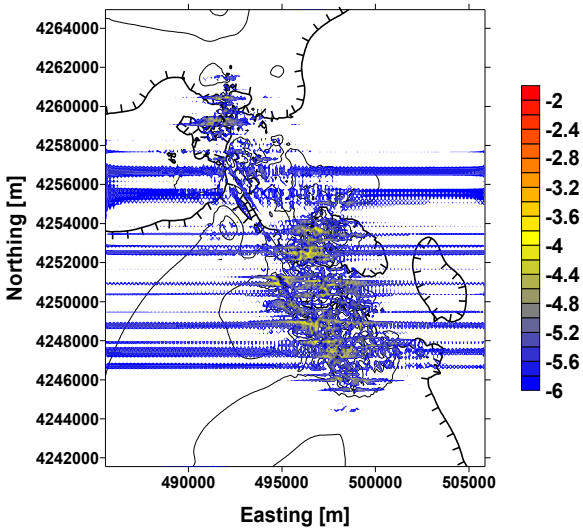


figure 5.1.4.3.6: lre Cooper approach FD2af

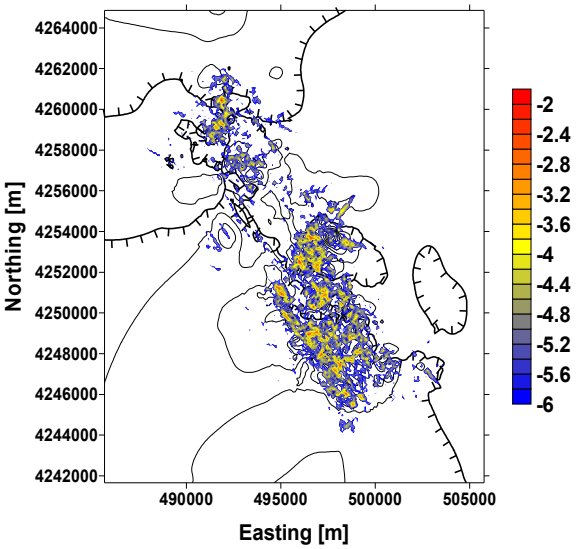


figure 5.1.4.3.7: lre ISVD 4 30

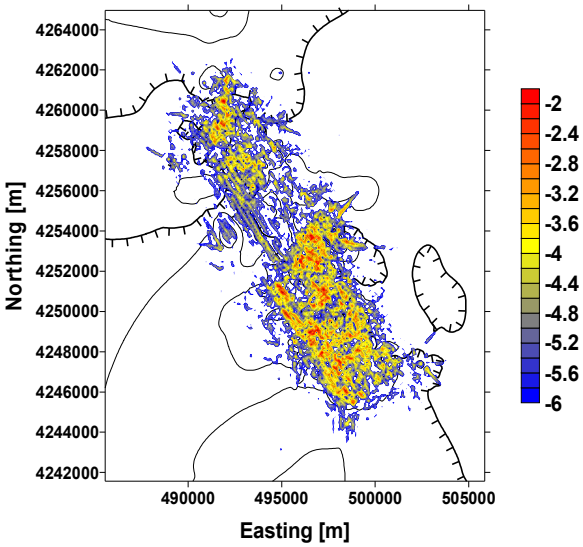


figure 5.1.4.3.8 lre Tikhonov / Pasteka

Again there are no visible differences in the approaches of the best ISVD in the ranking and therefore only ISVD 4 30 is shown and discussed here.

The logarithmic relative error once more shows a more detailed view on the results than the view of the errors alone. Again the Cooper approaches in figure 5.1.4.3.4 and figure 5.1.4.3.5 - both derivatives in GK-Y direction - are those with the smallest relative error scales. Nevertheless, the FFT approach seems to be the better choice, as the errors seem to be located only at the maxima of the field itself whereas the Cooper approaches have logarithmic relative error distributed all over the field in form of stripes most likely caused by the unidirectional horizontal derivatives. ISVD approaches again tend to have a similar logarithmic relative error structure like FFT but the error range is a lot bigger. The relative error of the ISVD approach(es) are around 1% of the maximum of the model-field. The advantage of ISVD at least compared to Cooper is that the errors are only located around the shallowest anomaly. Cooper on the contrary has smaller errors but they are spread along those typical stripe-formed areas depending on the derivatives

directions. This should be kept in mind when one uses this approaches in the future.

The relative error plots reveal the same picture as in the error plots for Tikhonov. The error maxima are located at the strongest anomalies. The amplitudes are bigger than those of ISVD and the relative error spreading is increased compared to ISVD.

The comparison of *impFD2af* and *FD2af* reveals no major advancement in using the error made by a certain Cooper approach in observation datum to correct the error in desired datum. Nevertheless, there is a small advancement visible at the location of the shallowest anomalies. (See figure 5.1.4.3.4 and figure 5.1.4.3.6)

5.1.4.4. Fields of the different approaches in -130m. Sampling interval 100m · 100m

All scale bars are in nT.

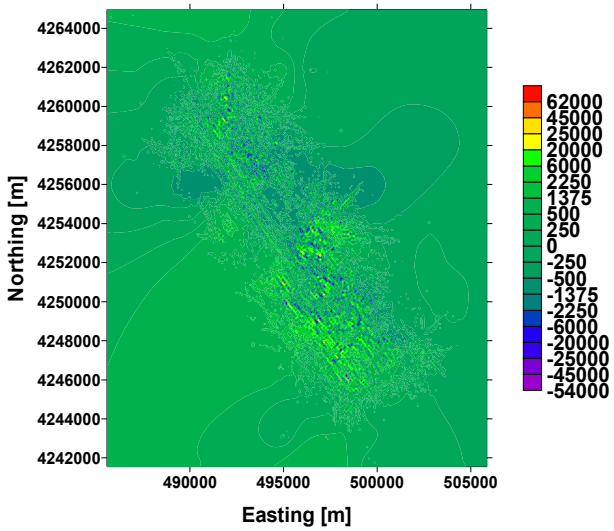


figure 5.1.4.4.1: model-field in 130m depth

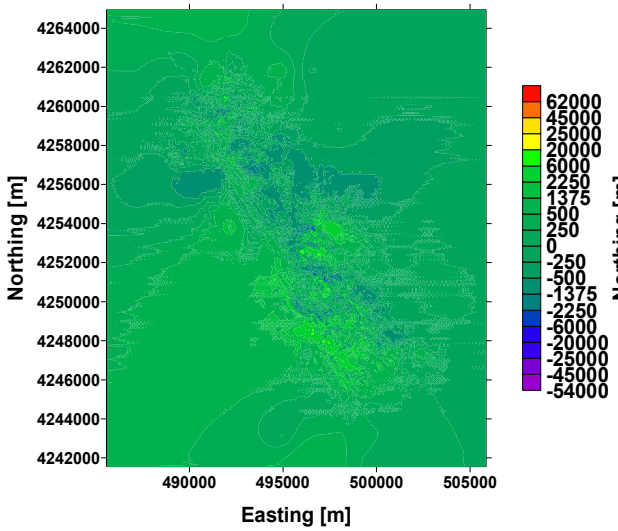


figure 5.1.4.4.2: Cooper approach impFD2fa

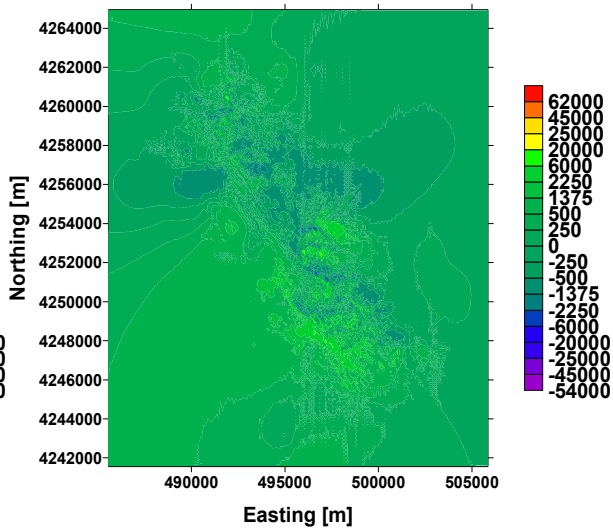


figure 5.1.4.4.3: Cooper approach impFD1af

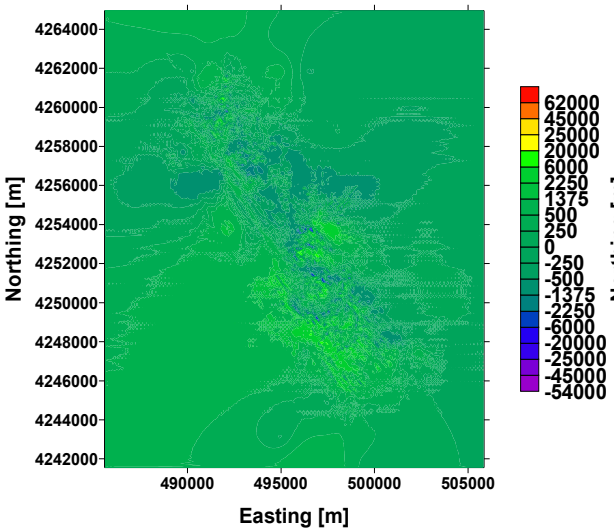


figure 5.1.4.4.4: Cooper approach impFD2af

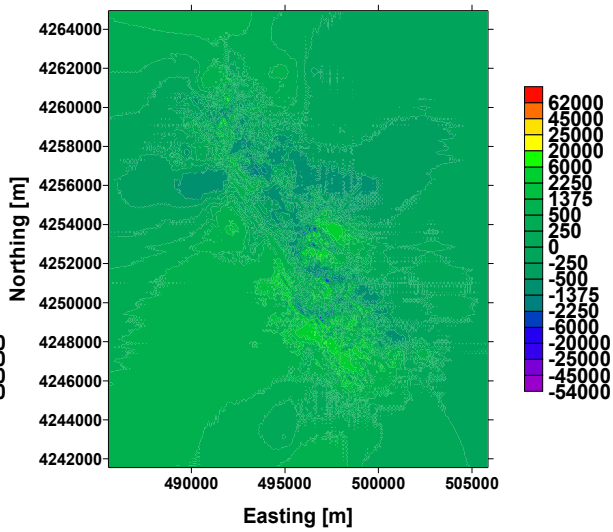


figure 5.1.4.4.5: Cooper approach FD0af

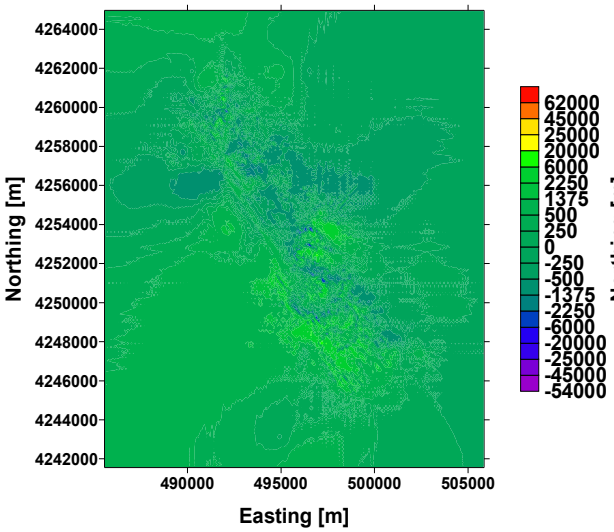


figure 5.1.4.4.6: Cooper approach impFD0fa

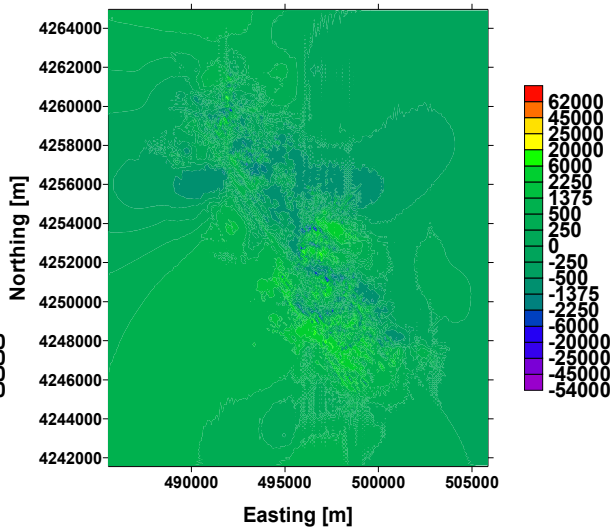


figure 5.1.4.4.7: Cooper approach FD1af

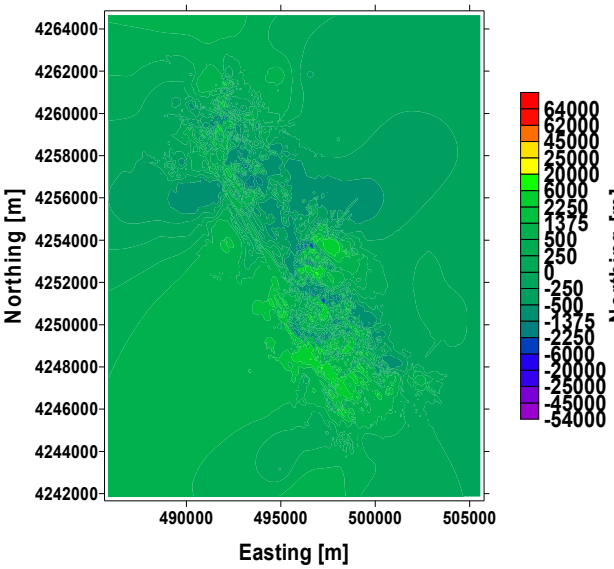


figure 5.1.4.4.8: ISVD 6 30

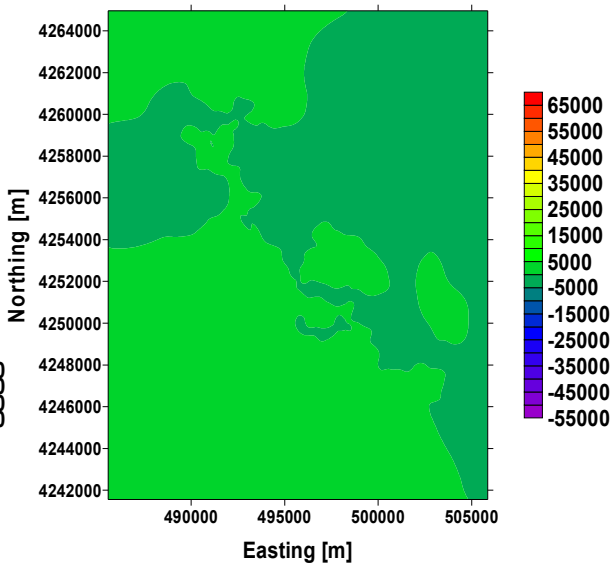


figure 5.1.4.4.9 Tikhonov / Pasteka

FFT is not as competitive as Cooper and/or ISVD approaches in this depth and so is not in the ranking any more.

The best ISVD approach here now is *ISVD 6 30* and *ISVD 4 30* is now the last in the ranking of the best 6 ISVD approaches. Nevertheless this fact again there seem to be no visible difference between the particular ISVD approaches. The ISVD approaches in the ranking are from the 2nd to the 6th. *ISVD 20 10, ISVD 8 30, ISVD 5 30, 20 9* and *ISVD 4 30.* As all of them look the same only *ISVD 6 30* will be shown and discussed here.

All the cooper approaches do have the already mentioned artefacts perpendicular to the derivation direction. Due to the fact that mixed-horizontal derivatives need derivatives in two directions additionally artefacts in both directions are visible. Again there is no 1st or 2nd order vertical derivative in the ranking of the best 6.

Tikhonov / Pasteka deliver a result which looks to be over-regularized at all. So field continuation close to the source layer (~140m) leads to over-regularization when Tikhonov's / Pasteka approach is used.

5.1.4.5. Errors of the different approaches in -130m. Sampling interval 100m · 100m.

All scale bars are in nT.

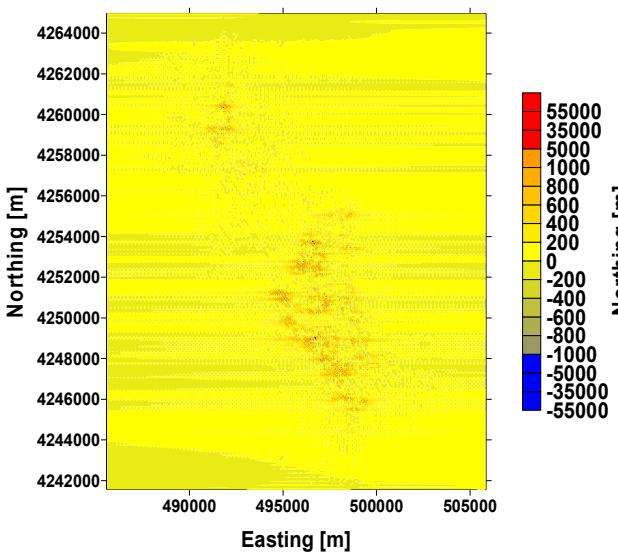


figure 5.1.4.5.1: error Cooper approach impFD2fa

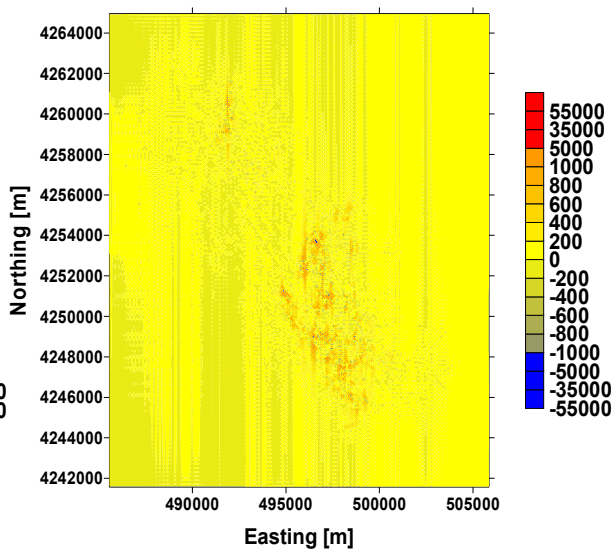


figure 5.1.4.5.2: error Cooper approach impFD1af

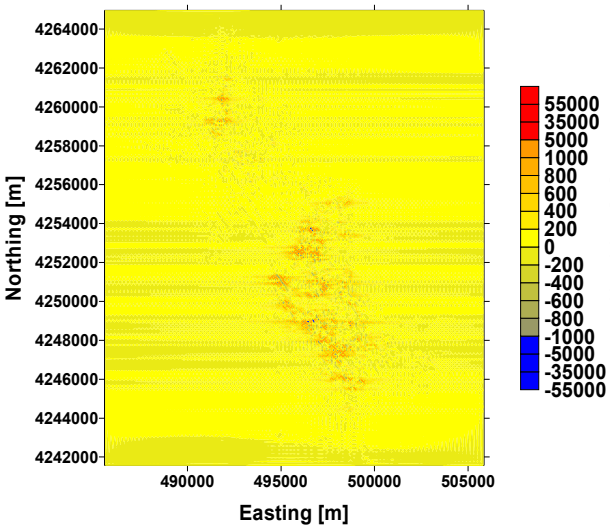


figure 5.1.4.5.3: error Cooper approach impFD2af

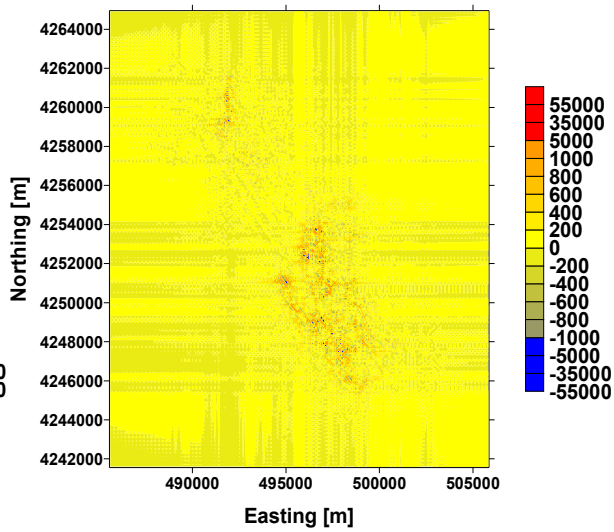


figure 5.1.4.5.4: error Cooper approach FD0af

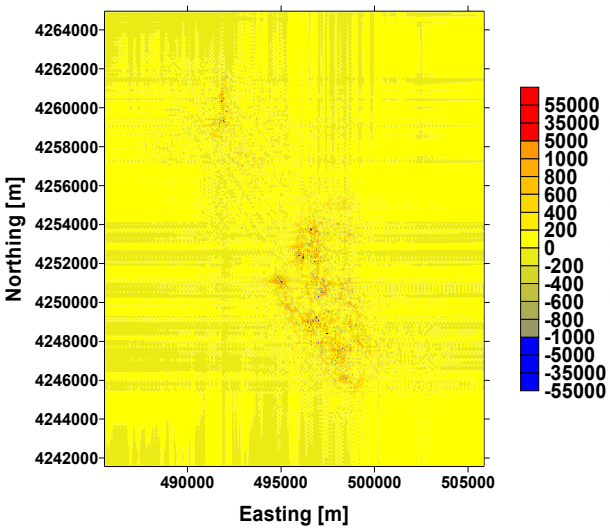


figure 5.1.4.5.5: error Cooper approach impFD0fa

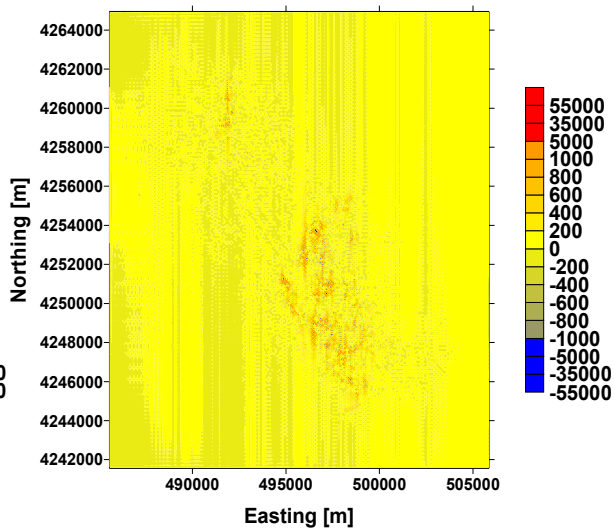


figure 5.1.4.5.6: error Cooper approach FD1af

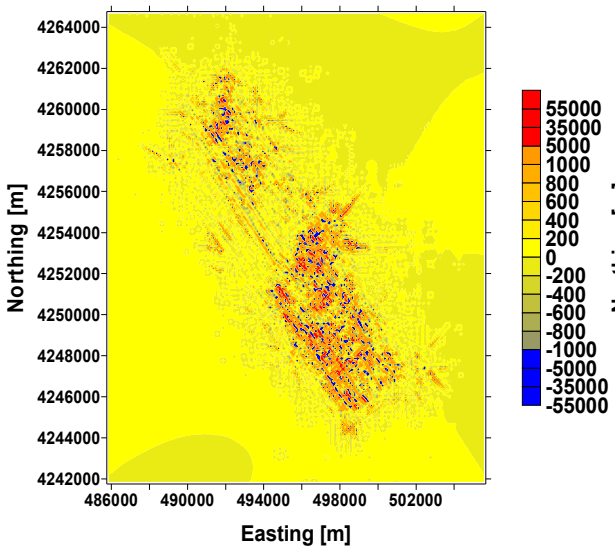


figure 5.1.4.5.7: error ISVD 6 30

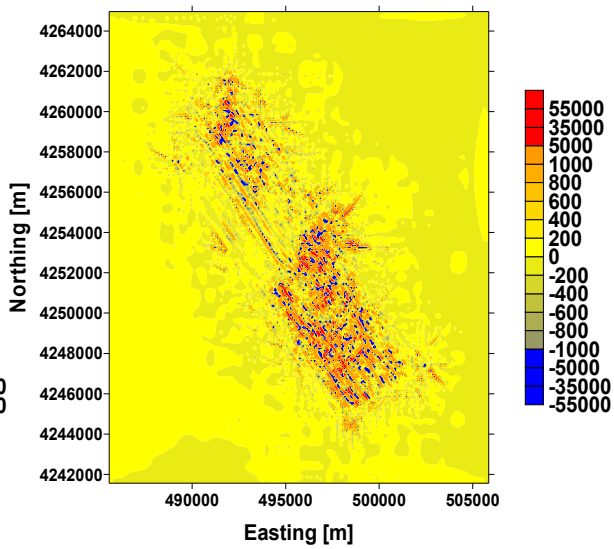


figure 5.1.4.5.8 error Tikhonov / Pasteka

Due to the recent results in -50m the reader of this thesis could believe that the mixed horizontal derivatives are not even anyhow useful. The results in -130m confute this results. In fact here the mixed horizontal derivatives have one of the smallest error ranges but it can't be said for sure if unidirectional horizontal derivatives or the mixed horizontal derivatives should be preferred.

The ISVD as well as Tikhonov have the worst errors, but still looks similar to the results of ISVD and FFT in -50m. Tikhonov's /Pasteka's approach investigated from this point of view does not seem to be over-regularized so much than the the view in the last chapter would have made one believe. Nevertheless, is it definitely over-regularized which can be easily seen by comparison with ISVD's error. Again FFT itself is not any more in the ranking of the first six best Cooper/FFT results. All shown results seem to oscillate already which is certainly caused by the close continuation level to the shallowest sources included in the model-field. It is also interesting that the horizontal derivative in GK-Y seems to be the better approach, at least for this model-field than the derivative in GK-X direction. This is a interesting fact when one remembers the results of this model-field in -50m where the GK-X direction derivatives seem to be better than the GK-Y derivatives.

Tikhonov's errors seem to be a bit bigger than those made by ISVD.

5.1.4.6. relative error in -130m. Sampling interval 100m · 100m

All scale bars are dimensionless.

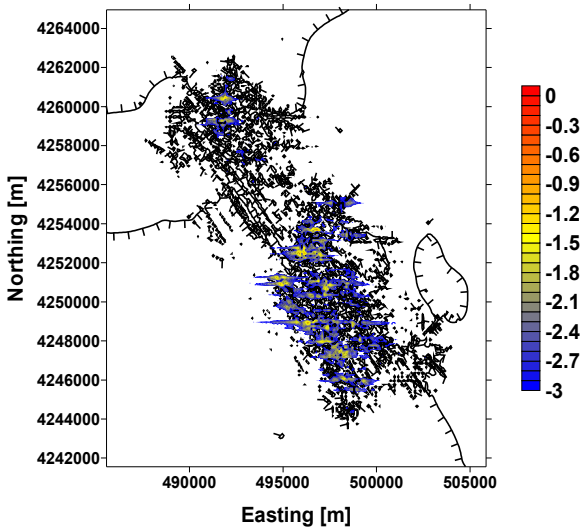


figure 5.1.4.6.1: lre Cooper approach impFD2fa

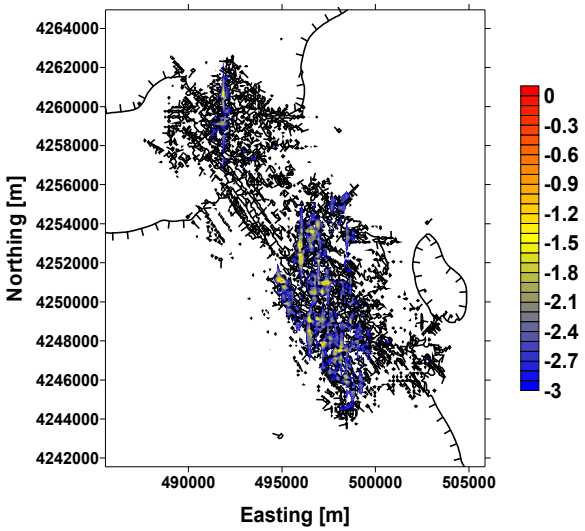


figure 5.1.4.6.2: lre Cooper approach impFD1af

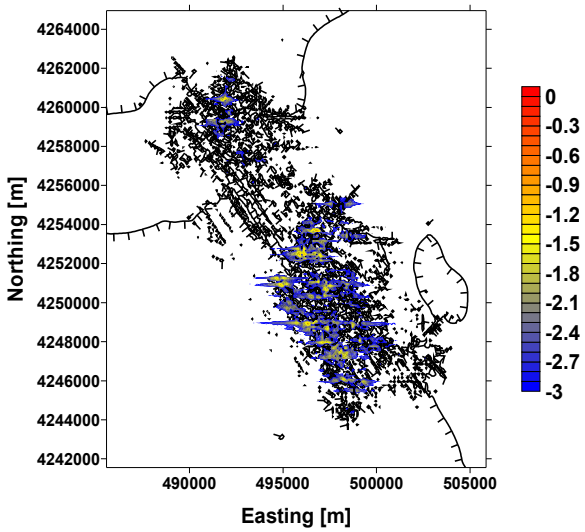


figure 5.1.4.6.3: lre Cooper approach impFD2af

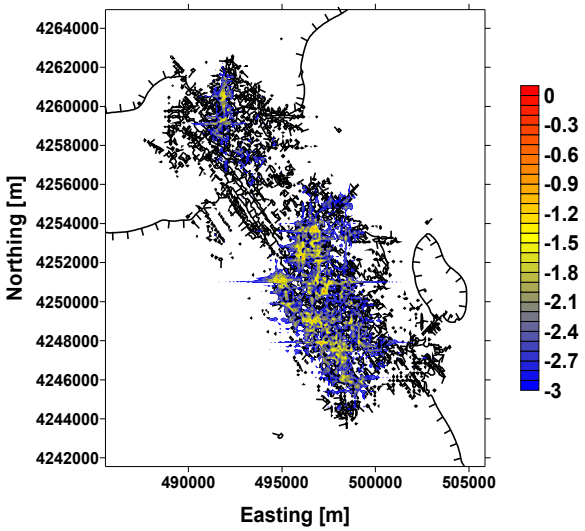


figure 5.1.4.6.4: lre Cooper approach FD0af

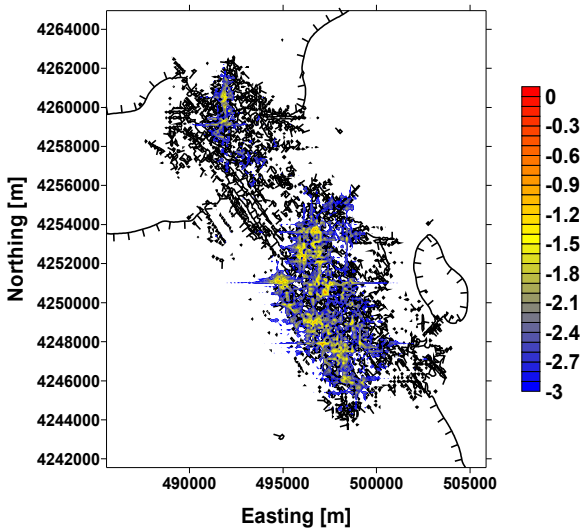


figure 5.1.4.6.5: lre Cooper approach impFD0fa

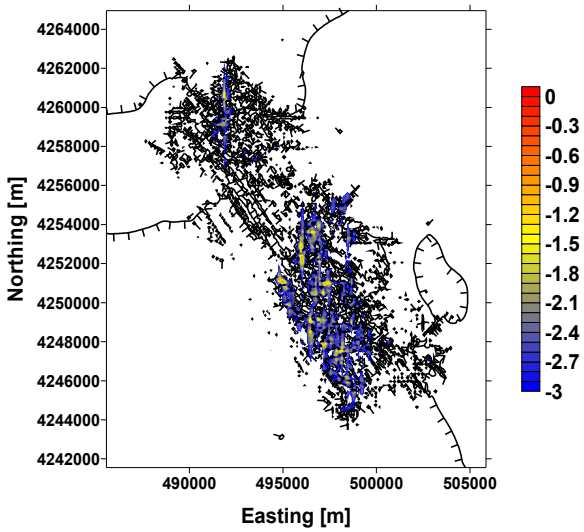


figure 5.1.4.6.6: lre Cooper approach FD1af

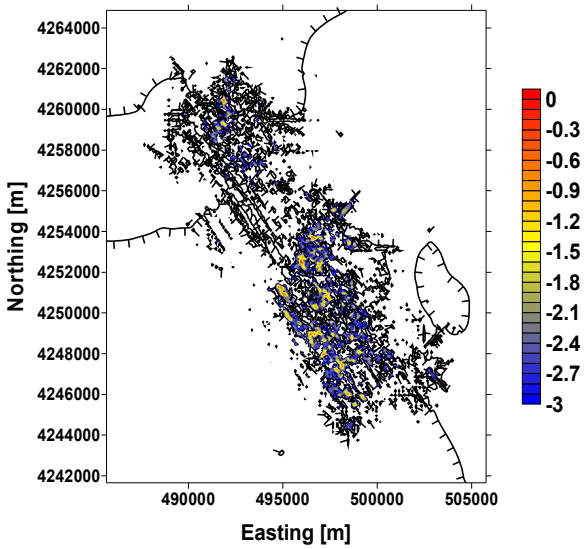


figure 5.1.4.6.7: lre ISVD 6 30

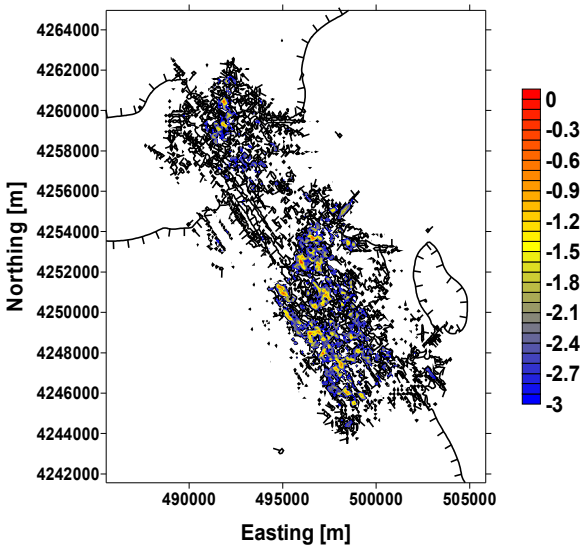


figure 5.1.4.6.8 lre Tikhonov / Pasteka

Once more the ISVD approaches can not be differed from each other and so only the best in the ranking will be discussed here. The experienced reader of this thesis may recognize that the ISVD approaches do have a smaller areas where the big errors occur but the magnitude is a bit bigger than that of the Cooper approaches. Therefore maybe the Cooper approaches should be preferred in this depth. Comparing the mixed-horizontal derivatives with the unidirectional ones it can be easily seen that the area with the biggest errors is a lot bigger than that of the unidirectional derivatives. Which horizontal derivative should be preferred depends on the measured field. In this special case the *impFD1af* seemed to be the best choice but as a general recommendation the mixed horizontal derivatives would be the best one cause they are independent of the direction and at least the magnitude of the errors seem to be smaller than that of the ISVD approaches. As the continuation level is so close to the sources in this case it seem to make no difference if one uses the *impFD0af* or the *impFD0fa* approach.

Unfortunately the lre-plots are not able to pinpoint out the over-regularization of the Tikhonov but again the astonishing similarity by ISVD and Tikhonov can be seen.

5.2. Results, reduction to pole (RTP) on arbitrary surface

5.2.1. Simple datasets

All datasets in this chapter are compared to the model-fields in 2.2.2 Simple datasets. Always the first four scale bars are in nT. The last two are always dimensionless. The lre plots include the isolines of the topography.

5.2.1.1. Inclination 10°

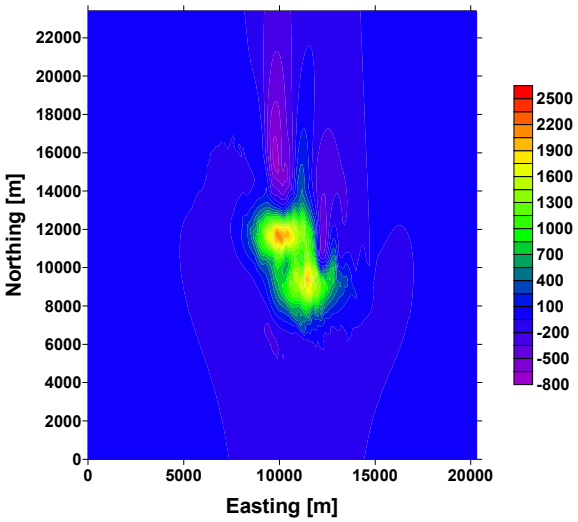


Figure 5.2.1.1.1: RTP field, neglecting topography, inclination 10°

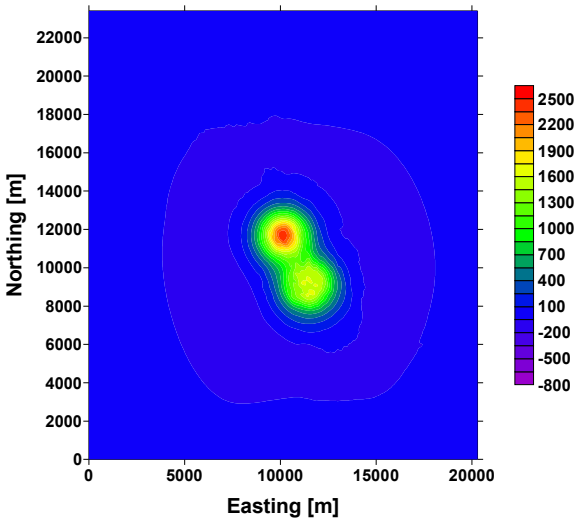


Figure 5.2.1.1.2: RTP field, considering topography, inclination 10° (Xia)

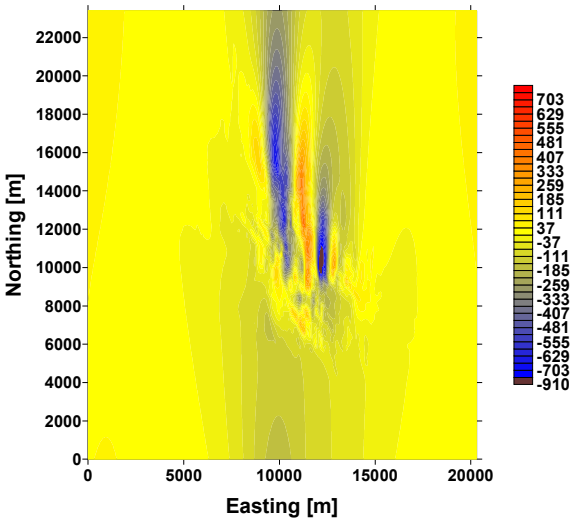


Figure 5.2.1.1.3: error RTP field, neglecting topography, inclination 10°

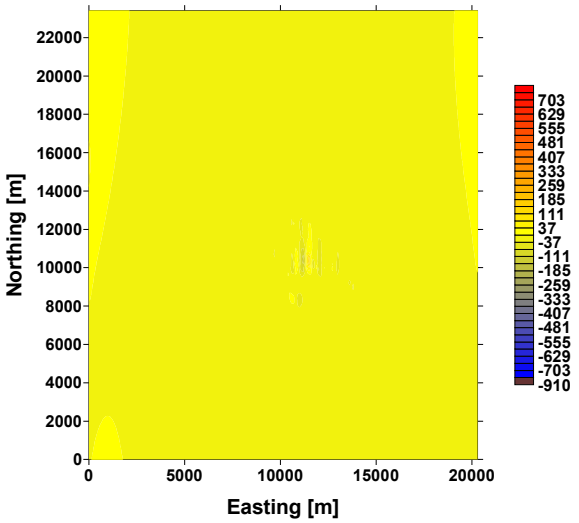


Figure 5.2.1.1.4: error RTP field, considering topography, inclination 10°

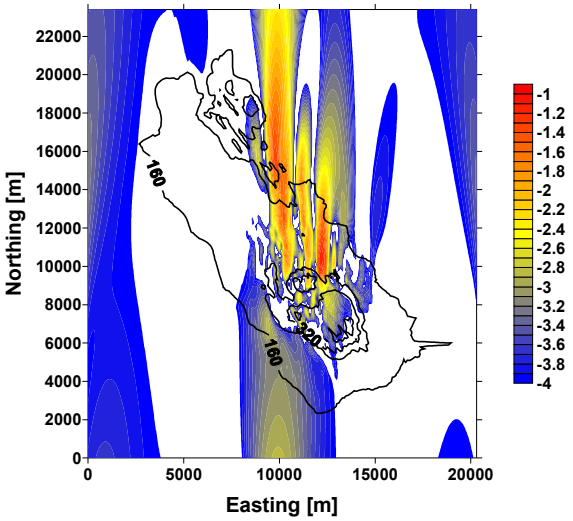


Figure 5.2.1.1.5: lre RTP field, neglecting topography, inclination 10°

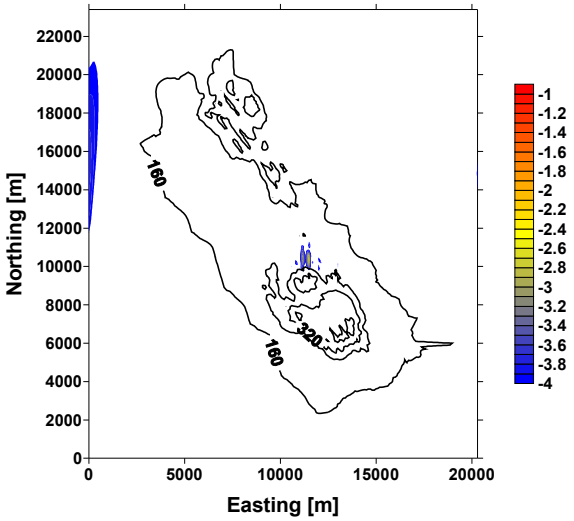


Figure 5.2.1.1.6: lre RTP field, considering topography, inclination 10°

Even comparing the RTP fields in Figure 5.2.1.1.1 and Figure 5.2.1.1.2 depict that the classical pole-reduction neglecting the topography with 10° inclination leads to big differences which is most likely caused by the small inclination and therefore can be seen as close to the magnetic equator where reduction to pole operator leads to singularities. This thesis may also be based on the *strong stripe formed errors*. *Xia*'s adjusted results on the contrary still looks quite good. The error fields just point this out more clearly. Even the magnitude of the errors of classical reduction to pole is around 10% of the model-field data as can be seen in the *lre*-plot. Xia's errors are just around 0.1% of the maximum of the model-field.

5.2.1.2. Inclination 30°

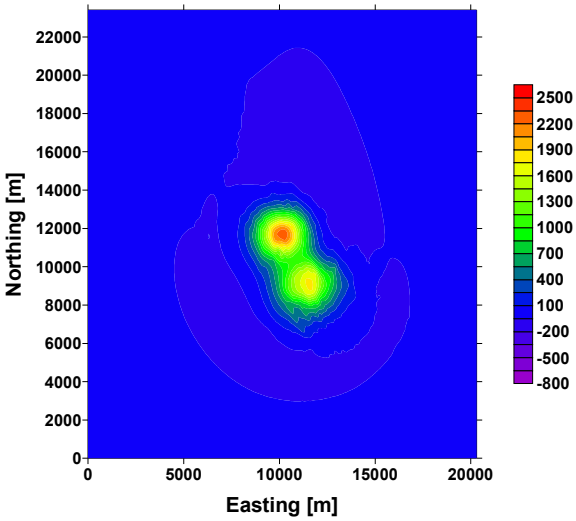


Figure 5.2.1.2.1: RTP field, neglecting topography, inclination 30°

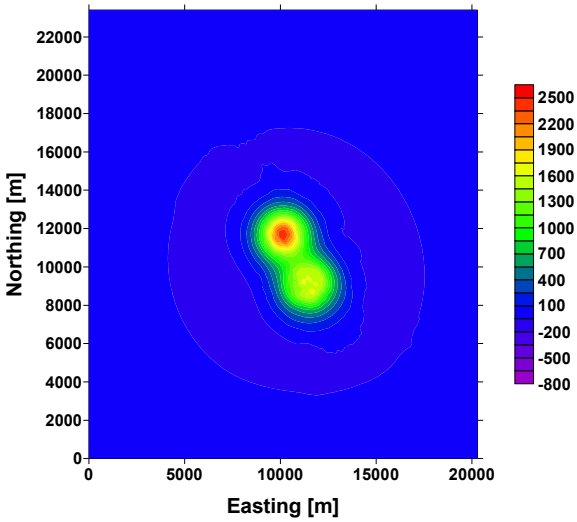


Figure 5.2.1.2.2: RTP field, considering topography, inclination 30° (Xia)

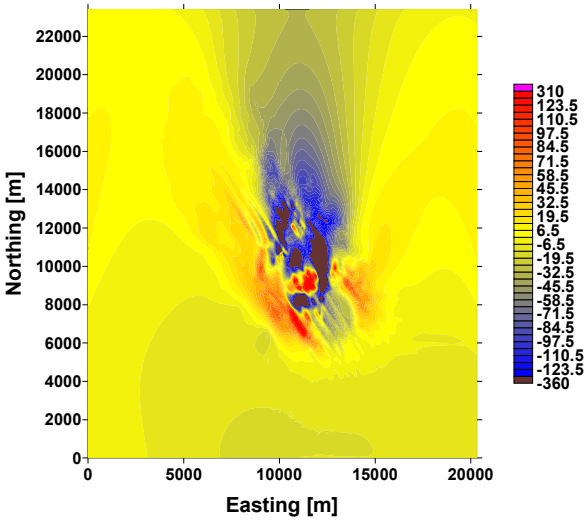


Figure 5.2.1.2.3: error RTP field, neglecting topography, inclination 30°

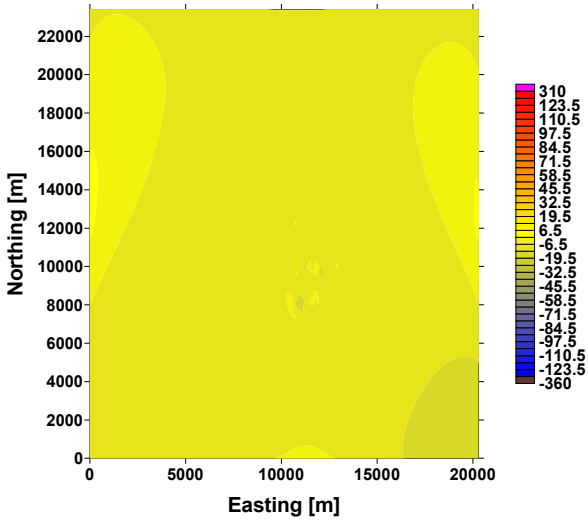


Figure 5.2.1.2.4: error RTP field, considering topography, inclination 30°

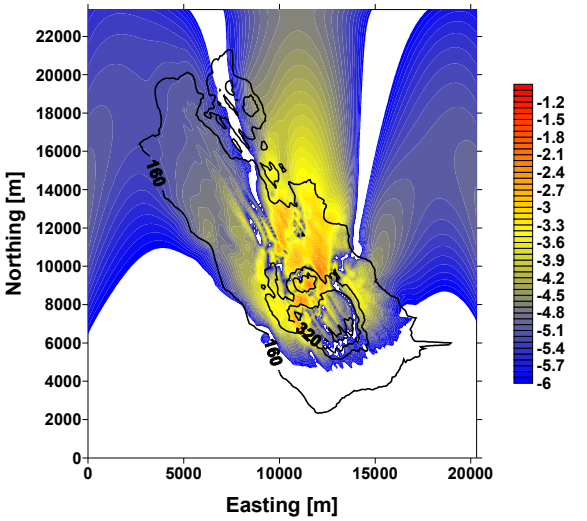


Figure 5.2.1.2.5: lre RTP field, neglecting topography, inclination 30°

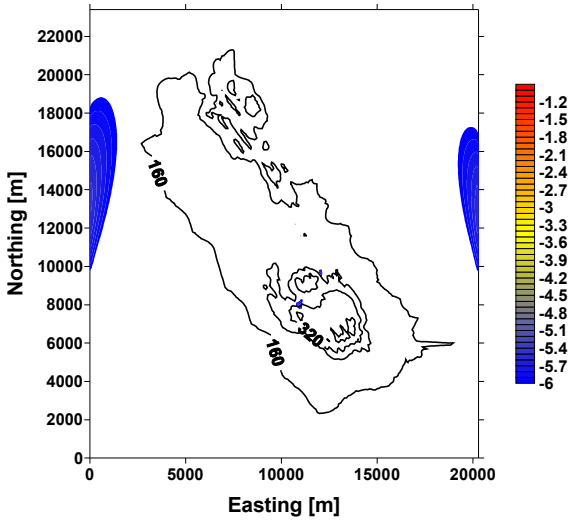


Figure 5.2.1.2.6: lre RTP field, considering topography, inclination 30°

Now that the inclination is a bit more higher than before the field gained by classical RTP does look more like the true RTP field. Nevertheless the error still is quite big and there are some major differences between the true RTP field and the *RTP* neglecting topography. Again *Xia*'s adjustment and *reduction to pole* considering the topography is much better. The error in the same scaling is nearly not existent and of course also *lre* of both errors shows the advantage of Xia's adjustment and reduction to pole. The lre plots reveal a maximum of around 6,5% of relative error for the RTP neglecting the topography and around 0.0004% for the Xia's approach considering the topography.

5.2.1.3. Inclination 50°

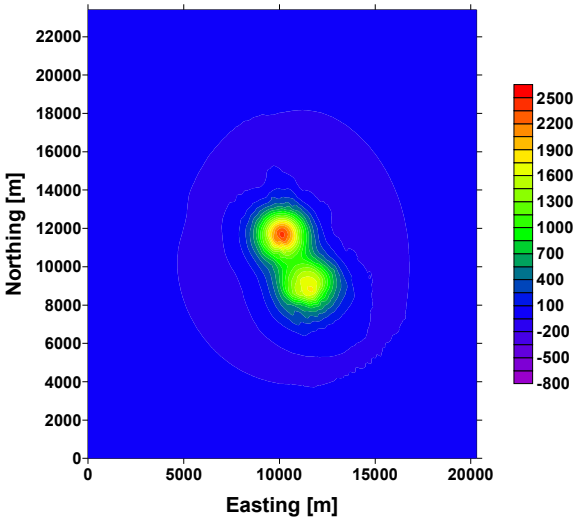


Figure 5.2.1.3.1: RTP field, neglecting topography, inclination 50°

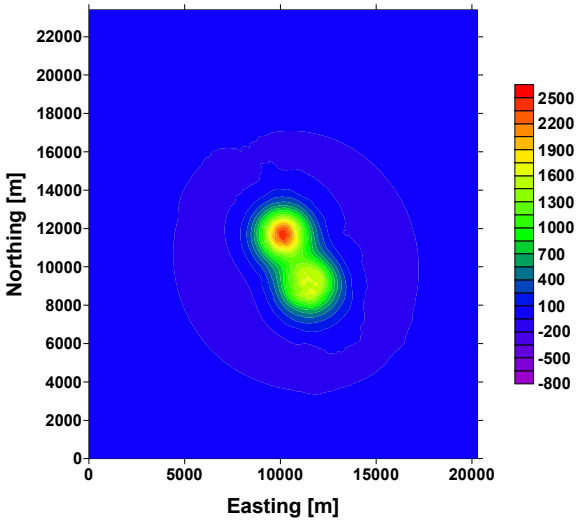


Figure 5.2.1.3.2: RTP field, considering topography, inclination 50° (Xia)

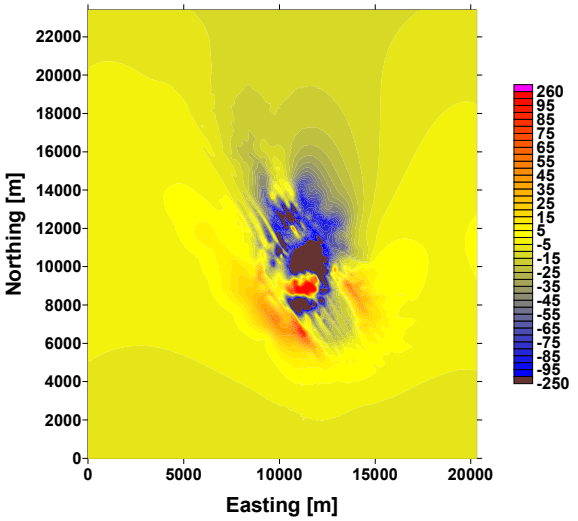


Figure 5.2.1.3.3: error RTP field, neglecting topography, inclination 50°

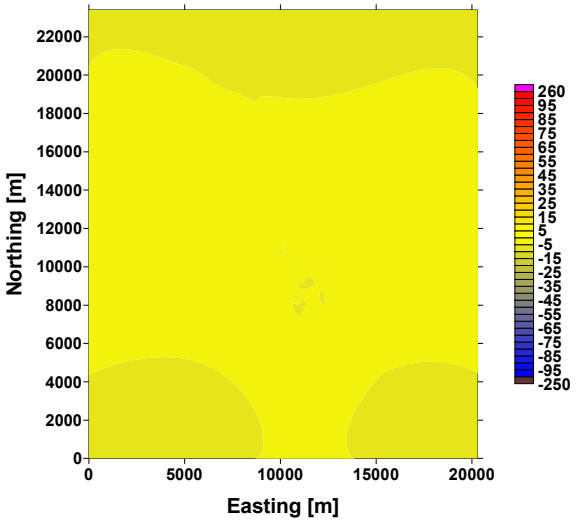


Figure 5.2.1.3.4: error RTP field, considering topography, inclination 50°

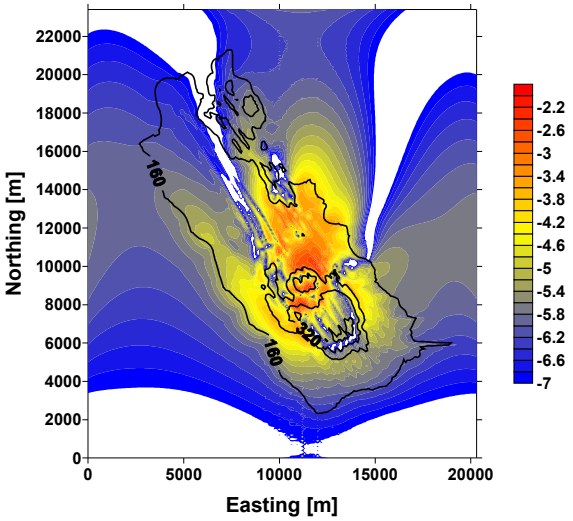


Figure 5.2.1.3.5: lre RTP field, neglecting topography, inclination 50°

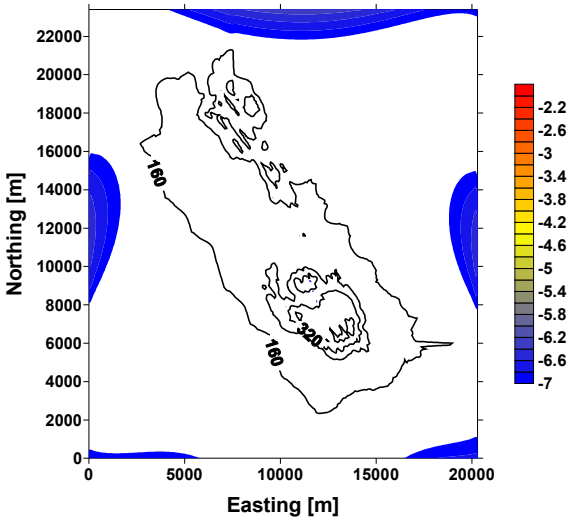


Figure 5.2.1.3.6: lre RTP field, considering topography, inclination 50°

Again Xia turns out to be the better approach. Here now the *lre* plots shows 1.6% relative error for the RTP neglecting the topography and around 0.00006% relative error for the Xia approach.

5.2.1.4. Inclination 70°

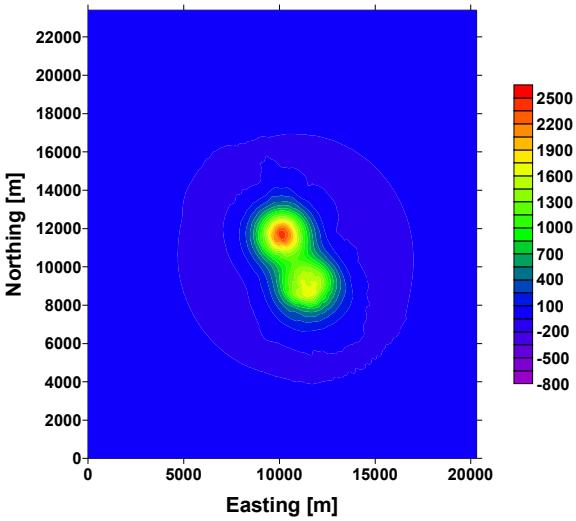


Figure 5.2.1.4.1: RTP field, neglecting topography, inclination 70°

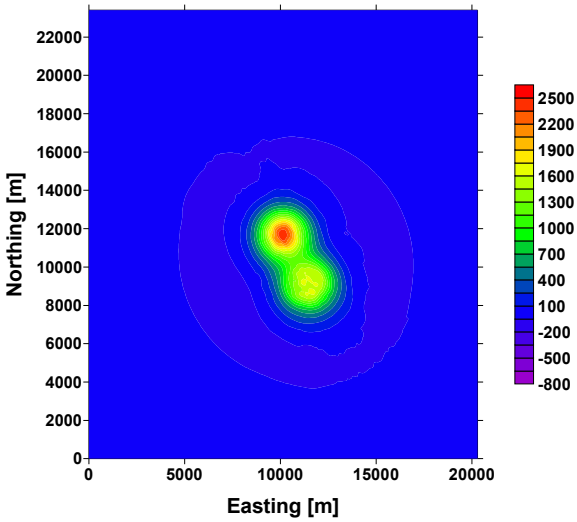


Figure 5.2.1.4.2: RTP field, considering topography, inclination 70° (Xia)

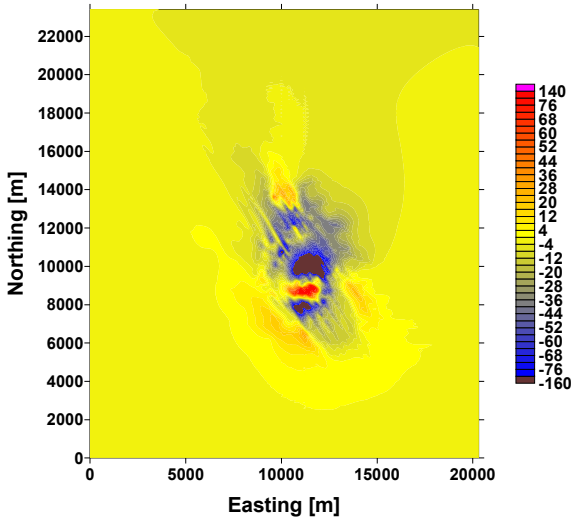


Figure 5.2.1.4.3: error RTP field, neglecting topography, inclination 70°

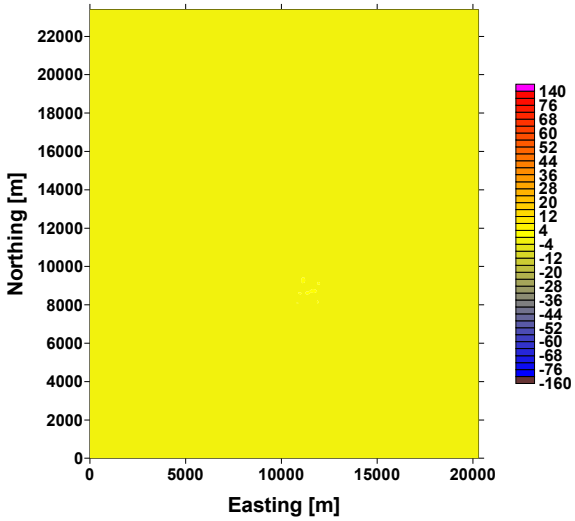


Figure 5.2.1.4.4: error RTP field, considering topography, inclination 70°

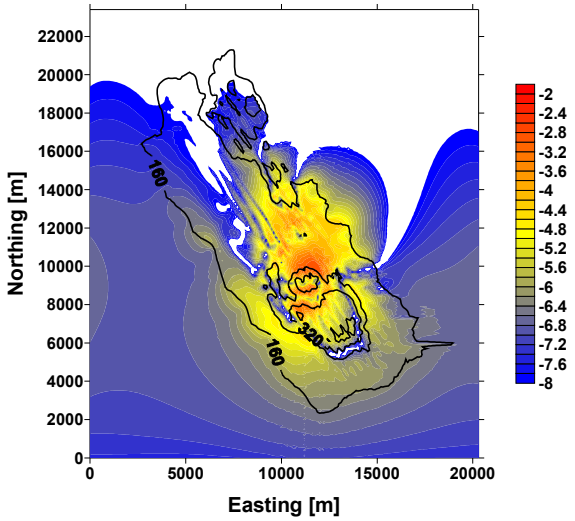


Figure 5.2.1.4.5: lre RTP field, neglecting topography, inclination 70°

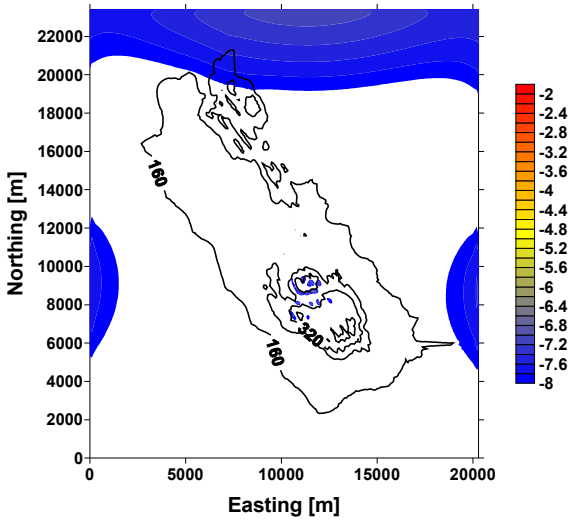


Figure 5.2.1.4.6: lre RTP field, considering topography, inclination 70°

The RTP neglecting the topography again has the bigger errors even if they are small compared to the true RTP field. The biggest of those errors seem to be located at the biggest changes in the RTP field with around 140 nT. Relative to the absolute field maximum the biggest errors occurring are about 1% for the RTP neglecting topography and $2 \cdot 10^{-5}$% for the *Xia* approach at a inclination of 70°.

So the Xia approach considering the topography is always better than the RTP neglecting the topography. The maximum relative error with 1% at a inclination of 10° for the Xia approach and 10% relative error for the RTP neglecting topography reveals an at least 10 times better result for the Xia approach than with simple RTP neglecting topography. Therefore in the further discussions Xia's RTP results considering the topography will be treated as the “true” RTP field in lack of other options. The adjusted field-plots will always include information about the standard-deviation of the adjusted fields – not the RTP fields - and their absolute maximum error. This may be kept in mind for the further chapters.

5.2.2. More realistic dataset of Vulcano 500m · 500m

The scale bar for all fields is in nT, except for the logarithmic relative error plot which is dimensionless. The *lre* field includes the isolines of the topography field.

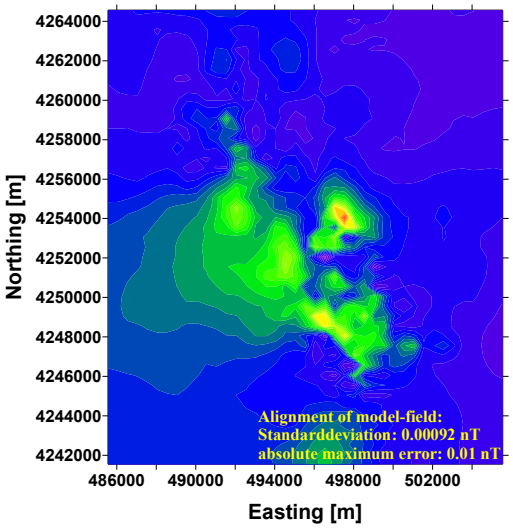


Figure 5.2.2.1: RTP field gained by Xia considering topography

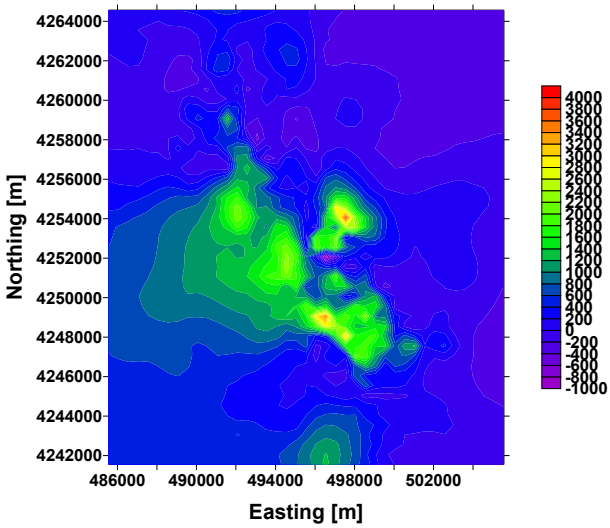


Figure 5.2.2.2: RTP field neglecting topography

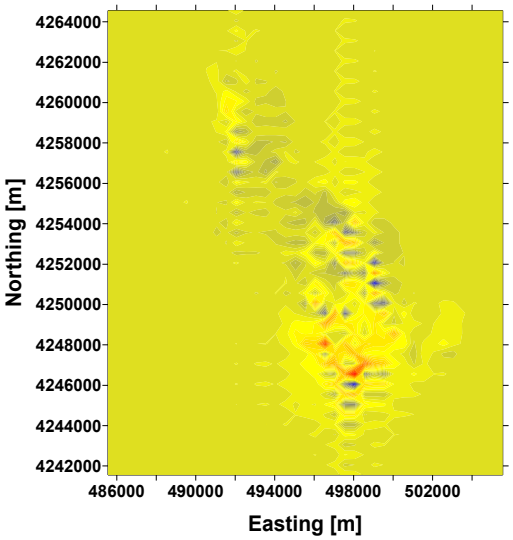


Figure 5.2.2.3: error RTP field neglecting topography (RTP-Xia)

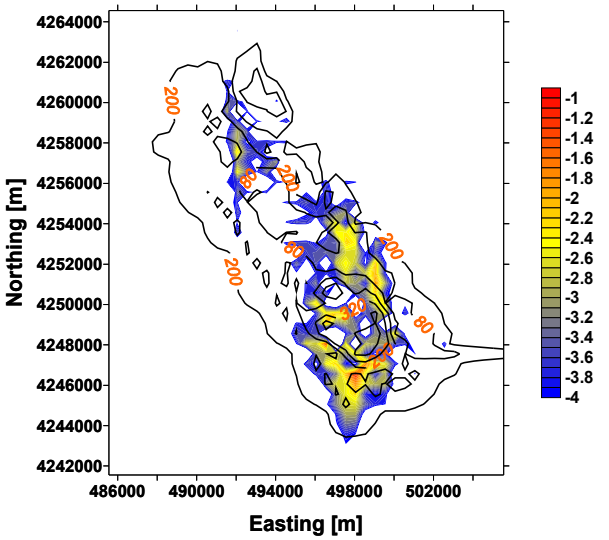


Figure 5.2.2.4: lre RTP field neglecting topography (lre (RTP-Xia))

The assumed inclination for the area of the island Vulcano was 57.8° and a declination of 0°. Other more accurate values may deliver different results but for this case this just should be assumed as a more realistic field. True field values will be discussed in the following chapters. For this dataset nearly the whole relative error was below 0.01% (white area, Figure 5.2.2.4). The maximum relative error is around 10% at approximately 4246000 north and 498000 east . The average relative error of the displayed scale is around 1% (4,5 nT) which seems to be a acceptable error. Unfortunately Xia's adjustment caused some clearly visible artefacts in the error.

5.2.3. More realistic dataset Vulcano 100m · 100m

The scale bar for all fields is in nT, except for the logarithmic relative error plot which is dimensionless. The *lre* field includes the isolines of the topography field.

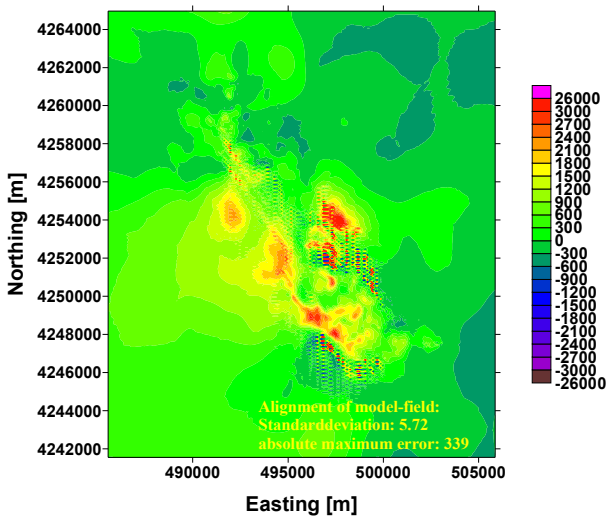


figure 5.2.3.1: RTP field gained by Xia considering topography

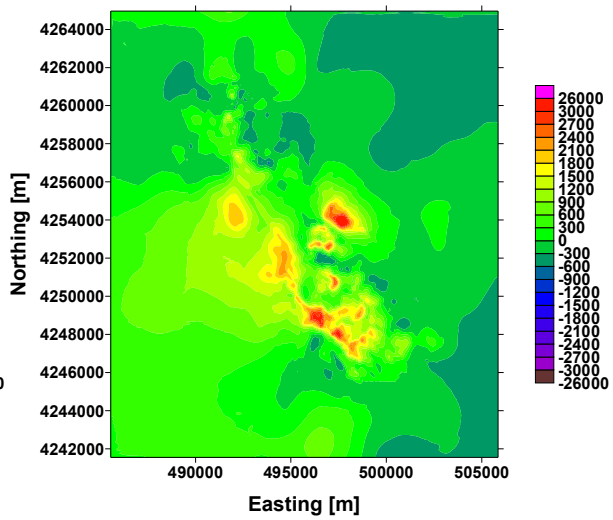


figure 5.2.3.2: RTP field neglecting topography

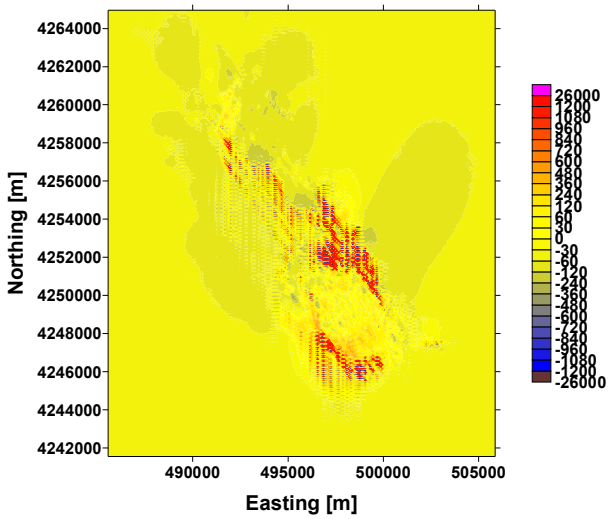


figure 5.2.3.3: error RTP field neglecting topography (RTP-Xia)

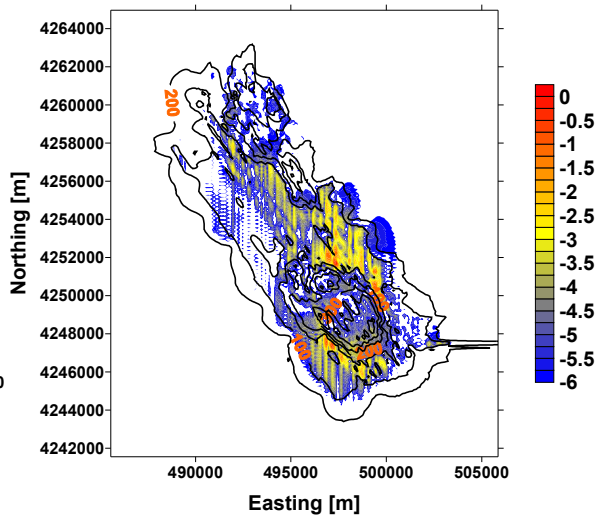


figure 5.2.3.4: lre RTP field neglecting topography (lre (RTP-Xia))

The comparison of the results of the Vulcano dataset with 500m times 500m grid spacing with the original grid spacing version of 100m times 100m clearly reveals the negative effect of Xia's influence in this case. Therefore the last dataset of Socorro was filtered before Xia's field adjustment process took place and the pole reduction operator was tested. As the adjustment was so bad further discussion on those results is useless with the exception that this is the proof the a better EQS algorithm is needed for magnetic field reproduction.

5.2.4. Real dataset of Socorro

The scale bar for all fields is in nT, except for the logarithmic relative error plot which is dimensionless. The *lre* and the error field includes the isolines of the topography field to pinpoint out may existing correlations.

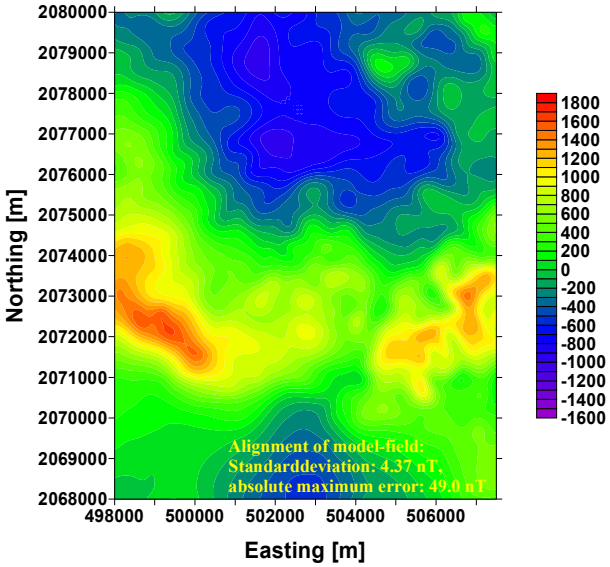


Figure 5.2.4.1: RTP field gaines by Xia considering topography

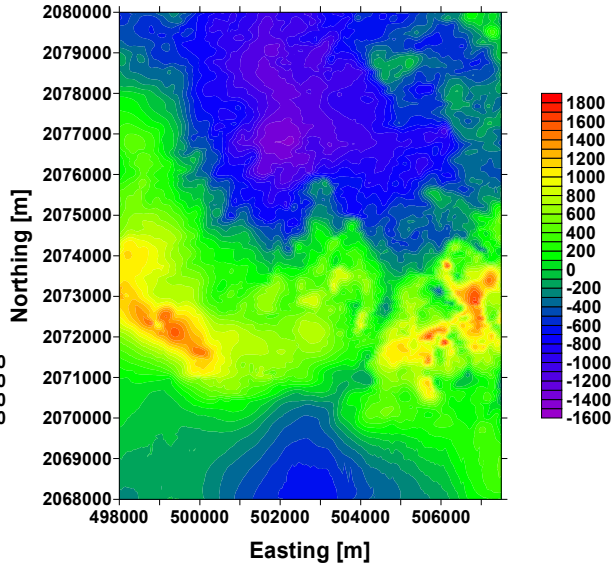


Figure 5.2.4.2: RTP field neglecting topography

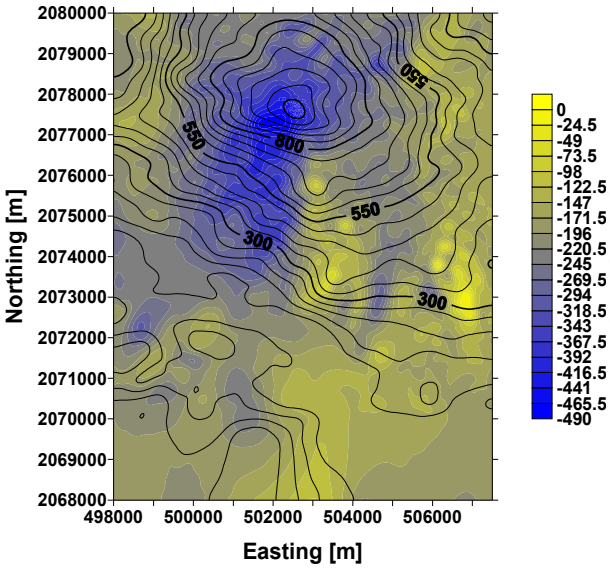


Figure 5.2.4.3: error RTP field neglecting topography (RTP-Xia)

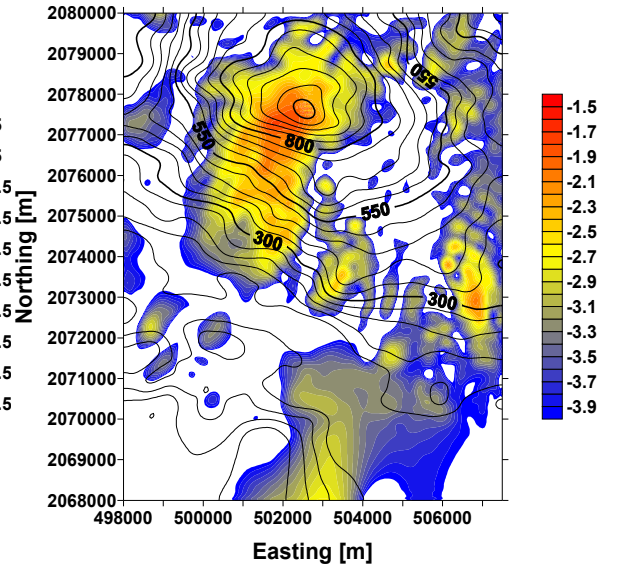


Figure 5.2.4.4: lre RTP field neglecting topography (lre(RTP-Xia))

The comparison with the dataset of Vulcano in the chapters above reveals one major difference. The errors made by *reduction to pole* neglecting the topography here only led to negative errors. In the simple dataset and in the dataset of Vulcano there the errors were positive as well as negative. Though nevertheless the Xia approach in this case

delivered a quite bad adjustment as can be seen in Figure 5.2.4.1 there could be positive errors too. Even if these errors aren't that exact, it may shows how big the errors can be, which was the aim of that part of the thesis. For this adjustment (with 10000 iteration steps) of the field reduction to pole neglecting the topography led to a maximum relative errors of about 3%. The mean of the displayed relative errors is around 0.2% which seems to be quite good. Even the maximum with 3% is quite astonishing compared to the Vulcano results. The bad adjustment of the Xia approach in this case may also be seen while simply comparing the RTP field data neglecting topography and the Xia field data. RTP neglecting topography has a lot more high-frequency content inbound than the Xia approach which maybe was not able to adjust this accurate enough. The weak oscillating character of the error data as well as the *lre*-plot depicts this more clearly.

6. Conclusion / Zusammenfassung

6.1. ...for downward field continuation / für die Feldfortsetzung nach unten

6.1.1. FFT

For depth smaller than the grid spacing FFT works just fine. Nevertheless, there are small oscillations existent especially at the locations of the shallowest anomalies.
/ Für *Tiefen kleiner* dem *gewählten Stützstellenabstand funktioniert die FFT* sehr *gut.* Nichtsdestotrotz, sind schon hier leichte *Oszillationen erkennbar,* speziell *an den* Stellen *der seichtesten Quellen.*

On the contrary, for depth bigger than the grid spacing interval FFT is a lot worse than all the other results, especially if the the field continuation is done close to the depth of the shallowest anomaly.
/ Auf der anderen Seite, für Tiefen größer als der gewählte Stützstellenabstand liefert die FFT sehr viel schlechtere Ergebnisse, im speziellen dann, wenn die Feldfortsetzung nach unten knapp über die seichtesten Quellen durchgeführt wird.

The results of the small aperture of the Vulcano field with 10m · 10m spacing showed that FFT is not or too less improved if no classical field augmentation like an regional field is used. When a regional field was used as “augmented area” and the field continuation depth is a multiple of the grid spacing FFT is not competitive enough compared to the other approaches.
/ Die Ergebnisse des kleinen Ausschnitts aus dem Vulcano Feld mit 10m · 10m Stützstellenabstand zeigen dass die FFT nicht, oder zu schwach durch die Verwendung von Regionalfelddaten verbessert wird. Auch die Feldfortsetzung in Tiefen die einem Vielfachen des Stützstellenabstandes entsprechen, wird nicht ausreichend verbessert, um gegen die anderen Verfahren konkurrenzfähig zu bleiben.

6.1.2. Cooper

The simple datasets show a long-wavelength character in the remaining error if no “zero-level-error-correction” as proposed by Cooper is applied. The improvement

through this proposal removes long-wavelength character partly but not completely but no high-frequency content.
/ Die simplen Datensätze weisen einen langwelligen Charakter in den verbleibenden Fehlern auf, wenn die von Cooper vorgeschlagene Subtraktion des Fehler im Beobachtungsniveau nicht vom Fehler in der Tiefe Z abgezogen wird. Diese Verbesserung führt allerdings dazu das der langwellige Fehler zumindest teilweise aus Daten verschwindet. Hochfrequente Anteile hingegen, bleiben davon völlig unberührt.

When field continuation is done to depth bigger than the grid spacing, all Cooper approaches start to oscillate. Furthermore interesting is that the best results were made by bi-cubic Laplace Equation approaches using 2nd and 1st vertical derivatives when the simple datasets were used and the finite-difference mixed horizontal derivatives approaches for the more realistic fields (Except for the local field plus the regional part of Vulcano where Cooper delivered so strong oscillations that there was not even any field data recognizable.).
/ Bei einer Feldfortsetzung in Tiefen größer dem gewählten Stützstellenabstand beginnen alle erwähnten Cooper Ansätze zu oszillieren. Des Weiteren interessant ist dass die besten Ergebnisse mit den bi-kubischen-Spline-Ansätzen unter Verwendung der Laplace Gleichung entstanden sind (1. und 2. vertikale Ableitungen), solange die simplen Datensätze verwendet wurden. Auf der anderen Seite, lieferten bei den realistischeren Datensätzen die gemischt horizontalen finiten-Differenzen-Ansätze von Cooper die besten Cooper-Ranking Ergebnisse (Mit Ausnahme des kleinen Datensatzes aus Vulcano wo über die Tiefe, die dem Stützstellenabstand entsprach, feldfortgesetzt wurde. Bei diesem Datensatz lieferten selbst die besten Cooper Ansätze stark oszillierende - Mit Amplituden größer den verwendeten Modelfelddaten. - Ergebnisse).

Influence from field-augmentation and filtering order are most of the time marginal. Nevertheless the simple dataset results revealed a small advancement if filtering in space domain is done before augmentation to reduce edge effects like oscillations.
/ Der Einfluss der Reihenfolge von Felderweiterung vor und nach dem Anbringen des Filters im Raumbereich war meist marginal. Nichtsdestotrotz zeigten die Ergebnisse der simplen Datensätze eine kleine Verbesserung, wenn die Filterung im Raumbereich vor der Felderweiterung durchgeführt wurde, um Randeffekte besser zu unterdrücken.

For depths a multiple deeper than the grid spacing, all of Coopers results are oscillating extremely. Even when a “high sophisticated” field-augmentation is used. The amplitudes of the errors as well as the frequency of them are far away from a acceptable range (Which was maybe caused by the different spacing of the regional and the local part of the field's sampling points and the resulting interpolation errors.). The improvement proposed by Cooper to remove the long-wavelength character of the errors by subtracting the error made in measurement datum from the error in depth Z turned out to work only partly. Especially for depths deeper than the used grid spacing Cooper's approaches all start to oscillate. These oscillations can't be removed by this “improvement”. Nevertheless there where always some improvement made by this idea but the benefits were nearly negligible.
/ Die Ergebnisse der Feldfortsetzung in Tiefen die einem Vielfachen des verwendeten Stützstellenabstand entspricht führt bei allen Ansätzen von Cooper zu massiven Oszillationen, die das gesamte Datenfeld unkenntlich machen. Auch deren Amplituden sind weit ab von einem akzeptablen Bereich. Dies könnte durch den unterschiedlichen Stützstellenabstand im Regional- und Lokal-feldbereich und die dadurch entstehenden Interpolationsfehler, hervorgerufen worden sein. Die bereits erwähnte und von Cooper vorgeschlagene Methode zur Unterdrückung langwelliger Fehlerstrukturen funktioniert

auch bei diesem Beispiel nur teilweise. Da dieser Vorschlag von Cooper auf den langwelligen Anteil zielt, bleiben somit auch die Oszillationen nahezu unberührt. Lediglich eine marginale Verbesserung der Amplituden ist erkennbar.

6.1.3. ISVD

For the simple datasets ISVD delivered good results with clearly visible errors only at the shallowest anomaly. There was no real difference recognizable between 4 to 7 Taylor series terms. The use of the truncation-parameter instead of the amount of Taylor series terms didn't show any remarkable improvement as the interpreter is not able to tell if the standard-deviation of the last series term is small compared to the whole series's standard-deviation for a given dataset. Especially ISVD showed a typical error structure. For all locations where anomalies existed, there were the biggest errors and those errors always had negative peaks at those locations. Everywhere else the errors were quite small. This effect became stronger for closer field continuation levels to the shallowest source layer.
/ Mit den simplen Datensätzen liefert auch die ISVD gute Ergebnisse, mit klar erkennbaren Fehlerstrukturen an den horizontalen Positionen der seichtesten Anomalien. Es ist kein Unterschied erkennbar zwischen 4 und 7 Taylor-Reihentermen. Die Verwendung des alternativen "truncation parameter" zeigt keine erkennbaren Vorteile, da für den Benutzer kaum klar ist wann die Standardabweichung des letzten Taylor-Reihenterms klein ist im Vergleich zur Standardabweichung des gesamten Feldes, für einen spezifischen Datensatz.

As field continuation was done to a depth deeper than the grid spacing the result oscillates a bit as can be seen in the simple dataset at -300m. Nevertheless the results for the local part of Vulcano with the regional field as "augmented area" turns out to be quite stable, at least in the inner area of the local field. And in this dataset the downward continuation was done to a multiplicity of the grid spacing distance. So at least for ISVD the regional field as "field-augmentation" seemed to be a good solution.
/ Als die Feldfortsetzung in Tiefen durchgeführt wurde, die größer als dem verwendeten Stützstellenabstand waren, fingen die Ergebnisse auch mit ISVD leicht zu oszillieren an, wie in den Ergebnissen der simplen Datensätze in -300m erkennbar ist. Nichtsdestotrotz, die Ergebnisse für den lokalen Bereich des Vulcano Teilausschnitts, mit Regionalfeldinformation als "Felderweiterung" sahen recht stabil aus, zumindest im inneren Bereich des lokalen Feldes. Hierbei ist auch zu berücksichtigen, dass die Feldfortsetzung in Tiefen durchgeführt wurde, die einem Vielfachen des Stützstellenabstandes entspricht.

The results for the whole Vulcano dataset in -50m and therefore within grid spacing distance and far away of the shallowest source looked quite good and similar as FFT errors but with bigger magnitudes again at the locations of the shallowest sources. ISVD used for field continuation to -130m delivered errors that were a lot bigger than that of Cooper in this depth. A maximum of around 50% relative error was visible in the centre of the field at that depth, with respect to the model-field maximum.
/ Die Ergebnisse für den kompletten Vulcano Datensatz mit Tiefen (-50m) kleiner als der verwendete Stützstellenabstand und noch weit weg von der seichtesten Quelle sehen recht gut aus und sogar ähnlich dem FFT Ergebnis in dieser Tiefe. Lediglich die Amplituden der ISVD Fehler waren etwas größer an den Stellen der seichtesten Quellen. Die Fehler der ISVD in -130m Tiefe und damit knapp oberhalb der seichtesten Quellen waren größer als die von Cooper in der selben Tiefe. Der relative Fehler im

Zentrum des Feld betrug etwa 50% des absoluten Maximums des verwendeten Modellfeldes in der selben Tiefe.

6.1.4. Tikhonov

The synthetic dataset led to the first assumption that the Tikhonov / Pasteka approach is the best approach to be used for field continuation to depth smaller than the grid spacing distance. Further investigations revealed that field continuation to depth bigger than the grid spacing distance works fine for the locations where no sources are to be assumed. Furthermore the magnitude of the maximum error was around ten times bigger than that of the best Cooper approach at the same depth.
/ Die Ergebnisse des synthetischen Datensatzes führten zur ersten Annahme das Tikhonov's / Pasteka's Ansatz der beste Ansatz für die Feldfortsetzung nach unten ist, solange die Tiefe kleiner ist als der verwendete Stützstellenabstand. Weitere Tests zeigten dass die Feldfortsetzung für Tiefen größer dem gewählten Stützstellenabstand gut funktioniert für Positionen an denen keine Quellen sind. Die Amplituden der größten vorkommenden Fehler in dieser Tiefe, mit den simplen Datensätzen, war allerdings um etwa zehnmal größer als die von Cooper.

Further tests on the smaller aperture including a regional and local field part with field continuation to 50m depth – 5 times the grid spacing distance – depicted very clearly the over-regularization of Tikhonov's / Pasteka's algorithm when a regional part assumed as a high sophisticated field-augmentation, was used. Due to the fact that the field continuation depth (50m) is not even close to the shallowest “source layer” at all, (~140m) this error may origins from the continuation depth exceedance of the grid spacing distance.
/ Weitere Tests am kleinen Teilausschnitt von Vulcano inklusive der Regionalfelddaten in 50m Tiefe, also 5 (fünf) mal dem verwendeten Stützstellenabstand, zeigten eine klare Überregularisierung durch Tikhonov's / Pasteka's Ansatz. Da diese Tiefe noch weit entfernt war von den seichtesten Quellen in ~140m Tiefe, kann dieser Fehler wohl nur durch das Überschreiten der Tiefe, die dem Stützstellenabstand entspricht, verursacht worden sein.

The results for the field-continuation to depths just a bit bigger than the grid spacing distance but close to the shallowest “source layer” again shows the over-regularization of Tikhonov's / Pasteka's approach. Due to this fact the biggest errors are again at the locations of the shallowest anomalies. The error pattern in this case is again very similar to the best ISVD approach but due to the over-regularization the amplitudes of those errors are just bigger.
/ Die Ergebnisse für die Feldfortsetzung in Tiefen knapp oberhalb der seichtesten Quellen, bei leichter Überschreitung der Tiefe, die dem Stüzstellenabstand entspricht, zeigten erneut das überregularisierende Verhalten von Tikhonov's / Pasteka's Ansatz. Die Fehlerstruktur ähnelte sehr stark dem ISVD-Fehler aber mit größeren Amplituden.

Generally Tikhonov delivers a astonishing similarity to the ISVD approach results which would be definitely a interesting point for further investigations.
/ Generell ist zu erwähnen das die Ergebnisse von Tikhonov erstaunlich Ähnlichkeit zu denen der ISVD hat. Hier wäre sicher ein interessanter Punkt für weitere Forschungen zu diesem Thema.

Concluding the results for field continuation downward, one can tell there is no general

best solution for field continuation but there are some recommendations which may help further interpreters to chose the right approach with a given dataset. First of all except for field continuation with Cooper approaches using bi-cubic splines to derive derivatives all approaches work fine for depths bigger than the grid spacing interval. The improvement proposed by Cooper to remove a long-wavelength character of the error by subtracting the error made by the field continuation process in measurement datum from the continued field in depth Z works only for long-wavelength errors. If field continuation is done to depths a multiplicity of the grid spacing distance Cooper's approaches are definitely not to be preferred cause the high-frequency content is not filtered at all through this “improvement” and the results extremely oscillate. Furthermore the investigations on filtering-field-augmentation-order showed a small advantage when filtering in space-domain is done before field augmentation and after that downward field continuation. To use FFT for field continuation is only reasonable for depths smaller than the grid spacing distance. FFT is even worse than Cooper's oscillating approaches when field continuation is done to depths a multiplicity of the grid spacing distance. The Cooper results for field continuation close to the shallowest “source layer” reveals unidirectional derivatives as best solutions. Nevertheless, their stripe-formed errors are distracting and the mixed-horizontal derivatives also in the ranking turned out to be only a bit worse. Therefore the mixed horizontal derivatives using finite-differences should be preferred to all other Cooper approaches. The “improvement”, proposed by Cooper did not help at all, close to the shallowest “source layer”. As all the Cooper approaches delivered bigger artefacts of some kind they are definitely out of competition even though their error-ranges where similar than ISVD and Tikhonov. The results for Tikhonov / Pasteka are quite good for synthetic datasets. The results for real datasets like Vulcano are partly different. Field continuation to depths deeper than the grid spacing distance leads to over-regularization of the Tikhonov / Pasteka approach and therefore continuation close to the shallowest sources is over-regularized if the shallowest source is close beneath the depth which is equal to the used grid-spacing distance. The errors made by Tikhonov and ISVD revealed a astonishingly similar pattern when continuation was done to depths bigger than the grid spacing distance which could be a starting point for further investigations. Through this over-regularization of Tikhonov's / Pasteka's approach the errors for Tikhonov are bigger than that of ISVD and therefore ISVD should be preferred to all others except for depths smaller than the grid spacing distance where FFT is the best choice. To chose the best ISVD approach is contrary to the proposed 7 terms by Fedi's and Florio's paper on this topic. The results in this thesis reveal an optimum of around 4 to 6 terms for real datasets. For depths close to shallowest sources 6 terms is better, for depths a multiplicity of the grid spacing – with a regional part as high-sophisticated field-augmentation – 4 to 6 terms should be preferred depending on the area of interest. This means 4 terms if the whole local part of a field is of interest and 6 terms if just the inner part is more interesting.

/ Zusammenfassend kann sicher gesagt werden, dass keine wirkliche beste Variante für die Feldfortsetzung exestiert aber es können zumindest ein paar Empfehlungen gegeben werden, um künftigen Interpreten die Wahl des richtigen Ansatzes, für unterschiedlichste Fälle zu erleichtern. Zuerst ist zu erwähnen, das für alle Ansätze, außer denen von Cooper mit bi-kubischen Splines, für Tiefen größer als der gewählte Stützstellenabstand recht gute Ergebnisse zu erwarten sind. Der Vorschlag von Cooper die Fehler einer jeweiligen Methode in Beobachtungsniveau zum Ergebnis in Tiefe Z hinzu zu addieren, funktioniert um den langwelligen Fehler-Anteil zu unterdrücken teilweise. Für Tiefen ein Vielfaches größer als der gewählte Stützstellenabstand ist Cooper definitiv nicht verwendbar weil zu starke Oszillationen im gesamten Datenfeld entstehen die nicht durch den vorher erwähnten Vorschlag von Cooper gefiltert werden.

Des Weiteren zeigen die Ergebnisse eine leichte Verbesserung wenn die Felderweiterung im Raumbereich nach der Filterung im Raumbereich aber vor der Feldfortsetzung nach unten stattfindet. Die FFT für die Feldfortsetzung nach unten zu verwenden ist eigentlich nur zu empfehlen für Tiefen die kleiner als der gewählte Stützstellenabstand sind. Für Tiefen darüber sind die Ergebnisse der FFT sogar schlechter als die der Cooper Ansätze. Für die Feldfortsetzung knapp oberhalb der seichtesten Quellen wären die unidirektionalen horizontalen Cooper Ansätze die beste Wahl unter den Cooper Ansätzen, solange die Tiefe nur leicht größer ist, als der gewählte Stützstellenabstand. Da aber die Entscheidung welche horizontale Richtung gewählt werden soll (und somit die beste wäre), davon abhängt wie die Potentialfeld-Struktur ist, sollte die Empfehlung eher lauten das die gemischt horizontalen Ableitungen zu bevorzugen sind. Deren Fehler sind zwar ein wenig größer aber zumindest besteht keine systematische Richtungsabängigkeit des Fehlers. Nahe an den seichtesten Quellen bringt Cooper's Vorschlag zur Unterdrückung des langwelligen Fehlers keinen erkennbaren Vorteil mehr. Im Vergleich zu ISVD sind die Amplituden des Fehlers von Cooper zwar etwas kleiner aber dafür ist der horizontale Ausdehnung größer. Tikhonov zeigt bei den simplen Datensätzen kaum Fehler, jedoch sind die Fehler bei den realistischeren Datensätzen dafür etwas größer als die der anderen Methoden. Die Feldfortsetzung in Tiefen größer dem gewählter Stützstellenabstand führt bei Tikhonov zur Überregularisierung und dementsprechend auf zu stark geglätteten Daten. Dies dürfte nicht wirklich mit der Quelltiefe in Zusammenhang stehen sondern eher mit der Überschreitung der Tiefe, die dem Stützstellenabstand entspricht. Der Ansatz von Tikhonov zeigt immer wieder äußerst erstaunliche Ähnlichkeiten in der Fehlerstruktur zu ISVD mit dem Unterschied, dass Tikhonov stärker glättet und dementsprechend die Amplituden der Fehler größer sind. Definitiv ein interessanter Punkt für weitere Forschungen in diesem Gebiet. Die ISVD liefert stark punktuelle Fehler an den Stellen der seichtesten Quellen. Dieses Verhalten ändert sich nur falls eine Feldfortsetzung in Tiefen größer dem gewählten Stützstellenabstand durchgeführt wird insoweit (inkl. Regionalfeldinformationen), dass stärkere Oszillationen in Form von Randeffekten auftreten. Da die ISVD, Tikhonov und FFT starke Ähnlichkeiten aufweisen und die FFT in Tiefen kleiner dem gewählten Stützstellenabstand auch die kleinsten Fehleramplituden liefert wäre diese hier auch zu bevorzugen. Bei Tiefen größer ist die ISVD zu bevorzugen, da die Fehleramplituden bei Tikhonov einfach größer sind als die beiden Vergleichbaren und Cooper Fehler liefert die zu breit "streuen". Im Gegensatz zu den Empfehlungen in Fedi's und Florio's Artikel 7 (sieben) Taylor-Reihenterm für die ISVD als Optimum zu verwenden, liefern die Ergebnisse der Tests hier eine klare Präferenz zwischen 4 (vier) und 6 (sechs) Taylor-Reihenterme. Dabei sollten je mehr Reihenterme verwendet werden, je kleiner das zu untersuchende Gebiet im Vergleich zum Gebiet ist von dem aus Daten miteinfließen. Die Randgebiete werden dabei stark verrauscht erscheinen. Für möglichst ausgewogene gleichmäßig verteilte Fehler ohne viel Rauschen sollten eher weniger Terme genommen werden. Vier Reihenterme schien in unseren Beispielen die besten Ergebnisse zu liefern.

6.2. ...for reduction to pole on arbitrary surfaces / für die Reduktion zum Pol auf beliebigen Flächen

6.2.1. ...for the simple dataset / für den simplen Datensatz

The simple dataset with two sources and different inclinations shows clearly the

increase of error of the classical *RTP* for small inclinations – close to the magnetic equator. The maximum of 10% relative error at 10° inclination depicts very palpably that the reduction to pole process leads to a relatively big error. Nevertheless the error made by reduction to pole neglecting the topography is around 1% at 30° and therefore astonishingly good. The maximum relative offset free error of 0.3% at 50° and 0.2% at 70° reveals that the errors made by *reduction to pole* while neglecting the topography is acceptable for simple cases and for inclinations at least bigger than 30°.
/ Der einfache Datensatz mit nur zwei Punktquellen zeigte einen klar erkennbaren Anstieg des Fehlers bei kleineren Inklinationen, nahe am magnetischen Equator. Das Maximum mit 10% relativem Fehler bei 10° Inklination machte das sehr schön klar. Der Fehler bei 30° Inklination war etwa 1% und damit überraschend klein. Bei 50° waren es noch maximal 0.3% und 0.2% relativer maximaler Fehler bei 70°. Somit für einfach Datensätze kann man ab etwa 30° Inklination von akzeptablem Fehler sprechen.

6.2.2. ...for the more realistic dataset of Vulcano / für den realistischeren Datensatz von Vulcano

The results for the more realistic case of Vulcano is a bit different. Here the errors made by classical pole reduction process is around 10% with respect to the model-field maximum with around 57° inclination. Though the adjusted field of Xia was taken as "true" field and the adjustment of this quite rough dataset (500m · 500m spacing) was good, reduction to pole process neglecting the topography here delivered a mean relative error of around 0.2% which is also quite good. The biggest errors seem to cumulate around the areas with steep topography in combination with big field magnitudes. As in the results of the simple datasets the errors were positive as well as negative.
/ Die Resultate für die realistischeren zwei Datensätze von Vulcano waren dann doch etwas unterschiedlich zu den einfachen Modelldaten. Die relativen Fehler der RTP durch die Vernachlässigung des topograpschien Einflusses lagen hier bei maximal 10% bei etwa 57° Inklination. Die Anpassung mit Xia für den einfachen Fall mit 500m · 500m Stützstellenabstand war äußerst gut. Die RTP liefert hier einen mittleren relativen Fehler um die 0.2%, was man auch als recht gut bezeichnen könnte. Dabei schienen die größten Fehler in Regionen aufzutreten, in denen es starke Höhenunterschiede in Kombination mit großen Potentialfeldwerten gab. Hier traten negative als auch positive Fehler auf.

The results for the original Vulcano dataset with 100m · 100m grid spacing was entirely different. The bad adjustment of Xia caused the "true" field to become extremely strong influenced by artefacts. This was the worst of all adjustments for this tests and therefore the results are shown but only pinpoints out how important a better field reproduction method for magnetic field data is, hopefully sometimes solvable by the means of some EQS algorithm.
/ Die Ergebnisse für den orginalen Vulcano Datensatz mit 100m · 100m Stützstellenabstand war komplett unterschiedlich zu den vorherigen. Da die Anpassung mit Xia nämlich nicht wirklich gut funktioniert sind auch die Ergebnisse dieses Datensatzes eher zu sehen als klare Forderung eine andere EQS-Methode für die Anpassung der Modell-felder zu verwenden. Diese müsste aber erst entwickelt werden, denn zum jetzigen Zeitpunkt exestiert keine bekannte Methode mit der magnetische Felddaten INKLUSIVE Inklination und Deklination genauer angepasst werden können als mit Xia.

6.2.3. ...for the real dataset of Socorro / für den echten Datensatz von Soccoro

It should be mentioned first, that the adjustment of the Socorro with Xia was better than the one with the 100m · 100m Vulcano dataset but was still bad, since the absolute maximum adjustment error of around 50 nT was already ~3% of the maximum magnitude of the model-field. Therefore the resulting errors of reduction to pole neglecting the topography are maybe not as distinct as requested. Furthermore, the real dataset of Socorro had to be low-pass filtered before the tests were done several times to achieve at least this adjustment with Xia. The maximum relative error of ~3% is therefore maybe for real somewhere around 5% or more. Very interesting in this result also is that here maximum relative errors are not only located at the steepest topographic locations but also at those regions with higher topographic undulations. This is maybe caused by the bad adjustment of the Xia approach and the resulting bad reproduction of the high-frequency content. Here again the adjustment with Xia shows its disadvantage. Maybe further investigations in this topic and an appropriate EQS algorithm development would solve the problem completely but at the moment no better way was found.
/ Als erstes sollte erwähnt werden, dass die Anpassung des Soccoro Datensatzes mit Hilfe von Xia besser war als die Anpassung an den Vulcano Datensatz mit 100m · 100m Stützstellenabstand, jedoch immer noch schlecht da der absolute maximale Fehler bei der Anpassung von Soccoro bei etwa 50nT lag und somit etwa 3% der maximalen Amplitude des Modellfeldes entsprach. Deshalb sollten die Ergebnisse hier nicht unbedingt so genau genommen werden wie vielleicht erhofft. Außerdem musste der Datensatz von Soccoro vor der Testreihe einige male tiefpass-gefiltert werden um zumindest diese Anpassung mit Xia zu ermöglichen. Der gefilterte Datensatz wurde anschließend für den RTP Prozess sowie für die Xia Anpassung verwendet. Daher könnten die maximalen relativen Fehler von ~3% vielleicht auch schon bei etwa 5% liegen. Hier auch wieder sehr interessant ist die Tatsache, dass die größten Fehler nicht an den steilsten Geländekanten in Kombination mit den größten Potentialwerten ist, sondern auch an den Stellen mit den größten topographischen Erhebungen. Dies könnte aber auch wieder eine Folge der schlechten Anpassung mit Xia sein und dem daraus resultierenden hochfrequenten Fehler. Hier zeigt leider Xia seine klaren Nachteile und die Notwendigkeit auf einen passenden EQS-Algorithmus zu entwickeln.

Concluding the results of reduction to pole while neglecting the topographic influence one can say that negligence of topography is allowed for regional field inclinations bigger than at least 30° but errors of around 10% of the maximum of the measured field may occur in steep topographic regions. The errors made in smoother areas is around 1%. The investigation of this topic is definitely not finished but with the limitations of Xia's bad adjustment, no more accurate result was possible. An outlook for further investigations in this topic would definitely be to replace Xia's method for reduction to pole on arbitrary surfaces with a more accurate one and then repeat those tests.
/ Zusammenfassend kann für die Reduktion zum Pol auf beliebigen Flächen gesagt werden, dass die Vernachlässigung der Topographie für Inklinationen zumindest größer 30° mit relativen Fehlern von etwa 10% zu Buche schlägt. Die größten Fehler treten dabei in den Regionen der stärksten topographischen Änderungen auf. Die relativen Fehler bei eher glatteren topograpischen Strukuren scheinen dabei um die 1% zu liegen. Die Untersuchung auf diesem Gebiet ist definitiv nicht abgeschlossen, jedoch

verhindert die schlechte Anpassung durch Xia genauere Aussagen zum jetzigen Zeitpunkt. Klarer Punkt für weitere Untersuchungen wäre das Ersetzen des Xia Algorithmus durch einen passenderen und die Wiederholung dieser Tests.

7. Acknowledgements

My utmost honest gratitude belongs to Prof. Dr. *Bruno Meurers* for his ongoing support and patience according to Fortran 77 compilers or the algorithms of *Cooper*, *Fedi and Florio*, *Cordell* and reduction to pole problem set as suggested by personal communication with *Dr. Andreas Ahl*, Geologische Bundesanstalt Wien (GBA). Without Dr. Bruno Meurers' sustaining hours of support it would have been hardly possible to do the step from theory to practice in Fortran 77, although I had some basic background on Fortran 77 according to a fine introduction in Fortran 77 by Mag. *Marc Merz* in "analysis of seismic data measurement". Furthermore I would like to thank Dr. *Roman Pasteka* from Comenius University in Bratislava for the support belonging to the Tikhonov algorithm and the comprehensible explanations in “Semi automated methods for potential fields” lessons, belonging his own developed source code, based on Tikhonov's papers and the application as well as precautions of and for the global minimum of the C-Norm function and hence the resulting fields.

8. References

BRACEWELL 1978: R. N. Bracewell, The Fourier transform and its applications, 1978, ISBN:, P, McGraw-Hill

XIA 1993: Geophysics Vol.:58 No.:4: Jianghai Xia, Donald R. Sprowl and Dana Adkins-Heljeson, Corrections of topographic distortions in potential-field data: A fast and accurate approach, 1993, P515-523

IVAN 1994: Geophysical Prospecting Vol.:42 No.:: Ivan, M., Upward continuation of potential fields from a polyhedral surface, 1994, P391-404

COOPER 2004: Exploration Geophysics Vol.:35 No.:: Gordon Cooper, The stable downward continuation of potential field data, 2004, P260-265

FEDI and FLORIO 2002: Geophys. J. Int. Vol.:151 No.:: M. Fedi and G. Florio, A stable downward continuation by using the ISVD method, 2002, P146-156

TIKHONOV 1968: Izv., Earth Physics, translated by F. Goodspeed Vol.: No.:12: A.N. Tikhonov, V.B. Glasko, O.K. Litvinenko and V.P. Melikhov, Analytic Continuation of a potential in the direction of the disturbing masses by the regularization method, 1968, P30-48

BLAKELY 1995: R.J. Blakely, Poential Theory in Gravity & Magnetic Applications, 1995, ISBN:0-521-57547-8, P178ff,

DOBRIN 1976: Dobrin, M. B., Introduction to geophysical prospecting, 1976, ISBN:, P483, McGraw-Hill Book Co.

OKUMA, S. et. al. 2006A: Geol. Surv. Japan Vol.:57 No.:: Okuma, S., Nakatsuka, R. Supper, M. Komazawa, High-resolution aeromagnetic anomaly map of the Vulcano-Lipari volcanic complex, Aeolian Islands , Italy., 2006, P177-190

OKUMA, S. et. al. 2006B: Explor. Geophys. Vol.:37 No.:: Okuma, S., Nakatsuka, M. Komazawa, M. Sugihara, S. Nakano, R. Furukawa, and R. Supper, Shallow subsurface structure of the Vulcano-Lipari volcanic complex, Italy, constrained by the helicopter-borne aeromagnetic surveys., 2006, P129-138

CORDELL 1992: Geophysics Vol.:57 No.:4: Lindrith Cordell, A scattered equivalent-source method for interpolation and gridding of potential-field data in three dimensions, 1992, P629-636

WHITTAKER AND WATSON 1962: Whittaker, E.T. and Watson, G.N., A course of modern analysis, 1962, ISBN:, P49, Cambridge Univ. Press.

BERES 2010: Jan Beres, Comparison and evaluation of three methods of analytic downward continuation,Comenius University in Bratislava, 2010

Bracewell 1978: R. N. Bracewell, The Fourier transform and its applications, 1978, ISBN:, P, McGraw-Hill

Geophys. J. Roy. Astr. Soc.,,447-455: Parker, R. L., The rapid calculation of potential anomalies, 1973

9. Appendix

9.1. Equations

9.1.1. Truncation parameter for ISVD approach

$$t-p.>\sqrt{\frac{\sum_{k=1}^{N}\{\frac{Z_D^k}{k!}\frac{\partial^k U(i,j)}{\partial z^k}\}^2-\sum_{k=1}^{N}\{\frac{Z_D^k}{k!}\frac{\partial^k U(i,j)}{\partial z^k}R^{-1}(k)\}}{\sum_{k=1}^{N}\{\sum_{k=1}^{N}[\frac{Z_D^k}{k!}\frac{\partial^k U(i,j)}{\partial z^k}]\}^2-\sum_{k=1}^{N}\sum_{k=1}^{N}\{\frac{Z_D^k}{k!}\frac{\partial^k U(i,j)}{\partial z^k}R^{-1}(k)\}}} \qquad (9.1.1.1)$$

Z_D...depth to continue to, U(i,j)...original field with dimension A · B

k...index of Taylor series term,

N...maximum amount of Taylor series terms to be calculated

t-p. ...truncation parameter defined by user

$$R^{-1}(k)=(A-2\cdot s(k)-1)(B-2\cdot s(k)-1),\ s(k)=\begin{cases}\frac{k}{2}, if\ mod(k,2)=0\\ \frac{k}{2}, if\ mod(k,2)\neq 0\end{cases} \qquad (9.1.1.2)$$

As soon as the 9.1.1.1 is valid or *N* is reached the program stops and puts the calculated field in a predefined grid file.

9.2. Index

adjustment-error....**14**
Ahl....**39**
Bi-cubic splines....**32**
boundary and continuity conditions....**32**
Bruno Meurers....**128**
BS0af....**33**
BS0fa....**33**
BS1af....**33**
BS1fa....**33**
BS2af....**33**
BS2fa....**33**
BS3af....**34**
BS3fa....**34**
BS4af....**34**
BS4fa....**34**
Cooper....**7, 14, 29, 128**

Cordell....**13, 128**
Cordell algorithm....**13p.**
Dr. Andreas Ahl....**11, 128**
EQS....**8**
equivalent source principles....**13**
equivalent-source....**8**
Fast Fourier Transform....**37**
FD0af....**31**
FD0fa....**31**
FD1af....**31**
FD1fa....**31**
FD2af....**31**
FD2fa....**31**
FD3af....**31**
FD3fa....**31**
FD4af....**32**
FD4fa....**32**
Fedi and Florio....**14, 35p., 50, 128**
FFT....**7, 14, 23**
FFT (BRACEWELL 1978)....**7**
finite differences....**32**
GBA....**13, 19, 39**
Geologische Bundesanstalt, Vienna. .**11, 13, 39**
helicopter flight height profile....**18**
IGRF....**9**
Integrated second vertical derivative....**7**
Integrated Second Vertical Derivative....**36**
ISVD....**7, 35**
ISVD N X....**36**
Laplace equation....**30pp.**
Lipari....**13**
logarithmic relative offset free error....**47**
lre....**57, 111p., 114, 116pp.**
Marc Merz....**128**
parameter C....**19**
Poisson's theorem....**10, 18**
R. Singleton 1968....**37**
reduction to pole....**9, 112, 118, 125**
Roman Pasteka....**23, 38, 128**
RTP....**9, 110, 112, 125**
Socorro....**19**
Stanford Research Institute....**37**
strong stripe formed errors....**111**
three layers....**14**
Tikhonov....**14, 38**
Tikhonov / Pasteka....**7**
Vulcano....**13, 18, 23, 55**
Xia....**19, 21, 111p., 115**

9.3. List of figures:

figure 2.1.1.1: model-field in 0m depth. Scale bar in mGal....**12**
figure 2.1.1.2: model-field in 50m depth. Scale bar in mGal....**13**

figure 2.1.1.3: model-field in 300m depth. Scale bar in mGal.....**13**

Figure 2.1.2.1: flowchart for model-field generation, RED = START, GREEN = model-fields used for the downward continuation tests.....**14**

figure 2.1.2.2: model-field in 0m depth 100m · 100m sampling interval. Scale bar in nT.....**15**

figure 2.1.2.3: model-field in 50m depth 100m · 100m sampling interval. Scale bar in nT.....**16**

figure 2.1.2.4: model-field in 130m depth 100m · 100m sampling interval. Scale bar in nT...**16**

figure 2.1.3.1 model-field in 0m depth, regional (100m · 100m samping point spacing) and local part (10m · 10m samping point spacing) interpolated to 10m · 10m sampling interval. The red rectangle marks the local part of the field which will be discussed in the results. Scale bar in nT.....**17**

figure 2.1.3.2 model-field in 50m depth 10m · 10m sampling interval. The red rectangle marks the local part of the field which will be discussed in the results. Scale bar in nT.....**17**

Figure 2.2.2.1: simple model-field 2 sources, inclination 10°.....**20**

figure 2.2.2.2: simple model-field 2 sources, inclination 30°.....**20**

figure 2.2.2.3: simple model-field 2 sources, inclination 50°.....**21**

figure 2.2.2.4: simple model-field 2 sources, inclination 70°.....**21**

figure 2.2.2.5 simple model-field 2 sources, inclination 90° (true pole-reduced field).....**21**

Figure 2.2.2.6: Topography for simple datasets. Scale bar in meter.....**21**

Figure 2.2.3.1: model-field of Vulcano dataset, re-sampled to 500m · 500m. Scale bar in nT.**22**

Figure 2.2.3.2: topography field for Vulcano dataset re-sampled to 500m · 500m. Heights in meter.....**22**

figure 2.2.4.1 model-field Vulcano 100m · 100m grid spacing. Scale bar in nT.....**22**

figure 2.2.4.2 topography for Vulcano dataset 100m · 100m grid spacing. Heights in meter...**22**

Figure 2.2.5.1: model-field of Socorro, no pole-reduction. Scale bar in nT.....**23**

Figure 2.2.5.2: topography of Socorro, heights in meter.....**23**

figure 3.1.1 potential field with problematic area (PINK) of two dimensional linearly interpolating field-augmentation for 1st and 2nd order vertical derivative calculation by Laplace's equation. Original field size marked by RED rectangular. Scale bar in nT per square-kilometer.....**27**

figure 3.3.1 ISVD flowchart for Taylor-series development.....**36**

figure 3.5.1 Tikhonov algorithm (with special thanks to Dr. Roman Pasteka, Comenius

University of Bratislava).....**38**

figure 4.3.1 Geometry of the plane of the equivalent source E (red) and the observation surface S (green) as well as the median topography height (blue).....**43**

figure 4.3.2 Magnitude of Poisson's theorem operator.....**45**

figure 4.3.3 Phase of Poisson's theorem operator.....**45**

figure 4.3.4 real part of A, a strong jump discontinuity as |K| approaches zero.....**46**

figure 4.3.5 imaginary part of A, another weaker jump discontinuity as |K| approaches zero. **46**

figure 5.1.1.1: FFT.....**48**

figure 5.1.1.2: Cooper approach BS4af.....**48**

figure 5.1.1.3: Cooper approach BS3fa.....**48**

figure 5.1.1.4: Cooper approach BS4fa.....**48**

figure 5.1.1.5: Cooper approach BS3af.....**49**

figure 5.1.1.6: Cooper approach FD3fa.....**49**

figure 5.1.1.7: ISVD 6 30.....**49**

figure 5.1.1.8: ISVD 20 6.....**49**

figure 5.1.1.9: ISVD 8 30.....**49**

figure 5.1.1.10: ISVD 4 30.....**49**

figure 5.1.1.11: ISVD 7 30.....**50**

figure 5.1.1.12: ISVD 5 30.....**50**

figure 5.1.1.13 Tikhonov / Pasteka.....**50**

figure 5.1.1.14: error FFT.....**51**

figure 5.1.1.15: error Cooper approach BS4af.....**51**

figure 5.1.1.16 error Cooper approach BS3fa.....**51**

figure 5.1.1.17: error Cooper approach BS4fa.....**51**

figure 5.1.1.18: error Cooper approach FD3fa.....**51**

figure 5.1.1.19 error Cooper approach BS3af.....**51**

figure 5.1.1.20: error ISVD 8 30.....**52**

figure 5.1.1.21: error ISVD 6 30.....**52**

figure 5.1.1.22: error ISVD 7 30.....**52**

figure 5.1.1.23: error ISVD 20 6.....**52**

figure 5.1.1.24: error ISVD 4 30.....**52**

figure 5.1.1.25: error ISVD 5 30.....**52**

figure 5.1.1.26 error Tikhonov / Pasteka.....**53**

figure 5.1.1.27: error Cooper approach impBS4af.....**54**

figure 5.1.1.28: error Cooper approach impBS3fa.....**54**

figure 5.1.1.29: error Cooper approach impBS4fa.....**54**

figure 5.1.1.30: error Cooper approach impBS3af.....**54**

figure 5.1.1.31: error Cooper approach impFD3fa.....**54**

figure 5.1.1.32: Cross-section path.....**56**

figure 5.1.1.33: CS error FFT.....**56**

figure 5.1.1.34: CS error Cooper approach impBS4af.....**56**

figure 5.1.1.35: CS error Cooper approach impBS3fa.....**56**

figure 5.1.1.36: CS error Cooper approach impBS4fa.....**56**

figure 5.1.1.37: CS error Cooper approach impBS3af.....**56**

figure 5.1.1.38: CS error Cooper approach impFD3fa.....**57**

figure 5.1.1.39: CS error ISVD 6 30.....**57**

figure 5.1.1.40 CS error Tikhonov / Pasteka.....**57**

figure 5.1.1.41: lre FFT.....**59**

figure 5.1.1.42: lre Cooper approach impBS4af.....**59**

figure 5.1.1.43: lre Cooper approach impBS3fa.....**59**

figure 5.1.1.44: lre Cooper approach impBS4fa.....**59**

Figure 5.1.1.45: lre Cooper approach impBS3af.....**59**

figure 5.1.1.46: lre Cooper approach impFD3fa.....**59**

figure 5.1.1.47: lre ISVD 6 30.....**60**

figure 5.1.1.48: lre ISVD 20 6.....**60**

figure 5.1.1.49: lre ISVD 8 30.....**60**

figure 5.1.1.50: lre ISVD 7 30.....**60**

figure 5.1.1.51: lre ISVD 4 30.....**60**

Figure 5.1.1.52: lre ISVD 5 30.....**60**

figure 5.1.1.53 lre Tikhonov / Pasteka.....**61**

figure 5.1.1.54: CS lre FFT.....**62**

figure 5.1.1.55: CS lre Cooper approach impBS4af.....**62**

figure 5.1.1.56: CS lre Cooper approach impBS3fa.....**62**

figure 5.1.1.57: CS lre Cooper approach impBS4fa.....**62**

figure 5.1.1.58: CS lre Cooper approach impBS3af.....**63**

figure 5.1.1.59: CS lre Cooper approach impFD3fa.....**63**

figure 5.1.1.60: CS lre ISVD 6 30.....**63**

figure 5.1.1.61 CS lre Tikhonov / Pasteka.....**63**

figure 5.1.1.62 model-field in -300m.....**64**

figure 5.1.1.63: Cooper approach BS3fa.....**65**

figure 5.1.1.64: Cooper approach BS3af.....**65**

figure 5.1.1.65: Cooper approach BS4af.....**65**

figure 5.1.1.66: Cooper approach BS0fa.....**65**

figure 5.1.1.67: Cooper approach BS0af.....**65**

figure 5.1.1.68: Cooper approach BS4fa.....**65**

figure 5.1.1.69: ISVD 8 30.....**66**

figure 5.1.1.70 Tikhonov / Pasteka.....**66**

figure 5.1.1.71: error Cooper approach BS3fa.....**66**

Figure 5.1.1.72: error Cooper approach BS3af.....**66**

figure 5.1.1.73: error Cooper approach BS4af.....**67**

figure 5.1.1.74: error Cooper approach BS0fa.....**67**

figure 5.1.1.75: error Cooper approach BS0af.....**67**

figure 5.1.1.76: error Cooper approach BS4fa.....**67**

figure 5.1.1.77: error ISVD 8 30.....**67**

figure 5.1.1.78: error ISVD 20 3.....**67**

figure 5.1.1.79 error Tikhonov / Pasteka.....**68**

figure 5.1.1.80: error Cooper approach impBS3fa.....**69**

figure 5.1.1.81: error Cooper approach impBS3af.....**69**

figure 5.1.1.82: error Cooper approach impBS4af.....**69**

figure 5.1.1.83: error Cooper approach impBS0fa.....**69**

figure 5.1.1.84: error Cooper approach impBS0af.....**70**

figure 5.1.1.85: CS error Cooper approach impBS3fa.....**70**

figure 5.1.1.86: CS error Cooper approach impBSaf.....**70**

figure 5.1.1.87: CS error Cooper approach impBS4af.....**71**

figure 5.1.1.88: CS error Cooper approach impBS0fa.....**71**

figure 5.1.1.89: CS error Cooper approach impBS0af.....**71**

figure 5.1.1.90: CS error Cooper approach BS4fa.....**71**

figure 5.1.1.91: CS error ISVD 8 30.....**71**

figure 5.1.1.92: CS error ISVD 20 3.....**71**

figure 5.1.1.93: CS error ISVD 7 30.....**72**

figure 5.1.1.94 CS error Tikhonov / Pasteka.....**72**

figure 5.1.1.95: lre Cooper approach impBS3fa.....**73**

figure 5.1.1.96: lre Cooper approach impBS3af.....**73**

figure 5.1.1.97: lre Cooper approach impBS4af.....**73**

figure 5.1.1.98: lre Cooper approach impBS0fa.....**73**

figure 5.1.1.99: lre Cooper approach impBS0af....**73**

figure 5.1.1.100: lre Cooper approach BS4fa....**73**

figure 5.1.1.101: lre ISVD 8 30....**74**

figure 5.1.1.102 lre Tikhonov / Pasteka....**74**

figure 5.1.1.103: CS lre Cooper approach impBS3fa....**75**

figure 5.1.1.104: CS lre Cooper approach impBS3af....**75**

figure 5.1.1.105: CS lre Cooper approach impBS4af....**75**

figure 5.1.1.106: CS lre Cooper approach impBS0fa....**75**

figure 5.1.1.107: CS lre Cooper approach impBS0af....**75**

figure 5.1.1.108: CS lre Cooper approach BS4fa....**75**

figure 5.1.1.109: CS lre ISVD 8 30....**76**

figure 5.1.1.110: CS lre ISVD 20 3....**76**

figure 5.1.1.111: CS lre ISVD 20 4....**76**

figure 5.1.1.112: CS lre ISVD 20 5....**76**

figure 5.1.1.113: CS lre ISVD 20 6....**76**

figure 5.1.1.114: CS lre ISVD 7 30....**76**

figure 5.1.1.115 CS lre Tikhonov / Pasteka....**76**

figure 5.1.2.1 Error of Kriging interpolation in 0m. The red rectangle marks the local/regional field boundary. Scale bar in nT....**79**

figure 5.1.2.2 The black lines mark the 100m grid, the grey lines mark the 10m grid. Upper left corner of the model-field. The biggest errors are in the regional part. Smaller errors are also in the local part of around ± 3nT....**79**

figure 5.1.2.3: local part of the model-field with 10m · 10m sampling interval in -50m....**81**

figure 5.1.2.4: Cooper approach impBS3af....**81**

figure 5.1.2.5: ISVD 4 30....**81**

figure 5.1.2.6: ISVD 6 30....**81**

figure 5.1.2.7: ISVD 5 30....**81**

figure 5.1.2.8 ISVD 3 30....**81**

figure 5.1.2.9: ISVD 2 30.....**81**

figure 5.1.2.10: ISVD 1 30.....**81**

figure 5.1.2.11: local part of the model-field with 10m · 10m sampling interval in -50m.....**82**

figure 5.1.2.12 Tikhonov without field-augmentation.....**82**

figure 5.1.2.13 Tikhonov with 15% field-augmentation (standard setting).....**82**

figure 5.1.2.14 Tikhonov with 50% field-augmentation.....**82**

figure 5.1.2.15 ISVD 4 30 (regional part exchanged by linear field augmentation to same field size like regional field).....**82**

figure 5.1.2.16 Tikhonov with 67% field augmentation (corresponds to same amount of nodes like regional field + local field).....**82**

figure 5.1.2.17: error distribution Cooper approach impBS3af, bin width 100nT.....**83**

figure 5.1.2.18: error ISVD 4 30.....**83**

figure 5.1.2.19: error ISVD 6 30.....**83**

figure 5.1.2.20: error ISVD 5 30.....**83**

figure 5.1.2.21 error ISVD 3 30.....**84**

figure 5.1.2.22: error ISVD 2 30.....**84**

figure 5.1.2.23: error ISVD 1 30.....**84**

figure 5.1.2.24 error Tikhonov without field-augmentation.....**84**

figure 5.1.2.25 error Tikhonov with 15% field-augmentation (standard setting).....**84**

figure 5.1.2.26 error Tikhonov with 50% field-augmentation.....**84**

figure 5.1.2.27 error ISVD 4 30 (regional part exchanged by linear field augmentation to same field size like regional field).....**85**

figure 5.1.2.28 error Tikhonov with 67% field augmentation (corresponds to same amount of nodes like regional field + local field).....**85**

figure 5.1.2.29: cross-section path for local field in Vulcano without regional field part.....**86**

figure 5.1.2.30: CS error ISVD 4 30.....**86**

figure 5.1.2.31: CS error ISVD 6 30.....**86**

figure 5.1.2.32: CS error ISVD 5 30.....**86**

figure 5.1.2.33 CS error ISVD 3 30.....**87**

figure 5.1.2.34: CS error ISVD 2 30.....**87**

figure 5.1.2.35: CS error ISVD 1 30.....**87**

figure 5.1.2.36 CS error Tikhonov without field-augmentation.....**87**

figure 5.1.2.37 CS error Tikhonov with 15% field-augmentation.....**87**

figure 5.1.2.38 CS error Tikhonov with 50% field-augmentation.....**87**

figure 5.1.2.39 CS error ISVD 4 30 (regional part exchanged by linear field augmentation to same field size like regional field).....**88**

figure 5.1.2.40 CS error Tikhonov with 67% field-augmentation (corresponds to same amount of nodes like regional field + local field).....**88**

figure 5.1.2.41: lre ISVD 4 30.....**89**

figure 5.1.2.42: lre ISVD 5 30.....**89**

figure 5.1.2.43: lre ISVD 6 30.....**89**

figure 5.1.2.44 lre ISVD 3 30.....**89**

figure 5.1.2.45: lre ISVD 2 30.....**89**

figure 5.1.2.46: lre ISVD 1 30.....**89**

figure 5.1.2.47 lre Tikhonov without field-augment.....**90**

figure 5.1.2.48 lre Tikhonov with 15% field-augmentation.....**90**

figure 5.1.2.49 lre Tikhonov with 50% field-augmentation.....**90**

figure 5.1.2.50 lre ISVD 4 30 (regional part exchanged by linear field augmentation to same field size like regional field).....**90**

figure 5.1.2.51 lre Tikhonov with 67% field-augmentation (corresponds to same amount of nodes like regional field + local field).....**90**

figure 5.1.2.52: CS lre ISVD 4 30.....**91**

figure 5.1.2.53: CS lre ISVD 6 30.....**91**

figure 5.1.2.54: CS lre ISVD 5 30.....**91**

figure 5.1.2.55 CS lre ISVD 3 30.....**91**

figure 5.1.2.56: CS lre ISVD 2 30.....**91**

figure 5.1.2.57: CS lre ISVD 1 30.....**91**

figure 5.1.2.58 CS lre Tikhonov without field-augmentation.....**92**

figure 5.1.2.59 CS lre Tikhonov with 15% field-augmentation.....**92**

figure 5.1.2.60 CS lre Tikhonov with 50% field-augmentation.....**92**

figure 5.1.2.61 CS lre ISVD 4 30 (regional part exchanged by linear field augmentation to same field size like regional field).....**92**

figure 5.1.2.62 CS lre Tikhonov with 67% field-augmentation (corresponds to same amount of nodes like regional field + local field).....**92**

figure 5.1.3.1: true derivative.....**93**

figure 5.1.3.2: BS3af / BS3fa derivative.....**93**

figure 5.1.3.3: error BS3af / BS3fa derivative.....**93**

figure 5.1.3.4: lre BS3af / BS3fa derivative.....**93**

Figure 5.1.3.5: true derivative.....**94**

figure 5.1.3.6: BS4af / BS4fa derivative.....**94**

figure 5.1.3.7: error BS4af / BS4fa derivative.....**94**

figure 5.1.3.8 lre BS4af / BS4fa derivative.....**94**

figure 5.1.3.9 BS4af / BS4fa derivative including regional part. Scale bar in nT/km.....**95**

figure 5.1.4.1: model-field in 50m depth.....**96**

figure 5.1.4.2: FFT.....**96**

figure 5.1.4.3: Cooper approach impFD1af.....**96**

figure 5.1.4.4: Cooper approach impFD2af.....**96**

figure 5.1.4.5: ISVD 4 30.....**97**

figure 5.1.4.6 Tikhonov / Pasteka.....**97**

figure 5.1.4.7: error FFT.....**98**

figure 5.1.4.8: error Cooper approach impFD1af.....**98**

figure 5.1.4.9: error Cooper approach impFD1fa.....**98**

figure 5.1.4.10: error Cooper approach impFD2af.....**98**

figure 5.1.4.11: error Cooper approach impFD2fa....**99**

figure 5.1.4.12: error Cooper approach FD2af....**99**

figure 5.1.4.13: error ISVD 4 30....**99**

figure 5.1.4.14 error Tikhonov / Pasteka....**99**

figure 5.1.4.15: lre FFT....**100**

figure 5.1.4.16: lre Cooper appraoch impFD1af....**100**

figure 5.1.4.17: lre Cooper approach impFD1fa....**100**

figure 5.1.4.18: lre Cooper approach impFD2af....**100**

figure 5.1.4.19: lre Cooper approach impFD2fa....**101**

figure 5.1.4.20: lre Cooper approach FD2af....**101**

figure 5.1.4.21: lre ISVD 4 30....**101**

figure 5.1.4.22 lre Tikhonov / Pasteka....**101**

figure 5.1.4.23: model-field in 130m depth....**102**

figure 5.1.4.24: Cooper approach impFD2fa....**102**

figure 5.1.4.25: Cooper approach impFD1af....**102**

figure 5.1.4.26: Cooper approach impFD2af....**103**

figure 5.1.4.27: Cooper approach FD0af....**103**

figure 5.1.4.28: Cooper approach impFD0fa....**103**

figure 5.1.4.29: Cooper approach FD1af....**103**

figure 5.1.4.30: ISVD 6 30....**103**

figure 5.1.4.31 Tikhonov / Pasteka....**103**

figure 5.1.4.32: error Cooper approach impFD2fa....**104**

figure 5.1.4.33: error Cooper approach impFD1af....**104**

figure 5.1.4.34: error Cooper approach impFD2af....**105**

figure 5.1.4.35: error Cooper approach FD0af....**105**

figure 5.1.4.36: error Cooper approach impFD0fa....**105**

figure 5.1.4.37: error Cooper approach FD1af.....**105**

figure 5.1.4.38: error ISVD 6 30.....**106**

figure 5.1.4.39 error Tikhonov / Pasteka.....**106**

figure 5.1.4.40: lre Cooper approach impFD2fa.....**107**

figure 5.1.4.41: lre Cooper approach impFD1af.....**107**

figure 5.1.4.42: lre Cooper approach impFD2af.....**107**

figure 5.1.4.43: lre Cooper approach FD0af.....**107**

figure 5.1.4.44: lre Cooper approach impFD0fa.....**108**

figure 5.1.4.45: lre Cooper approach FD1af.....**108**

figure 5.1.4.46: lre ISVD 6 30.....**108**

figure 5.1.4.47 lre Tikhonov / Pasteka.....**108**

Figure 5.2.1.1: RTP field, neglecting topography, inclination 10°.....**110**

Figure 5.2.1.2: RTP field, considering topography, inclination 10° (Xia).....**110**

Figure 5.2.1.3: error RTP field, neglecting topography, inclination 10°.....**110**

Figure 5.2.1.4: error RTP field, considering topography, inclination 10°.....**110**

Figure 5.2.1.5: lre RTP field, neglecting topography, inclination 10°.....**111**

Figure 5.2.1.6: lre RTP field, considering topography, inclination 10°.....**111**

Figure 5.2.1.7: RTP field, neglecting topography, inclination 30°.....**111**

Figure 5.2.1.8: RTP field, considering topography, inclination 30° (Xia).....**111**

Figure 5.2.1.9: error RTP field, neglecting topography, inclination 30°.....**112**

Figure 5.2.1.10: error RTP field, considering topography, inclination 30°.....**112**

Figure 5.2.1.11: lre RTP field, neglecting topography, inclination 30°.....**112**

Figure 5.2.1.12: lre RTP field, considering topography, inclination 30°.....**112**

Figure 5.2.1.13: RTP field, neglecting topography, inclination 50°.....**113**

Figure 5.2.1.14: RTP field, considering topography, inclination 50° (Xia).....**113**

Figure 5.2.1.15: error RTP field, neglecting topography, inclination 50°.....**113**

Figure 5.2.1.16: error RTP field, considering topography, inclination 50°.....**113**

Figure 5.2.1.17: lre RTP field, neglecting topography, inclination 50°.....**114**

Figure 5.2.1.18: lre RTP field, considering topography, inclination 50°.....**114**

Figure 5.2.1.19: RTP field, neglecting topography, inclination 70°.....**114**

Figure 5.2.1.20: RTP field, considering topography, inclination 70° (Xia).....**114**

Figure 5.2.1.21: error RTP field, neglecting topography, inclination 70°.....**115**

Figure 5.2.1.22: error RTP field, considering topography, inclination 70°.....**115**

Figure 5.2.1.23: lre RTP field, neglecting topography, inclination 70°.....**115**

Figure 5.2.1.24: lre RTP field, considering topography, inclination 70°.....**115**

Figure 5.2.2.1: RTP field gained by Xia considering topography.....**116**

Figure 5.2.2.2: RTP field neglecting topography.....**116**

Figure 5.2.2.3: error RTP field neglecting topography (RTP-Xia).....**116**

Figure 5.2.2.4: lre RTP field neglecting topography (lre (RTP-Xia)).....**116**

figure 5.2.3.1: RTP field gained by Xia considering topography.....**117**

figure 5.2.3.2: RTP field neglecting topography.....**117**

figure 5.2.3.3: error RTP field neglecting topography (RTP-Xia).....**117**

figure 5.2.3.4: lre RTP field neglecting topography (lre (RTP-Xia)).....**117**

Figure 5.2.4.1: RTP field gaines by Xia considering topography.....**118**

Figure 5.2.4.2: RTP field neglecting topography.....**118**

Figure 5.2.4.3: error RTP field neglecting topography (RTP-Xia).....**118**

Figure 5.2.4.4: lre RTP field neglecting topography (lre(RTP-Xia)).....**118**

10. Lebenslauf

PERSÖNLICHE DATEN

Niko Kompein

geboren am: 9.3.1981 in Graz

ledig

Anschrift: Meidlgasse 43/5/4, 1110 Wien

e-mail: niko.kompein@gmx.at

SCHULAUSBILDUNG

09/1987	-	*07/1991:*	*Volksschule Graz, Neubaugasse 12, 8020 Graz und Zeltgasse 7, 1080 Wien*
09/1991	-	*07/1994:*	*Bundesgymnasium, Bundesrealgymnasium und Wirschaftskundliches Bundesrealgymnasium Albertgasse 38, 1080 Wien*
09/1994	-	*07/1995:*	*Hauptschule, 2232 Deutsch Wagram*
09/1995	-	*06/2001:*	*HTBLA 22, Donaustadtstraße 45, 1220 Wien, Ausbildungsschwerpunkt Telekommunikation Reifeprüfung am 8.6.2001*

HOCHSCHULAUSBILDUNG

10/2005	-	07/2006:	Diplomstudium Meteorologie und Geophysik, 1. Studienabschnitt
07/2006	-	09/2011:	Diplomstudium Geophysik, 2. Studienabschnitt

BERUFLICHER WERDEGANG

06/2002 - 10/2005: *Systemtechniker für Kommunikationstechnik bei VA TECH, SAT GmbH & Co. Zuständig für:*

- *Anlagendesign und Projektierung*
- *Parametrierung und Inbetriebnahme der Anlagen*
- *Laufende Betreuung und Ausbau von Telekomnetzen*
- *Unterstützung von Vertriebsmitarbeitern bei der Angebotserstellung*
- *Projektleitung von Projekten innerhalb Österreichs*

KENNTNISSE

EDV:

- *Erfahrung in der Netzwerkadministration von Breitbandnetzen (HP-UX, SOLARIS, UNIX, EM-OS, etc.) sowohl als auch LAN-Netzen*
- *Grundlegende Kenntnisse von Datenbanken*
- *Grundlegende Kenntnisse in Matlab 7.0*
- *Gute Kenntnisse in Golden Software Surfer 8 sowie Fortran 77*
- *Gute Kenntnisse in Open-Office 3.0 sowie Microsoft Office Anwendungen*

FREMDSPRACHEN:

- *Englisch*